

# DISENTANGLING DROUGHT-RESPONSIVE TRAITS WITH FOCUS ON ARABIDOPSIS

AJAREE THONGLIM





**Disentangling drought-responsive traits  
with focus on Arabidopsis**

Ajaree Thonglim. 2023. *Disentangling drought-responsive traits with focus on Arabidopsis*.

PhD Thesis at the University of Leiden, The Netherlands.

ISBN: 978-94-6483-426-0

***This PhD research was financially supported by:***

Institute for the Promotion of Teaching Science and Technology.  
Dutch Research Council NWO (grant ALWOP.488).

***This PhD research was carried out at:***

Naturalis Biodiversity Center, The Netherlands.  
Leiden University, The Netherlands.  
University of Bordeaux, France.

***Editorial layout and cover design:***

Ajaree Thonglim



# **Disentangling drought-responsive traits with focus on Arabidopsis**

Proefschrift

ter verkrijging van  
de graad van doctor aan de Universiteit Leiden,  
op gezag van rector magnificus prof.dr.ir. H. Bijl,  
volgens besluit van het college voor promoties  
te verdedigen op donderdag 9 november 2023  
klokke 11:15 uur

door

**Ajaree Thonglim**  
geboren te Nakhon Pathom, Thailand  
in 1993

**Promotor:**

Prof. Dr. E. Smets

**Co-promotor:**

Dr. F. Lens

**Promotiecommissie:**

Prof. Dr. A.H. Meijer

Prof. Dr. P. van Welzen

Dr. S. Balazadeh

Prof. Dr.ir. K. Steppe (Ghent University, Belgium)

Prof. Dr. S. Jansen (Ulm University, Germany)

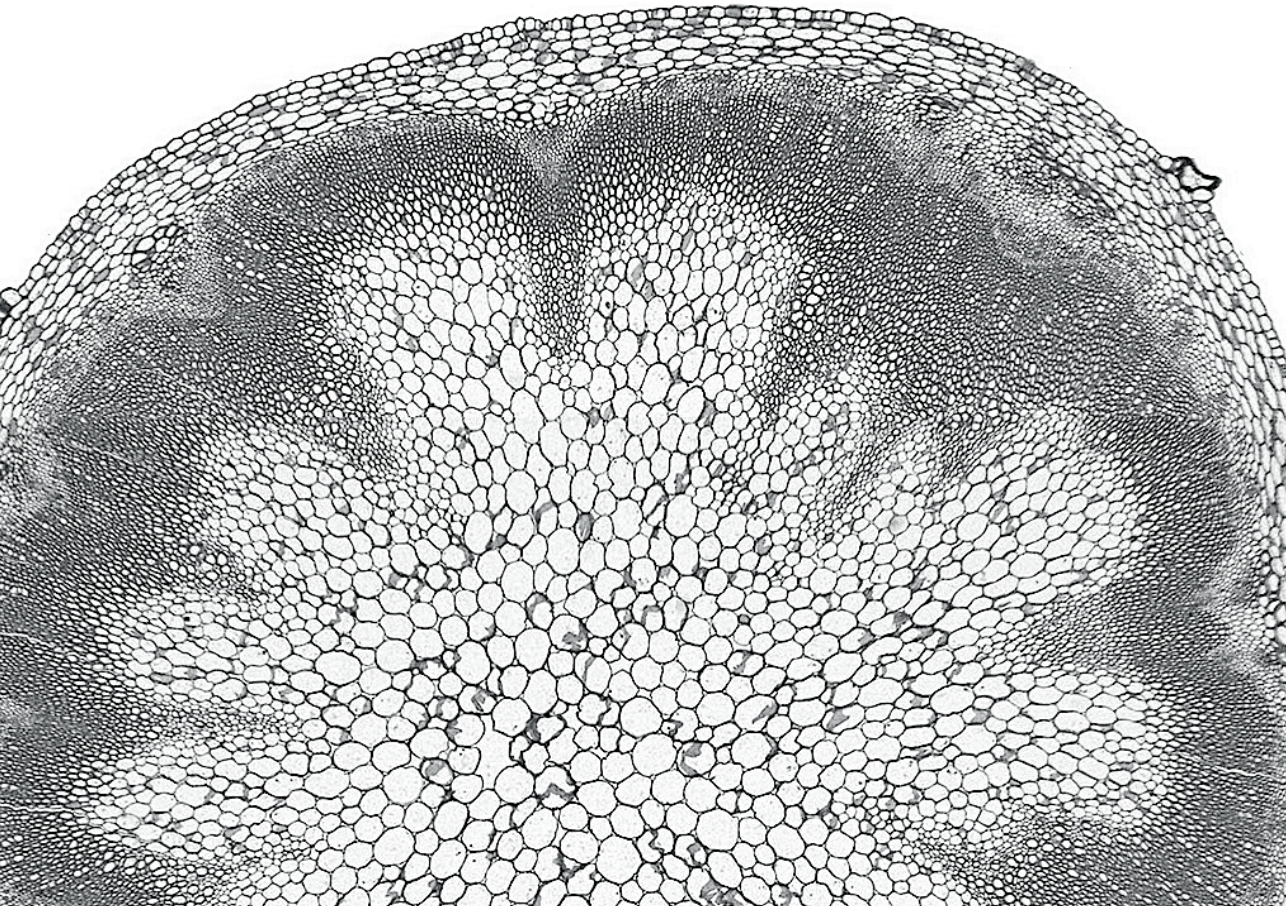
# TABLE OF CONTENTS

<b>CHAPTER 1</b> .....	7
General introduction and thesis outline	
<b>CHAPTER 2</b> .....	43
Intervessel pit membrane thickness best explains variation in embolism resistance amongst stems of <i>Arabidopsis thaliana</i> accessions	
<b>CHAPTER 3</b> .....	79
Drought response in Arabidopsis displays synergistic coordination between stems and leaves	
<b>CHAPTER 4</b> .....	125
High leaf water potential: a key to drought resilience in <i>JUB1</i> overexpression lines of Arabidopsis and tomato	
<b>CHAPTER 5</b> .....	159
General discussion and future perspectives	
<b>SUMMARIES</b> .....	173
<b>REFERENCES</b> .....	177
<b>ACKNOWLEDGEMENTS</b> .....	225
<b>CURRICULUM VITAE</b> .....	227



## Chapter 1

# **GENERAL INTRODUCTION AND THESIS OUTLINE**





## ***Impact of global warming on forest mortality and crop yield***

Temperature and precipitation patterns are shifting globally due to ongoing global warming. As a result, we are witnessing an increase in the severity and frequency of drought periods, even in countries that have not previously suffered drought stress (Corso *et al.*, 2020; Gleason *et al.*, 2022). These droughts have caused large-scale mortality events in various types of forests and ecosystems (Allen *et al.*, 2009, 2015; Hartmann *et al.*, 2018; Hammond *et al.*, 2022), such as temperate deciduous and evergreen forests (Crouchet *et al.*, 2019; Schuldt *et al.*, 2020), semi-arid woodlands and savannahs (Swemmer, 2020; Kannenberg *et al.*, 2021), dry tropical forests (Powers *et al.*, 2020), and tropical rainforests (Feldpausch *et al.*, 2016; Esquivel-Muelbert *et al.*, 2020) (Figure 1). Extensive and severe drought periods are also causing significant reductions in crop yield globally, with about 75% of the global harvested area experiencing drought-related yield losses (IPCC, 2022). Climate change has significantly impacted yields of nearly all important crops in Europe, particularly in southern Europe, resulting in recent yield stagnation and crop losses that have tripled over the past 50 years (Agnolucci and De Lipsis, 2020; Brás *et al.*, 2021). In western Africa, the declining precipitation and rising temperatures decrease millet and sorghum yields by 10–20% and 5–15%, respectively (Sultan *et al.*, 2019). Moreover, the combined effects of increased temperature and drought diminish the global yields of wheat, maize, and soybean by 9.2%, 11.6%, and 12.4%, respectively (Matiu *et al.*, 2017). Both crop yield decline and forest mortality are predicted to drastically accelerate at a global scale in the near future (Allen *et al.*, 2009; Lesk *et al.*, 2016; Klein and Hartmann, 2018; Goulart *et al.*, 2021; McDowell *et al.*, 2022). Moreover, drought stress frequently interacts with wildfires, windthrow (Brando *et al.*, 2014), or insect attacks (Temperli *et al.*, 2013; Sangüesa-Barreda *et al.*, 2015; Kolb *et al.*, 2016; Canelles *et al.*, 2021), which can exacerbate changes in the structure and function of natural ecosystems and agriculture (Waring *et al.*, 2009; Adams *et al.*, 2012; Clark *et al.*, 2016). Given the significant ecological and economic impacts of climate change, understanding drought-related plant death and its underlying mechanisms is crucial for accurately estimating the risk of forest and agricultural loss and implementing suitable management strategies (Anderegg *et al.*, 2013; Hartmann *et al.*, 2018).

The mechanisms underlying drought-induced mortality are complex. They involve the interplay between water, carbon, and biotic interdependencies (Anderegg *et al.*, 2015; McDowell *et al.*, 2022). The water and carbon supply are crucial for the survival of plants since they provide the basis for osmoregulation and cell maintenance (Koster and Leopold, 1988; Yu, 1999; Hoekstra *et al.*, 2001; Ramel *et al.*, 2009; Matros *et al.*, 2015; Martinez-Vilalta *et al.*, 2019; Mantova *et al.*, 2021; Sapes *et al.*, 2021), as well as the production of compounds used in a defense system against the attack of biotic agents (Goodsman *et al.*, 2013; Netherer *et al.*, 2015; Wiley *et al.*, 2016; Rissanen *et al.*, 2021). Furthermore, a decrease in carbon pool sizes and fluxes can impair resistance to embolism because carbohydrate is required to avoid, or tolerate cell dehydration, which is essential for maintaining the integrity of the hydraulic system (Tomasella *et al.*, 2019). Among all the processes involved in drought-induced plant mortality, carbon starvation and hydraulic failure have been proposed as the main mechanisms. Hydraulic failure occurs when the root-to-shoot water transport system collapses due to the accumulation of drought-induced embolism inside xylem conduits that exceeds the point at which water transport is irrecoverable (Sperry and Tyree, 1988; Venturas *et al.*, 2017; McDowell *et al.*, 2022; Johnson *et al.*, 2022). Carbon starvation occurs when the carbon-metabolic functions are impaired due to a limited supply of carbohydrates caused by a decrease in photosynthesis and available carbon storage (McDowell *et al.*, 2008, 2011). Although these two mechanisms are not mutually exclusive processes, many studies have shown that hydraulic failure is the primary cause of intense, short-to-longer periods of drought (Urli *et al.*, 2013; Salmon *et al.*, 2015; Adams *et al.*, 2017; Mantova *et al.*, 2022b), while carbon starvation is more likely to happen during prolonged moderate drought conditions (McDowell *et al.*, 2008; Creek *et al.*, 2020).



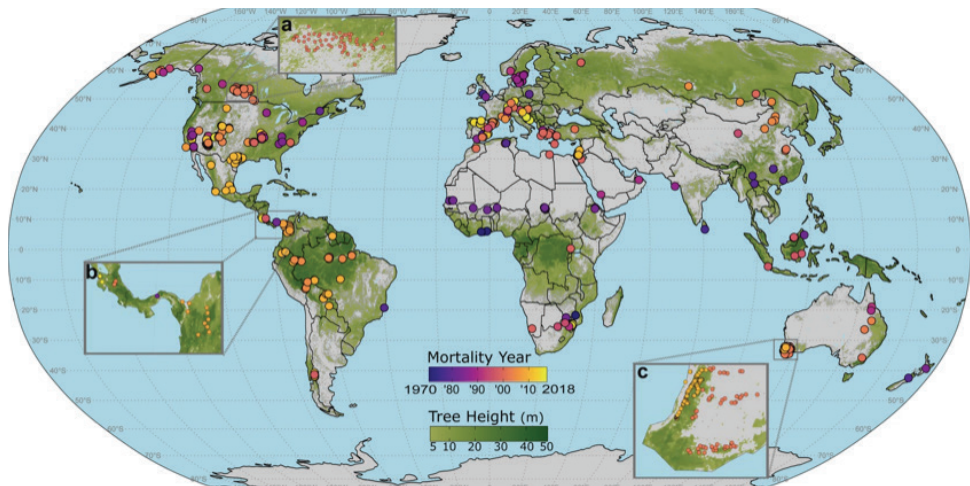


**Figure 1** A global map showing forest mortality locations associated with drought and high temperatures induced by climate change. Each dot represents a color-coded forest mortality event according to the year of mortality. Taken from Hammond *et al.* (2022).

### ***Plant vascular tissue: development and growth***

To understand the mechanisms behind water transport in plants, it is important to first become familiar with the tissues involved in this process. The vascular tissue is a crucial component of plants, originating from meristem cells called procambium located in the plant axis (root and stem) during embryonic development and beyond. These procambium strands produce vascular bundles comprising (primary) xylem that is lignin-rich and phloem that usually lacks lignin in the cell walls (Esau, 1965; Evert, 2006). Xylem transports water and nutrients upwards, whereas phloem transports sugars and other organic compounds from leaves to all living cells (Evert, 2006; Lucas *et al.*, 2013). The development of vascular tissues in the stem can be divided into two main stages: primary growth and (if available) secondary growth. *Primary growth* gives rise to all primary tissues by apical meristems in stems and roots, as well as by the procambium strands that produce the vascular bundles, and typically leads to plant elongation (Figure 2, i). *Secondary growth* is the developmental process in woody species – i.e., trees, shrubs, and lianas – that increases stem and root thickness through the activity of two lateral (secondary) meristems, known as vascular cambium and cork cambium. During secondary growth, vascular cambium

cells divide and differentiate into wood (i.e., secondary xylem) towards the inside and secondary phloem towards the outside of the hollow cylindrical meristem that connects the (intrafascicular) vascular cambium parts among adjacent vascular bundles via the formation of interfascicular cambium (Figure 2, ii-iv). Wood formation accumulates much faster than secondary phloem, which enlarges the vascular cambium and subsequently triggers the formation of cork cambium that produces the periderm with many cork cells (Figure 2, iii-iv). These cork cells act as a secondary protective barrier that helps to prevent water loss, protects the woody plant from physical damage, provides insulation (Esau, 1965; Pereira, 2007), and replaces the initial (primary) protective layer – epidermis in stems and rhizodermis in roots – that will rupture during the initial stages of the lateral growth. As the woody plant ages, the secondary xylem accumulates, forming a wood cylinder that provides essential structural stability and supports to the stem, and becomes responsible for a large part of the root-to-shoot water transport (Esau, 1965; Lucas *et al.*, 2013). At the same time, the bark tissues outside the vascular cambium develop as well, including secondary phloem that remains active for a limited amount of time, cortex parenchyma that often has the ability to undergo cell divisions to avoid rupturing during dilation, and (one or multiple) periderm(s) that include a cork cambium generating radial rows of cork cells towards the outside and one cell layer of phelloderm towards the inside (Esau, 1965; Pereira, 2007). These primary and secondary growth processes continue throughout the plant's lifetime, resulting in the continuous addition of new (primary and secondary) xylem and phloem and cork tissue, and a corresponding increase in vertical and lateral growth (Esau, 1965; Evert, 2006; Lucas *et al.*, 2013; Lopez and Barclay, 2017).

Unlike woody plants, herbaceous species rarely undergo secondary growth, and their lignified xylem tissue is mainly formed by the primary xylem inside the vascular bundles (Figure 2, i). Nevertheless, many non-monocot herbaceous angiosperm species have some degree of wood formation, although this is typically limited to the base of their stems (Schweingruber, 2006, 2007; Schweingruber *et al.*, 2011; Lens *et al.*, 2012*a*). In some cases, the limited amount of wood formation is confined to the vascular bundle regions at the base of the stem, while in others, a complete vascular cambium may be formed, producing a small cylinder of wood (Altamura *et al.*, 2001; Chaffey *et al.*, 2002; Lens *et al.*, 2012*a*; Ragni and Greb, 2018) (Figure 2, ii-iii). Due to the negligible presence of secondary

development in herbaceous plants, their stems are mechanically weaker than those of woody species. Subsequently, lignification in cells outside the xylem plays a vital role in increasing the tensile strength and stiffness of herbaceous stems, thereby reducing the risk of breakage or damage (Barros *et al.*, 2015) (Figure 2, iii). In addition, lignified cells provide a barrier against pathogens and pests, protecting plants from disease (Barros *et al.*, 2015; Liu *et al.*, 2018), and also occur in other cell types in different organs of the plant, such as seeds and fruits (Barcelo, 1997; Barros *et al.*, 2015; Emonet and Hay, 2022). In conclusion, lignification and wood formation are two distinct processes in plant development. Yet, they resemble each other in incorporating lignin inside the cell walls, either inside the secondary xylem tissue during wood formation or outside the xylem tissue (lignified sclerenchyma cells in stems, roots, leaves, and fruits).

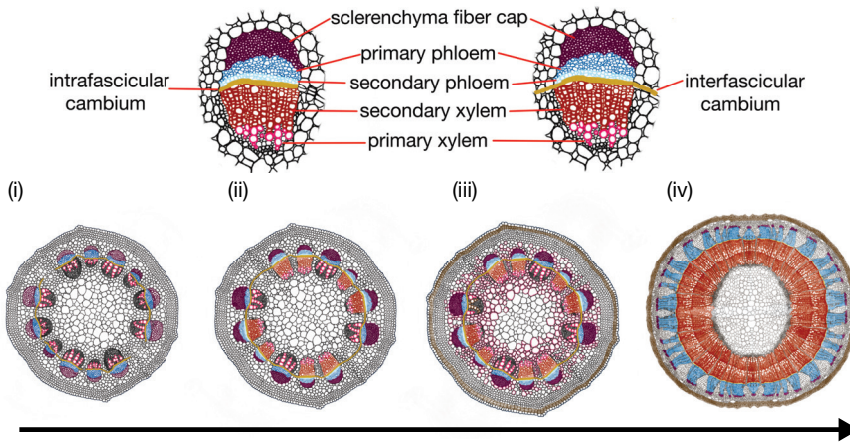


**Figure 2** A diagram illustrating the transition from primary to secondary growth in the stem (i to iv).

The process leads to an increase in the stem's thickness. It originates by connecting the intrafascicular cambium (within the vascular bundles) with interfascicular cambium parts (between the vascular bundles). At the beginning of secondary growth, the parenchyma cells close to the intrafascicular cambium dedifferentiate and undergo periclinal cell divisions, thereby forming a closed vascular cambium ring as viewed in a cross-section (i-ii). the vascular cambium ring is completely closed (ii), which later produces secondary xylem (wood) and secondary phloem (iii-iv). In herbaceous plants, secondary growth is limited, meaning that lignification in the cells outside the xylem tissue (dark purple fiber caps on top of the vascular bundles) is essential to strengthening the stems (iii).

## ***Exploring xylem anatomy***

Xylem is a complex tissue comprising various cell types, including water-conducting tracheary elements, non-tracheary elements, and parenchyma cells (Evert, 2006; Pittermann, 2010; Słupianek *et al.*, 2021). Tracheary elements, including water-conducting vessel elements and tracheids, are essential components of the xylem tissue. Vessel elements are dead, tubular cells with two large, perforated openings in their lower and upper walls that connect to each other and form an axial row of vessel elements, known as vessels. Vessels typically occur in angiosperms and are, on average, between 1-50 cm long and relatively wide (up to 0.8 mm). Tracheids are mainly present in gymnosperms and are relatively narrow and much shorter and narrower than vessels (ranging from 0.5-4 mm in length and 8-80  $\mu\text{m}$  in diameter; Pittermann, 2010). During development, both types of tracheary elements undergo programmed cell death, resulting in hollow, tube-like cells with lignified secondary walls, which impart mechanical strength to the xylem and allow efficient water transport while preventing cell collapse when xylem sap is under negative pressure (Evert, 2006; Pittermann, 2010; Słupianek *et al.*, 2021). Importantly, both vessels and tracheids are connected laterally and longitudinally via interconduit pits, forming a 3D network of short hollow tubes enabling an efficient long-distance water transport system from roots to leaves (Esau, 1965; Evert, 2006).

Interconduit pits are crucial structures for effective water transport because water needs to pass through millions of these pits in tall trees in order to reach the leaves, simply because the length of tracheary elements is much shorter than the total plant height. Each interconduit pit comprises pit borders, sections of the secondary cell wall that arch over a small aperture and widen into a larger pit chamber. These tiny gaps in the secondary cell wall allow water flow between neighbouring conduits. The intervessel pit membrane, which lies at the center of the pit-pair, is formed by hydrolysis of the middle lamella and primary walls of the two adjacent conduits. In angiosperms, the thickness of the intervessel pit membrane ranges from 70-1200 nm (Meyra *et al.*, 2007; Jansen *et al.*, 2009), and consists of modified porous structures, including microlayers of tightly woven cellulose microfibrils and hemicelluloses, which form a tortuous path

of nanoscale pores. The highly interconnected pit membrane pores contain multiple constrictions, with the narrowest constriction in each pore regulating the flow of water, gas, and embolism spreading (Kaack *et al.*, 2019, 2021; Zhang *et al.*, 2020). Pit membranes can account for more than 50% of the total hydraulic resistance in the xylem and are important safety valves that can prevent the spread of embolisms between adjacent conduits, also known as air-seeding, highlighting their crucial role in maintaining the safety and efficiency of the hydraulic system in the xylem network (Sperry *et al.*, 2005; Wheeler *et al.*, 2005; Choat *et al.*, 2006, 2008; Jansen *et al.*, 2009).

Other cell types in angiosperm xylem are fibers, which often comprise the bulk of the xylem tissue, also undergo programmed cell death, and in many cases, surround the vessels. These non-tracheary elements have a short length and often thick lignified walls, which provide the required mechanical support (Jacobsen *et al.*, 2005; Déjardin *et al.*, 2010; Pittermann, 2010). In addition to the dead xylem fibers, angiosperm wood also shows two types of living parenchyma cells, axial parenchyma and ray cells forming radial rays, which remain metabolically active in mature sapwood and contribute to a range of functions, such as the transport of nonstructural carbohydrates and mineral inclusions (O'Brien *et al.*, 2014; Plavcová and Jansen, 2015), water storage (capacitance), xylem hydraulic conductance (Pfautsch *et al.*, 2015), and to a lesser extent, mechanical support (Reiterer *et al.*, 2002; Martínez-Cabrera *et al.*, 2009). Overall, the coordinated actions of these cell types are essential for the proper functioning of xylem tissue in plants.

## ***Ascent of sap***

Plants require a continuous water supply between the soil and the leaves in order to sustain essential processes such as photosynthesis, growth, and reproduction (Sperry, 2003; Brodribb, 2009; Lucas *et al.*, 2013; Choat *et al.*, 2018; Brodribb *et al.*, 2020). According to the cohesion-tension theory, water is transported throughout the plant by water-conducting cells (tracheids and/or vessels depending on the plant group), which ensure a chain of interconnected water molecules (Dixon and Joly, 1895; Tyree and Zimmermann, 2002). This theory implies that (1) the root-to-leaf water flow is driven by a gradient of negative pressure (aka tension) that is created in

the cell walls of the mesophyll cells in leaves during transpiration, and (2) cohesion forces among water molecules, which are maintained by hydrogen bonds, allow the xylem sap to remain intact under these negative pressures (Dixon and Joly, 1895; Pickard, 1981; Brown, 2013a). If the loss of water molecules is larger than the uptake of soil water via the roots, the tension in the xylem sap will increase (Konrad *et al.*, 2019). This negative pressure puts water in a metastable state, which triggers its conversion from the liquid to the vapour phase (i.e., cavitation), which may or may not lead to large gas bubble events (i.e., embolisms) that block the water transport inside the water-conducting cell (Steudle, 2001; Wheeler and Stroock, 2008; Brown, 2013a; Venturas *et al.*, 2017) (Figure 3).

Mechanisms involved in embolism formation are complex and poorly known, and involve interactions at the nano-scale inside xylem sap that includes not only water but also other compounds such as tiny (undissolved) gas bubbles, ions, proteins, sugars, and lipids that act as surface active agents (surfactants) (Lens *et al.*, 2022). Cavitation could happen via homogeneous nucleation when water molecules acquire sufficient energy to break intermolecular binding forces, resulting in the formation of an embryonic vapour bubble within the water column. However, this homogeneous nucleation is unlikely to occur since the tension in the xylem conduits is not high enough to allow the cohesion forces to break (Briggs, 1950; Pickard, 1981; Maris and Balibar, 2000; Chen *et al.*, 2016a; Kanduč *et al.*, 2020). One alternative hypothesis is that embolism is caused by pre-existing, tiny gas bubbles inside the xylem sap that expand due to various changes in temperature, pressure, surface tension, or gas oversaturation. These changes could trigger a tiny gas nanobubble, surrounded by a stabilizing sheath of surfactants, to expand beyond a critical size that leads to an embolism (Tyree *et al.*, 1994; Schenk *et al.*, 2015, 2017; Ingram *et al.*, 2021). Another alternative is that embolisms are induced by surface bubbles associated with hydrophobic vessel surfaces (Tyree *et al.*, 1994; Lohse and Zhang, 2015).

There is a consensus that the spread of air bubbles via the intervessel pit membranes among adjacent conduits (i.e., air-seeding) is more plausible than the formation of new embolisms in the xylem sap (Zimmermann, 1983; Kaack *et al.*, 2019; Guan *et al.*, 2021). In angiosperms, air-seeding occurs when the xylem sap pressure surpasses the threshold that intervessel pit

membranes can sustain, enabling air bubbles in an embolized vessel to be pulled into an adjacent, water-filled vessel through nanoscale pores in pit membranes (Pockman *et al.*, 1995; Sperry and Hacke, 2004; Choat *et al.*, 2008; Jansen *et al.*, 2009). Under drought conditions, low water availability in drying soil or high evaporative demand significantly increases the xylem tension, thereby increasing the risk of air-seeding between adjacent conduits and potentially leading to a cascade effect of more drought-induced embolism as drought progresses (Brodribb and Hill, 2000). If water stress persists, the spread of embolisms in the 3D vessel network continues to decrease hydraulic conductivity and could eventually lead to decreased photosynthesis, desiccation, dieback of tissues and organs, and, ultimately, plant mortality (Brodribb and Cochard, 2009; Urli *et al.*, 2013; Adams *et al.*, 2017; Mantova *et al.*, 2022a,b). Bearing this in mind, increasing evidence suggests that natural selection has shaped the hydraulic systems of plants in such a way that the impact of drought-induced embolism is minimized, meaning that plants do not suffer from major drought-induced embolism events in the field under daily, natural growing conditions (Cochard and Delzon, 2013; Delzon and Cochard, 2014; Martin-StPaul *et al.*, 2017; Creek *et al.*, 2020).

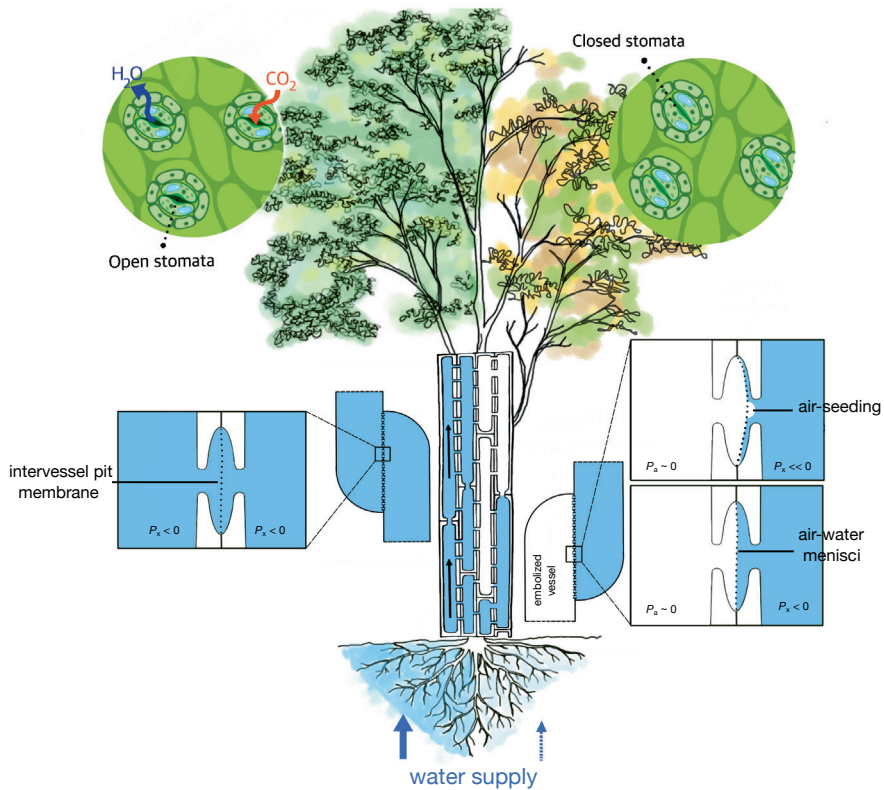


**Figure 3** The root-to-leaf water transport under well-watered (left) and water deficiency conditions (right). In the well-watered stage, water movement is driven by transpiration occurring through the open stomata during the day. As water evaporates from the leaves, it creates a negative pressure that draws water up from the roots, creating a continuous flow of water through the plant. During the onset of drought, the stomata close in an effort to prevent water loss and subsequently a continuously declining negative xylem sap pressure as this would otherwise promote embolism spread via air-seeding (visualized as a simplified 2D cartoon on the right-hand side). Air seeding thresholds in angiosperms are set by the thickness of the intervessel pit membrane, its associate pit membrane pore size, and the number of intervessel pits for a given conduit of average size. *Adapted from Venturas et al. (2017).*



## **Assessing plant vulnerability to embolism**

The vulnerability of plants to embolism can be measured by so-called vulnerability curves (VCs), in which the percentage loss of (measured or theoretical) hydraulic conductivity (PLC) is plotted against xylem sap pressure (measured in MPa) (Figure 4A) (Tyree and Sperry, 1989; Choat *et al.*, 2012). The VCs allow us to determine coefficients that have physiological relevance when describing the susceptibility of plants to xylem embolism, facilitating comparisons among plant organs and species (Tyree and Ewers, 1991; Tyree and Zimmermann, 2002). The xylem water potential inducing 50% loss of maximum conductivity ( $P_{50}$ ) is the main parameter derived from VCs. It is a proxy for a plant's drought tolerance (Tyree and Ewers, 1991; Maherali *et al.*, 2004; Choat *et al.*, 2012; Venturas *et al.*, 2017; Brodribb, 2017) (Figure 4A).  $P_{50}$  is strongly correlated with water availability reflected by species' distribution patterns and is considered relevant for drought-induced forest mortality modelling (Blackman *et al.*, 2012; Anderegg *et al.*, 2016; Larter *et al.*, 2017; Trueba *et al.*, 2017). Other parameters, such as  $P_{12}$  (xylem pressure causing a 12% loss of maximum conductivity) and  $P_{88}$  (xylem water potential inducing 88% loss of maximum conductivity), are also used to quantify embolism thresholds (Figure 4A).  $P_{12}$  can be interpreted as the 'air entry point', whereas  $P_{88}$  is thought to be the lethal threshold for irrecoverable embolism (Brodribb and Cochard, 2009; Meinzer *et al.*, 2009; Urli *et al.*, 2013; Li *et al.*, 2015; Dayer *et al.*, 2020). However, the  $P_{88}$  mortality thresholds may not be precise enough, as recent studies indicate that trees were able to recover from water stress beyond  $P_{80}$  in conifers or even higher levels of embolism in angiosperms (Hammond *et al.*, 2019; Johnson *et al.*, 2021; Mantova *et al.*, 2021, 2022b). Another cavitation index is sensitivity ( $S$ ), which is represented by the slope of VC. Species with shallow slopes gradually lose hydraulic conductivity over a wide range of xylem pressure. In contrast, the ones with steep slopes experience more rapid cavitation during a small range of  $P$  values (Sperry, 1995).

Several mathematical models, such as the Weibull, Gompertz, polynomial functions, and the exponential-sigmoid function, have been used to fit vulnerability curves. Among these, the exponential-sigmoid function is the most widely used model since its parameters represent both susceptibility ( $P_{50}$ ) and sensitivity ( $S$ ) (Rawlings and Cure, 1985; Neufeld *et al.*, 1992; Pammenter and Van der Willigen, 1998; Pockman and Sperry,

2000; Jacobsen *et al.*, 2007c). The vulnerability curves can be described as having two general shapes: (1) a sigmoid (s-shaped) curve, and (2) an exponential (r-shaped) curve (Figure 4B). There is increasing evidence that r-shaped curves are due to artefacts (Cochard *et al.*, 2010; Delzon and Cochard, 2014; Martin-StPaul *et al.*, 2014; Torres-Ruiz *et al.*, 2014). The so-called 'open vessel' artefact is the most important one and occurs when vessels are longer than the sample segments, causing multiple vessels to be cut at both ends. This leads to overestimating the vulnerability curve due to the air being sucked into these open vessels during the measurements, resulting in a rapid drop in the percentage loss of conductivity (PLC) at moderate xylem tension (Choat *et al.*, 2010; Cochard *et al.*, 2010; Wang *et al.*, 2014). However, some authors believe that exponential curves are legitimate and do not result from measurement artefacts (Jacobsen and Pratt, 2012; Sperry *et al.*, 2012; Tobin *et al.*, 2012; Hacke *et al.*, 2014).

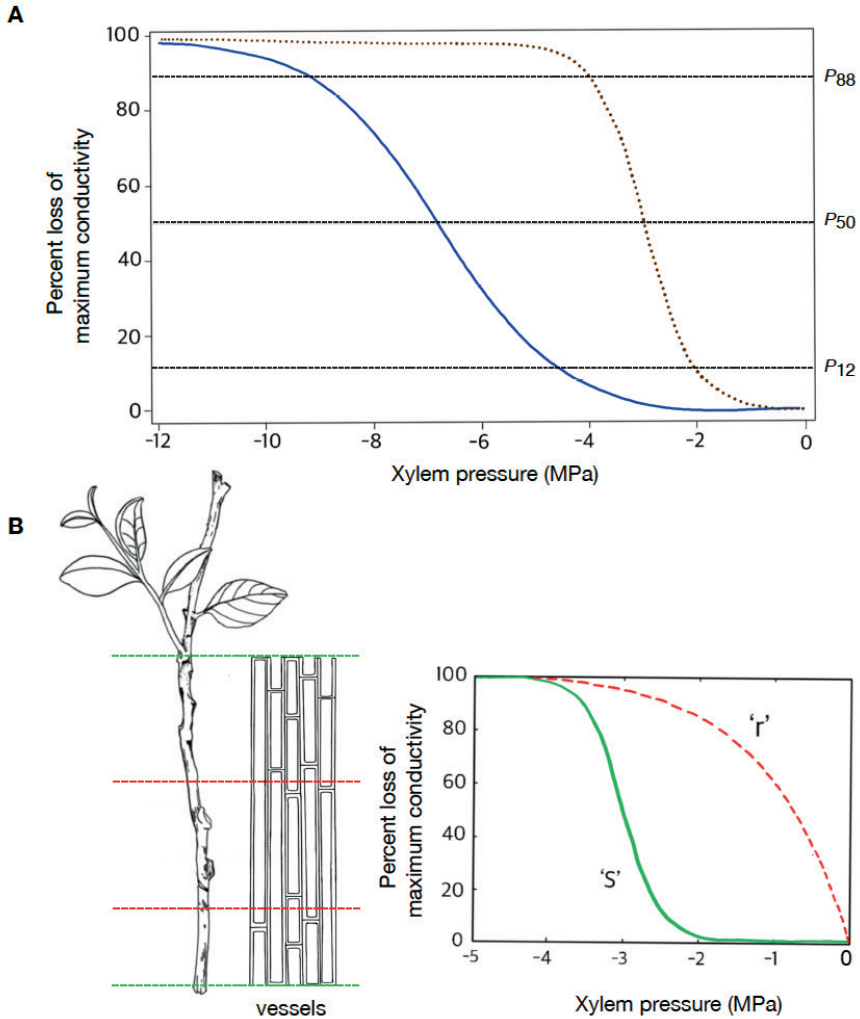


**Figure 4** The xylem vulnerability curve (VC) represents the relationship between the loss of maximum conductivity and xylem pressure. A) The VCs of drought-resistant (blue line) and sensitive species (brown-dotted line) show that a more tolerant plant has more negative  $P_{50}$  than a sensitive one, meaning it can withstand better drought-induced embolism inside the xylem. B) The VC is shown as a sigmoidal (green line) and exponential (red-dotted line) curve, demonstrating two different conductivity decline patterns. The r-shaped curve is often attributed to the 'open vessel artefact', which occurs when the stem segment is shorter than the maximum vessel length. These cut-open vessels can be embolized quickly, resulting in a rapid decrease in hydraulic conductivity.

## ***Various techniques to build vulnerability curves***

Various experimental methods have been developed to measure the hydraulic conductivity in different organs, ranging from basic approaches to more complex techniques that require special equipment. These techniques vary in the way embolism is induced and quantified (Cochard, 2006; Cochard *et al.*, 2013; Venturas *et al.*, 2017). The four invasive (i.e., requirement of cutting) approaches used to construct vulnerability curves are (1) bench dehydration, (2) air injection, (3) the centrifuge-based method, and (4) the pneumatic method, which are described below.

- (1) *Bench dehydration* is a basic procedure that best resembles actual drought-stress dehydration in plants (Figure 5A). With this technique, embolism is evaluated after whole intact plants (in situ or potted) or large excised segments (e.g., branches > 1 m long) are dehydrated freely in the air, expressing a range of different xylem pressures. During the drying process, leaf water potential is measured from a drying plant, and a stem segment close to the measured leaf is taken and plugged into water-filled tubes allowing to measure the amount of water flow through the stem segment at a given leaf water potential value. Bench dehydration is a time-consuming process, as dehydration of the samples might take days to weeks. In addition, several plant segments are required to construct one VC (Sperry and Tyree, 1988; Tyree *et al.*, 1992; Bréda *et al.*, 1993; Cochard *et al.*, 2013). This technique is preferred for long-vessel species (e.g., ring-porous trees and lianas) and was long considered as the golden standard to make VCs (Choat *et al.*, 2010).
- (2) The *air injection* method uses positive gas pressure to induce embolism in shorter sample segments (stems or roots) (Sperry and Tyree, 1988). Cavitation is induced by increasing the air pressure inside the chamber that holds the stem or root segment. The air can be injected into the segments when only one side is cut (single-end air injection) or through the segment surface in a double-ended pressure chamber with the two cut ends of the sample protruding out of the chamber (Cochard *et al.*, 1992; Salleo *et al.*, 1992; Sperry and Saliendra, 1994; Ennajeh *et al.*, 2011). Embolism is subsequently measured by measuring the water flow through the stems-roots at

different levels of positive pressure until the water flow drops to nearly zero (Figure 5B). The main advantage of this technique is that water flow can be controlled with great accuracy and applied to the sample within minutes (Ennajeh *et al.*, 2011; Cochard *et al.*, 2013), but is also prone to open vessel artefact (Cochard *et al.*, 2013).

- (3) The *centrifuge-based method* uses centrifugal force to generate a specific negative pressure in the middle part of the stem or root segment, after which the water flow in the segments is repeatedly measured at each centrifugation-induced pressure step (Pockman *et al.*, 1995; Alder *et al.*, 1997; Cochard, 2002; Cochard *et al.*, 2005, 2010) (Figure 5C). The centrifugation technique, as well as air injection, enables the construction of a whole VC on one sample, thus reducing sample variability (Cochard *et al.*, 2013; Martin-StPaul *et al.*, 2014; Venturas *et al.*, 2017). An additional advantage of the centrifugation technique is that it can also be applied to stems of small herbaceous species, such as *Arabidopsis*, which cannot be done with an air injection method (Tixier *et al.*, 2013).
- (4) The *pneumatic method* estimates xylem vulnerability for a single branch by extracting gas from xylem tissues through a partial vacuum applied to a cut segment (stem, petiole, or root) under various water potentials (Figure 5D). The advantage of this approach is that the pneumatic device is an easy, low-cost, and powerful tool for field measurements (Pereira *et al.*, 2016, 2020).

Despite numerous consistent results produced using these invasive methods, methodological debates have been raised over the years due to various potential artefacts that appear when investigating a system that is under negative pressure. Indeed, techniques that rely on cutting samples potentially allow air and other impurities to enter the segment, resulting in biased results (Wheeler *et al.*, 2013; Cochard *et al.*, 2013; Rockwell *et al.*, 2014; Martin-StPaul *et al.*, 2014; Wang *et al.*, 2014; Venturas *et al.*, 2017). One of the most influential artefacts is the open vessel artefact that regularly occurs when measuring angiosperm species with the popular centrifugation or air injection technique (Choat *et al.*, 2010; Cochard *et al.*, 2010; Martin-StPaul *et al.*, 2014; Torres-Ruiz *et al.*, 2014; Torres-Ruiz *et al.*, 2017). Therefore, in order to detect embolisms in a non-destructive manner,

non-invasive imaging approaches have been developed. High-resolution X-ray computed tomography (HRCT) is an imaging method that uses a high-intensity X-ray source with a micrometer-range resolution to detect whether a conduit is water-filled or air-filled (light grey or dark as viewed in virtual microCT images, respectively). The development of HRCT has made it possible to visualize the three-dimensional structure of the vessel network and simulate how embolisms propagate through the xylem network when the plant is subjected to drought (Brodersen *et al.*, 2010, 2011) (Figure 5E). Another non-invasive technique that visualizes the spatial, temporal spread of embolisms in the leaf venation network during water stress is the optical vulnerability (OV) approach (Figure 5F). By recording and comparing changes in the transmission of light through the veins of leaf samples, the OV method detects and follows the spread of embolisms as drought progresses (Brodrigg *et al.*, 2016b). Moreover, this method also allows for measuring embolism resistance in stems, roots as well as flowers (and leaves) of the same individual (Zhang and Brodrigg, 2017; Rodriguez-Dominguez *et al.*, 2018; Bourbia *et al.*, 2020; Song *et al.*, 2022), enabling to compare embolism resistance of different organs within the same individual. In addition to HRCT and OV, the acoustic emission method (AE) can be used as a non-invasive, real-time monitoring tool for assessing drought-induced embolism in plants. AE indirectly measures the loss of hydraulic conductivity by placing sensitive acoustic sensors, such as piezoelectric transducers, onto plant stems (with or without bark) or leaves (Figure 5G). These sensors can capture ultrasonic frequency ranges, including those emitted during cavitation events (100-200 kHz). Despite the practical advantages of this method, being automatic and less labour intensive compared to other techniques, AE requires precise setup and calibration of the sensors, which demands special expertise. Another challenge lies in effectively distinguishing the embolism-related AE signals from the signals caused by other processes, which is necessary to conduct precise data analyses and accurate interpretation (Vergeynst *et al.*, 2015a,b, 2016; De Roo *et al.*, 2016; Oletić *et al.*, 2023).

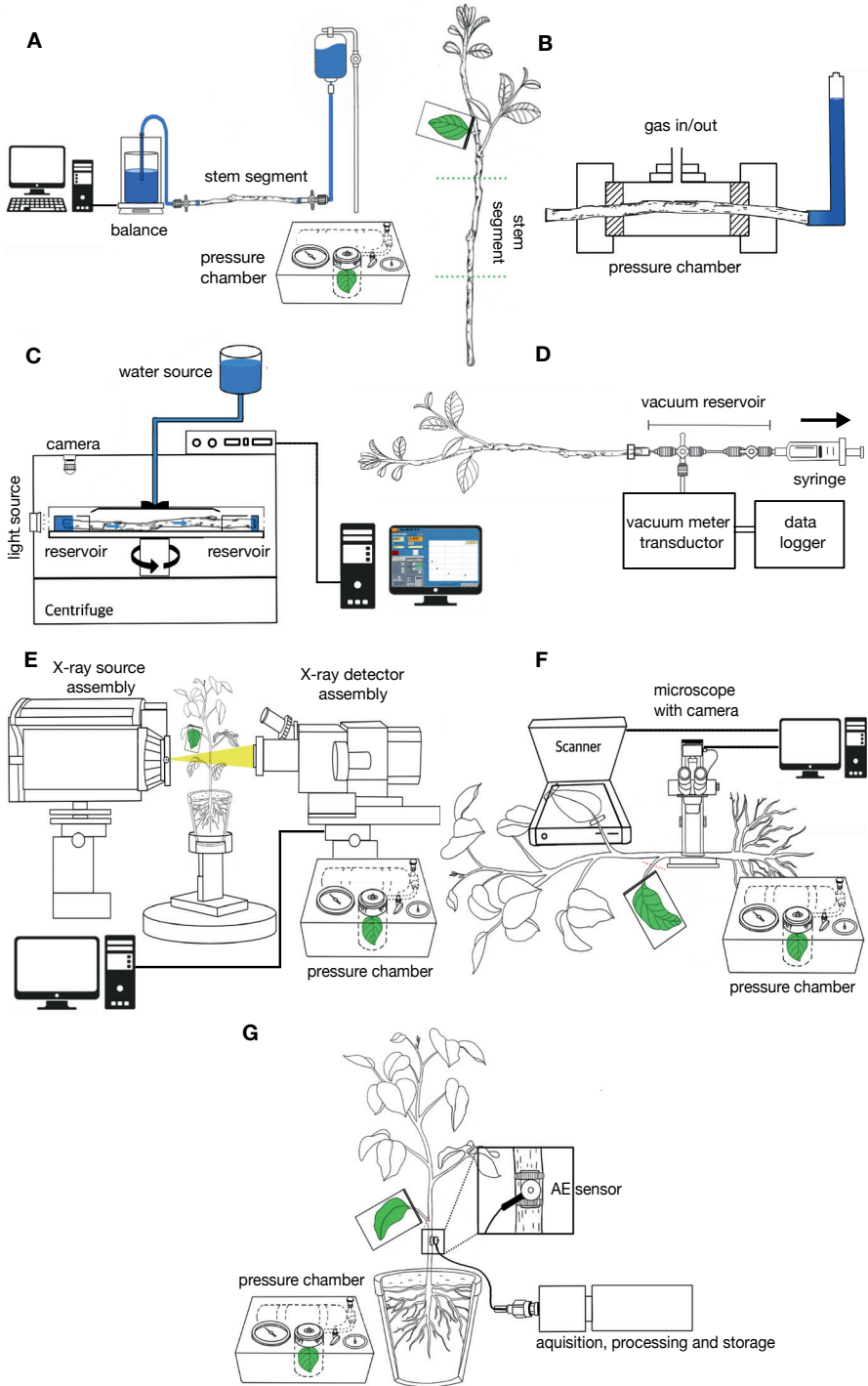


**Figure 5** The diagram illustrating different techniques used for measuring vulnerability curves (VCs). A) Bench dehydration technique measuring water transport in a freshly excised stem from a larger branch that is drying out in the lab; for each excised stem, the leaf water potential is measured until the water flow reduces to nearly zero in the last stem segment from the branch; *based on Sperry and Tyree (1988)*. B) Air injection method in double-end pressure chamber used for measuring the water flow through the stems-roots at different levels of positive pressure until the water flow drops to nearly zero; *adapted from Cochard et al. (1992) and Ennajeh et al. (2011)*. C) Custom-built cavitron centrifugation measuring water flow through the excised stem segment while simultaneously creating more negative xylem pressures by spinning the stems with increasing rotation speed steps; *adapted from Cochard et al. (2002, 2005)*. D) Pneumatic method is shown in the measurement position. The vacuum is created with a syringe directly connected to the tube, and the stopcocks are closed to the vacuum reservoir and open to the branch and vacuum meter. By pulling the syringe, the vacuum is created. Thereby the gas is sucked from the stem. The amount of gas/air discharged (AD) from the sample is measured over time while the plant tissue desiccates until AD reaches a plateau (stops increasing); *adapted from Pereira et al. (2016)*. E) High-resolution X-ray computed tomography (HRCT) makes virtual stem sections of living plants that are put under drought stress. These virtual sections can be used to visualize whether conduits are water-filled or gas-filled, and dynamics of embolism can be followed when plants are drying out more. Based on the proportion of the conduit area of all water-filled vessels compared to the total vessel area, and the leaf water potential at different time points, a VC can be made; *adapted from Brodersen et al. (2010)*. F) Optical vulnerability technique with scanner and microscope measuring intact plants that are put under drought stress. Every 5 minutes, images are taken from a leaf (with a scanner) and the stem (with a stereomicroscope equipped with a digital camera) from the same individual simultaneously. Subsequent images of the leaf and stem are analyzed, looking for differences in pixels that resemble the sudden change from water-filled to embolized conduits until nearly all conduits are embolized; *adapted from Brodribb et al. (2016)*. G) The acoustic emission (AE) method employs a transducer attached to the plant stem, which consistently captures AE signals emitted by the plant under drought stress conditions. The integrated AE sensor system runs signal acquisition, signal feature extraction, and results are logged onto a SD card; *adapted from Oletić et al. (2023)*.



## ***Surviving and thriving: how plants respond to drought***

Plant mortality is intimately linked to the balance between water supply and demand. However, carbohydrate availability also plays a role in the hydraulic function and associated failure, making both water and carbon supply crucial for plant survival (Allen *et al.*, 2015; Martinez-Vilalta *et al.*, 2019; Kannenberg *et al.*, 2021). To cope with water-deficit conditions, plants have evolved a range of strategies, including several functional traits in different organs that minimize the effects of drought stress and maximize their performance and fitness (Violle *et al.*, 2007). Resistance to drought-induced embolism can vary within and across species in response to various environmental factors such as water availability and shade (Stiller, 2009; Plavcová *et al.*, 2011). This resistance can be achieved by, among others, building the xylem resistance (Larter *et al.*, 2017), preventing sap pressure from reaching critical thresholds through early closure of the stomata (Martin-StPaul *et al.*, 2017), or contributing to hydraulic recovery by developing new wood tissue (Gauthey *et al.*, 2022). The coordination of drought-related features within and among organs is crucial in determining how long plants can maintain metabolic activities without risking hydraulic failure. For example, some plants may develop deep roots or other root-related traits that improve water uptake, while others may have leaf characteristics that limit water loss through transpiration (Allen *et al.*, 2009; Choat *et al.*, 2012; Mitchell *et al.*, 2013; Martínez-Vilalta and Garcia-Forner, 2017; Buckley, 2019; Creek *et al.*, 2020; Limousin *et al.*, 2022). By combining these traits, plants can optimize their water use efficiency and improve their chances of surviving periods of water shortage. Ultimately, understanding the mechanisms underlying plant responses to drought stress by investigating the diversity of drought-associated plant traits is essential for developing strategies to improve plant resilience and productivity in water-limited environments (Choat *et al.*, 2012, 2018; Blackman *et al.*, 2019; Rosas *et al.*, 2019; Venturas *et al.*, 2021; Lens *et al.*, 2022).

### ***Stomatal regulation***

Stomata are microscopic structures found on the surface of leaves. They regulate the exchange of gases, mainly carbon dioxide (CO<sub>2</sub>) and oxygen (O<sub>2</sub>), between plants and the atmosphere and the loss of water vapour by transpiration (Lawson and Vialet-Chabrand, 2019). Stomata are

pores surrounded by a pair of guard cells whose size can be altered in response to environmental signals, thereby regulating the rate of gas and water exchange (Wall *et al.*, 2022). This ability to adjust stomatal conductance ( $g_s$ ) is an essential adaptive feature that enables plants to maintain a balance of water use efficiency (WUE, defined as the ratio of photosynthesis and transpiration), especially under changing environmental conditions such as vapour pressure deficit (VPD), temperature, light levels, atmospheric CO<sub>2</sub>, and soil water availability (Assmann and Wang, 2001; Buckley, 2005; Messinger *et al.*, 2006; Ainsworth and Rogers, 2007). The regulation of stomatal opening and closure in response to drought is a complex process involving physical and biochemical changes. When the soil water becomes scarce, the plant senses the change and triggers a series of responses to reduce water loss through transpiration and delay xylem sap pressures from reaching critical thresholds (Brodribb and Holbrook, 2003; Pittermann, 2010; Buckley, 2019). One of the primary responses to drought is the closure of stomata, which considerably reduces the transpiration rate (although there will always be a residual stomatal conductance when the stomata are closed; see Billon *et al.*, 2020). Therefore, water is conserved for important processes, such as maintaining cellular turgor pressure. However, stomatal closure also results in a decline in carbon uptake as photosynthetic rates drop in response to decreased gas exchange (McDowell *et al.*, 2008; Brodribb *et al.*, 2017b; Martínez-Vilalta and Garcia-Forner, 2017; Martin-StPaul *et al.*, 2017; Knipfer *et al.*, 2020). As drought progresses, xylem water potential starts to become slightly more negative, leading to a decline in stomatal conductance to near zero. This closure is usually performed before the onset of substantial embolism formation to avoid the possibility of hydraulic failure (Brodribb *et al.*, 2003; Martin-StPaul *et al.*, 2017; Scoffoni *et al.*, 2017; Choat *et al.*, 2018). However, some plants try to keep their stomata open during drought as long as possible to maximize carbon assimilation, especially in species that are extremely resistant to embolism formation (see next paragraph). In other words, plants have evolved a range of stomatal conductance regulation mechanisms to achieve optimal water use efficiency in response to drought. These responses can vary across plant species, depending on their control strategies and physiological traits (Klein, 2014; Buckley, 2019; Papastefanou *et al.*, 2020; Joshi *et al.*, 2022).

Two stomatal regulation behaviors in response to drought stress have been described: isohydric and anisohydric (Bonal and Guehl, 2001;

West *et al.*, 2007; McDowell *et al.*, 2008). Isohydic species or drought avoiders ( $P_{50}$  value close to zero) tend to maintain a constant level of leaf water potential, even under severe drought stress, by tightly regulating the stomatal openings. In reaction to periods of water shortage, these plants close their stomata very early, regardless of the potential carbon loss. This strategy permits greater control over the plant's water balance but can come at the cost of diminished photosynthetic rates and growth due to limited gas exchange. Anisohydric plants or drought-tolerant species (much more negative  $P_{50}$  value), however, exhibit a more relaxed control over the stomatal aperture. These plants tend to keep their stomata open longer for greater photosynthesis and growth rates under mild drought stress. However, as drought stress intensifies, anisohydric species also ultimately close their stomata to conserve water and to avoid hydraulic failure (McDowell *et al.*, 2008; Klein, 2014; Joshi *et al.*, 2022). Importantly, recent research has demonstrated that isohydric, and anisohydric strategies are not fixed to one extreme side but rather exhibit dynamic responses to changes in water availability (Papastefanou *et al.*, 2020).

### ***Stomatal safety margin***

As mentioned above, stomatal regulation is crucial for plants to maintain the water balance and prevent hydraulic failure during drought stress (McDowell *et al.*, 2008; Brodribb *et al.*, 2017b; Martínez-Vilalta and Garcia-Forner, 2017; Martin-StPaul *et al.*, 2017; Knipfer *et al.*, 2020). Therefore, measuring  $P_{50}$  alone may not accurately reflect plant embolism resistance, as it does not account for the role of stomatal regulation. In addition,  $P_{50}$  values are typically considered constant over time by taking only a single point during the season (Lobo *et al.*, 2018; Mauri *et al.*, 2020; Martínez-Vilalta *et al.*, 2021). However, this is not entirely accurate, as research has shown that  $P_{50}$  can vary across seasons. For instance,  $P_{50}$  values may become more negative at the end of the growing season when conditions are becoming drier and warmer (Kolb and Sperry, 1999; Jacobsen *et al.*, 2007b; Charrier *et al.*, 2018; Sorek *et al.*, 2022). Consequently, combining stomatal closure with  $P_{50}$  results is a more physiologically relevant approach to estimating the ability of a plant species to withstand drought-induced embolism (Meinzer *et al.*, 2009; Anderegg *et al.*, 2016; Martin-StPaul *et al.*, 2017; Creek *et al.*, 2020; Dayer *et al.*, 2020; Skelton *et al.*, 2021). This is captured in the so-called stomatal safety margin (SSM),

defined as the difference between the water potential at stomatal closure ( $\Psi_{gs90}$ ) and the pressure inducing 50% loss of hydraulic conductivity ( $P_{50}$ ) (Figure 6). By measuring SSM, it is possible to evaluate the level of native embolism resistance in plants at a given drought period, which will be negligible in species with a wide SSM showing a large buffer between the point of stomatal closure and the point of hydraulic failure (often around or beyond  $P_{88}$ ). In contrast, plants with narrower (or even negative) safety margins operate closer to their hydraulic limit and will therefore develop high levels of native embolism - i.e. will more likely face hydraulic failure - even at relatively mild drought periods (Choat *et al.*, 2012; Anderegg *et al.*, 2016; Martin-StPaul *et al.*, 2017; Eller *et al.*, 2018; Creek *et al.*, 2020; Skelton *et al.*, 2021; Oliveira *et al.*, 2021).

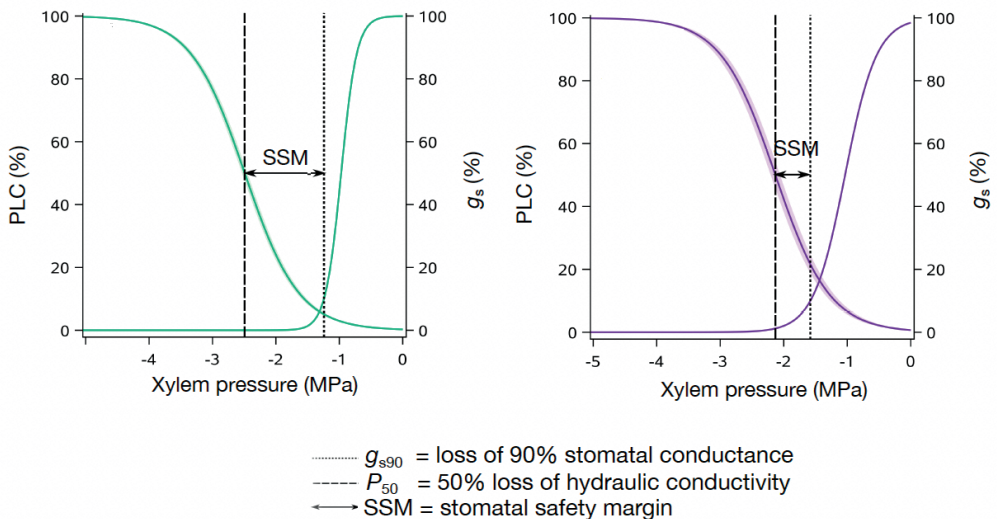


**Figure 6** The graph displaying the stomatal safety margin (SSM), which is the difference between the water potential at near stomatal closure ( $\Psi_{gs90}$ ) and the xylem pressure inducing 50% loss of hydraulic conductivity ( $P_{50}$ ). Species with a higher SSM (left) operate further from their hydraulic threshold, either by being more resistant to embolism formation and/or by rapidly closing their stomata during the onset of drought, while species with a low or even negative SSM (right) develop relatively high levels of native embolism even under mild drought stress and will soon reach the critical point of hydraulic failure as the drought intensifies.

## ***Ecological trends and trade-offs in xylem anatomy***

In addition to their rapid physiological responses to changes in water availability, plants also have the ability to modify their hydraulic architecture over longer-term responses (Tng *et al.*, 2018). Modifications to the anatomy of xylem tissue are essential for maintaining water transport efficiency and preventing cavitation or embolism under drought stress. The potential roles of different xylem cell types, sizes, and arrangements, as well as their environmental factors, were first explored in studies that compared the wood anatomy of different species growing in contrasting environments, a subdiscipline known as ecological wood anatomy (Carlquist, 1975, 1980; Baas, 1976; Baas *et al.*, 1983; Alves and Angyalossy-Alfonso, 2000; Segala Alves and Angyalossy-Alfonso, 2002; Lens *et al.*, 2004). As a result, numerous ecological trends associated with wood anatomical variation from diverse habitats, varying in water availability, temperature, and elevation, have been suggested. For instance, in drier environments, woody species tend to have narrower vessels with higher density, and thicker fiber walls compared to closely related species thriving in wetter conditions (Carlquist, 1966, 1977; Baas *et al.*, 1983; Carlquist and Hoekman, 1985; Bosio *et al.*, 2010).

Xylem tissue of plants provides two fundamental functions, water transport and mechanical support, which create competing demands. These conflicts can lead to a trade-off between efficiency and safety, meaning that when plants prioritize one function, such as water transport efficiency, they may compromise their ability to provide mechanical support (Tyree and Sperry, 1989; Baas *et al.*, 2004; Hacke *et al.*, 2006; Sperry *et al.*, 2006, 2008; Venturas *et al.*, 2017) (Figure 7). A pervasive hypothesis concerning the trade-off between hydraulic safety and efficiency has been proposed for a very long time (Zimmerman and Brown, 1971). Larger and longer vessels are linked to more efficiency in water conduction than narrower and shorter vessels, allowing plants to photosynthesize more and grow faster under favorable conditions (Poorter *et al.*, 2010; Gleason *et al.*, 2012, 2016a; Bouda *et al.*, 2019). However, enhancing embolism resistance, which requires investing more in increasing conduit wall and fiber wall thickness, might impair hydraulic efficiency (Tyree *et al.*, 1994; Hacke *et al.*, 2001, 2006; Jacobsen *et al.*, 2007b; Sperry *et al.*, 2008; Meinzer *et al.*, 2010). To achieve a balance between safety and efficiency, plants have developed different strategies depending on their ecological and environmental

conditions. Some species value safety over efficiency, while others value efficiency more than safety (Tyree *et al.*, 1994; Hacke *et al.*, 2006; Sperry *et al.*, 2008; Meinzer *et al.*, 2010). Interestingly, there is a substantial number of species that exhibit no trade-off because they have poor performance in both efficiency and safety (Choat *et al.*, 2005; Gleason *et al.*, 2016b).

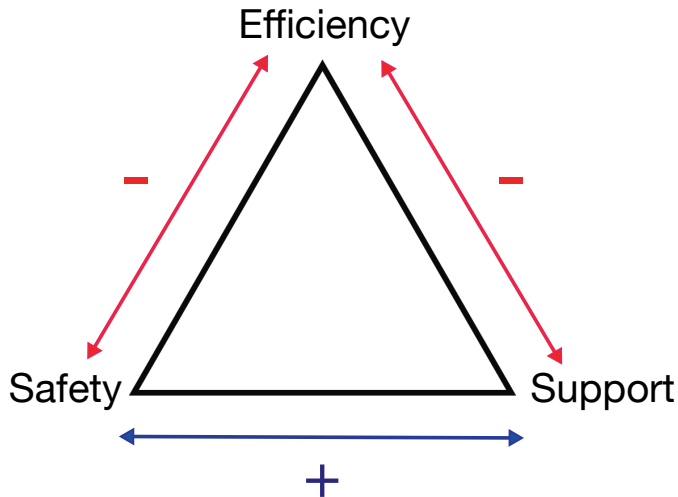


**Figure 7** “Trade-off” triangle showing the relationships amongst xylem functions. Efficiency refers to conductivity efficiency ( $K_s$  in  $\text{m}^2\text{MPa}^{-1}\text{s}^{-1}$ ); safety refers to resistance to embolism (MPa), and support refers to mechanical strength (vessel and fiber wall thickness). The conductive efficiency is inversely proportional to both mechanical strength and resistance to embolism. Adapted from Baas *et al.*, 2004.

### ***Structure-function relationships in the xylem***

A range of wood traits has been found to be associated with resistance to embolism. One such trait is wood density (WD), which is believed to impact water transport because of its correlation with the total area of the conduit area (Pratt *et al.*, 2007b; Chave *et al.*, 2009). Increased wood density tends to decrease hydraulic capacity, low water storage capacity and high construction costs (Pratt *et al.*, 2007a; Meinzer *et al.*, 2008a,b; Scholz *et al.*, 2011). Species with high wood density typically resist drought-induced embolism (Hacke *et al.*, 2001; Jacobsen *et al.*, 2007a; Willson *et al.*, 2008; Hoffmann *et al.*, 2011), mechanical breakage (Niklas, 1997; Poorter, 2008), and attack by pathogens and fungi (Augspurger and Kelly, 1984). In addition, recent studies have shown convincing physiological evidence that species with dense wood are better able to survive at low

water potentials due to their lower leaf/xylem turgor loss point (Fu and Meinzer, 2019; De Guzman *et al.*, 2021). Consequently, tree species with greater wood density tend to have lower mortality rates but are known to grow more slowly (Chao *et al.*, 2008; Nardini *et al.*, 2013; Greenwood *et al.*, 2017). WD is associated with the investment in various anatomical features, including vessel wall thickness and the surrounding fiber matrix that is hypothesized to protect vessels from collapsing during progressive xylem tension (although conduit collapse has only been sporadically observed in leaves) (Hacke *et al.*, 2001; Jacobsen *et al.*, 2005, 2007; Pratt *et al.*, 2007; Russo *et al.*, 2010; Zheng and Martínez-Cabrera, 2013; Fortunel *et al.*, 2014; Dória *et al.*, 2018; Zhang *et al.*, 2023). Plants with a greater degree of embolism resistance are also thought to develop thicker vessel walls relative to their lumen diameter (higher thickness-to-span ratio expressed by  $(t/b)$ ) (Hacke *et al.*, 2001; Sperry and Hacke, 2004; Jacobsen *et al.*, 2005, 2007a; Pittermann *et al.*, 2006). Likewise, the surrounding fiber cells might also contribute to embolism resistance by reinforcing the vessel wall, regardless of changes in vessel wall thickness or lumen diameter (Jacobsen *et al.*, 2005). Thus, greater investment in the vessel and fiber walls results in higher wood density, which reflects the ability of a plant to resist embolism. In herbaceous species, which lack a woody structure, higher stem density results from increased lignification in the stem. In addition, the amount of lignin accumulated in the cell wall could influence the speed of embolism by affecting gas diffusion kinetics across vessel walls, suggesting that stems with higher lignification levels may have a slower rate of embolism propagation (Lens *et al.*, 2016; Pereira *et al.*, 2018; Dória *et al.*, 2018; Lens *et al.*, 2022). Lastly, modifications of lignin concentration and composition in different cell types, such as vessels or fibers, can influence the mechanical and hydraulic properties of the stem. These alterations can boost cell stiffness, flexibility, and hydrophobicity of the cell wall, which can impact the plant's ability to withstand and recover from drought stress (Pereira *et al.*, 2018; Ménard *et al.*, 2022).

Vessel connectivity is another trait that has been linked to drought-induced embolism (Levionnois *et al.*, 2021; Mrad *et al.*, 2021; Ewers *et al.*, 2023). The average vessel connectivity (C) represents the number of neighboring vessels averaged over all vessels in the xylem segment (Loepfe *et al.*, 2007; Martinez-Vilalta *et al.*, 2012). Unfortunately, due to methodological constraints, vessel connectivity has rarely been

investigated. Instead, the vessel grouping index ( $V_G$ ) has been widely quantified and used as a 2D proxy of  $C$  (Mrad *et al.*, 2021). Some studies have found that high vessel grouping is associated with increased embolism resistance (Lens *et al.*, 2011; Levionnois *et al.*, 2021; Lemaire *et al.*, 2021b). This is because it provides a hydraulic redundancy pathway, which reduces the potential loss of water transport capacity associated with the embolism (Carlquist, 1984; Tyree *et al.*, 1994). In other words, connections with adjacent vessels offer alternative routes for water transport when some vessels are embolized (Carlquist, 1984; Tyree *et al.*, 1994; Levionnois *et al.*, 2021). However, some studies suggested that high  $V_G$  increases the likelihood of embolism spreading, resulting in a lower hydraulic safety (Loepfe *et al.*, 2007; Martinez-Vilalta *et al.*, 2012; Scholz *et al.*, 2013b). Therefore, there is controversy about the impact of the degree of vessel grouping on embolism resistance. Interestingly, Mrad *et al.* (2021), based on wood anatomy in *Acer*, simulated xylem segments and linked vessel connectivity to VC and hydraulic conductivity, suggesting that increasing vessel connectivity and grouping improves the resistance to embolism without compromising hydraulic efficiency. Additionally, the simulation showed that vessel connectivity significantly affects the slope of the VC. Thus, vessel grouping is necessary for the resistance to embolism spread, yet it also needs to be accompanied by variations in pits and other vessel traits (Lemaire *et al.*, 2021b; Mrad *et al.*, 2021).

One of the most frequently measured and debated anatomical traits associated with resistance to drought-induced embolism is vessel diameter ( $D$ ). Comparative and ecological wood anatomy studies have suggested a positive correlation between conduit diameter and embolism resistance. Several arguments have been raised (see Olson *et al.*, 2023 for an overview). Experimental research on xylem vulnerability to drought-induced embolism, however, shows no solid evidence for a direct link between vessel diameter and embolism resistance. For instance, several studies have found that narrow vessels in leaves are more vulnerable to embolism than wider vessels in shoots (Pivovarovoff *et al.*, 2014; Charrier *et al.*, 2016; Johnson *et al.*, 2016; Creek *et al.*, 2018; Skelton *et al.*, 2019), which may also suggest a vulnerability segmentation hypothesis (Tyree and Ewers, 1991). This hypothesis assumes that xylem in different plant organs has varying levels of embolism resistance, with more distal tissues, such as leaves and twigs, being more vulnerable than more proximal tissues (Tyree and Ewers, 1991).



However, recent studies have found that the xylem tissue in leaves, stems, and roots has (more or less) the same embolism resistance although the vessel diameter considerable changes among organs (Skelton *et al.*, 2017; Creek *et al.*, 2018; Wason *et al.*, 2018; Losso *et al.*, 2019; Levionnois *et al.*, 2020; Smith-Martin *et al.*, 2020; Lübbe *et al.*, 2022). Other traits that might involve in the mechanisms underlying drought-induced embolism, such as intervessel pit traits, may be better predictors of embolism vulnerability than vessel diameter (Lens *et al.*, 2022).

During the last two decades, it has become increasingly clear that intervessel pit membranes are key structures in the root-to-shoot water transport, which considerably impact the resistance to flow, and function as a safety valve by minimizing the spread of embolism from non-functional vessels to neighbouring functional conduits (Sperry and Tyree, 1988; Tyree and Zimmermann, 2002; Meyra *et al.*, 2007; Choat *et al.*, 2008). This protective function in intervessel pit membranes is enabled by the pit membrane's tiny pore constrictions and high permeability, which enable the flow of gas between adjacent vessels (Wheeler *et al.*, 2005; Jansen *et al.*, 2009). The thickness of the intervessel pit membrane ( $T_{PM}$ ) is strongly associated with the plant's ability to resist the spread of embolism, making it one of the main determinants of embolism resistance in angiosperms (Li *et al.*, 2016). Species with thicker pit membranes are more resistant to drought-induced embolism than those with thinner membranes (Jansen *et al.*, 2009; Lens *et al.*, 2011, 2013; Scholz *et al.*, 2013*b*; Schuldt *et al.*, 2016; Li *et al.*, 2016; Bai *et al.*, 2020; Kaack *et al.*, 2021; Isasa *et al.*, 2023) (Figure 8). The relationship between  $T_{PM}$  and  $P_{50}$  can be functionally explained by the effect that membrane thickness has on the number, size, and distribution of pore constrictions located in these membranes that are considered as nonwoven porous media (Bai *et al.*, 2020). According to the 3D-nanoscale pit membrane structure, the pores between the microfibril layers of pit membranes are extensively interconnected and contain multiple tiny pore constrictions that operate as the bottlenecks for the fluid transport across the pit membrane pathway (Kaack *et al.*, 2019, 2021; Yang *et al.*, 2020; Zhang *et al.*, 2020). Since the thickness of the pit membranes increases with the length of the multiconstriction path, it may be expected that thicker membranes will have a narrower maximum pore constriction size than thinner membranes. In addition, gas bubble snap-offs, which are assumed to occur spontaneously at the air-water interface in pore constrictions,

thereby possibly creating surfactant-coated nanobubbles, tend to increase with an increasing number of pore constrictions (Berg *et al.*, 2013; Schenk *et al.*, 2015; Park *et al.*, 2019; Lens *et al.*, 2022)

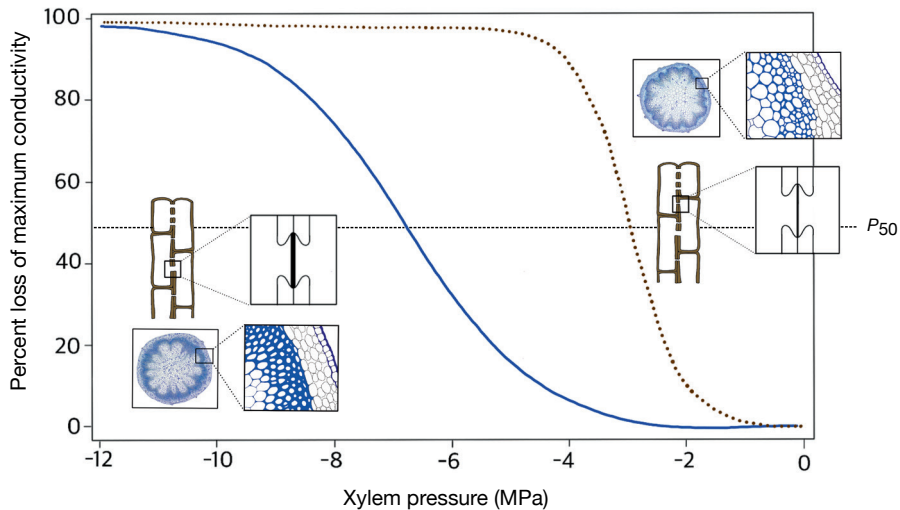


**Figure 8** The xylem vulnerability curve (VC) represents the relationship between the loss of maximum conductivity and xylem pressure. The VCs show that drought-resistant species (more negative  $P_{50}$ : blue curve) have a woodier or more lignified stem with thicker intervessel pit membranes than the sensitive species (less negative  $P_{50}$ : brown-dotted curve).

### ***Gene networks underlying plant responses to drought stress***

In addition to a multitude of physiological and anatomical traits, plants also respond and adapt to water shortage through molecular mechanisms, which include modifications to the activity of phytohormones, metabolites and signalling pathways, as well as transcriptional regulation cascades (Singh *et al.*, 2022). One of the phytohormones that is well-known for its role in plant acclimatization under stress conditions is abscisic acid (ABA). Under water deficit, ABA is produced, controlling root development, stomata closure, and activating stress-related genes (Nakashima *et al.*, 2014; Förster *et al.*, 2019). After ABA has been accumulated (mainly in leaves), it regulates the expression of downstream drought-inducible genes via *cis*-elements called ABRE (ABA-responsive element) and uses AREB (ABRE binding) genes as major transcriptional activators during ABA-

mediated signaling (Choi *et al.*, 2000; Uno *et al.*, 2000; Bauerle *et al.*, 2004; Cutler *et al.*, 2010; Maruyama *et al.*, 2012; Mehrotra *et al.*, 2014; Yoshida *et al.*, 2015; Chen *et al.*, 2020) (Figure 9). For instance, in many plant species, *AREB1* overexpression is associated with the improvement of drought resilience (Barbosa *et al.*, 2013; Yoshida *et al.*, 2015; Wang *et al.*, 2016a), whereas the triple knockout mutants of *AREB1*, *AREB2* and *ABF3* showed drought stress-sensitive phenotypes and had lower expression of drought-responsive genes (Yoshida *et al.*, 2010). Arabidopsis *AREB2* and *ABF3* also play a significant role in flowering time regulation by transcriptionally controlling the floral integrator *SUPPRESSOR OF OVEREXPRESSION OF CONSTANS1 (SOC1)* (Hwang *et al.*, 2019). Under drought stress, elevated ABA levels enhance the activity of *SOC1* through *AREB2* and *ABF3*, thereby accelerating the floral transition and enhancing reproductive success. This adaptive response enables plants to complete their life cycle before the onset of severe drought conditions, thereby mitigating the detrimental effects of water scarcity (Hwang *et al.*, 2019). *SOC1* also emerges as a crucial regulator of various developmental and stress responses (Kimura *et al.*, 2015; Aoki *et al.*, 2019). Moreover, *SOC1*, in conjunction with *FUL (FRUITFULL)* and *AHL15 (AT-HOOK MOTIF CONTAINING NUCLEAR LOCALIZED 15)* (Melzer *et al.*, 2008; Karami *et al.*, 2020; Rahimi *et al.*, 2022) plays a significant role in controlling meristem determinacy and cambial activity. A double loss-of-function mutant of *SOC1* and *FUL* has been shown to suppress axillary meristem maturation, resulting in later-flowering, polycarpic-like woody growth that is characterized by a much longer life span (Melzer *et al.*, 2008). *AHL15* has been found to act downstream of *SOC1* and *FUL*, and enhances vascular cambium activity and hence secondary xylem formation in Arabidopsis inflorescence stems (Rahimi *et al.*, 2022). These woody Arabidopsis genotypes allow us to investigate the role of increased woodiness in the inflorescence stem on the plant's drought response.

In addition to the ABA-dependent system, a number of stress-related genes can be regulated by an ABA-independent regulatory pathway, which is an important process in drought stress response during the initial stages before the build-up of endogenous ABA (Soma *et al.*, 2021)(Figure 9). The important TFs in the ABA-independent system include NAC transcription factors and DRE-binding proteins (DREB), particularly *DREB2A* (Sakuma *et al.*, 2006a,b; Lata and Prasad, 2011; Soma *et al.*, 2021). *DREB2A*, expressed

under dehydration and osmotic stress, binds to the Dehydration Responsive Elements (DRE) motif to regulate drought-responsive genes (Maruyama *et al.*, 2012) (Figure 9). Interestingly, the interaction between ABA-dependent and ABA-independent pathways has been observed since several types of TFs control the cellular responses to drought stress. For example, AREB/ABFs can partially regulate the expression of *DREB2A*, showing the interaction between the early processes of drought prior to the accumulation of ABA and the later-occurring ABA-dependent signalling processes (Kim *et al.*, 2011). Furthermore, plant-specific NAC TFs that bind to NAC recognition sites (NACR) mediate environmental stress responses (Tran *et al.*, 2004; Takasaki *et al.*, 2010; Puranik *et al.*, 2012) (Figure 9). For instance, ANAC096 is a positive regulator activated in response to dehydration stress. It increases the expression of drought-responsive genes, specifically *Responsive to Dehydration 29A (RD29A)*, which is one of the important marker genes in ABA dependent drought stress signalling pathway (Xu *et al.*, 2013). In conclusion, both ABA-independent and ABA-dependent gene regulatory networks are essential molecular mechanisms that govern differential gene expression during early and later drought responses (Shinozaki *et al.*, 2003; Yamaguchi-Shinozaki and Shinozaki, 2005; Shinozaki and Yamaguchi-Shinozaki, 2006).

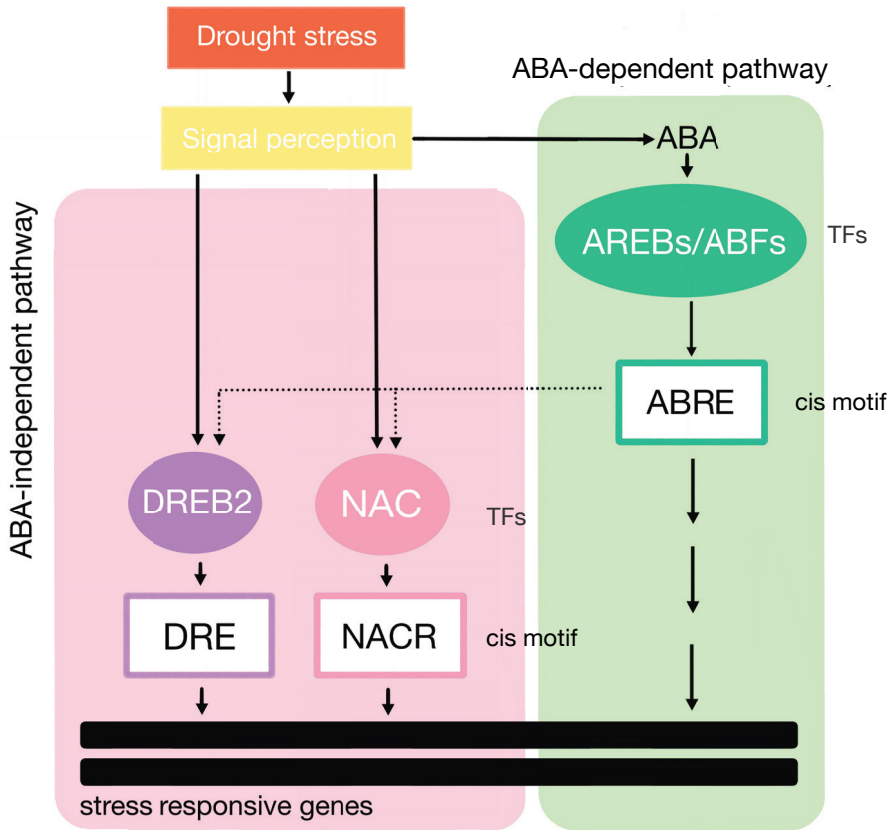


**Figure 9** A schematic model of plant signal perception and regulatory networks under drought stress via ABA-dependent and ABA-independent pathways. ABA signalling, phosphorylate AREB/ABF transcription factors, which in turn induce the expression of stress-responsive genes via an ABA-dependent pathway. DREB2 and NAC transcription factors are activated through an ABA-independent pathway. However, some transcription factors from these two groups, including DREB2A and ANAC096, mediate the crosstalk signal between ABA-dependent and ABA-independent systems. *Adapted from Soma et al. (2021).*

## Thesis outline

The aim of this thesis is to enhance our understanding of the complex mechanisms underlying drought responses in herbaceous species, providing insights into the various strategies that plants use to cope with drought stress. To achieve this, we investigate the relationship and coordination between xylem anatomical and hydraulic traits in stems and leaves and provide a preliminary analysis of the expression of drought-responsive genes. To address these objectives, we study various genotypes that exhibited contrasting levels of embolism resistance and lignification in the stems of *Arabidopsis thaliana*, a model herbaceous plant, and *Solanum lycopersicum* (tomato), an important crop species. This thesis comprises five chapters, with the first chapter serving as a general introduction and overview of the thesis, followed by the research chapters 2-4 that focus on the research specific objectives, and complemented with the last chapter that provides an overall discussion and conclusion of the PhD results.

### Chapter 2

This chapter delves into identifying the key anatomical and ecophysiological traits that best explain the variation in embolism in the inflorescence stems of four *Arabidopsis thaliana* genotypes with contrasting growth forms. Detailed stem anatomical observations serve as the basis for these explorations.

### Chapter 3

Building upon the previous chapter, this one focuses on studying the drought response strategies of the four *Arabidopsis* genotypes examined in chapter 2 in more detail, with the addition of two additional genotypes. This investigation combines stem anatomical observations, hydraulic measurements in stems and leaves (during well-watered and drought conditions), and gene expression studies in leaves (during well-watered and drought conditions) to gain comprehensive insights into the plants' adaptive responses to drought.

## Chapter 4

This chapter focuses on investigating the mechanisms underlying the increased drought tolerance observed in *JUNGBRUNNEN1* (*JUB1*) overexpression transgenic lines of both *Arabidopsis* and *Solanum lycopersicum* L. (tomato). This chapter employs detailed stem anatomy observations in combination with hydraulic traits in stems and leaves of *Arabidopsis* and tomato plants that differed in expression of *JUB1*, within the context of a drought experiment.





## Chapter 2

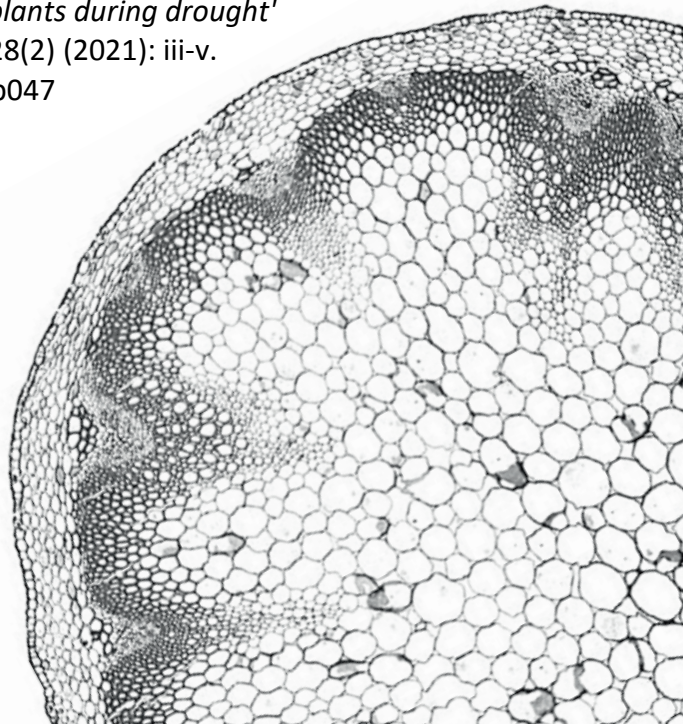
# Intervessel pit membrane thickness best explains variation in embolism resistance amongst stems of *Arabidopsis thaliana* accessions

Ajaree Thonglim<sup>1\*</sup>, Sylvain Delzon<sup>2</sup>, Maximilian Larter<sup>1</sup>, Omid Karami<sup>3</sup>, Arezoo Rahimi<sup>3</sup>, Remko Offringa<sup>3</sup>, Joost J. B. Keurentjes<sup>4</sup>, Salma Balazadeh<sup>3</sup>, Erik Smets<sup>1</sup>, and Frederic Lens<sup>1\*</sup>

*Adapted from*

**Annals of Botany** 128(2) (2021, first published online in 2020): 171-182.  
<https://doi.org/10.1093/aob/mcaa196>

A commentary paper by Craig R. Brodersen, entitled '*By the narrowest of margins: nano-scale modification of pit membranes and the fate of plants during drought*' is published in *Annals of Botany* 128(2) (2021): iii-v.  
<https://doi.org/10.1093/aob/mcab047>



<sup>1</sup> Naturalis Biodiversity Center, Functional Traits, PO Box 9517, 2300 RA Leiden, The Netherlands

<sup>2</sup> BIOGECO INRA, Université Bordeaux, 33615 Pessac, France

<sup>3</sup> Plant Developmental Genetics, Institute of Biology Leiden, Leiden University, 2333 BE Leiden, the Netherlands

<sup>4</sup> Laboratory of Genetics, Wageningen University, Droevendaalsesteeg 1, 6708 PB Wageningen, The Netherlands

\* For correspondence. E-mail: [ajaree.thonglim@naturalis.nl](mailto:ajaree.thonglim@naturalis.nl);  
[frederic.lens@naturalis.nl](mailto:frederic.lens@naturalis.nl)

## Abstract

The ability to avoid drought-induced embolisms in the xylem is one of the essential traits for plants to survive periods of water shortage. Over the past three decades, hydraulic studies have been focusing on trees, which limits our ability to understand how herbs tolerate drought. Here, we investigate the embolism resistance in inflorescence stems of four *Arabidopsis thaliana* accessions that differ in growth form and drought response. We assess functional traits underlying the variation in embolism resistance amongst the accessions studied using detailed anatomical observations. The vulnerability to xylem embolism was obtained via vulnerability curves using the centrifuge technique and linked with detailed anatomical observations in stems using light microscopy and transmission electron microscopy. The data show significant differences in stem  $P_{50}$ , varying twofold from -1.58 MPa in the Cape Verde Island accession to -3.07 MPa in the woody *soc1ful* double mutant. Out of all the anatomical traits measured, intervessel pit membrane thickness ( $T_{PM}$ ) best explains the differences in  $P_{50}$ , as well as  $P_{12}$  and  $P_{88}$ . The association between embolism resistance and  $T_{PM}$  can be functionally explained by the air-seeding hypothesis. There is no evidence that the correlation between increased woodiness and increased embolism resistance is directly related to functional aspects. However, we found that increased woodiness is strongly linked to other lignification characters, explaining why mechanical stem reinforcement is indirectly related to increased embolism resistance. In conclusion, the woodier or more lignified accessions are more resistant to embolism than the herbaceous accessions, confirming the link between increased stem lignification and increased embolism resistance as also observed in other lineages. Intervessel pit membrane thickness, and to a lesser extent theoretical vessel implosion resistance and vessel wall thickness, are the missing functional links between stem lignification and embolism resistance.

Keywords: *Arabidopsis thaliana*, embolism resistance, herbaceous species, intervessel pit membrane, lignification, stem anatomy, xylem hydraulics.

## Introduction

Long-distance water transport in the xylem connecting roots to leaves is essential for plant survival and distribution (Sperry, 2003; Brodribb, 2009; Lucas *et al.*, 2013; Lens *et al.*, 2016; Trueba *et al.*, 2017; Choat *et al.*, 2018; Brodribb *et al.*, 2020). Plants have developed an ingenious system to transport water upwards against gravity by a largely passive mechanism that is driven by a difference in negative xylem pressure created in the leaf mesophyll cell walls, known as the cohesion-tension theory (Dixon and Joly, 1895; Pickard, 1981; Brown, 2013). However, this negative or subatmospheric pressure inside the water-conducting xylem conduits puts water in a metastable liquid state, making it vulnerable to heterogeneous cavitation: the transition from liquid water to vapour by spontaneous destabilization of the hydrogen bonds between water molecules at nucleating sites (Steudle, 2001; Wheeler and Stroock, 2008; Brown, 2013; Venturas *et al.*, 2017). Under drought stress conditions, the xylem pressure becomes more negative, thereby increasing the risk of tiny vapour bubbles enlarging into a large embolism that blocks the water transport inside a conduit (Sperry and Tyree, 1988; Tyree and Zimmermann, 2002; Cochard, 2006). This embolized conduit can then cause gas bubbles to spread towards adjacent water-filled conduits via tiny pores in the interconduit pit membranes, a process called air-seeding. Air-seeding may lead to a rapid spread of drought-induced embolism throughout the plant, giving rise to hydraulic failure, i.e. a catastrophic loss of xylem hydraulic conductance, ultimately causing plant death (Brodribb and Cochard, 2009; Allen *et al.*, 2010; Urli *et al.*, 2013; Brodribb *et al.*, 2016, 2020; Anderegg *et al.*, 2016; Adams *et al.*, 2017; Kaack *et al.*, 2019; Zhang *et al.*, 2020). Acquiring a sufficient level of embolism resistance, therefore, represents one of the most essential adaptations for plant survival under drought conditions, along with other strategies such as reduced water-loss, increased water storage or root depth (Lens *et al.*, 2013; Gleason *et al.*, 2014; Martin-StPaul *et al.*, 2017; Billon *et al.*, 2020).

The relationship between the decline in hydraulic conductivity due to embolism and xylem pressure is plotted in a so-called vulnerability curve (VC), from which the pressure inducing 50% loss of hydraulic conductivity ( $P_{50}$ ) – the often-cited proxy for drought tolerance – is derived (Maherali *et al.*, 2004; Choat *et al.*, 2012; Venturas *et al.*, 2017). Hydraulic studies show

a wide range of  $P_{50}$  across species (from -0.5 MPa to -20 MPa), and species occupying dry habitats are generally more resistant to embolism formation (more negative  $P_{50}$ ) than species from wet habitats (Brodribb and Hill, 1999; Choat *et al.*, 2012; Larter *et al.*, 2015; Lens *et al.*, 2016; Trueba *et al.*, 2017). Xylem physiologists have measured  $P_{50}$  values in stems of over 2000 tree and shrub species. However, hydraulic measurements in herbaceous species are limited to only a few dozen species, despite the fact that a majority of our important food crops are herbs (Stiller, 2002; Holloway-Phillips and Brodribb, 2011; Lens *et al.*, 2013, 2016; Nolf *et al.*, 2016; Skelton *et al.*, 2017; Ahmad *et al.*, 2018; Dória *et al.*, 2018; Volaire *et al.*, 2018; Lamarque *et al.*, 2020; Bourbia *et al.*, 2020; Corso *et al.*, 2020) Therefore, it is essential to focus more on herb hydraulics and integrate these hydraulic traits in models that predict annual crop yields to consider the effects of drought and heatwave events (Asseng *et al.*, 2015).

In this paper, we focus on the model species *Arabidopsis thaliana* (L.) Heynh. This small herbaceous species is able to produce a limited amount of wood in the hypocotyl and at the base of the inflorescence stem (Chaffey *et al.*, 2002; Ko *et al.*, 2004; Nieminen *et al.*, 2004; Melzer *et al.*, 2008; Lens *et al.*, 2012). Wood formation can be moderately induced in wild-type accessions by either delaying flowering time under short days (Tixier *et al.*, 2013) or by clipping developing flowers (Chaffey *et al.*, 2002), by applying weights on the inflorescence stem (Ko *et al.*, 2004), or by increasing auxin levels (Agusti *et al.*, 2011; Brackmann *et al.*, 2018). A more extensive wood cylinder can be induced by modifying gene regulation that turns the herbaceous phenotype into a shrubby phenotype (Melzer *et al.*, 2008; Karami *et al.*, 2020), although this woodiness does not extend towards the upper parts of the inflorescence stems (Lens *et al.*, 2012). Since increased woodiness or lignification levels in stems have been linked to higher levels of embolism resistance in various plant groups (Tixier *et al.*, 2013; Lens *et al.*, 2013, 2016; Dória *et al.*, 2018, 2019), we selected three herbaceous wild-type accessions of *A. thaliana* with a different growth type and drought response (Columbia (Col-0), Cape Verde Islands (Cvi) and Shahdara (Sha); Bac-Molenaar *et al.*, 2016; Thoen *et al.*, 2017) and one woody mutant established in the Col-0 background (*soc1ful* knockout; Melzer *et al.*, 2008) to evaluate this potential correlation more closely. To this end, we applied the cavitron centrifuge method (Cochard *et al.*, 2013) to compare the xylem embolism resistance of inflorescence stems amongst the four accessions,

and assessed which xylem anatomical traits underlie the differences observed in  $P_{50}$  using detailed anatomical observations with light microscopy (LM) and transmission electron microscopy (TEM). Various hydraulically relevant stem traits were observed, such as the proportion of stem woodiness/lignification, intervessel pit membrane thickness, fiber wall thickness, theoretical vessel implosion index, and vessel grouping index (Table 1). We hypothesize that woodier or more lignified *Arabidopsis* stems are more resistant to embolism formation than less lignified stems and that this difference in embolism resistance is functionally driven by intervessel pit membrane thickness.

## Materials and methods

### *Plant material*

Three accessions and one woody mutant of *Arabidopsis thaliana* were chosen based on their contrasting growth form, the difference in drought tolerance and the minimum length of their inflorescence stems: (1) Columbia (Col-0, a direct descendant of Col-1 from Poland and Eastern Germany; Koornneef and Meinke, 2010; Passardi *et al.*, 2007; Somssich, 2019); (2) Shahdara (Sha, native to a low precipitation area of Shakhdarah valley, Tajikistan; Khurmatov, 1982; Trontin *et al.*, 2011); (3) Cape Verde Islands (Cvi, native to the high altitude region above 1,200 m on Cape Verde Islands; Lobin, 1983; Monda *et al.*, 2011); and (4) Col-0 accession in which two flowering time control genes *SUPPRESSOR OF OVEREXPRESSION OF CO 1* (*SOC1*) and *FRUITFULL* (*FUL*) are knocked out (*soc1ful* in Col-0 background; Melzer *et al.*, 2008). The three wild-type accessions were selected based on the length of their inflorescence stems (at least 30 cm required for the cavitron measurements, which exceeds by far the maximum vessel length of Col-0 reaching only 4 cm according to Tixier *et al.* (2013), to avoid potential open-vessel artefacts (Cochard *et al.*, 2013)), their differences in drought response (Bac-Molenaar *et al.*, 2016; Thoen *et al.*, 2017) and growth form. The *soc1ful* knockout was selected as the woody counterpart because of its extended levels of wood formation at the base of the inflorescence stems (Lens *et al.*, 2012). One hundred individuals from three accessions and one double knockout were grown from seeds sown directly in a mixture of soil and sand (4.5:1). After seed germination (10-12 days after sowing), the healthy seedlings were transferred and grown individually in 8 cm-diameter

pots in a growth chamber under controlled conditions of 20°C temperature and 16-h photoperiod, with 100  $\mu\text{mol m}^{-2} \text{s}^{-1}$  light intensity. Relative humidity (RH) was maintained at 70%. We synchronized the harvesting time for the four accessions, meaning that each accession was harvested at different ages (55-65 days for WT accessions, 80-90 days for *soc1ful*), depending on the time required for flowering and inflorescence stem development.

## ***Xylem vulnerability to embolism***

### *Sample preparation of inflorescence stems*

The plants were harvested – with roots, leaves and flowers still attached – in the growth chamber facilities at the Institute of Biology Leiden (Leiden University, The Netherlands). The basal part of the inflorescence stems of each accession was cut underwater with a sharp razor blade into a length at least of 30 cm, and then immediately wrapped in wet tissues, enclosed in plastic bags, and shipped to the PHENOBOIS platform (INRAE, University of Bordeaux, France) for the hydraulic experiments that were carried out within a week of harvest. Before running the cavitron centrifuge measurements, the samples were recut underwater to a standard length of 27 cm, after which both ends were trimmed to fit the cavitron rotor. All siliques, leaves and flowers were removed from the stems just before the measurement.

### *Cavitron centrifuge method*

Centrifugal force has been used to induce cavitation in stem segments by lowering the xylem pressure in the middle part of stems during spinning (Cochard, 2002; Cochard *et al.*, 2005). Vulnerability to embolism in the inflorescence stems was measured using ten individuals per vulnerability curve (VC) to generate sufficient hydraulic conductivity during the spinning experiment; about 10 VCs per accession were generated. A solution of deionized ultrapure water containing 1 mM  $\text{CaCl}_2$  and 10mM KCl was used as a reference for the hydraulic conductivity measurements. The theoretically maximum hydraulic conductivity ( $K_{\text{max}}$ ,  $\text{m}^2 \text{MPa}^{-1} \text{s}^{-1}$ ) of the ten inflorescence stems was firstly calculated at near-zero MPa (low speed). The xylem pressure was then gradually decreased by -0.2 to -0.4 MPa for each

spinning step. The hydraulic conductivities at every rotation speed ( $K$ ) were measured using Cavisoft software (Cavisoft v1.5, University of Bordeaux, France). The percentage loss of hydraulic conductivity ( $PLC$ ) was computed as:

$$PLC = 100 \cdot (1 - (K/K_{MAX})) \quad (1)$$

The vulnerability curves were constructed and fitted with a sigmoid function (Pammenter and Van der Willigen, 1998) using NLIN procedure in SAS 9.4 (SAS 9.4; SAS Institute, Cary, NC, USA) following the equation:

$$PLC = 100 / [1 + \exp ((S/25) \cdot (P - P_{50}))] \quad (2)$$

where  $P_{50}$  represents the xylem pressure inducing 50% loss of hydraulic conductivity and  $S$  (% MPa<sup>-1</sup>) is the slope of the VC at the inflexion point ( $P_{50}$ ).

## ***Stem anatomy***

### *Sample preparation*

Since the stem anatomy at the basal, more lignified part differs rather considerably compared to the middle part where the negative pressures were applied during the cavitron measurements, we made sections from both parts and performed the anatomical observations on the middle stem parts to match anatomy with  $P_{50}$ . From the 10 VCs we generated per accession, we selected three stems for three representative VCs (9 individuals per accession) for light microscopy (LM), and one stem for three representative VCs (3 individuals per accession) for transmission electron microscopy (TEM). The anatomical measurements (Table 1) were carried out using ImageJ (National Institutes of Health, Bethesda, USA) following the recommendations of (Scholz *et al.*, 2013).



### Light microscopy (LM)

The inflorescence stems were cut into small pieces, ca 1 cm long and stored in 70% ethanol. Fixed samples were then infiltrated and embedded in LR-White resin (Hamann *et al.*, 2011). The embedded samples were sectioned using a Leica RM 2265 microtome with disposable Tungsten carbon blades (Leica, Eisenmark, Wetzlar, Germany) at a thickness of 4  $\mu\text{m}$ . Subsequently, the sections were heat-fixed onto the slides with 40% acetone, stained with Toluidine blue (1% (w/v) toluidine blue (VWR chemical BDH<sup>®</sup>, Radnor, Pennsylvania, USA) in 1% (w/v) borax), rinsed with distilled water, air-dried, and mounted with DPX new-100579 mounting medium (Merck Chemicals B.V., Amsterdam, Northern Holland, The Netherlands). The anatomical features were observed under a Leica DM2500 light microscope and photographed with a Leica DFC-425 digital camera (Leica microscopes, Wetzlar, Germany). The diameter of vessels ( $D$ ) was calculated as:

$$D = (\sqrt{4A}) / \pi \quad (3)$$

where  $D$  represents the diameter of vessels, and  $A$  is the conduit surface area. The hydraulically weighted vessel diameter ( $D_H$ ) was calculated based on the diameter of vessels ( $D$ ) following the equation (Tyree and Zimmermann, 2002):

$$D_H = (\sum D^4 / N)^{1/4} \quad (4)$$

where  $D$  is the diameter of vessels measured using equation 3 and  $N$  is the number of conduits measured. All the measurements are explained in Table 1.

### Transmission Electron Microscopy (TEM)

After the cavitron experiment, 1 cm-long pieces from the middle part of the inflorescence stems were immediately collected and fixed in Karnovsky's fixative for 48 hr (Karnovsky, 1965). The samples were cleaned three times in 0.1M cacodylate buffer, then post-fixed with 1% buffered osmium tetroxide, rinsed again with buffer solution, stained with 1% uranyl acetate, and dehydrated in a series of ethanol: 1 % uranyl acetate

replacement, with increasing concentration of ethanol (30%, 50%, 70%, 96%, and twice in  $\geq 99\%$ ). The samples were then infiltrated with Epon 812 n (Electron Microscopy Sciences, Hatfield, England) and placed at 60°C for 48 hr in the oven. The Epon blocks were trimmed into 2  $\mu\text{m}$ -thick using a rotary microtome with a glass knife. Subsequently, the cross-sections with many vessel-vessel contact areas were cut into ultrathin sections of 90-95 nm using a Leica EM UC7 ultramicrotome with a diamond knife. The sections were dried and mounted on film-coated copper slot grids with Formvar coating (Agar Scientific, Stansted, UK), and post-stained with uranyl acetate and lead citrate. Ultrastructural observations of intervessel pits were performed and photographed using a JEM-1400 Plus TEM (JEOL, Tokyo, Japan), equipped with an 11 MPixel camera (Quemesa, Olympus). At least 25 relaxed, non-shrunken intervessel pit membranes were selected from 3 individuals per accession to observe intervessel pit membranes thickness and pit chamber depth (Table 1).

### ***Statistical analysis***

To assess the differences between embolism resistance among the four accessions studied, we performed General Linear Models (GLM). A Newman-Keuls post-hoc test was applied to test whether or not embolism resistance ( $P_{50}$ ) and anatomical characters differ amongst accessions. We carried out multiple linear regression models based on non-standardized and standardized data from the middle part of the stem segments to evaluate which stem anatomical traits (predictive variables) best explain embolism resistance, with  $P_{50}$ ,  $P_{12}$  (air entry point) and  $P_{88}$  as response variables. Predictors were firstly selected based on biological knowledge, followed by a collinearity analysis through pairwise scatterplots and variance inflation factor (VIF). To deduce the most parsimonious multiple linear regression model, we applied “step” function from “stats” package (R Core Team 2016; available in CRAN) to remove the least predictive variables each time according to Akaike Information Criterion (AIC). Robust fitting of linear models through iteratively reweighted least squares (IWLS) and MM estimation (M-estimation with Tukey’s bi-weight initialized by a specific S-estimator) was used to deal with the outliers and leverages. In addition, to assess the relative importance of the remaining explanatory variables of  $P_{50}$ , we calculated the relative importance of regressors in linear models. Pearson’s correlation analysis was applied to assess the correlation between

## **Chapter 2:** *Intervessel pit membrane thickness and embolism resistance*

the predictive variables and  $P_{50}$ . We used R version 3.6.3 in R Studio version 1.2.5033 for all analyses. All the differences were considered significant when p-value was  $<0.05$ .

**Table 1** List with the anatomical characters measured with reference to their acronyms, definitions, calculations, microscope techniques, and units.

Acronyms	Definition	Calculation	Number of measurements	Unit	Technique
A <sub>F</sub>	Fiber cell area	Area of single xylem fiber in cross-section	Min. 30 fibers	μm <sup>2</sup>	LM
A <sub>FL</sub>	Fiber lumen area	Area of single xylem fiber lumen in cross-section	Min. 30 fibers	μm <sup>2</sup>	LM
A <sub>FW</sub>	Fiber wall area	A <sub>F</sub> - A <sub>FL</sub> for the same fiber	Min. 30 fibers	μm <sup>2</sup>	LM
A <sub>LIG</sub>	Lignified stem area	Total xylem area + fiber caps area + lignified pith cell area in cross-section	9 stems per accession	mm <sup>2</sup>	LM
A <sub>PITH</sub>	Pith area	Total pith area in cross-section	9 stems per accession	mm <sup>2</sup>	LM
A <sub>S</sub>	Total stem area	Total stem area in cross-section	9 stems per accession	mm <sup>2</sup>	LM
D	Diameter of vessels	Equation 3	Min. 50 vessels	μm	LM
D <sub>H</sub>	Hydraulically weighted vessel diameter	Equation 4	Min. 50 vessels	μm	LM
D <sub>MAX</sub>	Maximum vessel lumen diameter	Diameter of single vessel	Min. 30 vessels	μm	LM
D <sub>PC</sub>	Pit chamber depth	Distance from the relaxed pit membrane to the inner pit aperture	Min. 25 pits	μm	TEM
P <sub>FWFA</sub>	Proportion of fiber wall area per fiber cell area	A <sub>FW</sub> /A <sub>F</sub> for the same fiber; a measure of xylem fiber wall thickness	Min. 30 fibers	-	LM

## Chapter 2: Intervessel pit membrane thickness and embolism resistance

Acronyms	Definition	Calculation	Number of measurements	Unit	Technique
P <sub>LIG</sub>	Proportion of lignified area per total stem area	$A_{LIG}/A_S$	9 stems per accession	-	LM
T <sub>PM</sub>	Intervessel pit membrane thickness	Thickness of intervessel pit membrane measured at its thickest point	Min. 25 measurements	μm	TEM
T <sub>V</sub>	Vessel wall thickness	Thickness of a single vessel wall	Min. 30 Vessels	μm	LM
T <sub>VW/D<sub>MAX</sub></sub>	Thickness-to-span ratio of vessels	Double intervessel wall thickness divided by the maximum diameter of the largest vessel	Min. 30 measurements	μm	LM
(T <sub>VW/D<sub>MAX</sub></sub> ) <sup>2</sup>	Theoretical vessel implosion resistance	(T <sub>VW/D<sub>MAX</sub></sub> ) <sup>2</sup>	Min. 30 measurements	-	LM
V <sub>D</sub>	Vessel density	Number of vessels per mm <sup>2</sup>	Min. 5 measurements	No. of vessels/mm <sup>2</sup>	LM
V <sub>G</sub>	Vessel grouping index	Ratio of total number of vessels to total number of vessel groupings (incl. solitary and grouped vessels)	Min. 50 vessel groups	-	LM

## Results

### ***Xylem vulnerability to embolism amongst the Arabidopsis accessions***

$P_{50}$  of each accession is significantly different from each other and varied twofold across the accessions studied ( $F = 57.70$ ;  $p$ -value  $< 0.001$ ) from  $-1.58$  MPa to  $-3.07$  MPa (Figure 1). Amongst the four accessions, stems of the *soc1ful* double mutant are the most resistant to embolism ( $P_{50} = -3.07 \pm 0.30$  (SD) MPa; Supplementary Table S1) with a slope of  $62\% \text{ MPa}^{-1}$  (Figure 1a), followed by Sha ( $P_{50} = -2.49 \pm 0.11$  MPa; slope =  $59\% \text{ MPa}^{-1}$ ), Col-0 ( $P_{50} = -2.14 \pm 0.18$  MPa; slope =  $38\% \text{ MPa}^{-1}$ ), and Cvi ( $P_{50} = -1.58 \pm 0.05$  MPa; slope =  $142\% \text{ MPa}^{-1}$ ) (Supplementary Table S1; Figure 1a). The  $P_{50}$  variation within accessions is remarkably low except for *soc1ful* ranging from  $-2.59$  MPa to  $-3.42$  MPa (Figure 1b). Similar significant variation in  $P_{12}$  ( $F = 26.79$ ;  $p$ -value  $< 0.001$ ) is observed; for  $P_{88}$ , Col-0 and Sha are not significantly different from each other ( $F = 34.8$ ;  $p$ -value =  $0.517$ ).

### ***Stem anatomical traits amongst the accessions studied***

The features that are significantly different from each other among the accessions studied are intervessel pit membrane ( $T_{PM}$ ) ( $F = 118.8$ ;  $p$ -value  $< 2e^{-16}$ ; Supplementary Figure S1a; Figures 2c-d; Figures 3c-d), theoretical vessel implosion resistance ( $T_{VW}/D_{MAX}$ )<sup>2</sup> ( $F = 37.35$ ;  $p$ -value =  $1.44e^{-10}$ ; Supplementary Figure S1b) and proportion of fiber wall area per fiber cell area ( $P_{FWFA}$ ) ( $F = 65.33$ ;  $p$ -value =  $9.75e^{-14}$ ; Supplementary Figure S1c). Meanwhile, proportion of lignified area per total stem area ( $P_{LIG}$ ) of Col-0 is different from *soc1ful* and Cvi ( $F = 18.68$ ;  $p$ -value =  $3.48e^{-07}$ ; Supplementary Figure S1d), which is similar to Sha. Furthermore, vessel grouping index ( $V_G$ ) of Col-0 and Cvi is similar, which is also the case for Sha and *soc1ful*;  $V_G$  of both groups, however, are significantly different from each other ( $F = 43.45$ ;  $p$ -value =  $2.17e^{-11}$ ; Supplementary Figure S1e). Vessel wall thickness ( $T_V$ ) of Col-0 and Cvi are different from each other, and different from Sha and *soc1ful* which have a similar  $T_V$  ( $F = 33.46$ ;  $p$ -value =  $5.52e^{-10}$ ; Supplementary Figure S1f).

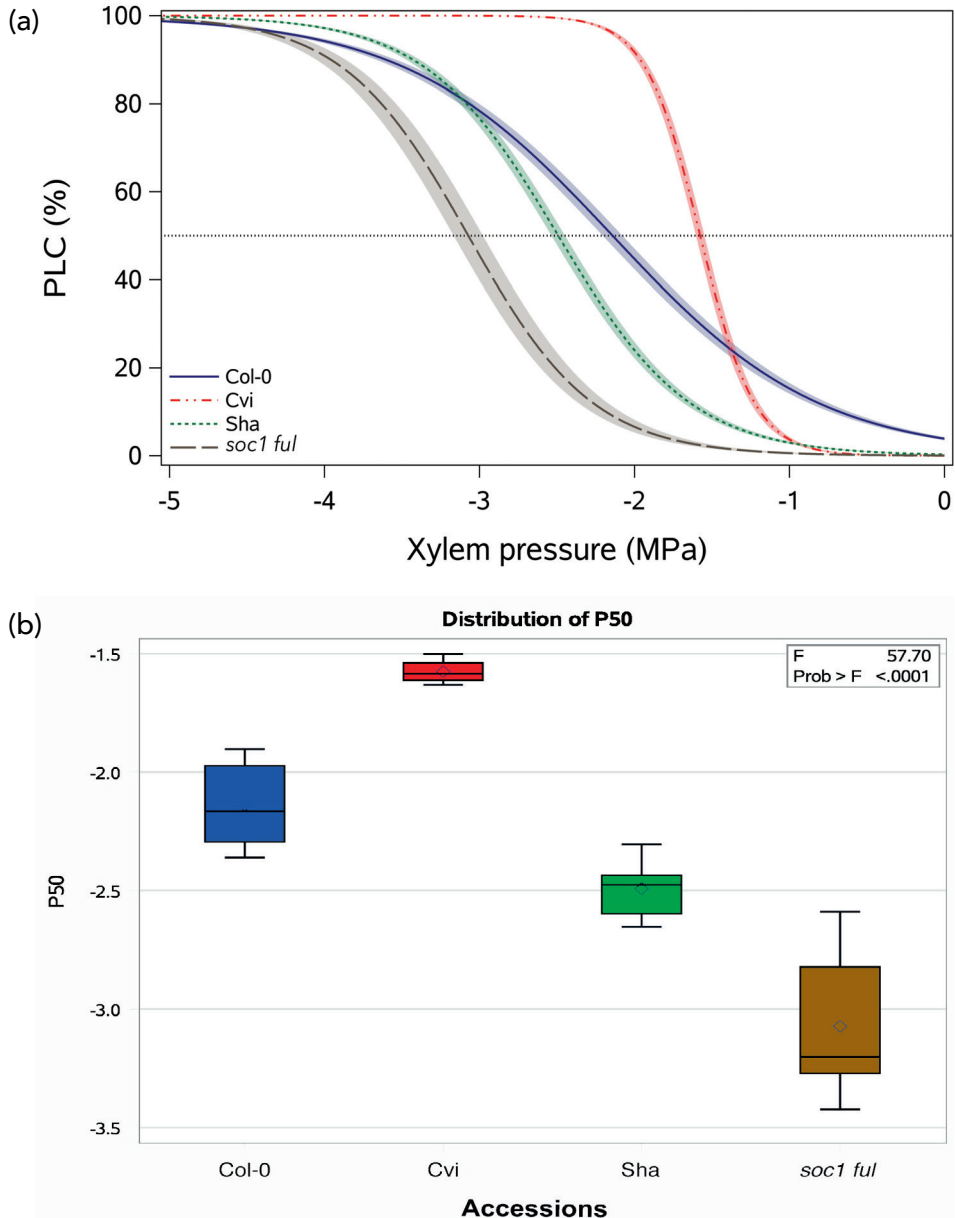


**Figure 1** Stem  $P_{50}$  is significantly different across *A. thaliana* accessions. (a) mean vulnerability curves (VCs) for each accession presents the percentage loss of conductivity (PLC) as a function of xylem pressure (MPa). The dotted line shows 50% loss of conductivity ( $P_{50}$ ). Shaded bands represent standard errors based on ca. 10 VCs per accession.; (b) boxplot showing  $P_{50}$  distribution and variation within and between accessions ( $p$ -value = 0.05).

## ***Relationship between embolism resistance and anatomical features***

Both  $T_{PM}$  and  $(T_{VW}/D_{MAX})^2$  strongly correlated positively with embolism resistance based on a Pearson correlation test ( $r = -0.93$ ,  $p$ -value =  $3.1e^{-16}$ ;  $r = -0.88$ ,  $p$ -value =  $2.1e^{-12}$ , respectively; Figures 4b-c). Furthermore, there are correlations between embolism resistance and vessel wall thickness ( $T_V$ ) ( $r = -0.86$ ,  $p$ -value =  $2.5e^{-11}$ ; Supplementary Figure S2a), between embolism resistance and vessel grouping index ( $V_G$ ) ( $r = -0.77$ ,  $p$ -value =  $3.6e^{-08}$ ; Supplementary Figure S2b), between embolism resistance and proportion of lignified area per total stem area ( $P_{LIG}$ ) ( $r = -0.67$ ,  $p$ -value =  $7.2e^{-06}$ ; Supplementary Figure S2c), and between embolism resistance and proportion of fiber wall per fiber cell area ( $P_{FWFA}$ ) ( $r = -0.73$ ,  $p$ -value =  $3.4e^{-07}$ ; Supplementary Figure S2d). Multiple regression analysis with robust fitting shows that the best predictors explaining  $P_{50}$  variation are the thickness of intervessel pit membrane ( $T_{PM}$ ; Figures 2c-d, 3c-d) and theoretical vessel implosion resistance ( $(T_{VW}/D_{MAX})^2$ ), followed by vessel wall thickness ( $T_V$ ), and vessel grouping index ( $V_G$ ) ( $R^2 = 0.9468$ ,  $p$ -value  $< 2.2e^{-16}$ ) (Table 2). However, only  $T_{PM}$  and  $(T_{VW}/D_{MAX})^2$  are highly significant in this model ( $p$ -value  $< 0.01$ ) (Table 2). According to the regressor analysis, the relative importance of  $T_{PM}$  and  $(T_{VW}/D_{MAX})^2$  in explaining  $P_{50}$  variation is 31% and 25%, respectively (Table 2, Figure 4a). The proportion of lignified area per total stem area ( $P_{LIG}$ ) does not explain embolism resistance based on the most parsimonious multiple regression model (AIC score = -134.39; Table 2, Supplementary Table S2), but is included in the second most parsimonious model (AIC = -132.44; Supplementary Table S3).

Correspondingly,  $T_{PM}$  also best explains  $P_{12}$  and  $P_{88}$  variations based on multiple regression models, followed by pit chamber depth ( $D_{PC}$ ) ( $R^2 = 0.9507$ ,  $p$ -value  $< 2.2e^{-16}$ ,  $R^2 = 0.8646$ ,  $p$ -value  $< 3.88e^{-13}$ , respectively) (Supplementary Tables S4, S5). In addition, theoretical vessel implosion resistance ( $(T_{VW}/D_{MAX})^2$ ) is included in  $P_{88}$  multiple regression model ( $p$ -value  $< 0.05$ ) (Supplementary Tables S5), while  $T_V$  is included in the  $P_{12}$  multiple regression model as a significant predictor ( $p$ -value  $< 0.001$ ) (Supplementary Tables S4). Correlations between the anatomical variables are the following: thickness of intervessel pit membrane is strongly correlated to theoretical vessel implosion resistance, vessel wall thickness, vessel grouping, and proportion of fiber wall per fiber cell area ( $r = 0.77, 0.76, 0.72$ , and  $0.68$ , respectively;  $p$ -value  $< 0.001$ ) (Supplementary Figure S3). Apart from that,



$(T_{VW}/D_{MAX})^2$  correlates with  $T_V$ ,  $V_G$ , and  $P_{FWFA}$  ( $r = 0.77, 0.62$ , and  $0.59$ ,  $p$ -value  $<0.001$ ),  $V_G$  is correlated with  $T_V$  ( $r = 0.63$ ;  $p$ -value  $<0.001$ ) (Supplementary Figure S3), and  $P_{LIG}$  shows correlations with  $T_{PM}$ ,  $V_G$ ,  $(T_{VW}/D_{MAX})^2$  and  $T_V$  ( $r = 0.67, 0.66, 0.58$  and  $0.58$ , respectively;  $p$ -value  $<0.001$ ; Supplementary Figure S3).

**Table 2** The best multiple regression model, based on AIC scores, of anatomical features explaining  $P_{50}$  variation in stems of the four *Arabidopsis thaliana* accessions studied.

Predictors	Estimate	Std. Error	z value	Pr ( $> z $ )
(Intercept)	0.901	0.315	2.858	0.004262
$T_{PM}$	-10.896	2.035	-5.356	$8.522e^{-08***}$
$(T_{VW}/D_{MAX})^2$	-35.174	10.927	-3.219	$0.001287**$
$T_V$	-0.516	0.239	-2.163	$0.031^*$
$V_G$	-0.280	0.183	-1.529	0.126

$T_{PM}$  = intervessel pit membrane thickness;  $(T_{VW}/D_{MAX})^2$  = theoretical vessel implosion resistance;  $T_V$  = vessel wall thickness;  $V_G$  = vessel grouping index; \*\*\*  $p$ -value  $< 0.001$ ; \*\*  $p$ -value  $< 0.01$ ; \*  $p$ -value  $< 0.05$

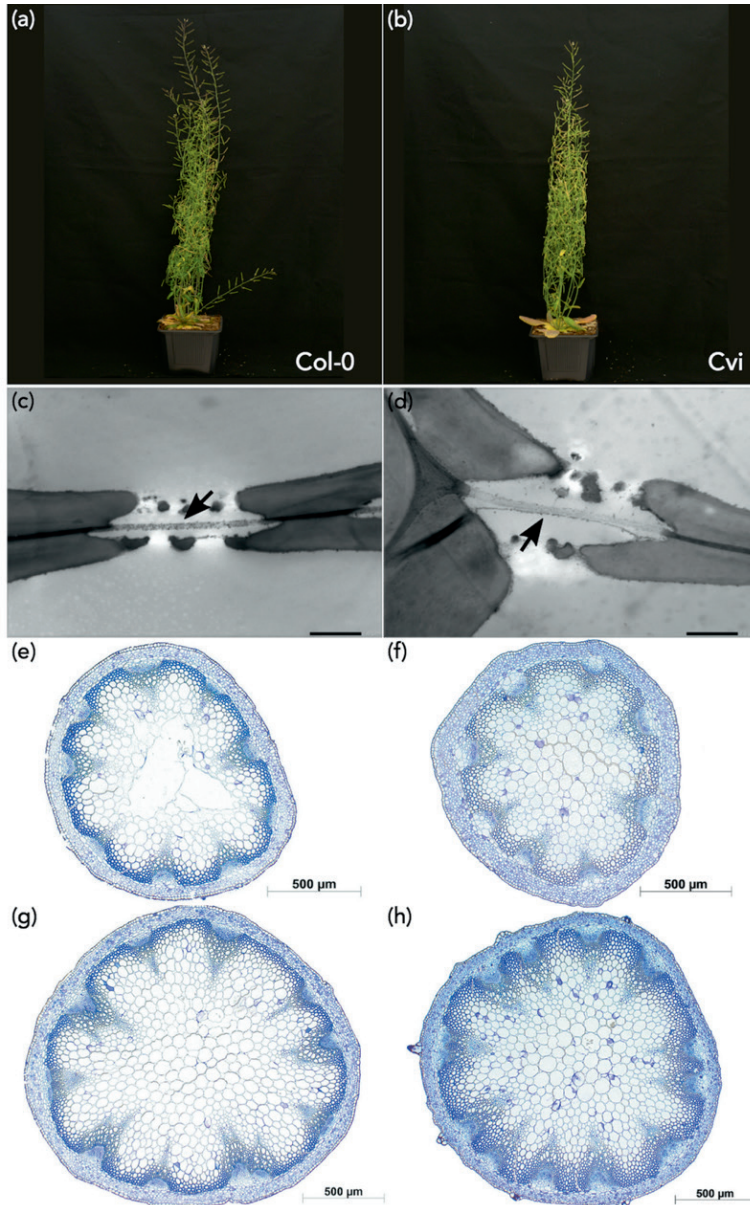


**Figure 2** Illustration of growth form and cross-sections of inflorescence stems of Col-0 (left, 57 days after sowing) and Cvi (right, 57 days after sowing). (a, b) growth form; (c, d) transmission electron microscope images of intervesel pit membranes (arrows); (e, f) light microscope images of the cross-section at the middle part of inflorescence stems; (g, h) light microscope images of the cross-section at the basal part of inflorescence stems. Scale bars represent 1  $\mu\text{m}$  (c-d), or 500  $\mu\text{m}$  (e-h).

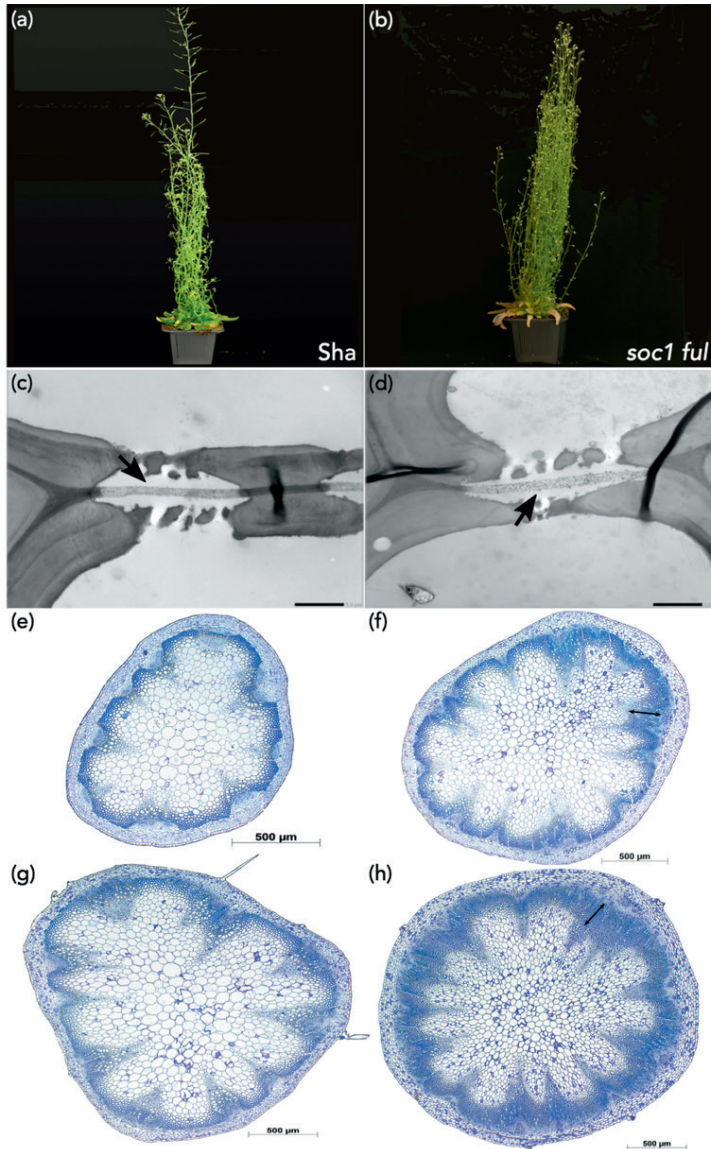


**Figure 3** Illustration of growth form and cross-sections of inflorescence stems of Sha (left, 57 days after sowing) and *soc1ful* (right, 80 days after sowing). (a, b) growth form; (c, d) transmission electron microscope images of intervessel pit membranes (arrows); (e, f) light microscope images of the cross-section at the middle part of inflorescence stems, the double-headed arrow shows the wood cylinder; (g, h) light microscope images of the cross-section at the basal part of inflorescence stems, the double-headed arrow shows the wood cylinder. Scale bars represent 1  $\mu\text{m}$  (c-d), 500  $\mu\text{m}$  (e-h).

## Discussion

We found a twofold variation in stem  $P_{50}$  amongst the *Arabidopsis thaliana* accessions studied (ranging from -1.5 to -3.0MPa; Figure 1), which is significantly associated with an increase in the thickness of the intervessel pit membrane ( $T_{PM}$ ; Figure 4) and is in line with the air-seeding hypothesis. Our findings confirm earlier reports that *Arabidopsis* inflorescence stems with increased levels of lignification are better able to avoid drought-induced embolism than stems that are less lignified (Figures 2-3), which is based on (1) a more elaborate set of wild-type accessions (three vs one), (2) multiple vulnerability curves (VCs) per accession compared to only one VC per accession, and (3) more detailed anatomical observations compared to previous structure-function papers in *Arabidopsis* (Lens *et al.*, 2013; Tixier *et al.*, 2013). We investigated correlations amongst a range of anatomical traits related to stem lignification and uncovered statistical associations between increased lignification vs  $T_{PM}$  and between vessel wall thickness vs  $T_{PM}$ . Our comparative approach suggests an indirect link between traits related to mechanical strength in stems and  $P_{50}$ , with  $T_{PM}$  serving as the missing functional link between stem reinforcement and vulnerability to embolism.

### ***Variation in stem $P_{50}$ amongst Arabidopsis accessions agrees with other herbs and is best explained by intervessel pit membrane thickness ( $T_{PM}$ )***

Our embolism resistance measurements with the cavitron technique support earlier papers reporting values for the same species based on the more traditional centrifuge technique in combination with a portable water flow device (XYL'EM) (from -2.25 to -3.5 MPa; Lens *et al.*, 2013; Tixier *et al.*, 2013). Our data also fall within the range of the published  $P_{50}$  values for herbaceous eudicot species (Tyree *et al.*, 1986; Stiller, 2002; Saha *et al.*, 2009; Li *et al.*, 2009; Rosenthal *et al.*, 2010; Nolf *et al.*, 2014; Skelton *et al.*, 2017; Dória *et al.*, 2018, 2019; Bourbia *et al.*, 2020), although more negative  $P_{50}$  values (up to -7.5 MPa) of herbaceous stems, especially in grasses, have been reported in some papers (Lens *et al.*, 2016; Volaire *et al.*, 2018). Amongst the anatomical traits we observed,  $T_{PM}$  strongly correlates with  $P_{50}$  and explains best the variation in  $P_{50}$  observed based on a statistical test showing the relative importance of regressors in our most parsimonious multiple linear regression model (Table 2; Figures 4a-b). Our observations in *Arabidopsis* fit well with other published data of woody and herbaceous

species where properly fixated intervessel pit membranes have been measured in stems that were subjected to  $P_{50}$  measurements (Li *et al.*, 2016; Dória *et al.*, 2018, 2019; Supplementary Figure S4).

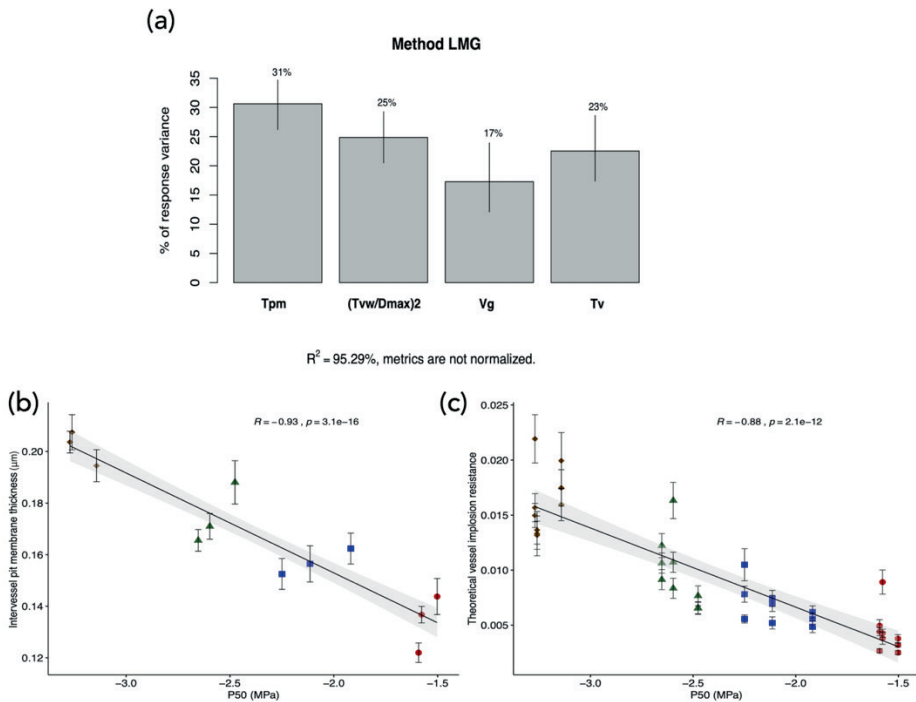


**Figure 4** The relative importance and correlations of intervessel pit membrane thickness and theoretical vessel implosion resistance to  $P_{50}$  (a) Relative importance of  $P_{50}$  variation is mainly explained by intervessel pit membrane thickness ( $T_{PM}$ ) and theoretical vessel implosion resistance  $(T_{VW}/D_{MAX})^2$  based on  $R^2$  contribution averaged over orderings among regressors; (b) negative correlation between thickness of intervessel pit membrane ( $T_{PM}$ ) and  $P_{50}$ ; (c) negative correlation between theoretical vessel implosion resistance  $(T_{VW}/D_{MAX})^2$  and  $P_{50}$ . Colours and styles refer to the accession studied: Col-0 (blue-filled square), Cvi (red-filled circle), Sha (green-filled triangle) and *soc1ful* (brown-filled diamond).

Furthermore, intervessel pit membrane thickness is the only trait that is also significant in the  $P_{12}$  and  $P_{88}$  multiple regression models, which emphasizes the functional relevance of  $T_{PM}$  in our dataset (Supplementary Tables S4, S5). As highlighted before, this  $T_{PM}$ - $P_{50}$  correlation is undoubtedly functionally relevant because it nicely fits with the air-seeding mechanism. Although we do not fully understand exactly how this mechanism works at the ultrastructural level, the oversimplified 2D view suggesting that air-

seeding occurs via the single largest pit membrane pore should be abandoned (Wheeler *et al.*, 2005). Instead, a more realistic 3D structure of intervessel pit membranes shows that a single pit membrane pore – being highly interconnected with other pores – has multiple constrictions that are often narrower than 50 or 20 nm when pit membranes are thinner or thicker than 300 nm, respectively (Zhang *et al.*, 2020). In other words, the chance of having a smaller pore constriction becomes higher with thicker pit membranes as this elongates the multiconstriction pit membrane pore. Consequently, air-seeding is not determined by the single largest pore in a pit membrane, but by the minimum constriction across all the interconnected pores in a given pit membrane (Kaack *et al.*, 2019; Zhang *et al.*, 2020). This explains why species with thicker intervessel pit membranes are better able to withstand air bubble spread between adjacent conduits under drought conditions than species with thinner intervessel pit membranes (Jansen *et al.*, 2009; Li *et al.*, 2016; Dória *et al.*, 2018). However, more ultrastructural observations of intact pit membranes and the role of surface-active substances such as phospholipids in the xylem sap and pit membranes should be carried out to improve our understanding of air bubble formation and spread at the ultrastructural level (Schenk *et al.*, 2017, 2018; Zhang *et al.*, 2020).

### ***Disentangling the correlation between traits impacting mechanical strength and embolism resistance***

Based on Pearson's correlation test, the proportion of lignified area per total stem area ( $P_{LIG}$ ) is significantly correlated to  $P_{50}$  (Supplementary Data Figures S2c, S3). This is in line with our previous results in *Arabidopsis* (Lens *et al.*, 2013), in other lineages of Brassicaceae and Asteraceae (Dória *et al.*, 2018, 2019), and in grasses (Lens *et al.*, 2016) showing that more woody/lignified stems are more resistant to embolism formation compared to close relatives with less woody/lignified stems. However,  $P_{LIG}$  is not included in the most parsimonious multiple regression  $P_{50}$  model (Table 2); it is retained in the second most parsimonious model (Supplementary Table S3), though, explaining only 10% of the  $P_{50}$  variation (results not shown). Consequently, in our dataset,  $P_{LIG}$  is not a key functional trait contributing to vulnerability to embolism in stems of the *Arabidopsis* accessions studied. Still, it does have predictive value due to its correlation with other traits that are considered to be more relevant. Interestingly,  $P_{LIG}$  is significantly

correlated to several other lignification traits, of which intervessel pit membrane thickness ( $T_{PM}$ ), theoretical vessel implosion resistance ( $T_{VW}/D_{MAX}$ )<sup>2</sup> and vessel wall thickness ( $T_V$ ) are prime examples (Supplementary Figure S3). These three traits explain altogether, 79% of the  $P_{50}$  variation in the most parsimonious multiple regression model (Figure 4a). When comparing the three  $P_{12}$ - $P_{50}$ - $P_{88}$  multiple regression models, it is interesting to note that the depth of pit chamber ( $D_{PC}$ ) is absent in the  $P_{50}$  model (Table 2) but pops up as highly significant in both  $P_{12}$ - $P_{88}$  models (Supplementary Tables S4, S5). It is hypothesized that shallower pit chambers minimize interconduit pit membrane stretching during aspiration and thereby reducing the mechanical stresses on the membranes in both angiosperms as gymnosperms (Hacke and Jansen, 2009; Lens *et al.*, 2011). However,  $D_{PC}$  does not seem to be generally correlated with embolism resistance across all lineages observed (Dória *et al.*, 2018).

The (indirect) correlation between  $P_{50}$  and traits impacting mechanical strength has also been highlighted in other studies that have found links between embolism resistance vs thickness-to-span ratio of conduits (Hacke *et al.*, 2001; Bouche *et al.*, 2014), vs vessel wall thickness (Jansen *et al.* 2009; Li *et al.* 2016; see also next paragraph), vs wood density (Jacobsen *et al.*, 2005; Hoffmann *et al.*, 2011; Anderegg *et al.*, 2016; Gleason *et al.*, 2016), vs fiber wall thickness (Jacobsen *et al.*, 2005, 2007), vs lignin content (Pereira *et al.*, 2018), and vs lignin composition (Awad *et al.*, 2012; Lima *et al.*, 2018). Out of all these lignification characters, vessel wall reinforcement for a given lumen area – expressed either as thickness-to-span ratio of vessels or theoretical vessel implosion resistance – explains 25% of the  $P_{50}$  variation (Figure 4a), but only 3% of the  $P_{88}$  variation (results not shown), and could potentially present a secondary functional link due to its direct association with the long-distance water flow in plants that is prone to negative pressures. Also, in conifers, the pressure causing conduit implosion is correlated with embolism resistance, but it is more negative than  $P_{50}$  for most species. Since vessel collapse due to negative pressures has never been observed in woody nor herbaceous stems, it suggests that embolism occurs before the critical vessel implosion threshold is reached (Choat *et al.*, 2012; Bouche *et al.*, 2014), which is likely also the case for herbaceous species. Only a few reports of (reversible) vessel collapse in the smallest leaf veins are reported, which could be a mechanism to prevent embolism upstream in the major veins (Zhang *et al.*, 2016).

Variation in theoretical vessel implosion resistance ( $(T_{VW}/D_{MAX})^2$ ) among *Arabidopsis thaliana* stems studied is mainly determined by the changes of vessel wall thickness ( $T_V$ ), explaining 64% of the variation, whereas the maximum vessel lumen diameter ( $D_{MAX}$ ) only accounts for 31% (Supplementary Figure S5). This result is in line with Bouche *et al.* (2014), who found that  $T_V$  drives the variation in  $T_{VW}/D_{MAX}$ , suggesting that species tend to mechanically reinforce their conduits by increasing wall thickness instead of reducing conduit size in order to maintain a minimum level of hydraulic conductance. But, at the same time,  $T_V$  also positively correlates with  $T_{PM}$  (Supplementary Figure S3), with thicker vessel walls leading to thicker intervessel pit membranes (Jansen *et al.*, 2009) and thus higher embolism resistance ( $T_V$  explaining 23% of the  $P_{50}$  variation (Figure 4a) and 18% of the  $P_{12}$  variation (results not shown)). On the other hand, other studies investigating the driver for  $T_{VW}/D_{MAX}$  variation found that  $D_{MAX}$  is more important (Pittermann *et al.*, 2006; Sperry *et al.*, 2006), thereby reducing the relevance of conduit wall thickening. Vessel grouping ( $V_G$ ), the final anatomical variable in the multiple regression  $P_{50}$  model, is the only character independent from lignification, and only accounts for 17% of the variation (Figure 4a) and 5% of the  $P_{88}$  variation. Pearson's correlation analysis shows a significant positive correlation between  $V_G$  and embolism resistance. Increased vessel connectivity safeguards all pathways in the 3D vessel network when only one vessel in a vessel multiple is embolized (Carlquist, 1984; Lens *et al.*, 2011). This can only work when the intervessel pit membranes are sufficiently thick to isolate the embolisms in a given vessel multiple at a normal drought stress level, which seems to be the case in *Arabidopsis*. If  $T_{PM}$  is too thin, greater vessel connectivity increases the probability of embolism spreading via air-seeding, potentially leading to lethal levels of hydraulic failure (Tyree and Zimmermann 2002; Loepfe *et al.*, 2007; Johnson *et al.*, 2020).



In conclusion, we found a twofold difference in stem  $P_{50}$  across the *Arabidopsis* accessions studied, with the woody mutant (*soc1ful*) being most resistant to embolism compared to the wild-type accessions. This confirms earlier studies that found a link between increased stem lignification and increased embolism resistance in *Arabidopsis* and other lineages. However, a higher degree of stem lignification cannot functionally explain the pattern observed, and therefore has to co-evolve with traits that functionally impact  $P_{50}$ . Intervessel pit membrane thickness ( $T_{PM}$ ), and to a lesser extent theoretical vessel implosion resistance ( $(T_{VW}/D_{MAX})^2$ ), vessel wall thickness ( $T_V$ ) and pit chamber depth ( $D_{PC}$ ), are strongly correlated with vulnerability to embolism and contribute most to the  $P_{12}$ - $P_{50}$ - $P_{88}$  variation observed, making  $T_{PM}$  the main functional missing link between stem lignification and embolism resistance. Adding more accessions and performing complementary measurements related to drought tolerance in stems, leaves and roots will undoubtedly shed more light into the complex mechanism that this short-lived, herbaceous model species has developed in order to cope with periods of water shortage.

## Acknowledgements

We thank Gaëlle Capdeville, Regis Burrett, Anne-Isabelle Gravel and Laurent Lamarque for technical support. We also acknowledge the statistical support of Pablo Cisneros Araujo. This work is funded by a PhD scholarship awarded to AT from the Institute for the Promotion of Teaching Science and Technology (IPST), Thailand, and by the Dutch Research Council NWO (grant number ALWOP.488)

## Supplementary data

**Table S1**  $P_{50}$  and anatomical traits measured (mean $\pm$ SD) of the four *Arabidopsis thaliana* accessions.

Traits/ accessions	Col-0	Cvi	Sha	<i>soc1ful</i>
$P_{50}$	-2.14 $\pm$ 0.18	-1.58 $\pm$ 0.05	-2.49 $\pm$ 0.11	-3.07 $\pm$ 0.30
$P_{LIG}$ (middle part of stem)	0.175 $\pm$ 0.001	0.193 $\pm$ 0.016	0.210 $\pm$ 0.009	0.252 $\pm$ 0.013
$T_{PM}$ ( $\mu$ m)	0.157 $\pm$ 0.005	0.134 $\pm$ 0.011	0.175 $\pm$ 0.012	0.202 $\pm$ 0.007
$D_{PC}$ ( $\mu$ m)	0.438 $\pm$ 0.015	0.357 $\pm$ 0.017	0.400 $\pm$ 0.010	0.353 $\pm$ 0.022
$D$ ( $\mu$ m)	20.954 $\pm$ 0.154	22.577 $\pm$ 1.202	20.714 $\pm$ 1.211	20.036 $\pm$ 2.155
$D_H$ ( $\mu$ m)	21.995 $\pm$ 0.189	23.456 $\pm$ 1.384	21.403 $\pm$ .127	20.625 $\pm$ 1.967
$D_{MAX}$ ( $\mu$ m)	25.992 $\pm$ 0.828	23.854 $\pm$ 0.744	25.837 $\pm$ 2.834	21.562 $\pm$ 0.870
$T_V$	0.996 $\pm$ 0.048	0.723 $\pm$ 0.082	1.179 $\pm$ 0.133	1.284 $\pm$ 0.045
$(T_{VW}/D_{MAX})^2$	0.007 $\pm$ 0.001	0.004 $\pm$ 0.001	0.010 $\pm$ 0.003	0.016 $\pm$ 0.002
$P_{FWFA}$	0.528 $\pm$ 0.063	0.397 $\pm$ 0.049	0.786 $\pm$ 0.047	0.671 $\pm$ .045
$V_D$	116.444 $\pm$ 5.251	102.706 $\pm$ 9.753	120.756 $\pm$ 14.931	127.756 $\pm$ 10.735
$V_G$	1.782 $\pm$ 0.057	1.829 $\pm$ 0.115	2.329 $\pm$ 0.108	2.342 $\pm$ 0.050

$P_{LIG}$  = proportion of lignified area per total stem area;  $T_{PM}$  = intervessel pit membrane thickness;  $D_{PC}$  = pit chamber depth;  $D$  = vessel diameter;  $D_H$  = hydraulically weighted vessel diameter;  $D_{MAX}$  = maximum vessel diameter;  $T_V$  = vessel wall thickness;  $(T_{VW}/D_{MAX})^2$  = theoretical vessel implosion resistance;  $P_{FWFA}$  = proportion of fiber wall area per fiber cell area;  $V_D$  = vessel density;  $V_G$  = vessel grouping index

**Table S2** The most parsimonious multiple regression model with standardized data of anatomical features explaining  $P_{50}$  variation in stems of the four *Arabidopsis thaliana* accessions studied.

Predictors	Estimate	Std. Error	z value	Pr (> z )
<b>(Intercept)</b>	-1.237988	0.079647	-15.5435	< 2.2e <sup>-16</sup>
<b>T<sub>PM</sub></b>	-0.931430	0.173915	-5.3557	8.524e <sup>-08***</sup>
<b>(T<sub>VW</sub>/D<sub>MAX</sub>)<sup>2</sup></b>	-0.683314	0.212280	-3.2189	0.001287**
<b>T<sub>V</sub></b>	-0.533092	0.246432	-2.1632	0.030522*
<b>V<sub>G</sub></b>	-0.274562	0.179581	-1.5289	0.126288

T<sub>PM</sub> = intervessel pit membrane thickness; (T<sub>VW</sub>/D<sub>MAX</sub>)<sup>2</sup> = theoretical vessel implosion resistance; T<sub>V</sub> = vessel wall thickness; V<sub>G</sub> = vessel grouping index; \*\*\* *p*-value < 0.001; \*\* *p*-value < 0.01; \* *p*-value < 0.05

**Table S3** Second most parsimonious multiple regression model of anatomical features explaining  $P_{50}$  variation in stems of the four *Arabidopsis thaliana* accessions studied, including proportion of lignified area per total stem area ( $P_{LIG}$ ).

Predictors	Estimate	Std. Error	z value	Pr (> z )
<b>(Intercept)</b>	0.902453	0.321147	2.81010	0.004953
<b>T<sub>PM</sub></b>	-10.94886	2.29588	-4.76890	1.852e <sup>-06</sup> ***
<b>(T<sub>VW</sub>/D<sub>MAX</sub>)<sup>2</sup></b>	-35.08942	11.41948	-3.07280	0.002121**
<b>T<sub>V</sub></b>	-0.51645	0.25839	-1.99870	0.045636*
<b>V<sub>G</sub></b>	-0.28617	0.19144	-1.49480	0.134960
<b>P<sub>LIG</sub></b>	0.09505	1.28027	0.07420	0.940816

T<sub>PM</sub> = intervessel pit membrane thickness; (T<sub>VW</sub>/D<sub>MAX</sub>)<sup>2</sup> = theoretical vessel implosion resistance; T<sub>V</sub> = vessel wall thickness; V<sub>G</sub> = vessel grouping index; P<sub>LIG</sub> = proportion of lignified area per total stem area; \*\*\* *p*-value < 0.001; \*\* *p*-value < 0.01; \* *p*-value < 0.05

**Table S4** The best multiple regression model, based on AIC scores, of anatomical features, explaining  $P_{12}$  variation in stems of the four *Arabidopsis thaliana* accessions studied.

Predictors	Estimate	Std. Error	z value	Pr (> z )
<b>(Intercept)</b>	-1.84631	0.52630	-3.50810	0.0004513
<b>T<sub>PM</sub></b>	-25.44504	2.57654	-9.87560	< 2.2e <sup>-16</sup> ***
<b>P<sub>FWFA</sub></b>	0.73844	0.52827	1.39790	0.1621552
<b>T<sub>V</sub></b>	-0.80998	0.22178	-3.65220	0.0002600***
<b>D<sub>PC</sub></b>	12.34489	1.17463	10.5096	< 2. 2e-16***

T<sub>PM</sub> = intervessel pit membrane thickness; P<sub>FWFA</sub> = proportion of fiber wall area per fiber cell area; T<sub>V</sub> = vessel wall thickness; D<sub>PC</sub> = pit chamber depth; \*\*\* *p*-value < 0.001; \*\* *p*-value < 0.01; \* *p*-value < 0.05

**Table S5** The best multiple regression model, based on AIC scores, of anatomical features, explaining  $P_{88}$  variation in stems of the four *Arabidopsis thaliana* accessions studied.

Predictors	Estimate	Std. Error	z value	Pr (> z )
<b>(Intercept)</b>	4.16481	0.67485	6.17150	6.764e <sup>-10***</sup>
<b>T<sub>PM</sub></b>	11.37418	3.08554	3.68630	0.0002276***
<b>(T<sub>VW</sub>/D<sub>MAX</sub>)<sup>2</sup></b>	-42.08524	16.36473	-2.57170	0.0101199*
<b>P<sub>FWFA</sub></b>	-1.24828	0.62798	-1.98780	0.0468351*
<b>V<sub>G</sub></b>	-0.77311	0.46031	-1.67950	0.0930509
<b>D<sub>PC</sub></b>	-15.82159	1.66181	-9.52070	< 2.2e <sup>-16***</sup>

T<sub>PM</sub> = intervessel pit membrane thickness; (T<sub>VW</sub>/D<sub>MAX</sub>)<sup>2</sup> = theoretical vessel implosion resistance; P<sub>FWFA</sub> = proportion of fiber wall area per fiber cell area; V<sub>G</sub> = vessel grouping index; D<sub>PC</sub> = pit chamber depth; \*\*\* *p*-value < 0.001; \*\* *p*-value < 0.01; \* *p*-value < 0.05

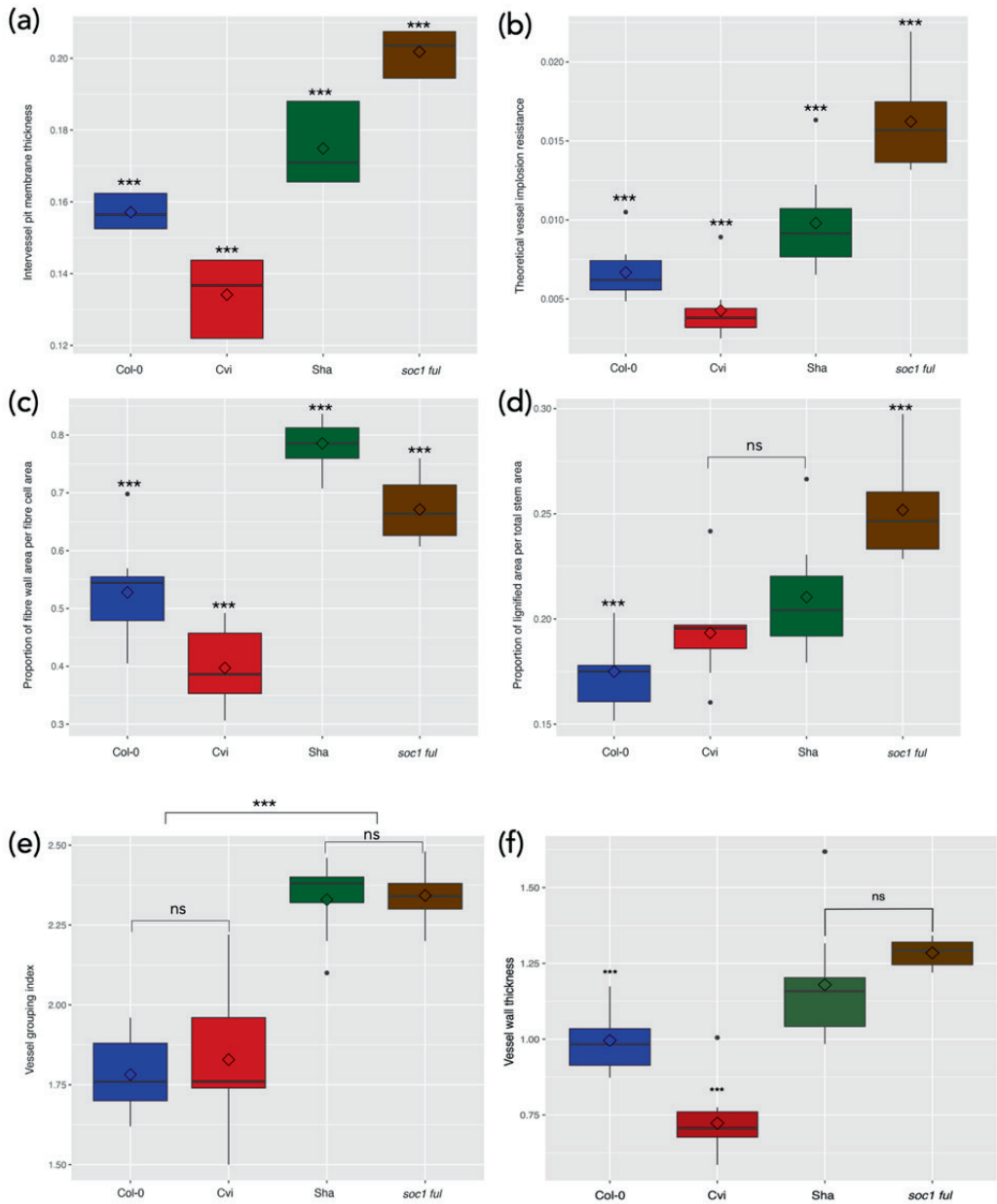


**Figure S1** Boxplots showing anatomical variation within and between accessions. (a) boxplot of intervessel pit membrane thickness ( $T_{PM}$ ); (b) boxplot of theoretical vessel implosion resistance ( $T_{VW}/D_{MAX}^2$ ); (c) boxplot of proportion of fiber wall area per fiber cell area ( $PF_{WA}$ ); (d) boxplot of proportion of lignified area per total stem area ( $P_{LIG}$ ); (e) boxplot of vessel grouping index ( $V_G$ ); ns =  $p$ -value > 0.05; \*\*\*  $p$ -value < 0.01

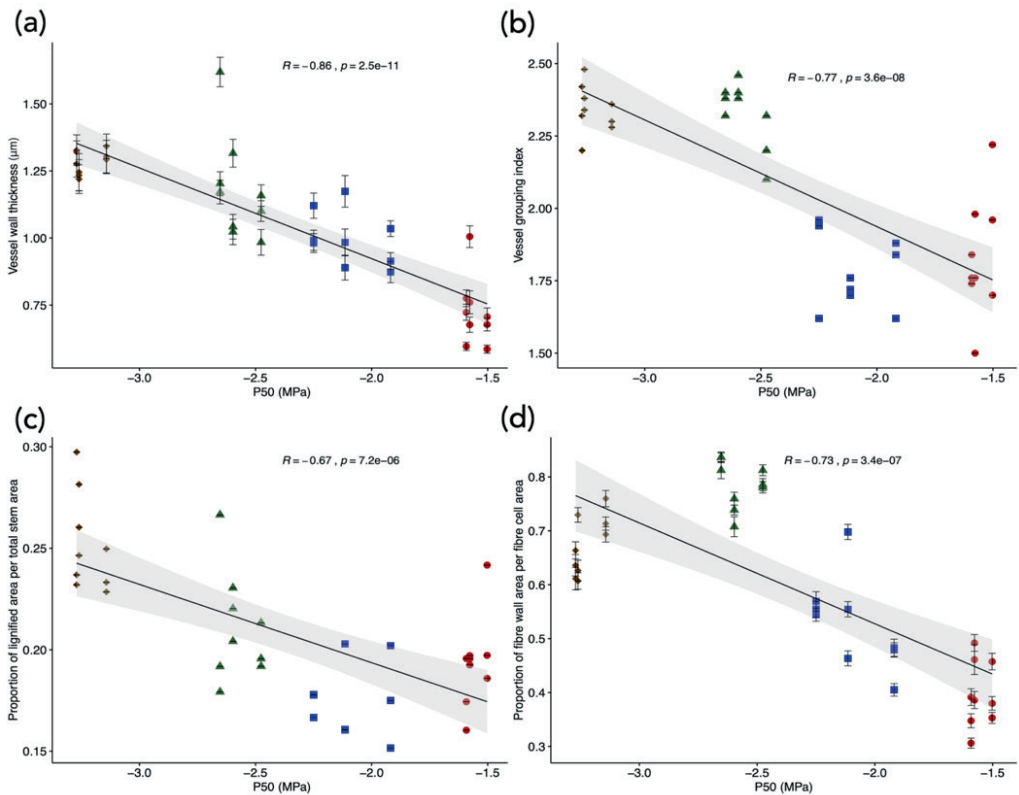


**Figure S2** Scatter plots with regression lines showing the relationships between anatomical characters and  $P_{50}$ . (a) the negative correlation between vessel grouping index ( $V_G$ ) and  $P_{50}$ ; (b) negative correlation between proportion of fiber wall area per fiber cell area ( $P_{FWFA}$ ) and  $P_{50}$ ; (c) negative correlation between proportion of lignified area per total stem area ( $P_{LIG}$ ) and  $P_{50}$ . Colours and styles refer to the accession studied: Col-0 (blue-filled square), Cvi (red-filled circle), Sha (green-filled triangle) and *soc1ful* (brown-filled diamond).



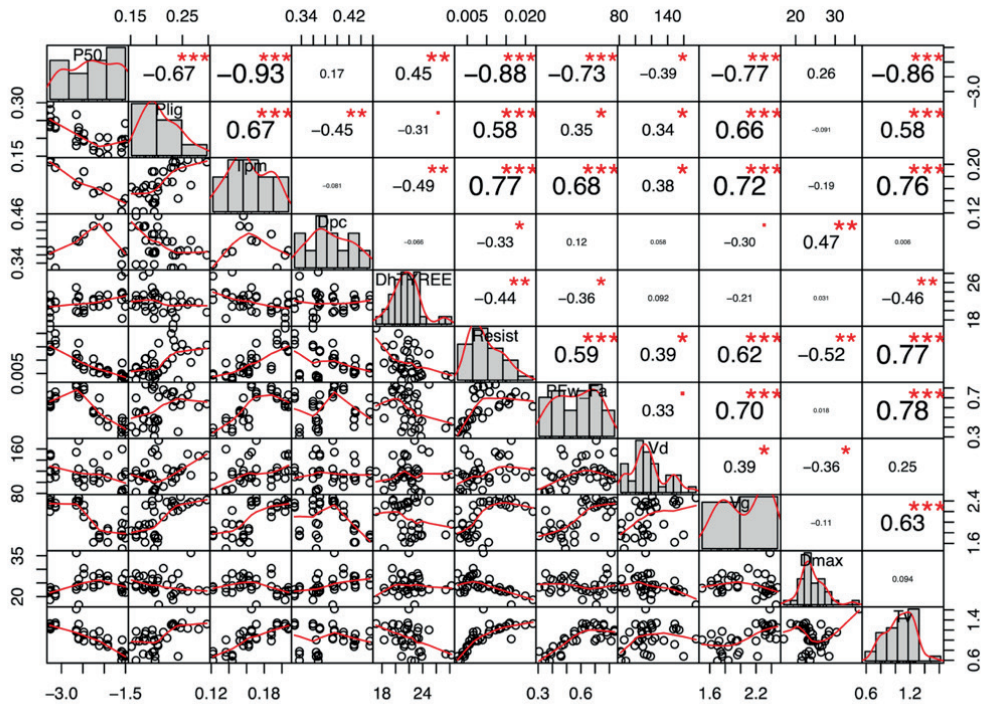


**Figure S3** The pairwise scatter plots based on Pearson’s correlation analysis showing the correlations of  $P_{50}$  (response variable) and each stem anatomical trait studied (predictive variables) and between all the predictive variables comprising proportion of lignified area per total stem area ( $P_{LIG}$ ), intervessel pit membrane thickness ( $T_{PM}$ ), pit chamber depth ( $D_{PC}$ ), hydraulically weighted vessel diameter ( $D_H$  or  $D_{HTYREE}$ ), theoretical vessel implosion resistance ( $(T_{VW}/D_{MAX})^2$  or Resist), proportion of fiber wall area per fiber cell area ( $P_{FWFA}$ ), vessel density ( $V_D$ ), vessel grouping index ( $V_G$ ), maximum vessel lumen diameter ( $D_{MAX}$ ), and vessel wall thickness ( $T_V$ ) \*\*\*  $p$ -value < 0.01; \*\*  $p$ -value < 0.01; \*  $p$ -value < 0.05.

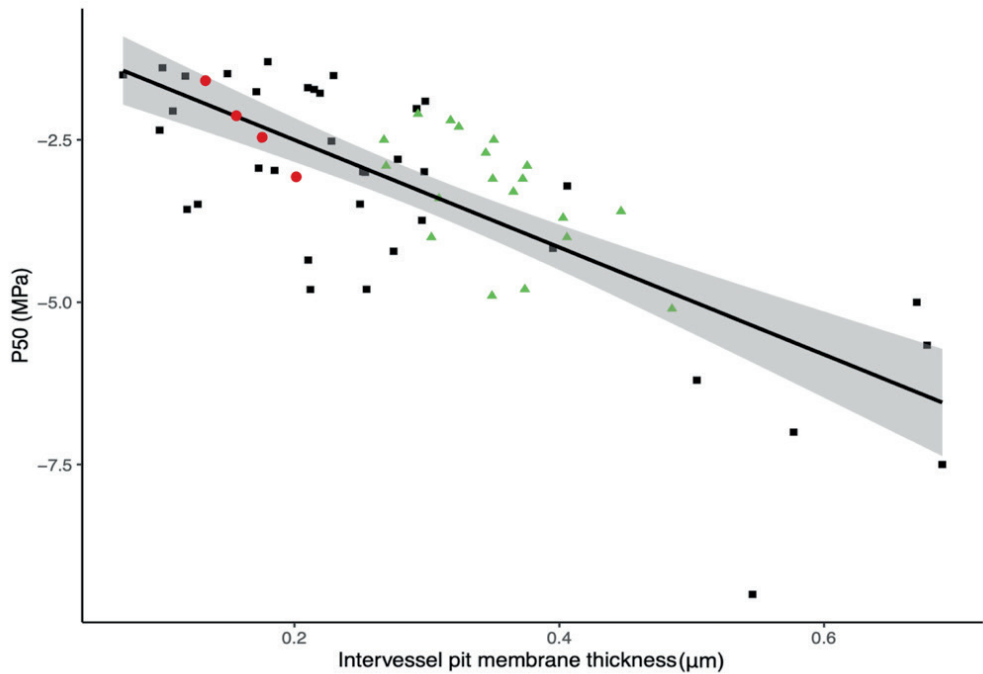


**Figure S4** Scatter plot with regression line showing the relationship between  $P_{50}$  and intervessel pit membrane thickness ( $T_{PM}$ ) of published woody and herbaceous angiosperms from Li *et al.* (2016; woody species marked as black-filled squares), Dória *et al.* (2018, 2019; mostly herbaceous species marked as green-filled triangles), and this study (red-filled circles).

## Chapter 2: Intervessel pit membrane thickness and embolism resistance

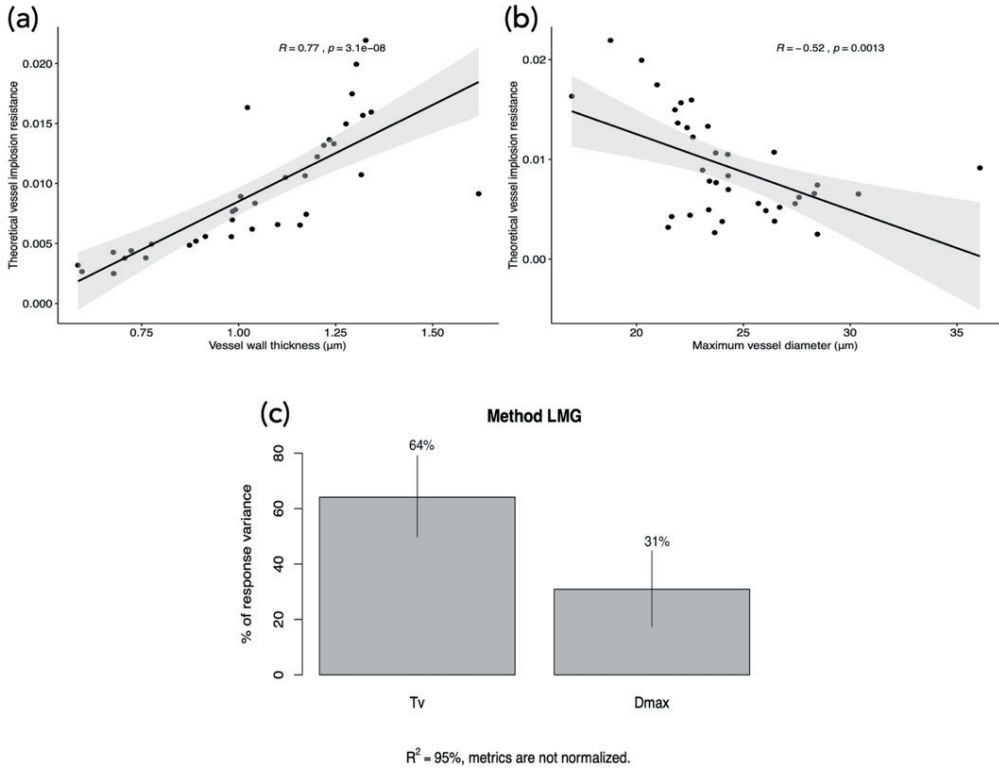


**Figure S5** Scatter plots with regression lines showing the relationship between (a) theoretical vessel implosion resistance ( $(T_{VW}/D_{MAX})^2$ ) and vessel wall thickness ( $T_V$ ), and (b) theoretical vessel implosion resistance ( $(T_{VW}/D_{MAX})^2$ ) and maximum vessel lumen diameter ( $D_{MAX}$ ); (c) the relative importance of theoretical vessel implosion resistance variation is mainly explained by vessel wall thickness ( $T_V$ ) based on  $R^2$  contribution averaged over orderings among regressors.



## Chapter 3

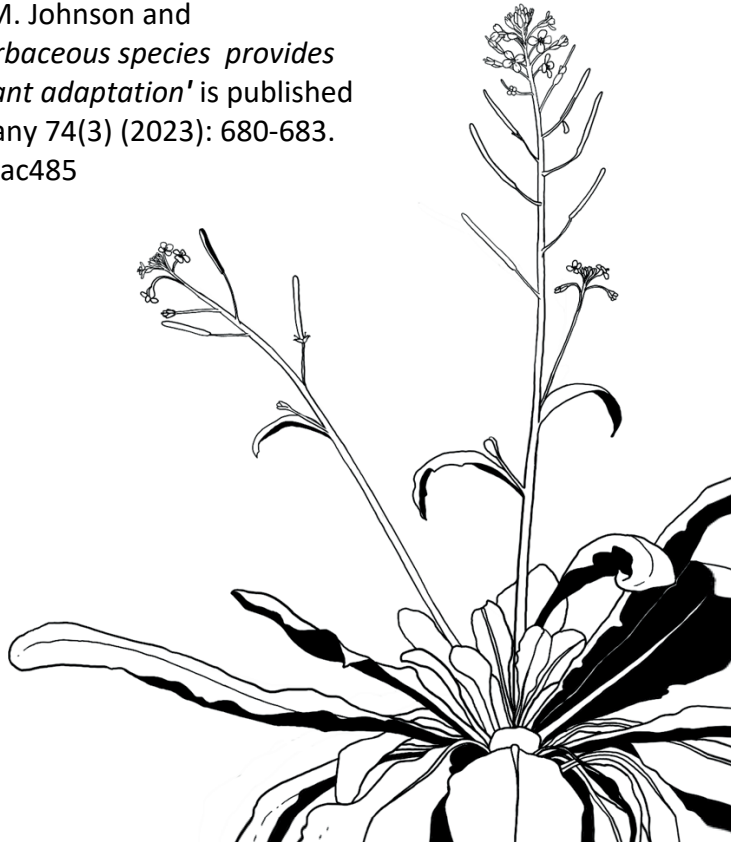
# Drought response in *Arabidopsis* displays synergistic coordination between stems and leaves

Ajaree Thonglim<sup>1,\*</sup>, Giovanni Bortolami<sup>1</sup>, Sylvain Delzon<sup>2</sup>, Maximilian Larter<sup>2</sup>, Remko Offringa<sup>3</sup>, Joost J.B. Keurentjes<sup>4</sup>, Erik Smets<sup>1,5</sup>, Salma Balazadeh<sup>6,†</sup> and Frederic Lens<sup>1,5,†,\*</sup>

*Adapted from*

**Journal of Experimental Botany** 74(3) (2023s, first published online in 2022): 1004-1021.  
<https://doi.org/10.1093/jxb/erac446>

A commentary paper by Kate M. Johnson and Leila R. Fletcher, entitled '*A herbaceous species provides insights into drought-driven plant adaptation*' is published in *Journal of Experimental Botany* 74(3) (2023): 680-683.  
<https://doi.org/10.1093/jxb/erac485>



<sup>1</sup> Naturalis Biodiversity Center, Research Group Functional Traits, PO Box 9517, 2300 RA Leiden, The Netherlands

<sup>2</sup> BIOGECO INRA, Université Bordeaux, 33615 Pessac, France

<sup>3</sup> Leiden University, Institute of Biology Leiden, Plant Developmental Genetics, Sylviusweg 72, 2333 BE Leiden, The Netherlands

<sup>4</sup> Laboratory of Genetics, Wageningen University, Droevendaalsesteeg 1, 6708 PB Wageningen, The Netherlands

<sup>5</sup> Leiden University, Institute of Biology Leiden, Plant Sciences, Sylviusweg 72, 2333 BE Leiden, The Netherlands

<sup>6</sup> Leiden University, Institute of Biology Leiden, Molecular Plant Stress Biology, Sylviusweg 72, 2333 BE Leiden, The Netherlands

\*For correspondence. E-mail [ajaree.thonglim@naturalis.nl](mailto:ajaree.thonglim@naturalis.nl) and [Frederic.lens@naturalis.nl](mailto:Frederic.lens@naturalis.nl)

†Shared last author

## Abstract

The synergy between drought-responsive traits across different organs is crucial in the whole-plant mechanism influencing drought resilience. These organ interactions, however, are poorly understood, limiting our understanding of drought response strategies at the whole-plant level. Therefore, we need more integrative studies, especially on herbaceous species that represent many important food crops but remain underexplored in their drought response. We investigated inflorescence stems and rosette leaves of six *Arabidopsis thaliana* genotypes with contrasting drought tolerance and combined anatomical observations with hydraulic measurements and gene expression studies to assess differences in drought response. The *soc1ful* double mutant was the most drought-tolerant genotype based on its synergistic combination of low stomatal conductance, largest stomatal safety margin, more stable leaf water potential during non-watering, reduced transcript levels of drought stress marker genes, and reduced loss of chlorophyll content in leaves, in combination with stems showing the highest embolism resistance, most pronounced lignification, and thickest intervessel pit membranes. In contrast, the most sensitive Cvi ecotype shows the opposite extreme of the same set of traits. The remaining four genotypes show variations in this drought syndrome. Our results reveal that anatomical, ecophysiological, and molecular adaptations across organs are intertwined, and multiple (differentially combined) strategies can be applied to acquire a certain level of drought tolerance.

**Keywords:** *Arabidopsis thaliana*, chlorophyll content, drought response, embolism resistance, gene expression, intervessel pit membrane thickness, stem anatomy, stomatal control.

## Introduction

The increasing intensity and frequency of drought episodes are becoming major threats to current and future agricultural productivity around the globe. Even the countries that had not experienced drought stress during the last decades are now impacted by drought (Corso *et al.*, 2020; Gleason *et al.*, 2022). One of the major problems that plants experience when they are facing severe drought is that detrimental levels of drought-induced gas bubbles (embolisms) in the xylem sap generate massive obstruction of the root to shoot water transport (Sperry and Tyree, 1988; Tyree and Zimmermann, 2002; Cochard, 2006; Choat *et al.*, 2012; Venturas *et al.*, 2017; Johnson *et al.*, 2022), which happens after stomata are closed (Martin-StPaul *et al.*, 2017). Stomatal closure may result in reduced photosynthetic productivity, growth rate, and reproduction, and under conditions of intense and prolonged drought may eventually cause desiccation and dieback of tissues (Mantova *et al.*, 2022), organs, and entire plants (Davis *et al.*, 2002; Venturas *et al.*, 2016; Pratt *et al.*, 2020; Brodribb *et al.*, 2021). Lethal levels of embolism, from which plants are unable to recover, are thought to be reached when the hydraulic conductivity is reduced to ~88% of its maximum conductance ( $P_{88}$ ) (Urli *et al.*, 2013; Li *et al.*, 2015; but see Hammond *et al.*, 2019; Johnson *et al.*, 2021), although there are probably more accurate thresholds to drought-induced mortality than  $P_{88}$  (Mantova *et al.*, 2021, 2022). Due to the implications of dramatic levels of drought-induced embolism on productivity, tissue death, and long-term survival, there is increasing evidence that natural selection has shaped the hydraulic systems of plants to minimize embolism occurrence and water potential loss during periods of water shortage (Lens *et al.*, 2022). This can be made possible when many drought-related traits from different organs act in concert (Dayer *et al.*, 2022).

As an example, angiosperms can build more resistant xylem by modifying a whole array of xylem anatomical adaptations to prevent the spread of embolisms, such as fine-scale modifications of pits in vessel walls allowing lateral transport of water and gas between adjacent vessels (Lens *et al.*, 2011; Li *et al.*, 2016; Kaack *et al.*, 2019, 2021; Levionnois *et al.*, 2021), or increased levels of lignification (Lens *et al.*, 2013, 2016; Thonglim *et al.*, 2021). In addition, plants can also delay xylem sap pressures from reaching critical embolism thresholds throughout the whole-plant body by producing



the stress hormone abscisic acid (ABA) that induces stomatal closure in the leaves very rapidly at the onset of drought, well before embolism events start to exponentially increase (Brodribb *et al.*, 2017; Martin-StPaul *et al.*, 2017; Buckley, 2019; Creek *et al.*, 2020). Consequently, stomatal closure is one of the primary responses that helps restrict water loss, which safeguards the water potential in the leaves and buffers the negative pressure in xylem sap (Brodribb *et al.*, 2017; Martínez-Vilalta and Garcia-Forner, 2017; Martin-StPaul *et al.*, 2017; Knipfer *et al.*, 2020). The regulation of water potential in leaves during drought is crucial because it influences plant metabolic processes. However, declining transpiration rates reduce not only water loss but also carbon uptake, leading to decreased photosynthetic activity, which ultimately may lead to carbon starvation when stomata remain closed for a long time (McDowell *et al.*, 2008). In other words, the interplay between embolism resistance inside the plant's xylem and the onset and duration of stomatal closure at the level of leaves will determine how long leaves can remain metabolically active without risk of detrimental levels of drought-induced embolism (Allen *et al.*, 2010; Choat *et al.*, 2012; Mitchell *et al.*, 2013; Brodribb *et al.*, 2017; Martínez-Vilalta and Garcia-Forner, 2017; Buckley, 2019; Creek *et al.*, 2020; Limousin *et al.*, 2022). Accordingly, the stomatal safety margin (SSM), which can be defined as the difference between the water potential at stomatal closure ( $\Psi_{gs90}$ ) and the pressure inducing 50% loss of hydraulic conductance ( $P_{50}$ ) is physiologically more important to estimate a plant's ability to cope with massive levels of drought-induced embolism than only  $P_{50}$  (Sperry and Tyree, 1988; Meinzer *et al.*, 2009; Anderegg *et al.*, 2016; Martin-StPaul *et al.*, 2017; Creek *et al.*, 2020; Dayer *et al.*, 2020; Skelton *et al.*, 2021). It is widely accepted that species with a narrower safety margin are operating more closely to their hydraulic threshold, while species that have a wider safety margin have a lower risk of facing a detrimental level of drought-induced embolism (Choat *et al.*, 2012; Anderegg *et al.*, 2016; Martin-StPaul *et al.*, 2017; Eller *et al.*, 2018; Creek *et al.*, 2020; Oliveira *et al.*, 2021; Skelton *et al.*, 2021).

It is clear that anatomical and physiological traits need to be intertwined within and among organs, but the molecular mechanisms cross-linking different pathways remain elusive. For instance, there is increasing evidence from gene expression studies confirming the positive correlation between lignification and drought resilience in a whole range of species (Tu *et al.*, 2020; Xu *et al.*, 2020; Wen *et al.*, 2021; Yan *et al.*, 2021; Hou *et al.*,

2022; Li *et al.*, 2022). Regarding drought responses in plants, the ABA-mediated signalling pathway is probably the best-known pathway at the molecular level. ABA regulates the expression of stress-responsive genes via transcription factors (Bauerle *et al.*, 2004; Cutler *et al.*, 2010; Bauer *et al.*, 2013; Dodd, 2013; Mehrotra *et al.*, 2014; Chen *et al.*, 2020). Once ABA is accumulated, it regulates ABA-responsive genes via the *cis*-element called ABRE (ABA-responsive element) in their promoter regions using AREB (ABRE binding) transcription factors (Choi *et al.*, 2000; Uno *et al.*, 2000; Yoshida *et al.*, 2015; Chen *et al.*, 2020). In *Arabidopsis*, *AREB1* is mainly expressed in vegetative tissues and up-regulated during drought (Yoshida *et al.*, 2010; Fujita *et al.*, 2011, 2013; Singh and Laxmi, 2015; Chen *et al.*, 2020). Other drought-responsive genes are regulated by dehydration-responsive element-binding (DREB) proteins through an ABA-independent pathway (Bartels and Sunkar, 2005; Sakuma *et al.*, 2006; Song *et al.*, 2018). For example, DREB2 transcription factors are induced by dehydration and are involved in gene transcription under water shortage (Agarwal *et al.*, 2006; Song *et al.*, 2018). Interestingly, many stress-inducible genes contain both ABREs and DREs in their promoter regions, such as *Responsive to Desiccation 29 (RD29)* (Shinozaki and Yamaguchi-Shinozaki, 2007). Hence, gene expression of drought-responsive genes occurs via ABA-dependent and/or ABA-independent signal transduction pathways (Umezawa *et al.*, 2010; Rushton *et al.*, 2012; Song *et al.*, 2016), and allows us to evaluate the expression of drought-responsive genes during a drought experiment with a simultaneous assessment of physiological and anatomical traits involved in drought tolerance.

Most studies investigating drought-induced embolism in plants have been focusing on trees, while herbaceous plants have been largely ignored despite their importance as crops and food sources for humans and animals (Brodribb and Hill, 1999; Stiller and Sperry, 2002; Holloway-Phillips and Brodribb, 2011; Choat *et al.*, 2012; Ahmad, 2016; Lens *et al.*, 2016; Volaire *et al.*, 2018). In our previous study on the herbaceous model species, *Arabidopsis thaliana*, including genotypes with contrasting levels of embolism resistance and lignification in the inflorescence stems (Thonglim *et al.*, 2021), we found that the more lignified genotypes are more resistant to embolism and have thicker intervessel pit membranes. Surprisingly, in most structure–function studies published so far, the drought response is only partly observed due to methodological and time constraints. For

instance, resistance to embolism in branches/twigs is often recorded in xylem physiological studies (e.g. Choat *et al.*, 2012; Anderegg *et al.*, 2016), and less frequently integrated with leaf  $P_{50}$  data (e.g. Cochard *et al.*, 2004; Klepsch *et al.*, 2018; Skelton *et al.*, 2019; Levionnois *et al.*, 2021) and/or root  $P_{50}$  data (e.g. Rodriguez-Dominguez *et al.*, 2018), and sometimes linked with other leaf physiological traits such as stomatal conductance ( $g_s$ ) and water potential (e.g. Brodribb *et al.*, 2003; Li *et al.*, 2015; Cardoso *et al.*, 2018; Charrier *et al.*, 2018; Creek *et al.*, 2020; Chen *et al.*, 2021). Only occasionally are detailed hydraulic measurements in stems, leaves, and/or roots complemented with detailed anatomical traits on intervessel pits (Guan *et al.*, 2022). Other papers only focus on the molecular pathway and gene regulation during drought (e.g. Bhargava and Sawant, 2013; Pandey *et al.*, 2013; Janiak *et al.*, 2016; Ebrahimian-Motlagh *et al.*, 2017; Thirumalaikumar *et al.*, 2018; Roca-Paixão *et al.*, 2019; Zhang *et al.*, 2019), while publications that integrate gene function with xylem physiology are scarce (e.g. Kitin *et al.*, 2010; Lamarque *et al.*, 2020). Integration of drought-related traits across organs in structure–function studies and intensive collaboration among plant anatomists, xylem physiologists, and molecular biologists will help us to make considerable progress in a holistic understanding of drought response at the whole-plant level. To contribute to that whole-plant approach, we measured hydraulic traits in stems and leaves during a drought experiment, combined with detailed stem anatomical measurements and an assessment of transcript levels of drought stress marker genes across *Arabidopsis* genotypes (two transgenic lines and four natural accessions).

In this study, we investigate the following two questions. (i) Is there a coupling between drought-related stem (anatomy,  $P_{50}$ ) and leaf traits (stomatal regulation, leaf water potential, expression of drought marker genes) among *Arabidopsis* genotypes? (ii) Can these genotypes use different combinations of drought-response traits to reach a certain level of drought tolerance? To answer these questions, we investigated six genotypes with marked differences in embolism resistance and lignification of the inflorescence stems. We examined the detailed stem anatomical traits and hydraulic traits (stem  $P_{50}$ ) of each genotype and quantified the drought response for all six genotypes using a drought experiment, during which we measured  $g_s$  and leaf water potential ( $\psi_l$ ), allowing us to calculate the SSM (as defined by  $\psi_{g_s90}$  minus  $P_{50}$ ). In addition, we compared the expression of

four drought-responsive genes from the ABA-(in)dependent (*ABI2*, *AREB1*, *RD29A*, and *DREB2A*) pathways from the rosette leaves at the end of the drought experiment to validate the level of drought stress among the six genotypes. By integrating all traits mentioned above, we want to assess how anatomical and ecophysiological traits across organs are intertwined to acquire a certain level of drought tolerance, and how these traits relate to the drought stress level at the end of the drought experiment based on a limited number of drought stress marker genes.

## Materials and methods

### *Plant material*

In addition to the four *A. thaliana* genotypes with contrasting levels of stem  $P_{50}$  and stem lignification, we studied before the ecotypes Columbia-0 (Col-0; wild type with intermediate stem lignification), Shadarah (Sha; wild type with a higher level of stem lignification), Cape Verde Islands (Cvi; least lignified wild type), and the double loss-of-function mutant *SUPPRESSOR OF OVEREXPRESSION OF CONSTANS 1* and *FRUITFULL* (*soc1ful*; most lignified genotype) (see Thonglim *et al.*, 2021); we added one more wild type [Kelsterbach-4 Kel-4] and a *p35S:AHL15* line (*AHL15* overexpression) in the Col-0 background (Rahimi *et al.*, 2022). The two additional genotypes were selected based on their inflorescence length (at least 27 cm required for the centrifuge method used to estimate embolism resistance measurements) and their increased lignification in the basal parts of the inflorescence stem, respectively (Supplementary Figures S1A, B, G, H). Indeed, Kel-4, an early flowering ecotype from Germany, shows a relatively high proportion of lignification at the base of the inflorescence stem (Ak, 2020), and has been reported to be more drought tolerant compared with many other wild-type accessions (Bac-Molenaar *et al.*, 2016; Kooke *et al.*, 2016). The *AT-HOOK MOTIF CONTAINING NUCLEAR LOCALIZED 15* (*AHL15*) gene has been found to suppress axillary meristem maturation, and its overexpression extends plant longevity (Karami *et al.*, 2021), and promotes secondary growth in the inflorescence stem to a similar extent as the *soc1ful* mutant (Rahimi *et al.*, 2022).

## **Growing conditions**

The plants were grown at the Institute of Biology Leiden (Leiden University, The Netherlands) under the same controlled conditions as in Thonglim *et al.* (2020) to ensure comparable datasets. Briefly, we germinated the two additional genotypes from seeds directly into a mixture of soil and sand (4.5:1). After 10 d of germination, the healthy seedlings were transferred into pots. Plants were grown in a controlled growth chamber with the following parameters: 20 °C temperature during the day and 17 °C temperature at night, 70% relative humidity, and 16 h photoperiod condition with 100  $\mu\text{mol m}^{-2} \text{s}^{-1}$  light intensity. Sampling was synchronized based on differences in flowering time and subsequent inflorescence development. To synchronize flowering, *p35S:AHL15* plants were planted earlier (harvesting inflorescence stems 85 d after sowing). The *Kel-4* individuals were planted slightly later (harvesting inflorescence stems 65 d after sowing) (Supplementary Figure S1A, B).

## **Drought experiment**

A drought experiment was performed to assess the link between the anatomical and hydraulic traits and investigate the differences in drought tolerance across the six *A. thaliana* genotypes studied. The six genotypes were selected based on a previous screening of drought tolerance and the differences in stem lignification (Melzer *et al.*, 2008; Bac-Molenaar *et al.*, 2016; Thoen *et al.*, 2017; Thonglim *et al.*, 2021). The seeds of each genotype were directly sown in 6 cm pots (27 g) with the same amount of soil and sand mixture (4.5:1) at different times to synchronize flowering. The weight of the pot with dry and saturated soil was controlled (807 g and 1097 g, respectively). The pots were kept in a growth-controlled chamber under the same conditions as the individuals grown for stem  $P_{50}$  measurements. After germination, when seedlings were 10 d old, they were thinned to one healthy seedling per pot and remained well watered. We equally divided 30 individuals of each genotype into a control and a drought batch during the experiment. The control plants were well irrigated every day to keep the soil constantly hydrated ( $\psi_i$  was around  $-0.5$  MPa to  $-0.6$  MPa). The drought batch was subjected to water deficit by completely withholding watering for 3 weeks ( $\psi_i$  values ranged between  $-1.85$  MPa to  $-3.4$  MPa among genotypes), starting 1 week before all the genotypes began to flower. When

most genotypes started developing an inflorescence stem (7 d after watering was stopped), drought measurements were initiated. Rosette leaves were harvested on the last day of the drought experiment (depending on the water potential and phenotype), immediately frozen in liquid nitrogen, and stored in a  $-80\text{ }^{\circ}\text{C}$  freezer for further gene expression and chlorophyll analyses. We initially intended to have three biological replicates per genotype. However, during sample preparation, some tubes containing ground leaf material popped open in the freezer. We assume that some liquid nitrogen used for grinding the samples was still left in the tubes, causing several closed tubes to burst open and potentially contaminate the other open tubes containing different genotypes. We opted to discard all the open tubes due to potential contamination and use only the closed tubes. We were able to still use three biological replicates for Cvi, Sha, and *soc1ful*, but only two for Col-0, Kel-4, and *p35S:AHL15*. For the latter genotypes, we included two biological and two technical replicates.

### ***Chlorophyll content***

Chlorophyll content was determined based on three biological replications for Cvi, Sha, and *soc1ful*, and four replicates (two biological and two technical) for Col-0, Kel-4, and *p35S:AHL15*, using the 80% acetone method (Porra *et al.*, 1989). Ground leaf samples of  $\sim 0.5$  mg was transferred into 1.5 ml tubes containing 1 ml of 80% acetone. The mixtures were gently vibrated using a vortex to extract chlorophyll and centrifuged at 1000 *g* for 5 min to remove debris. The supernatants (800  $\mu\text{l}$ ) were then transferred to UV-transparent microplates. The absorbance was measured at 647 nm ( $A_{647}$ ), 664 nm ( $A_{664}$ ), and 750 nm ( $A_{750}$ ) using the DMF-chl conc.\_YU program. Chl *a* and *b* contents ( $\mu\text{g Chl ml}^{-1}$ ) in the extract were calculated with the following formulas:

$$\text{Chl } a = (12.25 \times (A_{664} - A_{750}) - 2.85 \times (A_{647} - A_{750})) / 0.29$$

$$\text{Chl } b = (20.31 \times (A_{647} - A_{750}) - 4.91 \times (A_{664} - A_{750})) / 0.29$$

$$\text{Total Chl } (a + b) = (17.76 \times (A_{647} - A_{750}) + 7.34 \times (A_{664} - A_{750})) / 0.2$$

### **RNA isolation and qRT-PCR**

Total RNA was extracted using the RNeasy Plant Mini kit (Qiagen, Hilden, Germany). Synthesis of cDNA, quantitative reverse transcription-PCR (qRT-PCR) using SYBR Green, and data analysis were performed as previously described (Balazadeh *et al.*, 2008). Gene expression was normalized with two reference genes (*ACTIN2* and *GADPH*). qRT-PCR primers were designed using QuantPrime ([www.quantprime.de](http://www.quantprime.de)) (Arvidsson *et al.*, 2008). Primer sequences are given in Supplementary Table S1. Experiments were conducted in three biological replications for Cvi, Sha, and *soc1ful*, and two biological replicates with two technical replicates for Col-0, Kel-4, and *p35S:AHL15*.

### **Leaf water potential ( $\Psi_l$ ) and stomatal conductance ( $g_s$ )**

After 7 d of water deficit (i.e., the time required to dehydrate the moisturized soil in the pots of the drought batch),  $\Psi_l$  was measured in both control and drought batches every day during the drought period until harvesting (15–17 d). The daily measurements were carried out using three mature leaves (one from control and two from drought treatment) for each method. Before the measurements, the leaves were covered with aluminium foil for 30 min. Subsequently, leaf discs were cut from the bagged leaves and placed in the PSYPRO leaf water potential system (Wescor, Inc., Logan, UT, USA) to measure the leaf water potential. At the same time,  $g_s$  ( $\text{mmol H}_2\text{O m}^{-2} \text{s}^{-1}$ ) was measured on single mature rosette leaves that were close to the leaves used for water potential measurements, using an SC-1 leaf porometer (METER Group, Pullman, WA, USA) that was calibrated every other day. The  $g_s$  was measured using Auto Mode configuration with desiccant.  $g_s$ , depending on leaf water potential, was fit according to the following sigmoid function for each genotype using the NLIN procedure in SAS:

$$g_s = g_{sm} \div [1 + \exp(S \times (\Psi - \Psi_{gs50}))]$$

$g_{sm}$  is the maximal stomatal conductance for  $\Psi_l=0$ ,  $S$  is the slope of the curve, and  $\Psi_{gs50}$  the water potential inducing 50% stomatal closure. We then estimated the water potential inducing 90% of the stomatal closure ( $\Psi_{gs90}$ ).

## ***Stomatal safety margin (SSM)***

The SSM was defined as the difference between the leaf water potential at 90% stomatal closure (Martin-StPaul *et al.*, 2017) calculated from the fitted curve ( $\Psi_{gs90}$ ) and the water potential at 50% loss of stem conductivity ( $P_{50}$ ):

$$SSM = \Psi_{gs90} - P_{50}$$

## ***Generating vulnerability curves (VCs) in stems***

### *Sample preparation of inflorescence stems*

All individuals (80 individuals per genotype) were harvested at the Institute of Biology Leiden with roots, leaves, and flowers still attached and immediately wrapped in wet tissue papers. They were then enclosed in plastic bags to avoid dehydration during the shipment to the PHENOBOIS platform (INRAE, University of Bordeaux, France), where the Cavitron centrifuge measurements were performed. Before the Cavitron measurements, the roots were cut off at the basal part of inflorescence stems and trimmed on both sides, obtaining a stem segment of 27 cm in length that matches a standard Cavitron rotor. The length of the stem segments exceeds by far the maximum vessel length of Col-0, reaching only 4 cm according to Tixier *et al.* (2013) to avoid potential open-vessel artefacts (Cochard *et al.*, 2013). Next, all siliques, leaves, and flowers were removed underwater immediately before placing the inflorescence stems in the Cavitron rotor (7–9 stem segments per VC).

Xylem vulnerability to embolism was evaluated using the Cavitron method, a custom-built centrifuge that allows measuring the water flow through the inflorescence stems while spinning them to create a negative pressure in the middle part of the stem segments (Cochard, 2002; Cochard *et al.*, 2005, 2013). The negative pressure was gradually increased in each spinning step, as described in Thonglim *et al.* (2020). The degree of embolism in the xylem segment was quantified as the percentage loss of conductivity (PLC), calculated as follows:

$$PLC = 100 \times (1 - (K/K_{MAX}))$$



where  $K_{MAX}$  ( $m^2 MPa^{-1} s^{-1}$ ) is the maximum hydraulic conductivity which was calculated when stem segments were fully functioning (no embolism) at low spinning speed (near 0 MPa), and  $K$  is the decreased hydraulic conductivity due to embolisms. The extent of embolism formation at every rotation speed was measured using the Cavisoft software (Cavisoft v1.5, University of Bordeaux, France). We fitted the data points to reconstruct the VCs using a sigmoid function based on the NLIN procedure in SAS 9.4 (SAS Institute, Cary, NC, USA) (Pammenter and Van der Willigen, 1998):

$$PLC = 100 \div \left[ 1 + \exp \left( \frac{S}{25} \times (P - P_{50}) \right) \right]$$

where  $P$  is the xylem pressure used at each rotation step,  $P_{50}$  is xylem pressure inducing 50% loss of hydraulic conductivity, and  $S$  ( $MPa^{-1}$ ) is the slope of the VC at  $P_{50}$ . Due to the low hydraulic conductivity of *Arabidopsis*, we measured vulnerability to embolism of 7–9 inflorescence stems to generate one vulnerability curve. Eight VCs were constructed for each genotype.

### **Stem anatomy**

Three stems from three representative VCs per genotype (nine stems per genotype) were randomly selected for light microscopy (LM) observations and one stem per VC from three VCs (three individuals per genotype) for TEM observations (Supplementary Figure S1C, D). Both basal and central parts of the 27 cm inflorescence stem segments were sectioned because they differ in the amount of lignification (Supplementary Figure S1E–H). We, however, invested more time in measuring trait data from the middle part than in the basal segment because that is the region where the negative pressures were applied during the Cavitron experiments, allowing us to accurately link the anatomical traits with embolism resistance ( $P_{50}$ ). The anatomical traits are represented in Supplementary Table S2. ImageJ (National Institutes of Health, Bethesda, MD, USA) was used, and the guidance of Scholz et al. (2013a) was followed to measure the anatomical features in digital images from both LM and TEM observations.

### *Light microscopy (LM)*

Inflorescence stems were cut into 1 cm long pieces and submerged in 70% ethanol. The samples were then gradually infiltrated in LR-white resin (Hamann *et al.*, 2011). After embedding in LR-white, specimens were sectioned with a rotary microtome (Leica RM 2265, Leica, Eisenmark, Wetzlar, Germany) with disposable tungsten carbon blades at 4  $\mu\text{m}$  thickness. Next, the sections were heat-fixed onto the slides, stained with 1% (w/v) toluidine blue (VWR Chemicals BDH<sup>®</sup>, Radnor, PA, USA), and mounted with DPX new-100579 mounting medium (Merck Chemicals, Amsterdam, the Netherlands). Finally, various anatomical traits (Supplementary Table S2) were observed using a Leica DM2500 light microscope equipped with a Leica DFC-425 digital camera (Leica microscopes, Wetzlar, Germany).

### *Transmission electron microscopy (TEM)*

The middle parts of inflorescence stem segments were collected immediately after Cavitron measurements and fixed in Karnovsky's fixative (Karnovsky, 1965). Subsequently, the samples were washed in 0.1 M cacodylate buffer and post-fixed with 1% buffered osmium tetroxide. The samples were then prepared for semi-thin and ultra-thin sectioning according to the protocol described in Thonglim *et al.* (2020) and were observed with a JEM-1400 Plus TEM (JEOL, Tokyo, Japan) with an 11 megapixel digital camera (Quemesa, Olympus). TEM observations were conducted to measure the intervessel pit membrane thickness and the pit chamber depth (Supplementary Table S2).

## **Statistical analysis**

R version 3.6.3 in R Studio version 1.2.5033 was used for the statistical analyses of all traits studied, of which all the differences were considered significant when the  $P$ -value was  $<0.05$ . First, general linear models with a Newman–Keuls post-hoc test were used to check the differences in embolism resistance ( $P_{50}$ ,  $P_{12}$ , and  $P_{88}$ ), anatomical features, leaf physiological traits, chlorophyll content, and gene expression among *Arabidopsis* genotypes studied. Then, multiple linear regression was applied to assess the anatomical traits (predictive variables) that explain the differences in embolism resistance (responsive variables, including  $P_{50}$ ,  $P_{12}$ , and  $P_{88}$ ). The collinearity between variables was firstly checked to select the predictors. Then, the ‘step’ function (stats package; R Core Team, 2016) was applied to achieve the most parsimonious linear regression model based on the least Akaike information criterion (AIC). Subsequently, the model’s residuals, heteroscedasticity, skewness and kurtosis, and variance inflation factor (VIF) were checked. Once we obtained the best model, the relative importance of each explanatory variable was analysed to assess the variable that explains the best  $P_{50}$ . Pearson’s correlation was applied to plot the relationship between  $P_{50}$  and predictive variables and leaf physiological traits, and among the variables. Lastly, we investigated whether the different *Arabidopsis* genotypes presented different  $g_s$  in well-watered control conditions using a generalized linear mixed model with the accession as a fixed effect, with the GLIMMIX procedure in SAS software (SAS 9.4; SAS Institute).

## **Gene codes**

*Arabidopsis* gene codes are: *ACTIN2*, *AT3G18780*; *GAPDH*, *AT1G13440*; *RD29A*, *AT5G52310*; *ABI2*, *AT5G57050*; *AREB1*, *AT1G45249*; and *DREB2A*, *AT5G05410*.

## Results

### ***Drought-response phenotyping, chlorophyll content, and expression of drought-responsive genes in the basal rosette leaves***

After 3 weeks of non-watering, we found differences in phenotypes of the drought-treated batch compared with the well-watered controls. The *soc1ful* mutant and the *p35S: AHL15* overexpression line were least affected by drought based on the rosette phenotype (less wilting of leaves, less reduction of rosette size) and the small reduction of chlorophyll content when compared with the control individuals. The droughted individuals of Sha showed intermediate phenotypic drought stress-related signs compared with the control batch, such as a minor reduction in leaf rosette size, more wilting of leaves, and a slightly higher decrease of chlorophyll content (Figure 1A, B). In contrast, the rosette leaves were more reduced in size in the droughted individuals of Col-0, Kel-4, and Cvi compared with the well-watered control plants (Figure 1A); likewise, leaves and inflorescence stems in the droughted batch of these three genotypes were considerably more wilted compared with the control plants (Figure 1A), along with the stronger chlorophyll reduction in the rosette leaves (Figure 1B). With regards to Chl *b* reduction during the drought experiment, two significantly different genotype groups could be defined: one group comprising Col-0, Cvi, and Kel-4 (62%, 67% and 46% reduction, respectively) and the other comprising Sha, *soc1ful*, and *p35S: AHL15* (31, 13, and 27% reduction, respectively) ( $F=15.83$ ,  $P=0.00212$ ). For Chl *a* reduction, significant differences were detected among the genotypes ( $F=181.6$ ,  $P=1.84e^{-06}$ ), except for *soc1ful* and *p35S: AHL15* that presented a similar reduced value (10% and 12% reduction). This is also the case for total chlorophyll (Chl *a+b*) reduction ( $F=168.1$ ,  $P=2.32e^{-06}$ ) (Figure 1B).

In order to estimate how each *Arabidopsis* genotype senses drought stress at the molecular level, we measured the expression of four selected drought marker genes at the end of the 15–17 d drought treatment. In the ecotypes with an intermediate level of stem lignification (Col-0 and Kel-4) and the one with the least lignified stems (Cvi), all four drought-responsive genes were up-regulated under drought compared with well-watered conditions (Figure 1C). In contrast, of the four drought-response genes in the more lignified genotypes Sha, overexpression *p35S: AHL15*, and *soc1ful*

were significantly less induced under drought treatment. Interestingly, *p35S: AHL15* showed no difference in *ABI2* and *AREB1* expression level between drought and control conditions ( $-0.45$  and  $-1.37$  log<sub>2</sub> fold change, respectively). Regarding the changes in the expression of each gene between drought and control conditions among genotypes studied, we found that the change of *RD29A* expression was similar between Col-0 and Cvi ( $\sim 6.9$  log<sub>2</sub> fold change). Still, these two genotypes were significantly different from the rest ( $2.8$ – $4.7$  log<sub>2</sub> fold change) ( $F=10.2$ ,  $P=0.00021$ ). For *DREB2A*, two significantly different groups were defined: one comprising Col-0, Cvi, and Kel-4 ( $4.55$ ,  $5.6$ , and  $5.57$ , respectively) and the other comprising Sha, *soc1ful*, and *p35S: AHL15* ( $3.37$ ,  $2.75$ , and  $2.87$ , respectively) ( $F=21.05$ ,  $P=2.71e^{-06}$ ). The changes of *AREB1* were significantly different among genotypes ( $F=13.28$ ,  $P=4.63e^{-05}$ ), except for Col-0, Cvi, and Kel-4 ( $3.48$ ,  $3.22$  and  $3.19$  log<sub>2</sub> fold change, respectively). Likewise, for *ABI2*, there was a significant difference among genotypes ( $F=40.95$ ,  $P=3.2e^{-08}$ ), except for Col-0 and Kel-4 ( $6.22$  and  $5.93$ ), and Sha and *soc1ful* ( $4.57$  and  $3.58$  log<sub>2</sub> fold change) (Figure 1C).

### **Leaf water potential ( $\Psi_l$ ) and stomatal conductance ( $g_s$ ) dynamics during drought**

$\Psi_l$  under well-watered conditions was similar in every genotype, ranging between  $-0.5$  MPa and  $-0.6$  MPa (Figure 2A). However,  $g_s$  of control plants was significantly different among the genotypes studied ( $F=236.12$ ,  $P<0.0001$ , Figure 2B). Cvi (least lignified wild type) had the highest  $g_s$  ( $384$  mmol m<sup>-2</sup> s<sup>-1</sup>), followed by Col-0, Sha, and Kel-4, while the more lignified *soc1ful* and *p35S: AHL15* genotypes presented the lowest  $g_s$  value (up to  $216$  mmol m<sup>-2</sup> s<sup>-1</sup>); only  $g_s$  values of Sha and Kel-4 were not statistically different from each other (Figure 2B). In addition, we noticed that Col-0 closed its stomata at a less negative leaf water potential compared with the other genotypes. It reached 90% of stomatal closure ( $g_{s90}$ ) at  $-0.9$  MPa, followed by Kel-4 ( $-1.13$  MPa), and the more lignified Sha ( $-1.27$  MPa), *soc1ful* ( $-1.43$  MPa), and *p35S: AHL15* ( $-1.6$  MPa). The least lignified Cvi reached more negative  $\Psi_l$ , even before closing its stomata ( $-1.75$  MPa; Figure 2A). When following stomatal conductance and leaf water potential decline during the drought experiment, we found that the lignified *soc1ful* and Sha genotypes never reached critical water potential values (i.e., the  $P_{50}$ ) even after 17 d of

drought, while other genotypes reached their respective  $P_{50}$  between 10 d and 14 d (Supplementary Figure S2A, B).

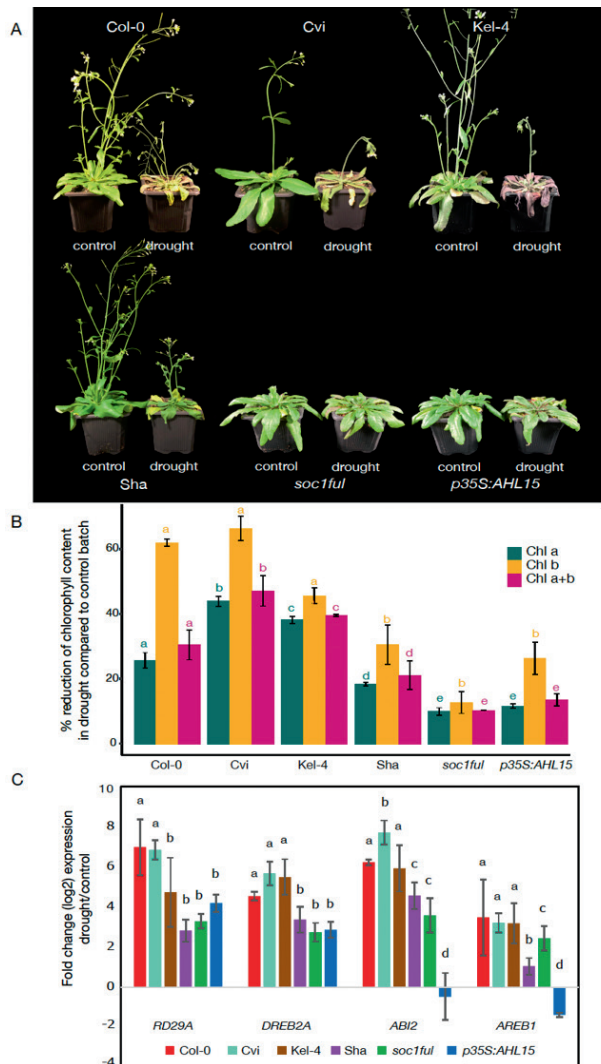


**Figure 1** (A) Phenotypic variation in response to drought. The phenotype of six *Arabidopsis* genotypes subjected to drought, by water withholding, after 3 weeks and their untreated counterparts. Nine plants per genotype and condition were analyzed, and representative images are shown. (B) The variation in chlorophyll contents (chlorophyll a, chlorophyll b, and chlorophyll a+b) among genotypes studied. The Y-axis represents the percent reduction of chlorophyll content in drought compared to the control batch. A student t-test was performed, showing the differences between each accession compared to Col-0. \*  $p$ -value < 0.05.

(C) qRT-PCR analysis of the expression of selected drought-responsive genes (RD29A, DREB2A, ABI2 and AREB1) in six *Arabidopsis* genotypes. The Y-axis represents the log<sub>2</sub> fold change of the gene expression between drought and control conditions. A student t-test was performed, showing the differences between each accession compared to Col-0. \* *p*-value < 0.05. Note: the genes are significantly less upregulated by drought in Sha, *p35S: AHL15*, and *soc1ful* plants.

### ***Stem vulnerability to embolism***

When comparing all six genotypes, the most lignified *soc1ful* was the most embolism resistant, with  $P_{50}$  of  $-3.07$  MPa (Figure 3; Table 1), whereas the least lignified Cvi remained the most vulnerable ( $P_{50} = -1.58$  MPa). For the two added genotypes, Kel-4 (wild type with intermediate lignified stems) was among the most vulnerable genotypes with  $P_{50} = -1.69$  MPa, whereas *p35S: AHL15* (overexpression line) was intermediate, almost identical to the common wild-type Col-0 with  $P_{50} = -2.13$  MPa. The  $P_{12}$  (stem water potential at onset of embolism) values of most of the genotypes studied were different from each other ( $F=420.6$ ;  $P < 2e^{-16}$ ), but Cvi and Kel-4 presented similar  $P_{12}$  ( $P=0.5424$ ). For  $P_{88}$ , *p35S: AHL15* and Kel-4 were different from other genotypes ( $F=75.09$ ;  $P < 2e^{-16}$ ) (Supplementary Figure S3). The slope of the vulnerability curve was similar across the genotypes, except Col-0, which had a lower slope (see Figure 3).

### ***Water potential and SSM during drought***

Assuming that leaf water potential values are similar to stem water potential values in the tiny *Arabidopsis* herbs, we calculated the SSM as the difference between  $\psi_{gs90}$  and  $P_{50}$ . The SSMs of all genotypes studied were positive (from  $+0.53$  MPa to  $+1.64$  MPa), except for the least lignified Cvi with a narrow and negative SSM ( $-0.17$  MPa) (Figure 4). Accordingly, Cvi also closed its stomata and reached a leaf water potential equivalent to  $P_{50}$  the soonest (10 d; Table 1). SSM was the widest in the most lignified *soc1ful* ( $+1.64$  MPa), followed by Col-0 and Sha ( $+1.24$  MPa and  $+1.22$  MPa, respectively; Table 1; Figure 4). Kel-4 and *p35S: AHL15* had intermediate SSMs ( $+0.56$  MPa and  $+0.53$  MPa, respectively).

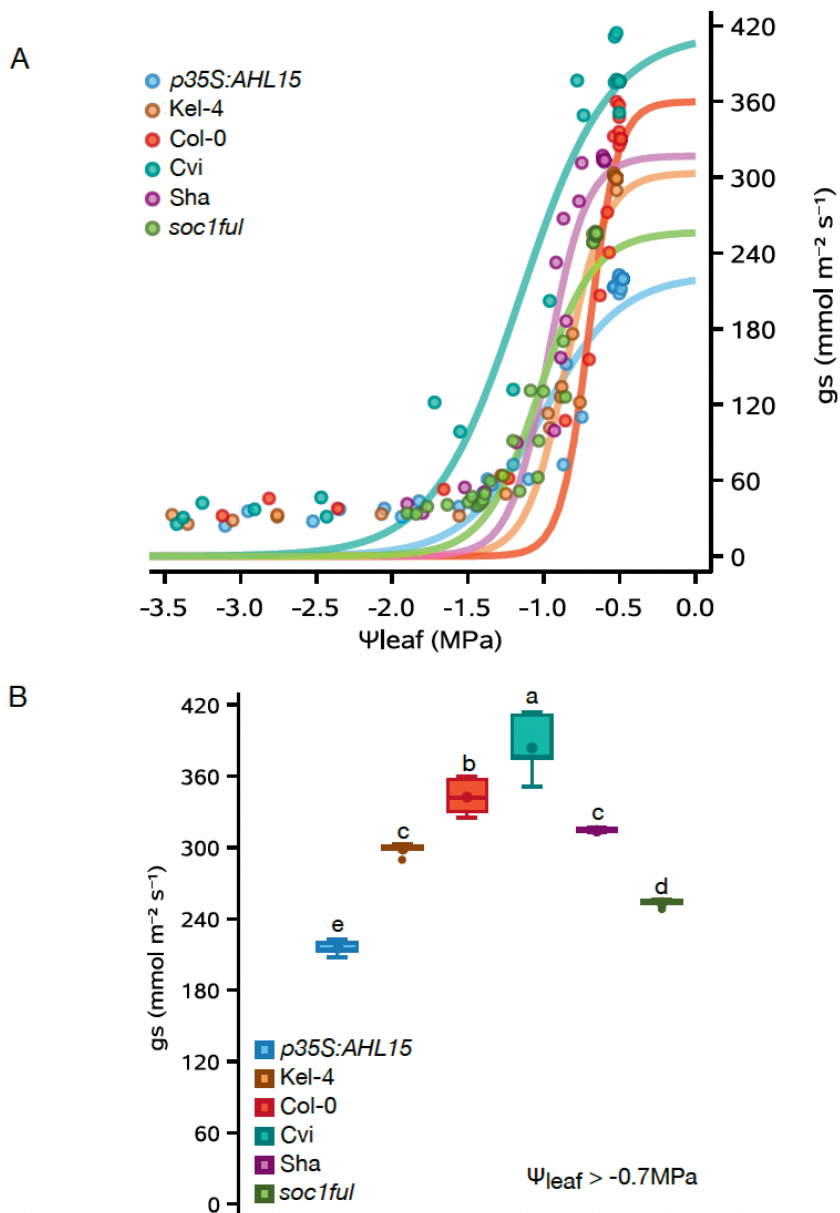


**Figure 2** Drought response traits for the six *A. thaliana* genotypes studied. (A) The relationship between leaf water potential ( $\Psi_l$ ) and stomatal conductance ( $g_s$ ). (B) Stomatal conductance ( $g_s$ ,  $\text{mmols}^{-1} \text{ m}^{-2}$ ) in control well-watered plants for the different *Arabidopsis* accession ( $\Psi_l > -0.7 \text{ MPa}$ ). Larger symbols within boxes correspond to means and smaller symbols outside boxes to outlier values. Colours refer to the genotype studied: *Col-0*, red; *Cvi*, turquoise; *Sha*, purple; *soc1ful*, green; *p35S:AHL15*, blue; *Kel-4* brown.



### ***The differences in anatomical features among genotypes studied***

When comparing the anatomical dataset across the six genotypes, we found that the lignified *soc1ful* and Sha genotypes had the thickest intervessel pit membranes ( $T_{PM}$ ), followed by an intermediate pit membrane thickness of *p35S: AHL15* and Col-0 ( $F=3.857$ ;  $P=0.0672$ ), and thinner pit membranes in Kel-4 and the least lignified Cvi ( $F=4.467$ ;  $P=0.0506$ ) (Supplementary Figure S4A). Results of vessel wall thickness ( $T_V$ ) showed the same pattern as that described for intervessel pit membrane thickness ( $F=2.546$ ;  $P=0.13$  and  $F=0.554$ ;  $P=0.468$ , respectively) (Supplementary Figure S4B). Vessel grouping index ( $V_G$ ) was markedly higher in the *p35S: AHL15* overexpression line than in all the other genotypes ( $F=27.38$ ;  $P=5.46e^{-13}$ ) (Supplementary Figure S4C), which was also the case for the proportion of lignified area per total stem area ( $P_{LIG}$ ;  $F=28.8$ ;  $P=2.25e^{-13}$ ) (Supplementary Figure S4D). The lignified *p35S: AHL15* overexpression line also had a higher proportion of fiber wall area per fiber cell area ( $PF_{WFA}$ ) than Kel-4, Col-0, and Cvi, but the fibers were less thick walled compared with the lignified genotypes *soc1ful* and Sha ( $F=49.05$ ;  $P<2e^{-16}$ ) (Supplementary Figure S4E). Surprisingly, *p35S: AHL15* showed no wood formation at the stem segment investigated (Supplementary Figure S1E) and was less lignified than *soc1ful*, although *AHL15–SOC1–FUL* belong to the same pathway. The vessel diameter ( $D$ ) of Kel-4 was significantly narrower than that of the other genotypes. Among the remaining genotypes, Cvi (least lignified wild type) had the widest mean  $D$ , which was significantly different from the *p35S: AHL15* overexpression line, but there was no statistical difference in  $D$  with Col-0, Cvi, Sha, and *soc1ful* ( $F=9.46$ ;  $P=2.52e^{-06}$ ) (Supplementary Figure S4F). For theoretical vessel implosion resistance ( $T_{VW}/D_{MAX}$ )<sup>2</sup>, the lignified *soc1ful* and Sha showed the highest values as well, while there was no difference among *p35S: AHL15*, Kel-4, Col-0, and Cvi ( $F=3.955$ ;  $P=0.0166$ ). Finally, vessel density ( $V_D$ ) of *p35S: AHL15*, Col-0, Cvi, Sha, and *soc1ful* was similar ( $F=1.899$ ;  $P=0.13$ ) and significantly higher than that of Kel-4.

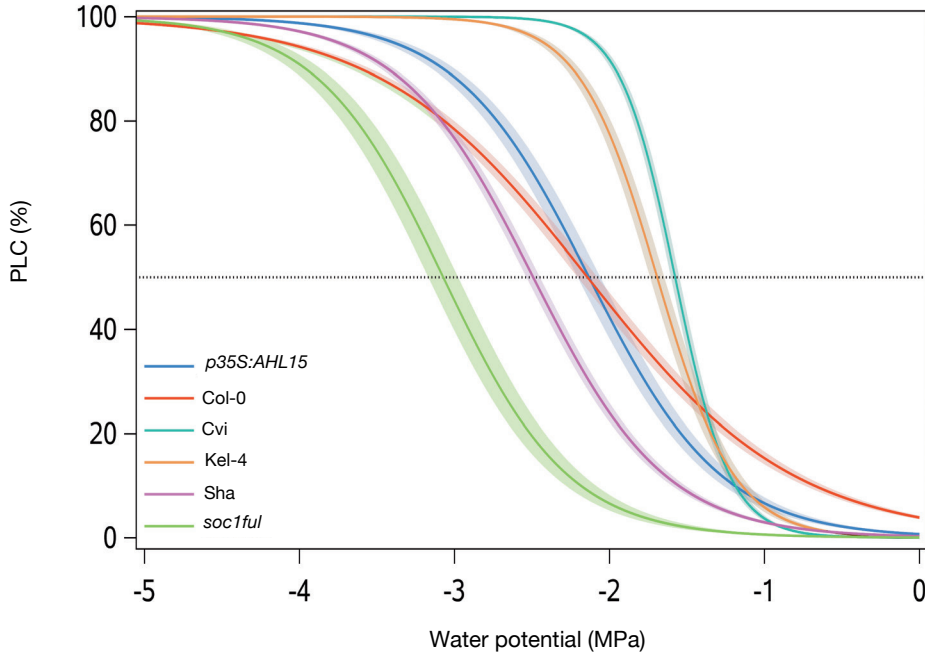


**Figure 3** Mean vulnerability curves present the percentage loss of conductivity (PLC) as a function of xylem pressure (MPa) of each genotype studied. Shaded bands represent standard errors based on five to ten vulnerability curves per genotype. Colours refer to the genotype studied: Col-0, red; Cvi, turquoise; Sha, purple; *soc1ful*, green; *p35S:AHL15*, blue; Kel-4 brown.

### ***Stem anatomical traits explaining variation in embolism resistance***

According to the most parsimonious model derived from multiple linear regression (AIC= -194.59), the stem anatomical predictors that explain the embolism resistance variation were  $T_{PM}$ ,  $T_V$ ,  $V_G$ , and maximum vessel lumen diameter ( $D_{MAX}$ ) ( $R^2=0.924$ ;  $P<2.2e^{-16}$ ) (Supplementary Table S3).  $T_{PM}$  was the anatomical feature explaining  $P_{50}$  variation best, with relative importance of 44%, followed by  $T_V$  (38%),  $V_G$  (9%), and  $D_{MAX}$  (2%) (Figure 5A). Likewise,  $T_{PM}$  and  $T_V$  together also explained most of the variation in  $P_{12}$ , with 41% relative importance ( $R^2=0.795$ ;  $P=1.135e^{-14}$ ) (Supplementary Table S4; Supplementary Figure S5A).  $P_{88}$  variation, on the other hand, was mostly explained by  $PF_{WFA}$  (25% relative importance) ( $R^2=0.516$ ;  $P=1.07e^{-07}$ ) (Supplementary Table S5; Supplementary Figure S5B).

### **The relationship among embolism resistance, anatomical traits, and hydraulic traits**

Based on a Pearson's correlation test,  $T_{PM}$  was strongly positively correlated with other anatomical traits, such as  $T_V$ ,  $(T_{VW}/D_{MAX})^2$ ,  $PF_{WF_A}$ , and  $V_D$  ( $r=0.77$  and  $P=1.108e^{-11}$ ;  $r=0.74$  and  $P=1.956e^{-10}$ ;  $r=0.61$  and  $P=8.96e^{-07}$ ,  $r=0.58$ ,  $P=4.472e^{-06}$ , respectively) (Supplementary Figure S6). Lastly,  $T_V$  and  $PF_{WF_A}$  were correlated as well ( $r=0.71$ ,  $P=2.3e^{-09}$ ) (Supplementary Figure S6). When also taking  $P_{50}$  into account, we saw that  $P_{50}$  was strongly correlated with  $T_{PM}$ ,  $(T_{VW}/D_{MAX})^2$ ,  $T_V$ , and  $PF_{WF_A}$  ( $r= -0.91$ ,  $-0.87$ ,  $-0.86$ , and  $-0.70$ ;  $P<2.2e^{-16}$ , respectively) (Figure 5B–E; Supplementary Figure S6). Similarly,  $P_{12}$  had strong relationships to  $T_{PM}$ ,  $(T_{VW}/D_{MAX})^2$ , and  $T_V$  ( $r= -0.77$  and  $P=6.41e^{-12}$ ;  $r= 0.84$  and  $P=3.93e^{-15}$ ;  $r= 0.68$  and  $P=1.38e^{-08}$ , respectively) (Supplementary Figure S6).  $P_{88}$  only showed a correlation with  $PF_{WF_A}$  ( $r= -0.54$ ;  $P=2.762e^{-05}$ ) and  $T_V$  ( $r= -0.44$ ;  $P=0.0008146$ ) (Supplementary Figure S6). We also found a strong correlation between  $P_{50}$  and the leaf water potential at the harvesting day ( $\psi_{lh}$ ), the number of days until reaching 90% stomatal closure ( $Day_{90}$ ), and the SSM ( $r= -0.9$ ,  $-0.85$ , and  $-0.84$ ;  $P<2.2e^{-16}$ , respectively), but not between  $P_{50}$  and  $\psi_{gs90}$ . Subsequently, the anatomical traits that were strongly correlated to  $P_{50}$ , such as  $T_{PM}$ ,  $T_V$ , and  $V_G$ , were also significantly correlated to  $\psi_{lh}$ ,  $Day_{90}$ , and SSM (Supplementary Figure S6).

## **Discussion**

We performed a drought experiment including six *Arabidopsis* genotypes, during which we compiled a detailed xylem anatomical–hydraulic dataset of inflorescence stems (among others intervessel pit membrane thickness, proportion of lignification, and  $P_{50}$ ) and leaves (rate of stomatal conductance, leaf water potential, and chlorophyll content), and validated the drought response of the genotypes with the transcript abundance of four known drought marker genes at the end of a 15–17 d treatment without watering. Based on anatomical, hydraulic, and gene expression results, it is clear that the most lignified mutant *soc1ful* (Melzer *et al.*, 2008; Lens *et al.*, 2012, 2013) is the most drought-tolerant genotype, closely followed by the lignified ecotype Sha and the *p35S: AHL15* overexpression line, while the lesser lignified Col-0, Kel-4, and especially Cvi ecotypes are much more sensitive. Interestingly, each genotype applies a unique combination of anatomical stem traits and hydraulic traits in stems

and leaves to acquire a certain level of drought tolerance, as will be discussed in the following sections.

**Table 1** The hydraulic data of *Arabidopsis* genotypes studied measured during the drought experiment.

Genotypes	$P_{50}$ (MPa)	$\psi_{gs90}$ (MPa)	SSM (MPa)	$\psi_{lh}$ (MPa)	Days until 90% stomatal closure	Days until $P_{50}$	PLC after 3 weeks of non- watering
<b>Cvi</b>	-1.58	-1.75	-0.17	-3.4	10	10	100%
<b>Kel-4</b>	-1.69	-1.13	0.56	-3.4	11	11	100%
<b>Col-0</b>	-2.14	-0.9	1.24	-2.97	10-11	12	75%
<b><i>p35S:AHL15</i></b>	-2.13	-1.6	0.53	-3.03	13	14	88%
<b>Sha</b>	-2.49	-1.27	1.22	-1.85	12	does not reach $P_{50}$	14%
<b><i>soc1ful</i></b>	-3.07	-1.43	1.64	-1.87	14	does not reach $P_{12}$	10%

$P_{50}$  = stem water potential at 50% loss of hydraulic conductivity,  $\psi_{gs90}$  = leaf water potential at 90% stomatal closure, SSM= stomatal safety margin,  $\psi_{lh}$  = leaf water potential at the harvesting day, PLC = percentage loss of hydraulic conductivity

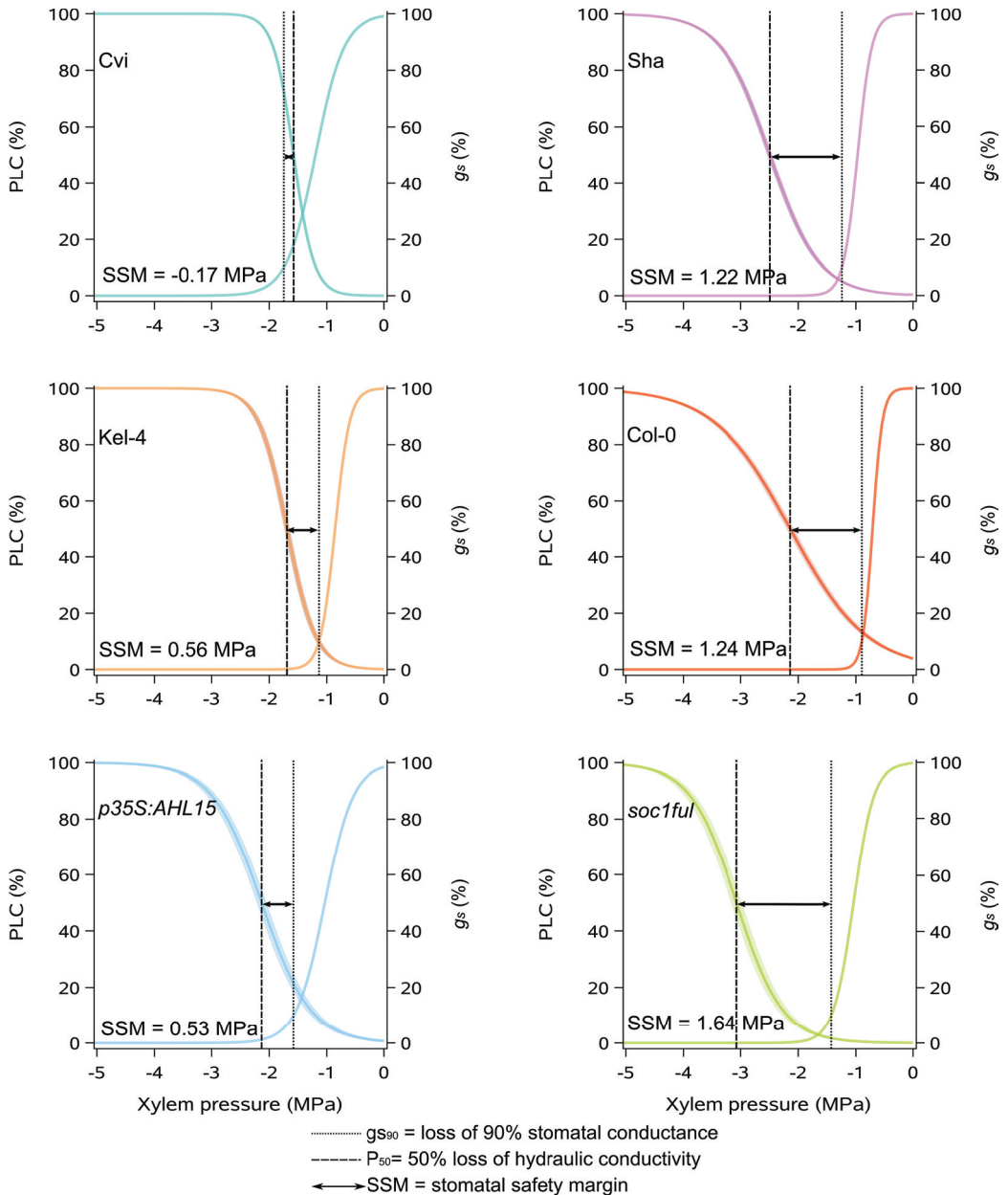


**Figure 4** Stomatal safety margin (SSM) of each genotype studied. The graphs show the percent loss of hydraulic conductivity (PLC) and the percent of stomatal conductance ( $g_s$ ) as a function of xylem pressure (MPa). The dotted lines represent water potential at 90% loss of stomatal conductance. The dashed lines show  $P_{50}$ . The difference between the dashed and the dotted line refers to the SSM.

## **Comparing extremes in drought response: most lignified *soc1ful* versus least lignified *Cvi***

Both the most drought-tolerant *soc1ful* and the most drought-sensitive *Cvi* use a similar set of traits with contrasting trait values to reach the two extremes of the drought tolerance spectrum among the genotypes studied. The drought-tolerant strategy of *soc1ful* (Figure 1A) is determined by a unique combination of traits, as exemplified by the most negative stem  $P_{50}$  (Figure 3; cf. Choat *et al.*, 2012; Lens *et al.*, 2016; Thonglim *et al.*, 2021), coupled with a low initial  $g_s$  that gradually slowed down during drought, allowing a more stable leaf water potential (Supplementary Figure S2A) (Li *et al.*, 2017; Dayer *et al.*, 2020; Lemaire *et al.*, 2021). In addition to its low  $g_s$ , *soc1ful* started closing its stomata rapidly at the onset of drought (at high water potential) to further reduce water loss, but at the same time it reached full stomatal closure later than in the other genotypes ( $\Psi_{gs90}$  was reached after 14 d of non-watering, Table 1). Although we had not quantified carbon uptake during drought, we observed that stomatal closure in *soc1ful* occurred gradually over a longer period during drought, probably extending photosynthetic activities without risking a detrimental level of drought-induced embolism (Figure 2A; Supplementary Figure S2). This is further supported by a low reduction of chlorophyll content in rosette leaves of droughted *soc1ful* individuals compared with the well-watered control batch (Figure 1B). Moreover, this mutant line had the widest positive SSM (Figure 4), which is essential in estimating a plant's drought response (Choat *et al.*, 2012; Delzon and Cochard, 2014; Anderegg *et al.*, 2016; Eller *et al.*, 2018; Oliveira *et al.*, 2021; Skelton *et al.*, 2021). Finally, as reported in Thonglim *et al.* (2020), this mutant also produced the thickest intervessel pit membranes and the largest wood cylinder at the base of the inflorescence stem. Both traits are thought to play an important role in preventing embolism spread (Lens *et al.*, 2022). In contrast, the least lignified *Cvi* was the most vulnerable genotype as it showed the least negative stem  $P_{50}$  combined with a rapid drop in leaf water potential during drought, leading to rapid wilting (Figure 1A) and a strong decrease of chlorophyll content (Figure 1B). In addition, *Cvi* had the highest initial  $g_s$ , and it closed its stomata at low water potential, which led to more water loss due to transpiration (Figure 2A; Supplementary Figure S2). Although it reached  $\Psi_{gs90}$  earlier than the more tolerant genotypes (Table 1), it seemed like *Cvi* could not close its stomata in time because all the water was already consumed, giving rise to

a rapid water potential drop during drought (Supplementary Figure S2A). Due to its less negative stem  $P_{50}$ , the  $\Psi_{gs90}$  exceeded stem  $P_{50}$ , leading to the only negative SSM among the six genotypes studied (Figure 4). This implies that Cvi experiences a considerable decrease in stem hydraulic conductivity right after or even before stomatal closure. In addition to all these physiological parameters pointing to the most sensitive drought response among the genotypes studied, Cvi also had the least lignified inflorescence stems with the thinnest intervessel pit membranes (Thonglim *et al.*, 2021).

### ***The role of embolism resistance and stomatal regulation in drought tolerance and its impact on the stomatal safety margin***

The previous section highlights the importance of embolism resistance as well as SSMs in determining drought tolerance, as has been demonstrated across many other lineages of plants (Meinzer *et al.*, 2009; McDowell, 2011; Choat *et al.*, 2012; Johnson *et al.*, 2012; Cochard *et al.*, 2013; Lens *et al.*, 2013; Skelton *et al.*, 2015, 2021; Martin-StPaul *et al.*, 2017; Creek *et al.*, 2020; Dayer *et al.*, 2020). However, our dataset suggests that stem  $P_{50}$ —which is probably a good proxy for whole-plant  $P_{50}$  based on our few leaf  $P_{50}$  measurements in the *p35S:AHL15* overexpression line and based on other herbaceous species showing no difference in  $P_{50}$  across organs (e.g., Skelton *et al.*, 2017)—outperforms SSM in explaining the responses to drought among the genotypes studied. This is because stomatal regulation in *Arabidopsis* genotypes that were equally drought tolerant could be substantially different, while  $P_{50}$  showed a more consistent pattern with whole-plant drought tolerance. However, it seems that the rate of  $g_s$  in *Arabidopsis* under well-watered conditions is more critical than the speed of stomatal closure, as shown by Cvi, Col-0, and Kel-4 (Table 1; Supplementary Figure S2B). Indeed,  $\Psi_{gs90}$  is not the driving force behind drought tolerance since the more drought-tolerant genotypes closed their stomata slightly later than the sensitive ones. In other words, Cvi, Col-0, and Kel-4 lost more water because of a higher transpiration rate, but they closed their stomata sooner than the more drought-tolerant genotypes (Table 1). These results align with previous studies stating that stomatal behavior only shows how each species respond to drought stress, but not how much they tolerate drought (Roman *et al.*, 2015; Combe *et al.*, 2016; Martínez-Vilalta and Garcia-Forner, 2017). Bearing this in mind, our observation shows that the two mutant genotypes studied in the Col-0 background (*soc1ful* and

*p35S: AHL15*)—both belonging to the same regulatory *SOC1–FUL–AHL15*–cytokinin pathway that induces wood formation in stems (Rahimi *et al.*, 2022)—also have by far the lowest initial  $g_s$  values across all six genotypes studied, including the Col-0 ecotype (Figure 2B). This makes it a promising gene regulatory pathway to discover how drought-responsive traits in stems (increased lignification or woodiness) and leaves (reduced  $g_s$ ) are linked to each other at the genetic level. Our dataset aligns with earlier studies showing that safety margins across (mainly woody) angiosperms are overall positive, and considerable levels of embolisms only happen under remarkable, intense drought events (Choat *et al.*, 2012; Delzon and Cochard, 2014; Martin-StPaul *et al.*, 2017; Creek *et al.*, 2020; Dayer *et al.*, 2020; Skelton *et al.*, 2021; Guan *et al.*, 2022; Lens *et al.*, 2022). The positive SSMs in five out of six genotypes indicate that stomatal closure typically occurs before embolism in order to prevent water loss and delay hydraulic dysfunction (Martin-StPaul *et al.*, 2017; Creek *et al.*, 2020). In contrast, Cvi—the only genotype with a negative SSM—closed its stomata at 70% loss of maximum conductance, highlighting its high sensibility to drought.

### ***Multiple strategies to acquire drought tolerance***

In addition to the drought-responsive traits discussed in *soc1ful* and Cvi, different combinations among these traits were observed in the remaining genotypes. This shows that even in a species with a short life cycle, multiple strategies can be applied to acquire a certain level of drought tolerance. For instance, Sha and *p35S: AHL15* had a similarly high level of drought tolerance based on their phenotype after 3 weeks of water shortage (Figure 1A), but their drought-responsive traits were different. Sha had high embolism resistance in stems combined with a relatively high initial transpiration rate in leaves that rapidly declines during drought, allowing a relatively stable leaf water potential (also confirmed by Bouchabke *et al.*, 2008) and a large SSM. On the other hand, *p35S: AHL15* had the lowest  $g_s$  of all the genotypes studied (Figure 2A), which means it can keep its leaf water potential relatively high during drought, whereas its stem  $P_{50}$  was intermediate and led to a smaller SSM compared with Sha (Figures 2–4). Another example is given by *p35S: AHL15* (overexpression line) and Col-0 common wild type, which both had a similar stem  $P_{50}$  (–2.1 MPa; Figure 3). However, Col-0 was more drought sensitive than *p35S: AHL15*, even though the former closed its stomata earlier during drought, resulting in a wider



SSM (Figure 4). The reason for Col-0 being more drought sensitive is that stomatal conductance is much higher, leading to more water loss and consequently a more rapid decline in leaf water potential during the drought experiment, while the leaf water potential during drought in *p35S:AHL15* drops more slowly (Supplementary Figure S2). Thus, a wider SSM does not always lead to prolonged survival during drought since the rate of  $g_s$  is not accounted for in the SSM. In other words, the width of the safety margin does not necessarily match all aspects of stomatal regulation and the resulting leaf water potential dynamics during drought (Martin-StPaul *et al.*, 2017; Martínez-Vilalta and Garcia-Forner, 2017; Knipfer *et al.*, 2020).

### ***Expression levels of drought-responsive genes agree with drought-response traits***

To assess the level of drought stress and compare it among the genotypes, we assessed the expression of selected drought-responsive genes on the final day of the drought treatment (15–17 d). As expected, the four drought-responsive genes *RD29A*, *DREB2A*, *ABI2*, and *AREB1* were most up-regulated in the more sensitive genotypes Col-0, Kel-4, and Cvi, and less up-regulated in the more tolerant genotypes Sha, *p35S:AHL15*, and *soc1ful* (Figure 1C). To study the casual relationship between physiological responses (e.g., stomatal closure) and gene activity (e.g., ABA biosynthesis genes), future work should focus on conducting a high-resolution time-course gene expression analysis, which is beyond the scope of this study.

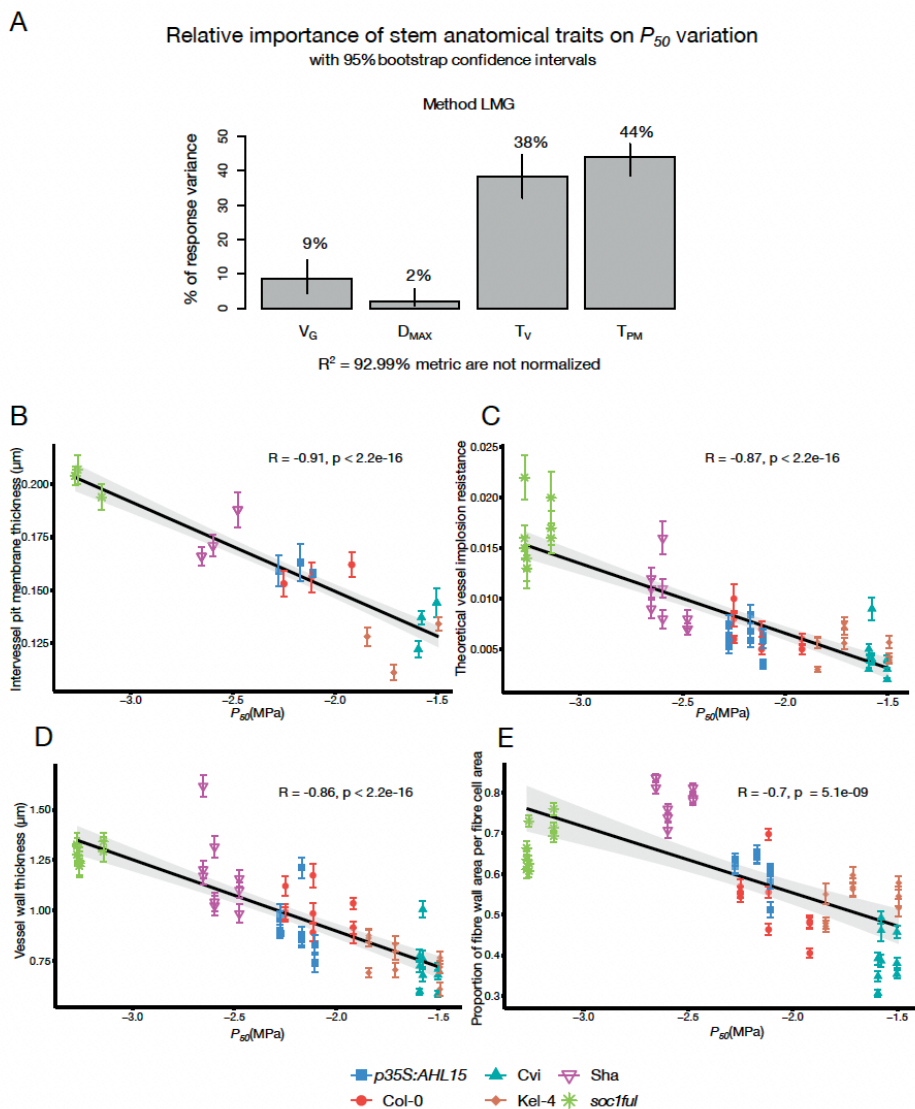


**Figure 5** (A) Relative importance of stem anatomical traits on  $P_{50}$  variation. The  $P_{50}$  variation is mainly explained by intervessel pit membrane thickness ( $T_{PM}$ ) and vessel wall thickness ( $T_V$ ) based on  $R^2$  contribution averaged over orderings among regressors (based on LMG method). (B) Negative correlation between  $T_{PM}$  and  $P_{50}$  (C) Negative correlation between  $(T_{VW}/D_{MAX})^2$  and  $P_{50}$  (D) Negative correlation between  $T_V$  and  $P_{50}$  (E) Negative correlation between  $PF_{WFA}$  and  $P_{50}$ . Colours and styles refer to the genotype studied: Col-0, red circles; Cvi, turquoise triangles point up; Sha, purple triangles point down; *soc1ful*, green stars; *p35S:AHL15*, blue squares; Kel-4, brown diamonds.

***Intervessel pit membrane thickness as an important anatomical driver of embolism resistance, and the potential effect of stem lignification on  $P_{50}$*** 

Our extended database confirms our previous results that intervessel pit membrane thickness is the anatomical trait that explains best the variation in  $P_{50}$  across all six genotypes studied (Figure 5A). These results are in line with several other angiosperm studies showing a strong positive correlation between embolism resistance and  $T_{PM}$ , both at the interspecies level (Jansen *et al.*, 2009; Lens *et al.*, 2011, 2022; Plavcová and Hacke, 2012; Plavcová *et al.*, 2013; Scholz *et al.*, 2013b; Li *et al.*, 2016; Dória *et al.*, 2018; Trueba *et al.*, 2019; Guan *et al.*, 2022) and within species (Schuldt *et al.*, 2016). The functional explanation for this relationship was intensively discussed in our previous paper (Thonglim *et al.*, 2021). In brief, there is convincing evidence based on microCT and/or optical technique observations in stems (Brodersen *et al.*, 2013; Knipfer *et al.*, 2015; Choat *et al.*, 2016; Skelton *et al.*, 2017; Torres-Ruiz *et al.*, 2017) and leaves (Brodrigg *et al.*, 2016a; Skelton *et al.*, 2017, 2018; Klepsch *et al.*, 2018; Lamarque *et al.*, 2018) that embolism spread between adjacent vessels predominantly happens via porous pit membranes located inside the bordered pits between adjacent vessels. Although this explains why the thickness of intervessel pit membrane plays an important role in embolism propagation and, by extension, also whole-plant drought tolerance, the detailed mechanisms behind this embolism spread remain poorly known due to the complex 3D structure/composition of pit membranes and the enigmatic behavior of gas–liquid–solid–surfactant interfaces at the nano-scale (Kaack *et al.*, 2019, 2021; Yang *et al.*, 2020; Zhang *et al.*, 2020; Lens *et al.*, 2022).

It has also been shown in previous studies that intervessel pit membrane thickness is strongly linked not only with  $P_{50}$ , but also with other anatomical traits assumed to be involved in drought-induced embolism resistance, such as vessel wall thickness (Jansen *et al.*, 2009; Li *et al.*, 2016), and the amount of stem lignification or woodiness (Li *et al.*, 2016; Dória *et al.*, 2018; Thonglim *et al.*, 2021). How exactly lignification would impact embolism spread in stems is the subject of ongoing research. One hypothesis is that the amount of lignification in secondary cell walls may determine gas diffusion kinetics across xylem cell walls and, therefore, could reduce the speed of embolism propagation in species with increased levels of lignification or woodiness (Li *et al.*, 2016; Dória *et al.*, 2018; Pereira *et al.*,

2018; Thonglim *et al.*, 2021; Lens *et al.*, 2022). This may imply that older stems from herbaceous species could lead to increased embolism resistance, resulting from a possible increase in stem lignification and/or the amount of wood. In our study, this may especially apply to the *p35S: AHL15* overexpression line, which has the ability to develop as much wood as the *soc1ful* double knockout genotype (Rahimi *et al.*, 2022). However, this study shows that wood development is delayed in *p35S: AHL15* (Supplementary Figure S1E, G) compared with *soc1ful* in 80-day-old plants, despite the fact that SOC1, FUL, and AHL15 belong to the same wood pathway (Rahimi *et al.*, 2022). Older individuals of *p35S: AHL15* will therefore develop more wood and probably also thicker intervessel pit membranes in their inflorescence stems, most probably resulting in both higher embolism resistance and higher SSM, which synergistically may increase total plant tolerance of the overexpression line to the level of *soc1ful*.

In conclusion, there is a considerable difference in drought response among the six *Arabidopsis* genotypes studied. The genotypes *soc1ful*, Sha, and *p35S: AHL15* synergistically increase their drought tolerance by building lignified inflorescence stems with thick intervessel pit membranes, developing the largest SSMs, keeping the water potential in their leaves pretty stable during periods of water shortage as a result of low stomatal conductance, maintaining relatively high chlorophyll content in rosette leaves, and by showing the lowest expression levels of drought-response genes compared with the control batch. In contrast, the most sensitive genotypes to drought (Cvi, Kel-4, and Col-0) are more susceptible to drought due to the opposite extreme of the same set of drought-responsive traits. This shows that stem anatomical traits and hydraulic stem and leaf traits are intertwined to acquire a certain level of drought tolerance. To further disentangle gene regulatory networks underlying drought-responsive traits across organs and to find out how they are linked with each other and synergistically strengthen the whole-plant drought response, future studies should combine a time series of gene expression data in roots, stems, and leaves during a drought experiment followed by rewatering. During such an experiment, a range of drought-responsive (anatomical and physiological) traits in all organs should be investigated. Only with this integrative approach, will we be able to make considerable progress in securing our food production by developing breeding tools that can make crops more

drought tolerant and propose solutions on how to protect our herbs and forests under the current global change scenario.

## **Acknowledgements**

We would like to thank Alex Bos (IBL) for support with the gene expression analysis, Omid Karami and Arezoo Rahimi (IBL) for providing seeds and their knowledge in taking care of Arabidopsis plants, and Gaëlle Capdeville (BIOGECO INRA) for technical support. This work is funded by a PhD scholarship awarded to AT from the Institute for the Promotion of Teaching Science and Technology (IPST), Thailand, and by the Dutch Research Council NWO (grant number ALWOP.488).

## Supplementary data

**Supplementary Table S1** Oligonucleotide sequences.

---

Primers for qRT-PCR			
Gene name	Gene ID	Primer Fwd sequence (5'-3')	Primer Rev sequence (5'-3')
<i>ACTIN2</i>	AT3G18780	TCCCTCAGCACATTCCAGCAGAT	AACGATTCTGGACCTGCCTCATC
<i>GAPDH</i>	At1G13440	TTGGTGACAACAGGTCAAGCA	AAACTTGTCGCTCAATGCAATC
<i>RD29A</i>	AT5G52310	TGGACAAAGCAATGAGCATGAGC	AGGTTTACCTGTTACGCCTGGTG
<i>ABI2</i>	ATG557050	CTCGCAATGTCAAGATCCATTGGC	TTACTCGCCGCACTGAAGTCAC
<i>AREB1</i>	AT1G45249	AGTTACAACGAAAGCAGGCAAGG	CCTCCTTGCAAGATTCTCATC
<i>DREB2A</i>	AT5G05410	CAGTGTTGCCAACGGTTCAT	AAACGGAGGTATTCCGTAGTTGAG

---

**Supplementary Table S2** The anatomical characters and hydraulic values measured with acronyms, definitions, calculations, units, and techniques.

Acronyms	Definition	Calculation	Number of measurements	Unit	Technique
A <sub>F</sub>	Fiber cell area	Area of single xylem fiber in cross-section	Min. 30 fibers	μm <sup>2</sup>	LM
A <sub>FL</sub>	Fiber lumen area	Area of single xylem fiber lumen in cross-section	Min. 30 fibers	μm <sup>2</sup>	LM
A <sub>FW</sub>	Fiber wall area	A <sub>F</sub> - A <sub>FL</sub> for the same fiber	Min. 30 fibers	μm <sup>2</sup>	LM
A <sub>LIG</sub>	Lignified stem area	Total xylem area + fiber caps area + lignified pith cell area in cross-section	9 stems per accession	mm <sup>2</sup>	LM
A <sub>PITH</sub>	Pith area	Total pith area in cross-section	9 stems per accession	mm <sup>2</sup>	LM
A <sub>S</sub>	Total stem area	Total stem area in cross-section	9 stems per accession	mm <sup>2</sup>	LM
Day <sub>90</sub>	Days until reaching 90% of stomatal closure	-	-	days	-
D <sub>MAX</sub>	Maximum vessel lumen diameter	Diameter of single vessel	Min. 30 vessels	μm	LM
D <sub>PC</sub>	Pit chamber depth	Distance from the relaxed pit membrane to the inner pit aperture	Min. 25 pits	μm	TEM
g <sub>s</sub>	Stomatal conductance	-	1 control sample and 2 drought samples each measurement	mmol m <sup>-2</sup> s <sup>-1</sup>	Porometer
SSM	Stomatal safety margin	$\Psi_{g_{50}} - P_{50}$	1 SSM per accession	MPa	-
P <sub>12</sub>	Stem water potential at 12% loss of hydraulic conductivity	-	8 values per each accession	MPa	Cavitron centrifuge
P <sub>50</sub>	Stem water potential at 50% loss of hydraulic conductivity	-	8 values per each accession	MPa	Cavitron centrifuge
P <sub>88</sub>	Stem water potential at	-	8 values per each accession	MPa	Cavitron centrifuge

	88% loss of hydraulic conductivity				
$P_{FWFA}$	Proportion of fiber wall area per fiber cell area	$A_{FW}/A_f$ for the same fiber; a measure of xylem fiber wall thickness	Min. 30 fibers	-	LM
$\psi_{gs90}$	Leaf water potential at 90% loss of stomatal conductance	-	1 control sample and 2 drought samples each measurement	MPa	PSYPRO meter
$\psi_{lh}$	Leaf water potential at the harvesting day	-	1 control sample and 2 drought samples each measurement	MPa	PSYPRO meter
$P_{LIG}$	Proportion of lignified area per total stem area	$A_{LIG}/A_s$	9 stems per accession	-	LM
$T_{PM}$	Intervessel pit membrane thickness	Thickness of intervessel pit membrane measured at its thickest point	Min. 25 pit membranes	$\mu m$	TEM
$T_v$	Vessel wall thickness	Thickness of a single vessel wall	Min. 30 vessels	$\mu m$	LM
$T_{VW}/D_{MAX}$	Thickness-to-span ratio of vessels	Double intervessel wall thickness divided by the maximum diameter of the largest vessel	Min. 30 measurements	$\mu m$	LM
$(T_{VW}/D_{MAX})^2$	Theoretical vessel implosion resistance	$(T_{VW}/D_{MAX})^2$	Min. 30 measurements	-	LM
$V_D$	Vessel density	Number of vessels per $mm^2$	Min. 5 measurements	No. of vessel per $mm^2$	LM
$V_G$	Vessel grouping index	Ratio of total number of vessels to total number of vessel groupings (incl. solitary and grouped vessels)	Min. 50 vessel groups	-	LM



**Supplementary Table S3** The most parsimonious multiple linear regression model (based on AIC scores) of anatomical traits, explaining stem  $P_{50}$  variation of the six *Arabidopsis thaliana* accessions studied.

Predictors	Estimate	Std. Error	t value	Pr (> t )
<b>(Intercept)</b>	0.435	0.239	1.825	0.074
<b>T<sub>PM</sub></b>	-11.096	1.329	-8.347	5.67e <sup>-11</sup> ***
<b>D<sub>MAX</sub></b>	0.028	0.007	4.149	0.000132***
<b>V<sub>G</sub></b>	-0.242	0.073	-3.331	0.001651**
<b>T<sub>V</sub></b>	-1.074	0.146	-7.360	1.84e <sup>-09</sup> **

T<sub>PM</sub> = intervessel pit membrane thickness; D<sub>MAX</sub> = maximum vessel lumen diameter; V<sub>G</sub> = vessel grouping index; T<sub>V</sub> = vessel wall thickness. \*\*\* *p-value* < 0.001; \*\* *p-value* < 0.01

**Supplementary Table S4** The most parsimonious multiple linear regression model (based on AIC scores) of anatomical traits explaining stem  $P_{12}$  variation of the six *Arabidopsis thaliana* accessions studied.

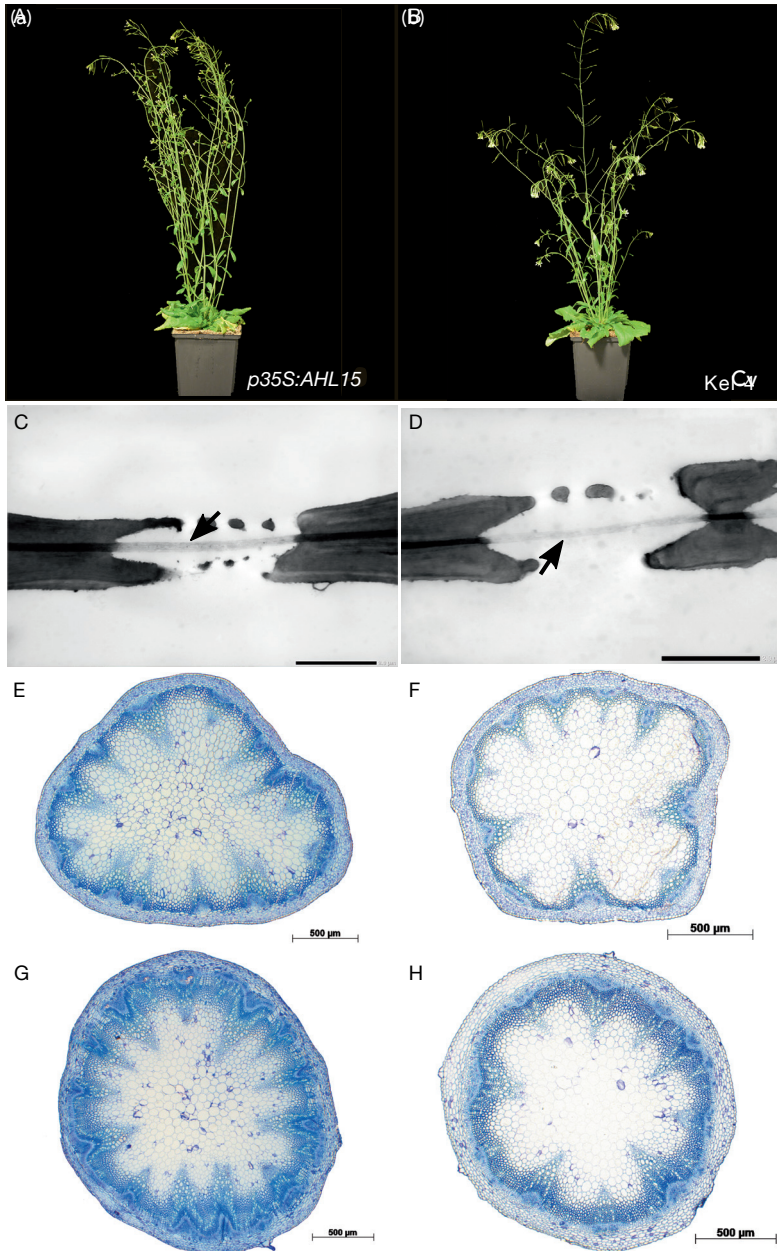
Predictors	Estimate	Std. Error	t value	Pr (> t )
<b>(Intercept)</b>	-0.599	0.687	-0.872	0.388
<b>P<sub>LIG</sub></b>	-3.365	1.793	-1.877	0.067
<b>T<sub>PM</sub></b>	-12.657	3.660	-3.458	0.001**
<b>D<sub>PC</sub></b>	1.926	0.756	2.546	0.014*
<b>D<sub>MAX</sub></b>	0.086	0.016	5.492	1.76e <sup>-06***</sup>
<b>P<sub>FwFA</sub></b>	1.093	0.660	1.656	0.105
<b>V<sub>D</sub></b>	0.006	0.003	2.443	0.019*
<b>V<sub>G</sub></b>	-0.511	0.261	-1.959	0.056
<b>T<sub>V</sub></b>	-1.416	0.404	-3.502	0.001**

P<sub>LIG</sub> = proportion of lignified area per total stem area; T<sub>PM</sub> = intervessel pit membrane thickness; D<sub>PC</sub> = pit chamber depth; D<sub>MAX</sub> = maximum vessel lumen diameter; P<sub>FwFA</sub> = proportion of fiber wall area per fiber cell area; V<sub>D</sub> = vessel density V<sub>G</sub> = vessel grouping index; T<sub>V</sub> = vessel wall thickness. \*\*\* *p*-value < 0.001; \*\* *p*-value < 0.01; \* *p*-value < 0.05

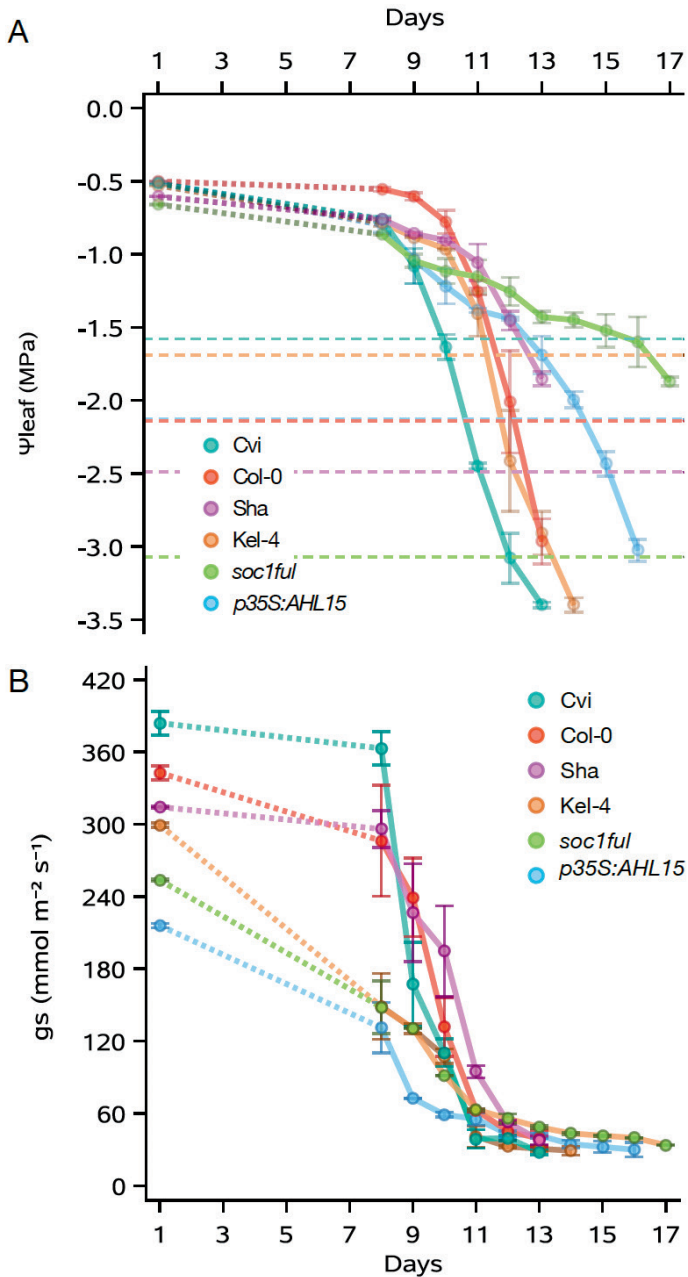
**Supplementary Table S5** The most parsimonious multiple linear regression model (based on AIC scores) of anatomical traits explaining stem  $P_{88}$  variation of the six *Arabidopsis thaliana* accessions studied.

Predictors	Estimate	Std. Error	t value	Pr (> t )
<b>(Intercept)</b>	1.414	0.701	2.018	0.049*
<b>P<sub>LIG</sub></b>	3.967	1.556	2.550	0.014*
<b>D<sub>PC</sub></b>	-1.932	0.726	-2.662	0.011*
<b>PF<sub>WFA</sub></b>	-2.208	0.469	-4.710	2.148e <sup>-05***</sup>
<b>V<sub>D</sub></b>	-0.010	0.003	-3.575	0.000810***
<b>D<sub>MAX</sub></b>	-0.072	0.018	-4.054	0.000184***

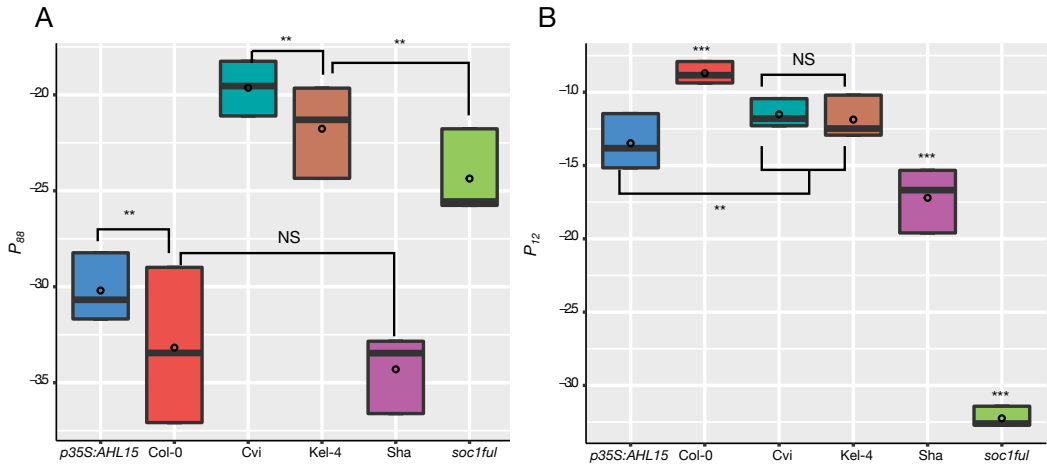
P<sub>LIG</sub> = proportion of lignified area per total stem area; D<sub>PC</sub> = pit chamber depth; PF<sub>WFA</sub> = Proportion of fiber wall area per fiber cell area; V<sub>D</sub> = vessel density; D<sub>MAX</sub> = maximum vessel lumen diameter. \*\*\* *p*-value < 0.001; \*\* *p*-value < 0.01; \* *p*-value < 0.05



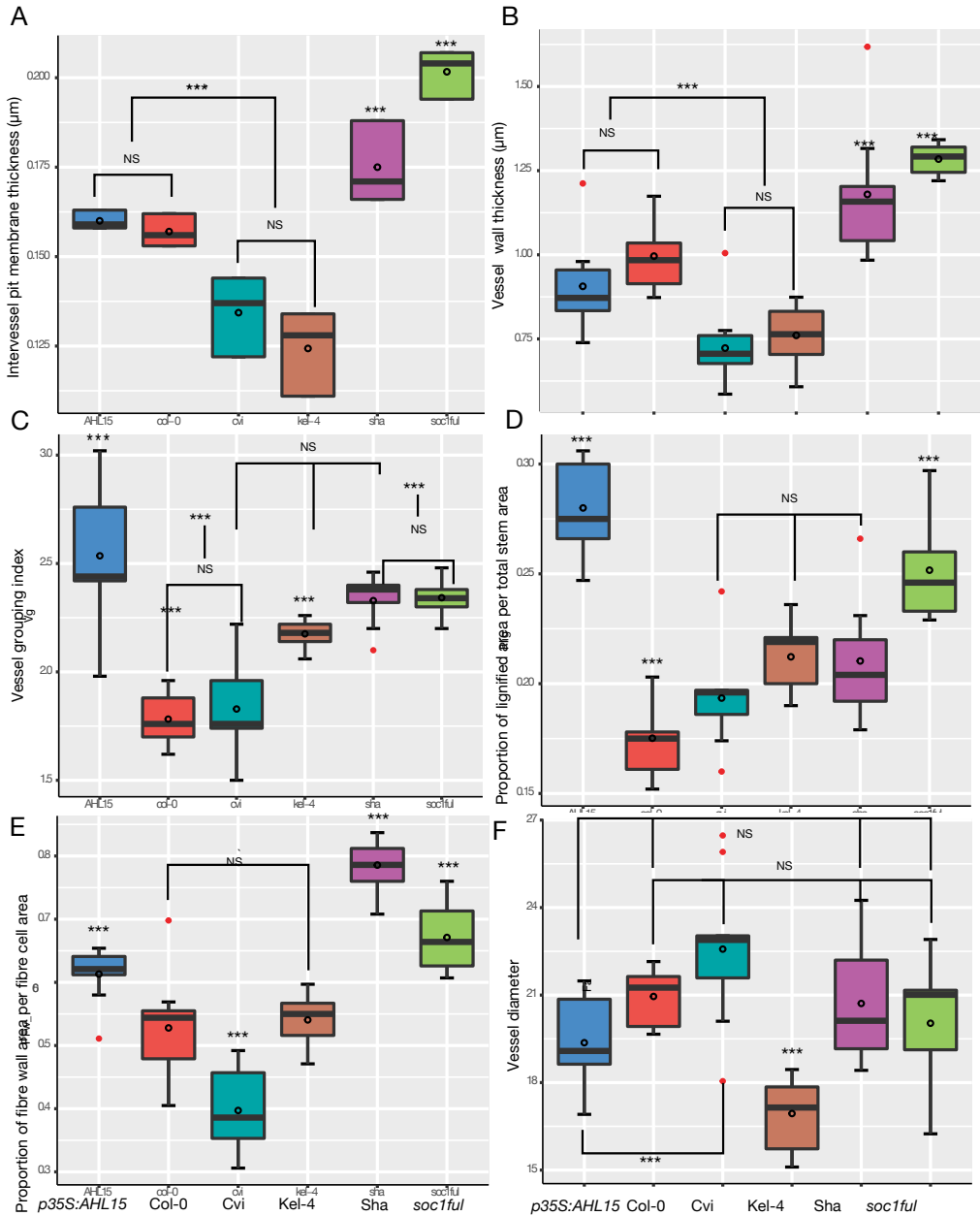
**Supplementary Figure S1** Growth form and cross-sections of inflorescence stems of *p35S:AHL15* (left, 85d after sowing) and *Kel-4* (right, 65d after sowing). (A, B) Growth form. (C, D) TEM images of intervessel pit membranes (arrows). Scale bars = 2 μm. (E, F) LM images of cross-sections at the middle part of inflorescence stems. Scale bars = 500 μm. (G, H) LM images of cross-sections at the basal part of inflorescence stems show more pronounced lignification. Scale bars = 500 μm.



**Supplementary Figure S2** Leaf water potential and stomatal conductance during drought experiment. (A) Leaf water potential ( $\Psi_l$ ) over time. Dotted lines represent  $P_{50}$  value of each genotype. (B) Stomatal conductance ( $g_s$ ) over time. Colours refer to the genotype studied: Col-0, red; Cvi, turquoise; Sha, purple; *soc1ful*, green; *p35S:AHL15*, blue; Kel-4, brown.

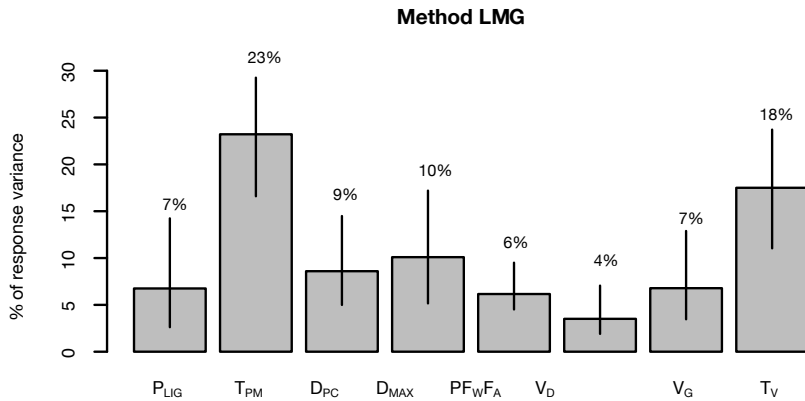


**Supplementary Figure S3** Boxplots showing  $P_{88}$  and  $P_{12}$  variation within and between genotypes. (A) Boxplot showing  $P_{88}$  of every genotype studied. (B) Boxplot showing  $P_{12}$  of every genotype studied; ns =  $p$ -value > 0.05; \*\*  $p$ -value < 0.05; \*\*\*  $p$ -value < 0.01.



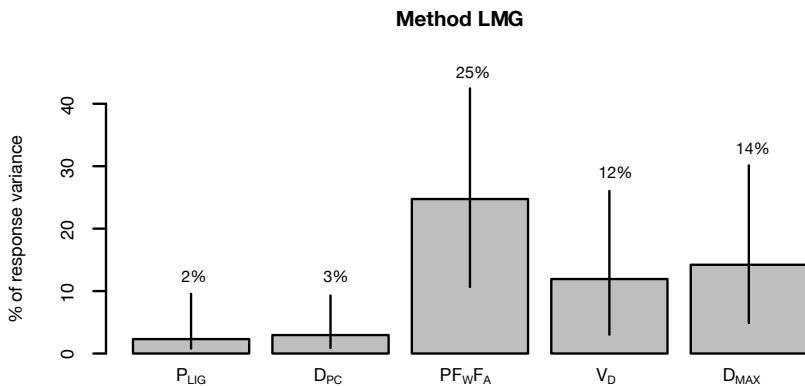
**Supplementary Figure S4** Boxplots showing anatomical variation within and between all genotypes. (A) Boxplot of intervessel pit membrane thickness ( $T_{PM}$ ). (B) Boxplot of vessel wall thickness ( $T_V$ ). (C) Boxplot of vessel grouping index ( $V_G$ ). (D) Boxplot of the proportion of lignified area per total stem area ( $P_{LIG}$ ). (E) Boxplot of the proportion of fiber wall area per fiber cell area ( $PF_{WFA}$ ). (F) Boxplot of vessel diameter ( $D$ ); ns =  $p$ -value > 0.05; \*\*  $p$ -value < 0.05; \*\*\*  $p$ -value < 0.01.

**A** Relative importance of stem anatomical traits on  $P_{12}$  variation  
with 95% bootstrap confidence intervals



$R^2 = 82.62\%$ , metrics are not normalized.

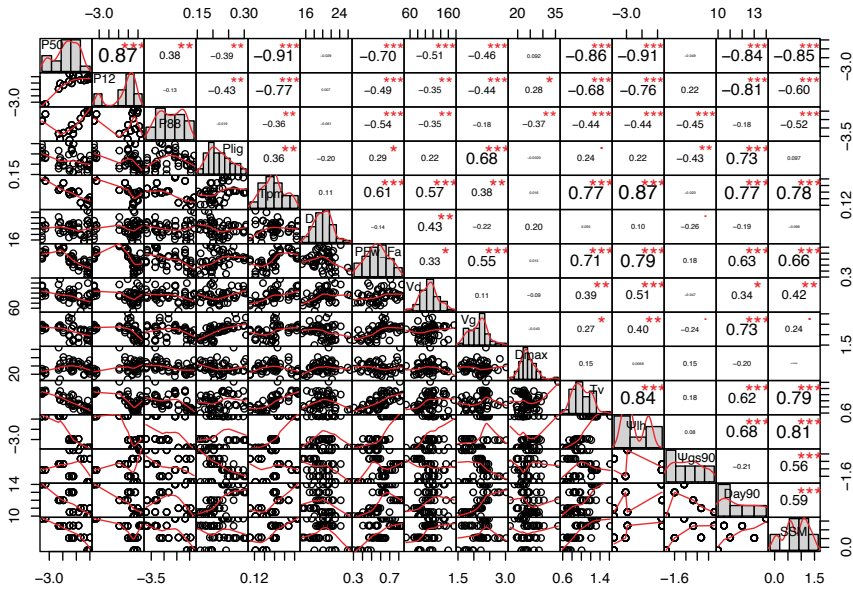
**B** Relative importance of stem anatomical traits on  $P_{88}$  variation  
with 95% bootstrap confidence intervals



$R^2 = 56.16\%$ , metrics are not normalized.

**Supplementary Figure S5** The relative importance of  $P_{12}$  and  $P_{88}$  evaluated. (A) The relative importance of  $P_{12}$  variation is mainly explained by intervessel pit membrane thickness ( $T_{PM}$ ) and vessel wall thickness ( $T_V$ ). (B) The relative importance of  $P_{88}$  variation is mainly explained by proportion of fiber wall area per fiber cell area ( $PF_{WFA}$ ).





**Supplementary Figure S6** The pairwise scatter plots based on Pearson's correlation analysis show the correlations of  $P_{50}$ ,  $P_{12}$  and  $P_{88}$  (response variables) and each stem anatomical and hydraulic traits studied (predictive variables) and between all the predictive variables. \*\*\*  $p$ -value < 0.01; \*\*  $p$ -value < 0.01; \*  $p$ -value < 0.05.



## Chapter 4

# High leaf water potential: a key to drought resilience in *JUB1* overexpression lines of *Arabidopsis* and tomato

*Ajaree Thonglim*<sup>1, \*</sup>, *Giovanni Bortolami*<sup>1</sup>, *Sylvain Delzon*<sup>2</sup>,  
*Maximilian Larter*<sup>2</sup>, *Erik Smets*<sup>1,3</sup>, *Salma Balazadeh*<sup>4</sup>, and  
*Frederic Lens*<sup>1,3, \*</sup>

Manuscript in preparation for publication



<sup>1</sup> Naturalis Biodiversity Center, Research Group Functional Traits, PO Box 9517, 2300 RA Leiden, The Netherlands

<sup>2</sup> BIOGECO INRA, Université Bordeaux, 33615 Pessac, France

<sup>3</sup> Leiden University, Institute of Biology Leiden, Plant Sciences, Sylviusweg 72, 2333 BE Leiden, The Netherlands

<sup>4</sup> Leiden University, Institute of Biology Leiden, Molecular Plant Stress Biology, Sylviusweg 72, 2333 BE Leiden, The Netherlands

\* Correspondence: [ajaree.thonglim@naturalis.nl](mailto:ajaree.thonglim@naturalis.nl) and [frederic.lens@naturalis.nl](mailto:frederic.lens@naturalis.nl)

## Abstract

Increased drought events caused by climate change are leading to yield stagnation and crop losses worldwide, emphasizing the importance of understanding drought tolerance mechanisms for resilient crop development. *JUNGBRUNNEN1* (*JUB1*), a multifunctional transcription factor, has been identified as a positive regulator of drought tolerance in various species. However, the mechanisms underlying *JUB1*'s enhancement of drought tolerance remain unexplored. To address this knowledge gap, our study comprehensively analyzed anatomical and hydraulic traits in well-watered and water deficit conditions, including intervessel pit membrane thickness ( $T_{PM}$ ), stem lignification, embolism resistance in stems ( $P_{50}$ ), stomatal safety margin (SSM), stomatal conductance ( $g_s$ ), and leaf water potential ( $\psi_l$ ), in wild-types and *JUB1* overexpression (OX) lines of *Arabidopsis thaliana* and *Solanum lycopersicum* (tomato). Our results highlight the pivotal role of maintaining high  $\psi_l$  in conferring drought tolerance in the more resilient *JUB1OX* genotypes, both in *Arabidopsis* and tomato. Interestingly, none of the stem anatomical features nor any of the hydraulic traits associated with drought tolerance in other *Arabidopsis* genotypes showed a correlation with the improved drought response of the *JUB1OX* genotypes. Even more surprisingly, *JUB1OX* plants exhibited traits typically associated with reduced resilience to drought, such as (slightly) less negative stem  $P_{50}$ , narrower SSMs, and thinner intervessel pit membranes. When looking more into stomatal conductance dynamics that may be involved in stabilizing  $\psi_l$  during drought between *JUB1OX* genotypes and wild-types in *Arabidopsis* and tomato, we see that A-*JUB1OX* plants lose less water via transpiration through a lower initial  $g_s$  during well-watered conditions and early drought compared to the wild-type and *jub1* knockdown mutant, while the stomata in A-*JUB1OX* plants take longer to completely close. In tomato *JUB1OX* plants, however, we observed elevated  $g_s$  during the initial stages of drought compared to the wild-type tomato plants, followed by a steep decline until the stomata are fully closed. In conclusion, our findings highlight that high leaf water potential is central in the mechanism contributing to the enhanced drought tolerance observed in *JUB1OX* plants, but none of the other traits investigated shows evidence of how these plants stabilize their  $\psi_l$  levels during conditions of water deficit. This opens the door to investigating in detail the role of *JUB1* on the accumulation of osmoprotectants such as proline in the leaves.

Keywords: *Arabidopsis thaliana*, *Solanum lycopersicum*, drought response, embolism resistance, leaf water potential, stem anatomy, stomatal conductance.

## Introduction

Water availability is a crucial factor that has a significant impact on plant growth and productivity. As plants rely on water for their development and functioning, limited water availability is a significant constraint on plant growth (Choat *et al.*, 2018; Martinez-Vilalta *et al.*, 2019; Sapes *et al.*, 2019; Brodribb *et al.*, 2020). Ongoing climate change has led to rising temperatures and shifting rainfall patterns, increasing the frequency and severity of droughts that exacerbate water scarcity worldwide (Kim and Jehanzaib, 2020; Fischer *et al.*, 2021). Approximately 75% of the global harvested area is affected by lower water availability (IPCC, 2022), resulting in reduced photosynthesis, yield stagnation, and crop losses that have been increasing globally in recent decades (Matiu *et al.*, 2017; Sultan *et al.*, 2019; Agnolucci and De Lipsis, 2020; Brás *et al.*, 2021). Ultimately, drought could lead to plant mortality, which is a complex process that associates the interplay between water and carbon interdependencies (Anderegg *et al.*, 2015; McDowell *et al.*, 2022). Among the various mechanisms involved in drought-induced plant mortality, hydraulic failure is considered the primary cause and occurs when plants experience extreme water stress due to short intense droughts, leading to the collapse of the water transport system (Sperry and Tyree, 1988; Venturas *et al.*, 2017; McDowell *et al.*, 2022; Johnson *et al.*, 2022). Under conditions of soil drying and high evaporative demand, the tension in the xylem increases, triggering the formation of large gas bubbles in the water-conducting cells (embolisms), although the precise mechanisms of embolism formation in the xylem remain incompletely understood (Lens *et al.*, 2022). There is increasing evidence, however, that embolisms spread via the interconduit pit membranes among adjacent conduits (air-seeding), causing a massive decline in hydraulic conductance that will provoke desiccation of plant tissues, cell death, and, ultimately, plant death (Brodribb and Cochard, 2009; Urli *et al.*, 2013; Adams *et al.*, 2017; Mantova *et al.*, 2022a,b; McDowell *et al.*, 2022).

Bearing this in mind, it is clear that determining the critical levels of embolism in plants' xylem is important for understanding their drought tolerance. The lethal level of embolism that is irrecoverable for plants is thought to be close to  $P_{88}$  (referring to xylem pressure leading to 88% loss of maximum conductance) (Hammond *et al.*, 2019; Johnson *et al.*, 2021; Mantova *et al.*, 2021, 2022b). While there are concerns that  $P_{88}$  may not be precise enough as an estimate of the point-of-no-return (Hammond *et al.*, 2019; Johnson *et al.*, 2021; Mantova *et al.*, 2021, 2022b),  $P_{50}$  or the pressure inducing 50% loss of hydraulic conductance is commonly used as a proxy for tolerance to xylem embolism (Tyree and Ewers, 1991; Maherali *et al.*, 2004; Choat *et al.*, 2012; Venturas *et al.*, 2017; Brodribb, 2017). The stomatal safety margin (SSM), referring to the difference between the water potential at stomatal closure ( $\Psi_{gs90}$ ) and  $P_{50}$ , is often regarded as an even more reliable parameter to estimate drought resilience, because it takes also into account dynamics of stomatal regulation (see next paragraph; Meinzer *et al.*, 2009; Choat *et al.*, 2012; Anderegg *et al.*, 2016; Martin-StPaul *et al.*, 2017; Eller *et al.*, 2018; Creek *et al.*, 2020; Dayer *et al.*, 2020; Skelton *et al.*, 2021; Oliveira *et al.*, 2021).

Plants have evolved a range of strategies to cope with the detrimental effects of drought-induced embolism on their growth and survival, and to maximize their performance and fitness during water shortages (Violle *et al.*, 2007). These mechanisms operate at various scales, involving processes at the morphological, anatomical, physiological, and molecular levels, and include multiple drought-related traits in different organs that act in concert to maintain metabolic activity without risking plant mortality (Allen *et al.*, 2009; Lata and Prasad, 2011; Choat *et al.*, 2012; Mitchell *et al.*, 2013; Basu *et al.*, 2016; Brodribb *et al.*, 2017b; Thonglim *et al.*, 2023; Limousin *et al.*, 2022). Stomata closure is one of the initial responses to drought, occurring before embolism formation (Brodribb *et al.*, 2003; Martin-StPaul *et al.*, 2017; Scoffoni *et al.*, 2017; Choat *et al.*, 2018). This process can be triggered by the production of abscisic acid (ABA) or ethylene in leaves as well as leaf turgor changes, which signals the guard cells in the stomata to close, leading to a significant reduction in water loss via transpiration and thereby helping to maintain high leaf water potential ( $\Psi_l$ ) (Desikan *et al.*, 2006; Tombesi *et al.*, 2015; Kuromori *et al.*, 2018). At the same time, stomatal closure also results in reduced CO<sub>2</sub> assimilation and photosynthetic activity (McDowell *et al.*, 2008; Brodribb *et al.*, 2017b;

Martínez-Vilalta and Garcia-Forner, 2017; Martin-StPaul *et al.*, 2017; Knipfer *et al.*, 2020). Plants also have the ability to modify their xylem anatomy to better avoid embolism formation and spread. For example, thicker intervessel pit membranes in angiosperms have been shown to better prevent the spread of embolisms between adjacent vessels (Lens *et al.*, 2011, 2022; Li *et al.*, 2016; Gao *et al.*, 2019; Kaack *et al.*, 2019, 2021; Zhang *et al.*, 2020; Thonglim *et al.*, 2021, 2023; Levionnois *et al.*, 2021; Isasa *et al.*, 2023). In addition, increasing stem lignification levels in otherwise non-woody lineages (Lens *et al.*, 2011, 2016; Dória *et al.*, 2018; Thonglim *et al.*, 2021, 2023) or modifying lignin composition enhances embolism resistance (Pereira *et al.*, 2018; Ménard *et al.*, 2022). Alternatively, plants can recover from massive embolism events by developing new wood tissue (Gauthey *et al.*, 2022), or they can prevent these detrimental embolism events by building more resistant xylem in combination with rapid stomatal closure leading to a large stomatal safety margin (SSM) (Creek *et al.*, 2020; Thonglim *et al.*, 2023). In addition to a wide range of physiological and anatomical adaptations, plants also respond to drought at the molecular level through the coordinated regulation of gene expression (Singh *et al.*, 2022). Under drought stress, water deficit triggers a reprogramming of the transcriptome, in which transcription factors (TFs), and gene regulatory networks (GRNs) play a critical role (Rabara *et al.*, 2014; Todaka *et al.*, 2015; Vermeirssen *et al.*, 2015; Chen *et al.*, 2016b; Joshi *et al.*, 2016). In the last decades, several NAC TFs in many different plant species have been identified as important regulators of responses to biotic and abiotic stresses, and have been shown to be useful for improving drought tolerance in crops (Le *et al.*, 2011; Al Abdallat *et al.*, 2014; Fang *et al.*, 2015; Sakuraba *et al.*, 2015; Wang *et al.*, 2016b).

JUNGBRUNNEN1 (*JUB1*) is a multifunctional TF of the NAC family in *Arabidopsis thaliana* that plays a central role in regulating plant longevity and the interplay between growth and stress responses (Shahnejat-Bushehri *et al.*, 2012, 2016; Wu *et al.*, 2012). *JUB1* functions as a positive regulator of drought tolerance not only in *Arabidopsis* but also in other species such as tomato and banana (Tak *et al.*, 2017; Thirumalaikumar *et al.*, 2018). The overexpression of *JUB1* (*JUB1OX*) strongly delays senescence and enhances drought tolerance, while the *JUB1* knockdown (*jub1kd*) mutant exhibits a drought sensitivity (Shahnejat-Bushehri *et al.*, 2012; Wu *et al.*, 2012; Ebrahimian-Motlagh *et al.*, 2017; Thirumalaikumar *et al.*, 2018). Even



though the mechanistic role of *JUB1* on drought tolerance is unclear, there is evidence suggesting its effect on enhancing the osmoprotectants accumulation (Wu *et al.*, 2012; Shahnejat-Bushehri *et al.*, 2017; Tak *et al.*, 2017; Alshareef *et al.*, 2019; Welsch, 2022) as well as lowering reactive oxygen species (ROS) levels in leaves (Shahnejat-Bushehri *et al.*, 2012, 2016; Wu *et al.*, 2012; Ebrahimian-Motlagh *et al.*, 2017; Thirumalaikumar *et al.*, 2018). In addition, nothing is known about *JUB1OX*'s impact on the underlying physiological response to drought and on the stem anatomical and hydraulic traits that are associated with embolism resistance.

In this study, we investigate the stem anatomical (proportion of stem lignification, intervessel pit membrane thickness) and hydraulic traits (stem  $P_{50}$ ), and quantified the drought response in wild-type and *JUB1* overexpression (*JUB1OX*) transgenic lines of *Arabidopsis thaliana* and tomato (*Solanum lycopersicum* L.). During the drought treatment, gas exchange, and leaf water potential ( $\psi_l$ ) dynamics were measured and complemented with stem  $P_{50}$  to calculate the SSM. We aimed to assess whether or not *JUB1OX* in *Arabidopsis* and tomato uses a set of integrated leaf and stem traits to enhance drought resilience. More in particular, we addressed the following research questions: (i) Do the *JUB1OX* transgenic lines in *Arabidopsis* and tomato develop the expected anatomical (more lignified stem, thicker intervessel pit membranes) and ecophysiological traits (more negative  $P_{50}$ , larger SSM, lower  $g_s$ , higher  $\psi_l$ ) that are known to be associated with improved drought response in other taxa? (ii) Are there any consistent differences in the traits investigated between the wild-type and *JUB1OX* genotypes in both species?

# Materials and methods

## ***Plant material and growth conditions***

The model plant, *Arabidopsis thaliana* (L.) Heynh. and the crop species *Solanum lycopersicum* L. (tomato) were investigated. For *Arabidopsis*, we studied the Columbia-0 (Col-0) ecotype (wild-type), and two transgenic lines in the Col-0 background: with one genotype with *JUNGBRUNNEN1* (*JUB1*) gene being overexpressed (*JUB1OX*), and another mutant line (*jub1kd*) where the expression of *JUB1* was knocked down. For tomato, we used one wild-type cultivar, *Solanum lycopersicum* L. cv. Moneymaker (MM), and one transgenic line *JUB1OX* in the MM background. To differentiate the same transgenic lines between both species, we added A- and T- prefixes to assign genotypes to either *Arabidopsis* or tomato.

### *Arabidopsis plants*

The seeds of each genotype were germinated directly into a mixture of soil and sand (ratio 4.5:1). At 10-12 days after germination, the healthy seedlings were transferred to 8 cm-diameter pots and grown individually under controlled growth chamber conditions. The growth chamber was set to maintain a 20°C temperature during the day and a 17°C temperature at night, with 70% relative humidity and a 16-hour photoperiod condition with 100  $\mu\text{mol m}^{-2} \text{s}^{-1}$  light intensity. The harvesting time between the wild-type and the transgenic lines was synchronized based on differences in inflorescence development and subsequent flowering time. To synchronize flowering, *JUB1OX* individuals were planted earlier, and their inflorescence stems were harvested 65 days after sowing for stem  $P_{50}$  and stem anatomical measurements. Col-0 and *jub1kd* plants were grown 10 days later, and their inflorescence stems were harvested 55 days after sowing (Supplementary Figure S1).

### *Tomato plants*

The seeds of each genotype were sowed in Murashige and Skoog (MS) agar medium containing 1% (w/v) sucrose. After three weeks, the seedlings with sufficiently developed roots were transferred to 15x15x19 cm (=3.3 L) pots. Pots contained a mixture of soil (basis biomix, Lensli®

substrates, Bleiswijk, the Netherlands), vermiculite and sand (ratio 25:8:2), and 3 spoons of osmocote fertilizer. All pots were placed in the same growth chamber with 70% relative humidity, 24 °C temperature, with a 16-hour photoperiod condition. (Supplementary Figure S1).

## **Generating stem vulnerability curves (VCs)**

### *Cavitron experiments in Arabidopsis*

At the Institute of Biology Leiden, *Arabidopsis* plants were harvested with roots, leaves, and flowers still intact. These individuals were then immediately wrapped in wet tissue paper and placed in plastic bags to prevent dehydration during the shipment to the PHENOBOIS platform (University of Bordeaux, France) for the Cavitron centrifuge measurements, which were carried out within a week of harvest. The roots were cut at the basal part of the inflorescence stems and the stems were trimmed to a length of 27 cm to match the standard Cavitron rotor. This 27 cm length exceeds the maximum vessel length of Col-0, which is only 4 cm (Tixier *et al.*, 2013), thereby preventing the open-vessel artefact. The siliques, leaves, and flowers were removed from the segments underwater right before placing the inflorescence stems in the Cavitron rotor. The xylem vulnerability to embolism was evaluated by measuring the water flow through the inflorescence stems via the increase of cavitation induced by lowering the xylem pressure at the middle part of stems during the spinning (Cochard, 2002; Cochard *et al.*, 2005). The negative pressure was gradually increased by -0.2 to -0.4 MPa in each spinning step. The degree of embolism in the xylem segment was then quantified as the percentage loss of conductivity (PLC). The PLC was calculated as

$$PLC = 100 \times (1 - (K/K_{max}))$$

where  $K$  is the decreased hydraulic conductivity due to embolisms.  $K_{max}$  ( $m^2 MPa^{-1} s^{-1}$ ) is the maximum hydraulic conductivity which was calculated when stem segments were fully functioning (no embolism) at a low spinning speed (near 0 MPa). The embolism formation at every rotation speed was measured using the Cavisoft software (Cavisoft v1.5, University of Bordeaux, France) and fitted the data points to reconstruct the VCs using a sigmoid

function based on the NLIN procedure in SAS 9.4 (SAS Institute, Cary, NC, USA) (Pammenter and Van der Willigen, 1998):

$$PLC = 100 \div [1 + \exp(\frac{S}{25} \times (P - P_{50}))]$$

where  $S$  ( $\text{MPa}^{-1}$ ) is the slope of the VC at  $P_{50}$ .  $P$  is the xylem pressure used at each rotation step, and  $P_{50}$  is the xylem pressure inducing 50% loss of hydraulic conductivity. We used seven to nine individuals to generate one vulnerability curve due to the low hydraulic conductivity of Arabidopsis. Four to eight VCs were constructed for each genotype.

### *Optical technique measurements in tomato*

The tomato plants with intact roots and leaves were transferred to the hydraulic laboratory at Naturalis Biodiversity Center (Leiden) and harvested. To prepare the plants for embolism visualization using the optical technique (Brodrigg *et al.*, 2017a), most of the soil was carefully removed from the root system using water to speed up the drying process. The stems were then secured underneath a stereomicroscope equipped with a camera and fixed with tape to minimize any movement during drought-induced shrinkage. Next, a razor blade was used to carefully remove the stem cortex to expose the xylem to the camera. Hydrogel was applied to the exposed surface to enhance light transmission and minimize the evaporation (Brodrigg *et al.*, 2017a). To visualize and quantify emboli in the stems through time, the plants were automatically photographed at five-minute intervals until the leaves were completely dry, and impossible to measure the water potential; this took approximately one week. Stem water potential was monitored in bagged leaves two to three times a day with a Scholander's pressure chamber (PMS Instrument Company, Albany, Oregon, USA). Fiji software (Schindelin *et al.*, 2012) and the OSOV toolbox plugin were used to analyze the optical data, following the open-source OV protocols on GitHub ([www.opensourceov.org](http://www.opensourceov.org)). The formation and spread of emboli over time were determined by subtracting the differences in pixels in the major veins (1<sup>st</sup> to 3<sup>rd</sup>-order veins) between subsequent images. Background noise, mainly caused by tissue shrinkage, was removed using mild filters for noise removal and manual inspection of the image and pixels. The VCs were reconstructed using the same sigmoid function (as in

Arabidopsis mentioned above). Four to seven VCs were constructed for each genotype.

### ***Stem anatomy***

To study stem anatomy, three representative stems per genotype of both Arabidopsis and tomato were randomly selected for light microscopy (LM) and transmission electron microscopy (TEM) observations. In Arabidopsis, the middle part of the 27 cm inflorescence stem segments, where negative pressures were applied during Cavitron measurements, were sectioned to obtain anatomical traits data. In tomato, basal stem parts were selected from areas close to the area where embolism resistance was measured. The features measured from this part provided accurate information linking anatomical traits and embolism resistance ( $P_{50}$ ). The measured traits are shown in Supplementary Table S1. We used ImageJ (National Institutes of Health, Bethesda, MD, USA) to measure the anatomical features in digital images from both LM and TEM observations, following the recommendations by Scholz *et al.* (2013).

#### *Light microscopy*

##### *Arabidopsis*

One cm long pieces of inflorescence stems were stored in 70% ethanol. The fixed samples were then gradually infiltrated and embedded in LR-White resin (Hamann *et al.*, 2011). The embedded samples were sectioned at 4  $\mu\text{m}$  thickness using a rotary microtome (Leica RM 2265, Leica, Eisenmark Wetzlar, Germany) with disposable tungsten carbon blades. Then, the sections were heat-fixed onto the slides, stained with 1% (w/v) toluidine blue (VWR Chemicals BDH., Radnor, PA, USA), and mounted with DPX new-100579 mounting medium (Merck Chemicals, Amsterdam, the Netherlands). Finally, the anatomical traits were observed using a Leica DM2500 light microscope and photographed with a Leica DFC-425 digital camera (Leica microscopes, Wetzlar, Germany).

## *Tomato*

The basal parts of the stems were cut into 40 µm thick transverse sections using a sliding microtome (Reichert) with N35 microtome blades. The sections were then bleached with household bleach containing 3% sodium hypochlorite (Acros), rinsed with demi water, and stained with a mixture of Safranin O (Chroma) and Alcian Blue (Sigma-Aldrich) in a ratio 35:65 (Lens *et al.*, 2007). The safranin was prepared as a 1% solution in 50% ethanol. The 1% alcian blue stain was dissolved in pure water. Subsequently, the stained sections were dehydrated in a series of ethanol (50%, 70%, and 96% respectively), treated with a 1:1 combination of 96% ethanol and the histological clearing agent Limonene (HISTO-CLEAR, EMS), and afterward cleared with 100% Limonene and finally mounted on a microscope slide using Euparal green (Chroma). The sections were observed using an AXIO Imager.M2 (Zeiss) motorized microscope with a camera and photographed using Axiovision software.

## *Transmission electron microscope (TEM)*

The 1 cm long stem pieces of *Arabidopsis* and tomato were fixed in Karnovsky's fixative for 48 h (Karnovsky, 1965), adjacent to the stem segments sampled for light microscopy. The samples were rinsed with 0.1 M cacodylate buffer and post-fixed with 1% buffer osmium tetroxide, and then stained with 1% uranyl acetate. The stained samples were dehydrated in a series of ethanol: 1% uranyl acetate replacement, with increasing concentration of ethanol. The dehydrated samples were then infiltrated with Epon 812n (Electron Microscopy Sciences, Hatfield, UK) and placed in the oven (60°C) for 48 h. The Epon blocks were cut into semi-thin (2 µm) and ultra-thin (90-95 nm) sections using a Leica EM UC7 ultramicrotome with a diamond knife. The sections were dried and mounted on film-coated copper slot grids, and post-stained with uranyl acetate and lead citrate. The sections were observed with a JEM-1400 Plus TEM (JEOL, Tokyo, Japan) with an 11-megapixel digital camera (Quemesa, Olympus).

## **Drought treatment**

### *Arabidopsis*

Seeds of each genotype were sown directly in 6x6x7 cm (=0.25 L) pots with the same ratio of soil and sand mixture (4.5:1) at different times to synchronize flowering (35 days after sowing for Col-0 and *A-jub1kd* and 45 days after sowing for *A-JUB1OX*). The weight of the pot with dry and saturated soil was controlled. The plants were grown in a growth chamber under controlled conditions similar to those used for anatomical and stem  $P_{50}$  measurements. During the experiment, thirty individuals of each genotype were equally divided into a control (well-watered) and a drought batch. The control group of plants received daily watering to keep the soil consistently hydrated, whereas the drought batch experienced a water deficit by completely abstaining from watering for three weeks, starting one week prior to flowering.

### *Tomato*

The tomato plants used in the drought experiment were grown in the same 3.3 L pots and under the same condition as those used for the anatomical and stem  $P_{50}$  measurements. After 55 days after potting, plants of both genotypes were randomly assigned to control and drought treatments (10 control and 10 drought individuals). The control plants were well-watered every day, while plants from the drought group did not receive any water for 10 days.

## **Leaf water potential ( $\Psi_l$ ), stomatal conductance ( $g_s$ ), and $CO_2$ assimilation rate ( $A$ )**

### *Arabidopsis*

The leaf water potential of well-watered and drought batches was measured every day until the end of the experiment (15-17 days), starting from a 7-d water deficit which is the required time to dehydrate the moisturized soil in the pots of the drought batch. To carry out the daily measurements, three mature rosette leaves, one from the control batch and two from the drought batch, were covered with aluminum foil for 30

minutes before the measurements. The leaf discs were then cut from the wrapped leaves and placed in the PSYPRO device (Wescor, Inc., Logan, UT, USA) to measure leaf water potential. Stomatal conductance ( $g_s$ ,  $\text{mmol m}^{-2} \text{s}^{-1}$ ) was measured daily on the mature rosette leaves that were close to those used for water potential measurements, using an SC-1 leaf porometer (METER Group, Pullman, WA, USA). The  $g_s$  was measured using Auto Mode configuration with desiccant. Due to the small size of Arabidopsis leaves, we encountered limitations in using Targas-1 (PP systems, Amesbury, MA, USA) for measuring stomatal conductance and  $\text{CO}_2$  assimilation rate. As a result, we were unable to obtain data on  $\text{CO}_2$  assimilation rate in Arabidopsis.

### Tomato

The  $\Psi_1$  measurements were carried out daily in both control and drought plants starting from the first day of withholding water until the end of the drought experiment (10 days). Four to five mature leaves of each genotype were bagged in aluminum zip-lock bags for at least 30 minutes before the measurements. The leaves were then cut at the base of the petiole with a fresh razor blade and  $\Psi_1$  was measured using a Model 1000 Pressure Chamber Instrument (PMS Instrument Company, Albany, Oregon, USA) (Rodriguez-Dominguez *et al.*, 2022). The  $g_s$  of the mature leaves was measured every day using an SC-1 leaf porometer (METER Group, Pullman, WA, USA) with the same mode as the one used for Arabidopsis and compared with a Targas-1 Portable Photosynthesis System (with a LED light unit; PP systems, Amesbury, MA, USA). To determine the water potential at 90% of the stomatal closure ( $\Psi_{gs90}$ ), the stomatal conductance of both species was fit according to the following sigmoid function for each genotype using the NLIN procedure in SAS:

$$g_s = g_{sm} \div [1 + \exp(S \times (\Psi_{gs} - \Psi_{gs50}))]$$

where  $g_{sm}$  is the maximal stomatal conductance for  $\Psi_1 = 0$ .  $S$  is the slope of the curve, and  $\Psi_{gs50}$  is the water potential inducing 50% stomatal closure.

Stomatal conductance data obtained from both the porometer and the Targas-1 instrument showed no significant differences between them, as shown in Supplementary Figure S2. Consequently, we chose to utilize the  $g_s$  data acquired from the Targas-1 instrument, along with the  $\text{CO}_2$  assimilation rate data, for our subsequent analyses.



## ***Stomatal safety margin (SSM)***

The SSM was defined as the difference between the leaf water potential at 90% stomatal closure and stem  $P_{50}$  (Martin-StPaul *et al.*, 2017). It can be calculated from the fitted curve ( $\Psi_{gs90}$ ) and the water potential at 50% loss of stem conductivity ( $P_{50}$ ) as follows:

$$SSM = \Psi_{gs90} - P_{50}$$

## ***Statistical analysis***

The statistical analyses of all traits studied were performed using R version 3.6.3 in R Studio version 1.2.5033. A  $P$ -value of  $<0.05$  was considered significant for all differences observed. Initially, general linear models were used to assess differences in embolism resistance ( $P_{50}$ ,  $P_{12}$ , and  $P_{88}$ ) and anatomical features among the genotypes studied, followed by a Newman-Keuls post-hoc test. Multiple linear regression was then applied to determine the anatomical traits (predictive variables) that explain differences in embolism resistance (responsive variables, including  $P_{50}$ ,  $P_{12}$ , and  $P_{88}$ ). Collinearity between variables was checked to select predictors, and the 'step' function (stats package; R Core Team, 2016) was used to obtain the most parsimonious linear regression model based on the least Akaike information criterion (AIC). Residuals, heteroscedasticity, skewness and kurtosis, and variance inflation factor (VIF) were checked once the best model was obtained. The relative importance of each explanatory variable was analyzed to determine the variable that best explains  $P_{50}$ . Pearson's correlation was used to plot the relationship between  $P_{50}$  and predictive variables. Lastly, a generalized linear mixed model was used to investigate whether the different genotypes exhibited different  $g_s$  in well-watered control conditions. The genotypes were used as a fixed effect using the GLIMMIX procedure in SAS (SAS 9.4; SAS Institute).

## Results

### ***Phenotypic variation in drought responses in Arabidopsis and tomato***

After subjecting Arabidopsis and tomato plants to a water deficit treatment for a period of up to 17 days and 10 days, respectively, we observed notable differences in the phenotypes of the drought-treated batches compared to the well-watered plants. The drought-treated plants were consistently smaller in size than the well-watered plants for each species, and the leaves of the drought-treated A-T-wild-types and *A-jub1kd* individuals showed strong signs of leaf wilting, as well as a higher incidence of yellow leaves and leaf senescence (Figure 1). Interestingly, the *JUB1OX* transgenic lines of both species demonstrated no leaf wilting, and the leaves retained their green color without any observation of leaf senescence (A-*JUB1OX* and T-*JUB1OX* shown in Figure 1).

### ***Leaf water potential ( $\psi_l$ ), dynamics of stomatal conductance ( $g_s$ ), and $CO_2$ assimilation rate ( $A$ ) under drought stress***

In well-watered plants,  $\psi_l$  was similar for each species, with Arabidopsis displaying a value of -0.5 MPa, and tomato exhibiting a range between -0.2 to -0.25 MPa for all genotypes studied (Figure 2A, 2C; Supplementary Figure S3). During the onset of drought, we observed a consistent difference between  $\psi_l$  decline in *JUB1OX* genotypes and the other genotypes studied: A-T-*JUB1OX* plants maintained a stable and high  $\psi_l$  for several days before exhibiting a gradual decline, while A-T-wild-types, and *A-jub1kd* mutant exhibited an earlier and more rapid  $\psi_l$  decline (Figure 2A, 2C). This more rapid  $\psi_l$  decline in the latter three genotypes means that  $P_{50}$  was reached after only 9 days of drought (T-wild-type) and 11 days of drought (A-wild-type and *A-jub1kd*); T- and A-*JUB1OX* plants reached  $P_{50}$  much later: later than 10 days after onset of water deficit and at day 14, respectively (Figure 2A, 2C; Table 1).



**Figure 1** Representative images showing phenotypic variation between well-watered and drought-treated individuals of *Arabidopsis* (68-72 days after sowing) and tomato (65 days after potting) across all the genotypes studied, taken at the end of the drought treatment (up to 17 days of water deficit in *Arabidopsis*, and 10 days of water deficit in tomato). At least seven plants per genotype and conditions were analyzed.

The patterns of stomatal conductance ( $g_s$ ) showed more variation between the two species. In Arabidopsis, the stomatal conductance of A-wild-type and *A-jub1kd* was similarly high before drought, approximately  $360 \text{ mmolm}^{-2}\text{s}^{-1}$ , and gradually declined during the first week of drought. This was followed by a steep decline in  $g_s$  on day 7 and day 9, respectively, until they reached 90% of stomatal closure ( $g_{s90}$ ) after 10-11 days of water deficit. *A-JUB1OX* genotype exhibited lower  $g_s$  at well-watered conditions ( $255 \text{ mmolm}^{-2}\text{s}^{-1}$ ) and maintained a gradual decline over time until it reached  $g_{s90}$  a few days later than the other two genotypes (14 days after onset of drought) (Figure 2B; Table 1). The well-watered tomato plants showed another pattern. The T-*JUB1OX* transgenic line displayed an equally high  $g_s$  as the T-wild-type, with a value of  $420 \text{ mmolm}^{-2}\text{s}^{-1}$ . Quickly after the onset of drought,  $g_s$  of T-wild-type declined steadily until it reached  $g_{s90}$  on day 6 of drought, while T-*JUB1OX* exhibited first a  $g_s$  plateau between day 3-6 after the onset of water deficit before declining rapidly, reaching  $g_{s90}$  one to two days later than the wild-type (Figure 2D; Table 1; Supplementary Figure S3).

Under well-watered conditions, the T-*JUB1OX* genotype displayed a significantly higher  $\text{CO}_2$  assimilation rate ( $A$ ) compared to the T-wild-type ( $F = 9.97$ ,  $P = 0.002$ ). Furthermore, the *JUB1OX* genotype could maintain a greater  $\text{CO}_2$  assimilation rate and exhibited a slower decline in assimilation than the wild-type during the drought experiment (Figure 2E; Supplementary Figure S3C).

### ***Stem vulnerability to embolism based on vulnerability curves (VCs)***

We observed different patterns of stem vulnerability between Arabidopsis and tomato among the genotypes studied. In Arabidopsis, the wild-type demonstrated the highest resistance to embolism, with a  $P_{50}$  value of  $-2.14 \text{ MPa}$ , followed by *A-JUB1OX* ( $P_{50}$ :  $-1.58 \text{ MPa}$ ) and *A-jub1kd* ( $P_{50}$ :  $-1.37 \text{ MPa}$ ). The slope of the VCs was more gradual in A-Col-0, but steeper in *A-JUB1OX* and *A-jub1kd* (Figure 3A). In tomato, however, T-wild-type and T-*JUB1OX* exhibited no significant difference in embolism resistance and slope, with  $P_{50}$  values of  $-1.54$  and  $-1.45 \text{ MPa}$ , respectively (Figure 3B). The  $P_{12}$  values (stem water potential at the onset of embolism) showed the same pattern in both Arabidopsis and tomato, with wild-types having less negative  $P_{12}$  values than the overexpression transgenic lines (Table 1). The  $P_{12}$  values of each genotype were significantly different from each other ( $F = 2.317$ ;  $P$

$< 2e^{-16}$ ). In contrast, the  $P_{88}$  values showed the opposite pattern, with wild-types of both species exhibiting more negative values than *JUB1OX* genotypes. The  $P_{88}$  values of each genotype in both species were also significantly different from each other ( $F = 2.704$ ;  $P < 2e^{-16}$ ) (Table 1).

**Table 1** The hydraulic data of Arabidopsis and tomato genotypes studied

Genotypes	$P_{12}$ (MPa)	$P_{50}$ (MPa)	$P_{88}$ (MPa)	$\Psi_{gs90}$ (MPa)	SSM (MPa)	Days until 90% stomatal closure	Days until $P_{50}$
<b>A-Col-0</b>	-0.78	-2.14	-3.51	-0.9	1.24	10	11
<b>A-<i>JUB1OX</i></b>	-0.94	-1.58	-2.21	-1.03	0.55	14	14
<b>A-<i>jub1kd</i></b>	-0.96	-1.37	-1.78	-1.05	1.32	11	11
<b>T-MM</b>	-1.12	-1.54	-1.96	-0.55	0.99	6	9
<b>T-<i>JUB1OX</i></b>	-1.21	-1.45	-1.69	-0.43	1.02	7	does not reach $P_{50}$

$P_{12}$  = stem water potential at 12% loss of hydraulic conductivity,  $P_{50}$  = stem water potential at 50% loss of hydraulic conductivity,  $P_{88}$  = stem water potential at 88% loss of hydraulic conductivity,  $\Psi_{gs90}$  = leaf water potential at 90% stomatal closure, SSM= stomatal safety margin

### **Stomatal safety margin (SSM)**

All the genotypes studied in both Arabidopsis and tomato exhibited positive SSMs. In Arabidopsis, the widest SSM was observed in A-wild-type with a value of 1.24. The A-*JUB1OX* and A-*jub1kd* mutants had narrower SSM values of 0.55 and 0.32, respectively. In tomato, T-*JUB1OX* showed a similar SSM compared to T-wild-type with values of 1.02 and 0.99, respectively (Table 1).

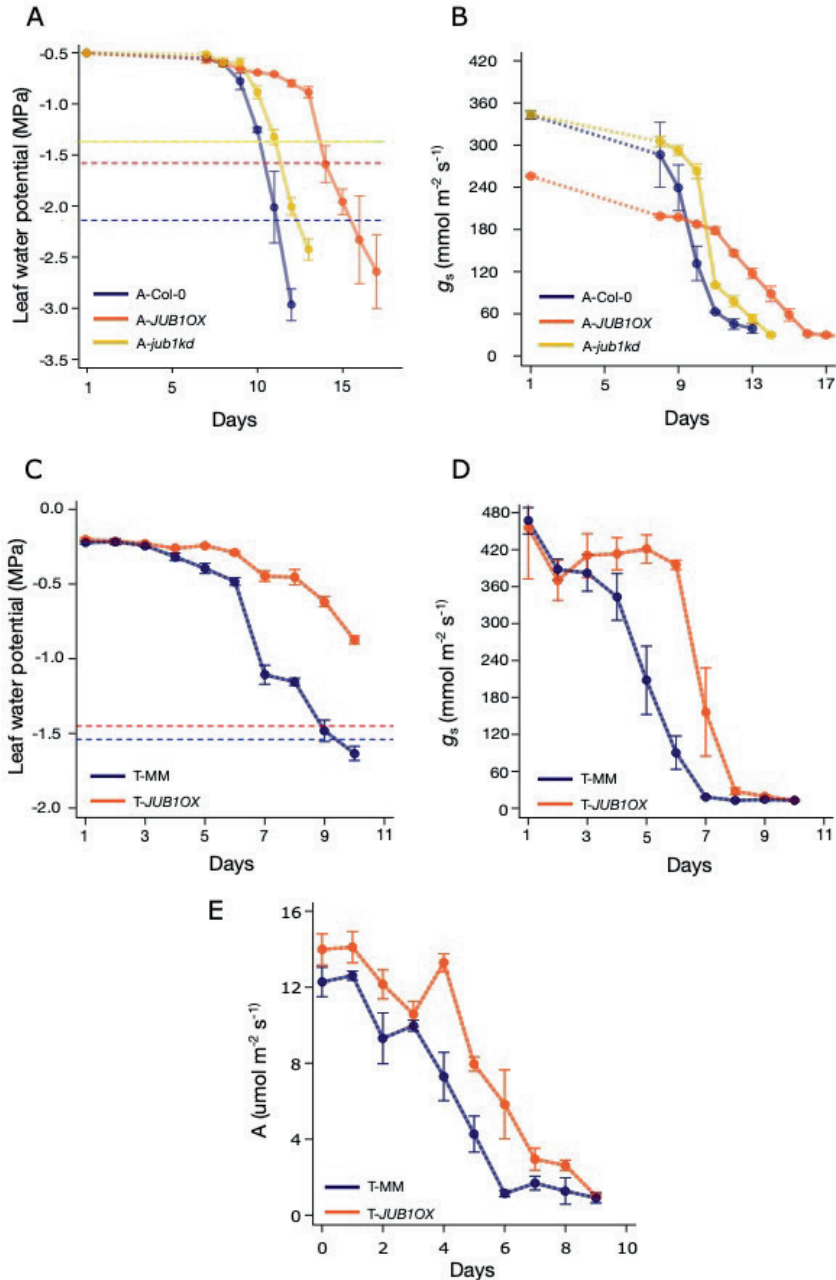


**Figure 2** Drought-responsive traits for the Arabidopsis and tomato genotypes measured during the drought experiment. (A) The leaf water potential ( $\psi_l$ ) over time. (B) The stomatal conductance ( $g_s$ ) of Arabidopsis over time. (C) Tomato  $\psi_l$  over time. (D) Tomato  $g_s$  over time. (E) Tomato CO<sub>2</sub> assimilation (A) over time. Colours refer to the genotype studied: wild-type (blue); *JUB1* overexpression (orange); *JUB1* knocked down (yellow).

### **Differences in stem anatomical traits among genotypes studied**

Our study revealed significant differences in various anatomical traits among genotypes within both species. Interestingly, in both *Arabidopsis* and tomato, the wild-types had thicker intervessel pit membranes ( $T_{PM}$ ) (Supplementary Figure S4) ( $F = 237.4$ ,  $P = 1.94e^{-06}$  and  $F = 10.76$ ,  $P = 0.03$ , respectively) and a higher proportion of fiber wall area per fiber cell area ( $PF_{WFA}$ ) ( $F = 54.53$ ,  $P = 0.0001$  and  $F = 334.8$ ,  $P = 5.25e^{-05}$ , respectively) compared to the overexpression transgenic lines (*JUB1OX*), while the knockdown line in *Arabidopsis* (*A-jub1kd*) had the thinnest  $T_{PM}$  and  $PF_{WFA}$ . The wild-types of both species had the widest maximum vessel diameter ( $D_{MAX}$ ) compared to other genotypes, followed by *JUB1OX* transgenic lines and the *jub1kd* line in *Arabidopsis* ( $F = 12.24$ ,  $P = 0.0076$  and  $F = 46.57$ ,  $P = 0.0024$ , respectively). Furthermore, vessel wall thickness ( $T_V$ ) was significantly different among *Arabidopsis* genotypes, with A-Col-0 (wild-type) having the thickest vessel walls and *A-jub1kd* possessing the thinnest walls ( $F = 45.95$ ,  $P = 0.0002$ ), but no differences were found in tomato. Likewise, the proportion of lignified area per total stem area ( $P_{LIG}$ ) showed significant differences among *Arabidopsis* genotypes, with A-Col-0 having the highest  $P_{LIG}$  followed by A-*JUB1OX* and *A-jub1kd* ( $F = 41.8$ ,  $P = 3e^{-04}$ ), whereas tomato genotypes did not show any difference. With respect to vessel grouping ( $V_G$ ), we measured the highest mean value in A-*JUB1OX*, and the lowest  $V_G$  in A-Col-0 ( $F = 59.38$ ,  $P = 0.0001$ ), but no differences were detected in tomato. For vessel density ( $V_D$ ), we found the opposite pattern:  $V_D$  of T-*JUB1OX* was significantly higher than that of the T-MM wild-type ( $F = 13.43$ ,  $P = 0.0215$ ), but no differences were observed among *Arabidopsis* genotypes.

### **Stem anatomical traits explaining the variation in embolism resistance**

Based on the most parsimonious model obtained through multiple linear regression (AIC = -245.59), we found that the stem anatomical predictors of embolism resistance variation were  $T_{PM}$ ,  $PF_{WFA}$ ,  $D_{MAX}$ , and  $T_V$  ( $R^2 = 0.910$ ,  $P < 2.2e^{-16}$ ). Among these,  $T_{PM}$  had the highest relative importance (34%) explaining  $P_{50}$  variation, followed by  $PF_{WFA}$  (28%),  $D_{MAX}$  (18%), and  $T_V$  (12%) (Supplementary Figure S5A). These anatomical traits also accounted for a significant proportion of the variation in  $P_{12}$  (62 % relative importance), with  $T_{PM}$  being also the most important predictor,

responsible for almost half of the variation ( $R^2 = 0.6931$ ,  $P = 3.699e^{-16}$ ) (Supplementary Figure S5B). Among the predictors of  $P_{88}$  variation,  $P_{FWFA}$  was found to be the most significant one with a relative importance of 41% ( $R^2 = 0.5269$ ,  $P = 3.62e^{-11}$ ) (Supplementary Figure S5C).

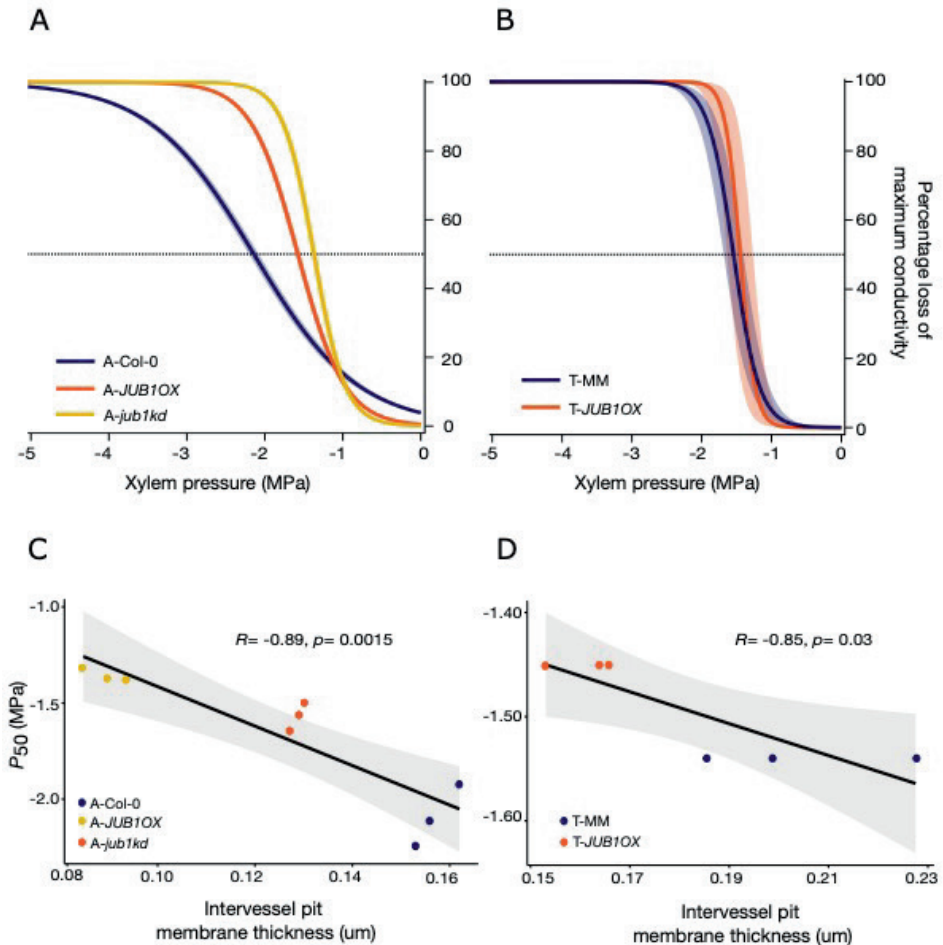


**Figure 3** Mean vulnerability curves (VCs) presenting the percentage loss of conductivity (PLC) as a function of xylem pressure (MPa) of (A) Arabidopsis and (B) tomato across the genotypes studied. Shaded bands represent standard errors based on four to eight VCs per genotype. (C) The scatter plots based on Pearson's correlation analysis show the correlations of  $P_{50}$  and intervesSEL pit membrane thickness ( $T_{PM}$ ) of Arabidopsis and (D) tomato. Colours refer to the genotype studied: wild-type (blue); *JUB1* overexpression (orange); *JUB1* knocked down (yellow).



## Discussion

This study presents for the first time a set of anatomical and hydraulic traits of stems and leaves in Arabidopsis and tomato plants to elucidate the *JUB1*-mediated mechanisms underlying the increased drought tolerance observed. Interestingly, among all the traits observed during the drought treatment, only the high and stable leaf water potential is in agreement with the increased drought resilience behaviour of *JUB1* overexpression (*OX*) plants compared to the wild-type plants in both species. Interestingly, the underlying anatomical and physiological modifications triggered by *JUB1* overexpression are not in line with traits associated with drought resilience as observed in many other studies, opening new perspectives on the role of *JUB1* in plant response to drought.

### ***High leaf water potential ( $\Psi_l$ ) is central in *JUB1OX* plants' drought resilience***

The improved drought tolerance of the *JUB1OX* plants in both Arabidopsis and tomato compared to the wild-types and the *JUB1* knockdown line in Arabidopsis (*A-jub1kd*) is attributed to their capacity to maintain high leaf water potential ( $\Psi_l$ ) during drought stress (Figures 1-2). In Arabidopsis, a lower initial stomatal conductance ( $g_s$ ) in *A-JUB1OX* compared to wild-type, gradually decreasing up to 10 days of withholding water followed by a steeper decline, is consistent with a high and relatively stable  $\Psi_l$  up to 13 days of water deficit (Figure 2A, 2B). In contrast, the Arabidopsis wild-type and *A-jub1kd* showed a considerably higher  $g_s$  followed by a more rapid decline of stomatal conductance after 8-9 days and a subsequent steep drop of  $\Psi_l$  at 9-10 days during drought (Li *et al.*, 2017; Dayer *et al.*, 2020; Lemaire *et al.*, 2021a; Welsch, 2022). Interestingly, *A-JUB1OX* reached full stomatal closure later than the wild-type and *A-jub1kd* (Figure 2B), enabling extended photosynthetic activity without risking detrimental levels of drought-induced embolism (Thonglim *et al.*, 2023). In contrast, *JUB1OX* in tomato displayed an equally high initial  $g_s$  compared to wild-type tomato plants and kept its stomata fully open for six days before showing a dramatic  $g_s$  drop (Figure 2D). Despite the greater loss of water through transpiration, *T-JUB1OX* plants were able to maintain a high  $\Psi_l$  for two more days (up to eight days of water deficit) before a more drastic decline compared to the *T-MM* wild-type (Figure 2C). In other words, the

inconsistency in  $g_s$  differences between the overexpression genotypes and the wild-types in Arabidopsis and tomato suggest that stomatal conductance does not explain why leaf water potential in *JUB1OX* plants remains high for a longer period of drought stress.

### ***Plants can exhibit markedly different mechanisms to drought within a single species***

Contrary to what we expected, the remaining hydraulic and stem anatomical traits that have often been shown to be associated with increased drought resilience in Arabidopsis and other species, such as more negative stem  $P_{50}$ , broader stomatal safety margins, thicker intervessel pit membranes and higher levels of stem lignification (Thonglim *et al.*, 2021, 2023; Lens *et al.*, 2022) are not observed in the more resilient *JUB1* overexpression lines in both Arabidopsis and tomato plants. Especially the presence of thinner intervessel pit membranes and less lignified stems in both A-*JUB1OX* and T-*JUB1OX* plants compared to wild-type plants is remarkable given the relevance of these traits in the improved drought response of Arabidopsis and beyond (Li *et al.*, 2016; Dória *et al.*, 2018; Thonglim *et al.*, 2021, 2023; Guan *et al.*, 2022; Lens *et al.*, 2022). It is remarkable to see that even in species with a short life cycle, such as Arabidopsis, substantially different strategies can be employed to acquire a certain level of drought tolerance. Therefore, our observations demonstrate that the increased drought tolerance of *JUB1* overexpression plants is not due to their drought-responsive anatomical and hydraulic traits. Instead, the only consistent observed trait that is in line with the improved drought stress behaviour of the A-T-*JUB1OX* plants is their ability to maintain high leaf water potential for a longer period of water shortage.

### ***Suggested mechanisms leading to increased drought response of JUB1OX plants***

Our results clearly indicate that the improved drought tolerance of *JUB1* overexpression plants is not due to their anatomical and hydraulic traits that are otherwise known to play a role in drought-induced mechanisms. But what are the potential drought-related traits that we have missed in our study? From the literature, there are two *JUB1*-mediated candidates that could offer an explanation for the elevated  $\psi_l$  during the

period of water deficit. One line of research indicates that *JUB1* overexpression leads to increased levels of the amino acid proline (Pro) in various species (Wu *et al.*, 2012; Shahnejat-Bushehri *et al.*, 2017; Tak *et al.*, 2017; Alshareef *et al.*, 2019; Welsch, 2022). Proline accumulation is crucial for the plants' ability to overcome lower water potential, as it acts as an osmolyte, facilitating additional water uptake and buffering the immediate impact of water scarcity. Furthermore, proline helps with cellular osmotic adjustment and stabilizes sub-cellular structures, thereby contributing to enhanced drought tolerance in plants (Heuer, 2010; Blum, 2017; Hasanuzzaman *et al.*, 2019; Ahmad *et al.*, 2020; Ozturk *et al.*, 2021). Additionally, the overexpression of *JUB1* could also result in a reduction of reactive oxygen species (ROS), particularly H<sub>2</sub>O<sub>2</sub>, through the accumulation of DELLA proteins (Shahnejat-Bushehri *et al.*, 2012, 2016; Wu *et al.*, 2012; Ebrahimian-Motlagh *et al.*, 2017; Thirumalaikumar *et al.*, 2018). ROS accumulation during stress can cause oxidative damage to various cellular components, leading to reduced photosynthetic efficiency, reduced cell membrane stability, metabolic dysfunction, and ultimately cell death (Benjamin and Nielsen, 2006; Cruz De Carvalho, 2008; Hanin *et al.*, 2011; Choudhury *et al.*, 2013, 2017). Unfortunately, our study did not analyze the concentration of osmoprotectants nor ROS, as this will be the focus of a follow-up study that will further disentangle whether and how *JUB1* regulates osmoprotectants accumulation and ROS mitigation at the molecular level. We did, however, observe that T-*JUB1OX* maintained higher CO<sub>2</sub> assimilation rates under well-watered conditions (Supplementary Figure S3C), and exhibited a slower decline of CO<sub>2</sub> assimilation rates during drought (compared to T-wild-type; Figure 2E) implying more efficient photosynthesis and possibly a faster production of osmoprotectants and antioxidant compounds under both drought and well-watered conditions. The potential role of *JUB1* serves as a promising initial step to dive deeper into the *JUB1*-mediated mechanistic role of improved drought tolerance, and further experiments should be conducted to confirm this.

In conclusion, the key factor for enhancing drought response in *JUB1OX* plants is the preservation of a high leaf water potential. However, unlike other *Arabidopsis* genotypes, none of the studied stem anatomical features or hydraulic traits, which were previously linked to enhanced drought tolerance, are involved in the underlying mechanisms. This suggests that *JUB1* acts on different gene regulatory pathways leading to drought

resilience, possibly via increased osmoprotectants and/or decreased ROS, compared to those activated in other resilient *Arabidopsis* genotypes which tend to develop more embolism resistant stems that are more lignified and have thicker intervessel pit membranes. The presence of multiple, contrasting drought strategies in a single annual species is remarkable and highlights the adaptive abilities of plants to cope with drought stress. It is therefore imperative to perform drought experiments across multiple accessions/genotypes in, for instance, crops to gain a better picture of their full potential to respond to drought.

## **Acknowledgements**

We would like to thank Rob Langelaan (Naturalis Biodiversity Center) and Gaëlle Capdeville (BIOGECO INRA) for technical support in TEM observations and Cavitron centrifuge measurements, respectively. This work was funded by a PhD scholarship awarded by the Institute for the Promotion of Teaching Science and Technology (IPST), Thailand, and by the Dutch Research Council NWO (grant ALWOP.488).

## Supplementary data

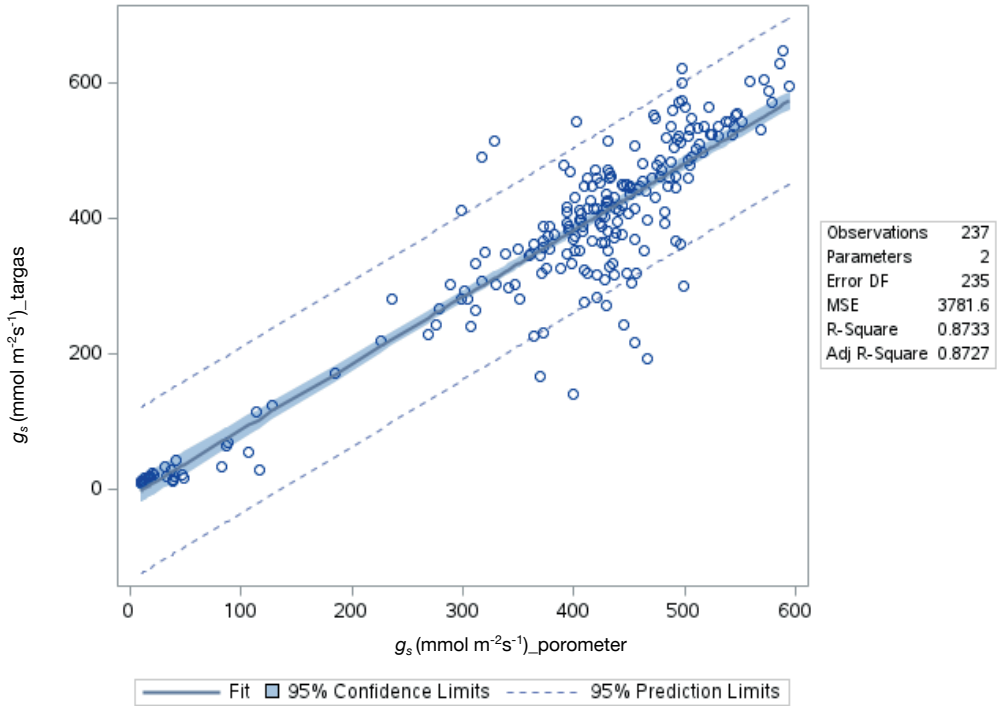
**Supplementary Table S1** The anatomical characters and hydraulic values measured with acronyms, definitions, calculations, units, and microscope techniques

Acronyms	Definition	Calculation	Number of measurements	Unit	Technique
A	CO <sub>2</sub> assimilation	$A = - [(C_{out} - C_{in}) \times W] + (C_{out} \times E)$	At least 1 control sample and 2 drought samples for each measurement	$\mu\text{mol m}^{-2}\text{s}^{-1}$	Targas-1
A <sub>F</sub>	Fiber cell area	Area of single xylem fiber in cross-section	Min. 30 fibers	$\mu\text{m}^2$	LM
A <sub>FL</sub>	Fiber lumen area	Area of single xylem fiber lumen in cross-section	Min. 30 fibers	$\mu\text{m}^2$	LM
A <sub>FW</sub>	Fiber wall area	$A_F - A_{FL}$ for the same fiber	Min. 30 fibers	$\mu\text{m}^2$	LM
A <sub>LIG</sub>	Lignified stem area	Total xylem area + fiber caps area + lignified pith cell area in cross-section	9 stems per accession	$\text{mm}^2$	LM
A <sub>S</sub>	Total stem area	Total stem area in cross-section	9 stems per accession	$\text{mm}^2$	LM
Day <sub>90</sub>	Days until reaching 90% of stomatal closure	-	-	days	-
D	Diameter of vessels	$D = (\sqrt{4A}/\pi)$	Min. 50 vessels	$\mu\text{m}$	LM
D <sub>MAX</sub>	Maximum vessel lumen diameter	Diameter of single vessel	Min. 30 vessels	$\mu\text{m}$	LM
D <sub>PC</sub>	Pit chamber depth	Distance from the relaxed pit membrane to the inner pit aperture	Min. 25 pits	$\mu\text{m}$	TEM
<i>g<sub>s</sub></i>	Stomatal conductance	-	1 control sample and 2 drought samples each measurement	$\text{mmol m}^{-2}\text{s}^{-1}$	Porometer
SSM	Stomatal safety margin	$\Psi_{gS90} - P_{50}$	1 SSM per accession	MPa	-

Acronyms	Definition	Calculation	Number of measurements	Unit	Technique
$P_{50}$	Stem water potential at 50% loss of hydraulic conductivity	-	8 values per each accession	MPa	Cavitron centrifuge
$P_{88}$	Stem water potential at 88% loss of hydraulic conductivity	-	8 values per each accession	MPa	Cavitron centrifuge
$P_{FWFA}$	Proportion of fiber wall area per fiber cell area	$A_{FW}/A_F$ for the same fiber; a measure of xylem fiber wall thickness	Min. 30 fibers	-	LM
$P_{LIG}$	Proportion of lignified area per total stem area	$A_{LIG}/A_S$	9 stems per accession	-	LM
$T_{PM}$	Intervessel pit membrane thickness	Thickness of intervessel pit membrane measured at its thickest point	Min. 25 pit membranes	$\mu\text{m}$	TEM
$T_V$	Vessel wall thickness	Thickness of a single vessel wall	Min. 30 vessels	$\mu\text{m}$	LM
$(T_{VW}/D_{MAX})^2$	Theoretical vessel implosion resistance	$(T_{VW}/D_{MAX})^2$	Min. 30 measurements	-	LM
$V_D$	Vessel density	Number of vessels per $\text{mm}^2$	Min. 5 measurements	No. of vessel per $\text{mm}^2$	LM
$V_G$	Vessel grouping index	Ratio of total number of vessels to total number of vessel groupings (incl. solitary and grouped vessels)	Min. 50 vessel groups	-	LM
$\psi_{gs90}$	Leaf water potential at 90% loss of stomatal conductance	-	At least 3 control and 3 drought samples each measurement	MPa	PSYPRO Meter and Pressure chamber
$\psi_l$	Leaf water potential	-	At least 3 control and 3 drought samples each measurement	MPa	PSYPRO Meter and Pressure chamber

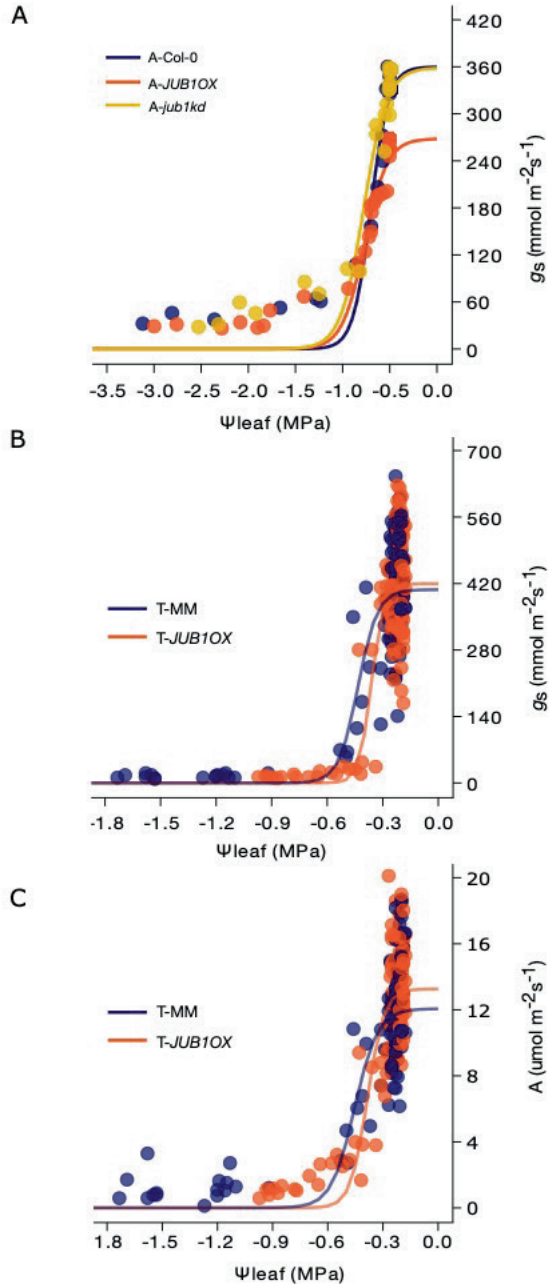


**Supplementary Figure S1** Growth form of genotypes of Arabidopsis and tomato used for stem anatomical and stem  $P_{50}$  studies. *A-JUB1OX* (top left, 65d after sowing), *A-Col-0* (top middle, 55d after sowing), *A-jub1kd* (top right, 55d after sowing), *T-JUB1OX* (bottom left, 55d after potting) and *T-MM* (bottom right, 55d after potting).

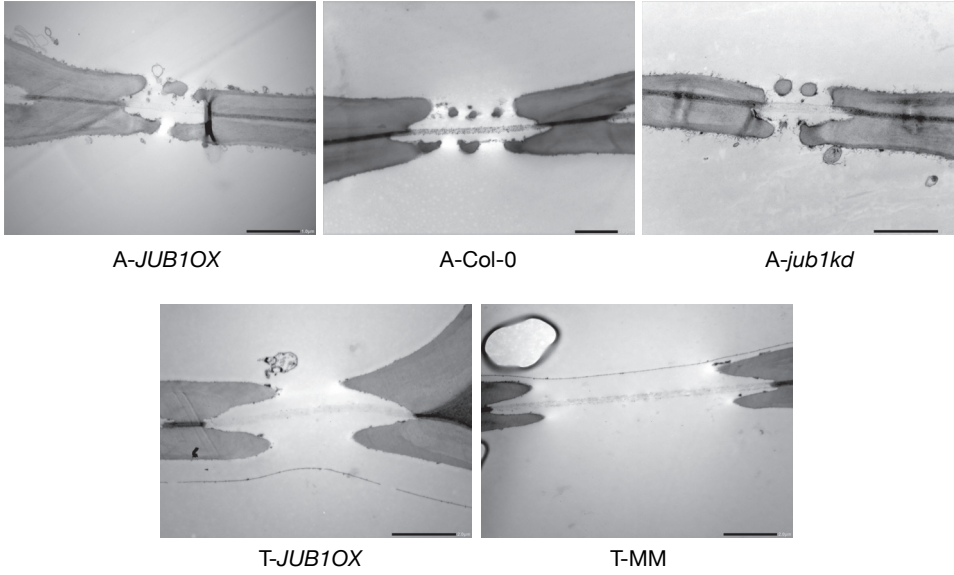


**Supplementary Figure S2** The relationship between stomatal conductance ( $g_s$ ) measured with Targas-1 and porometer. Shaded band represents the 95% confidence limits. The dotted lines represent 95% prediction limits.

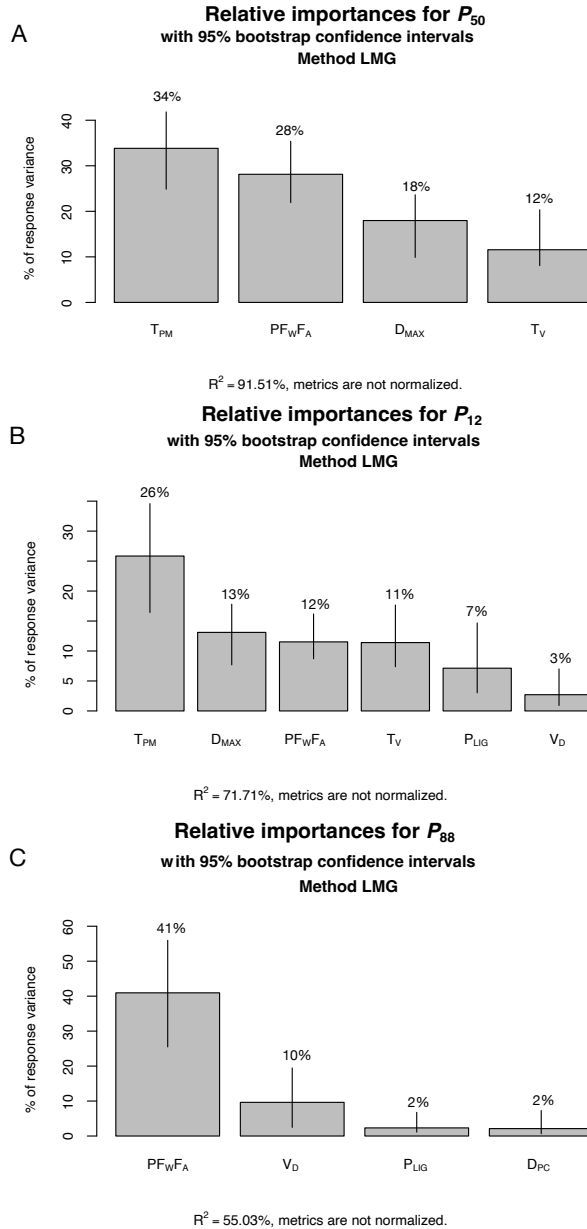




**Supplementary Figure S3** The relationship between leaf water potential and stomatal conductance during the drought experiment in (A) Arabidopsis and (B) tomato. (C) The relationship between leaf water potential and CO<sub>2</sub> assimilation ( $A$ ) of tomato. Colours refer to the genotype studied: wild-type (blue); *JUB1* overexpression (orange); *JUB1* knocked down (yellow).



**Supplementary Figure S4** TEM images of intervessel pit membranes. Scale bars = 1 μm and 2 μm.

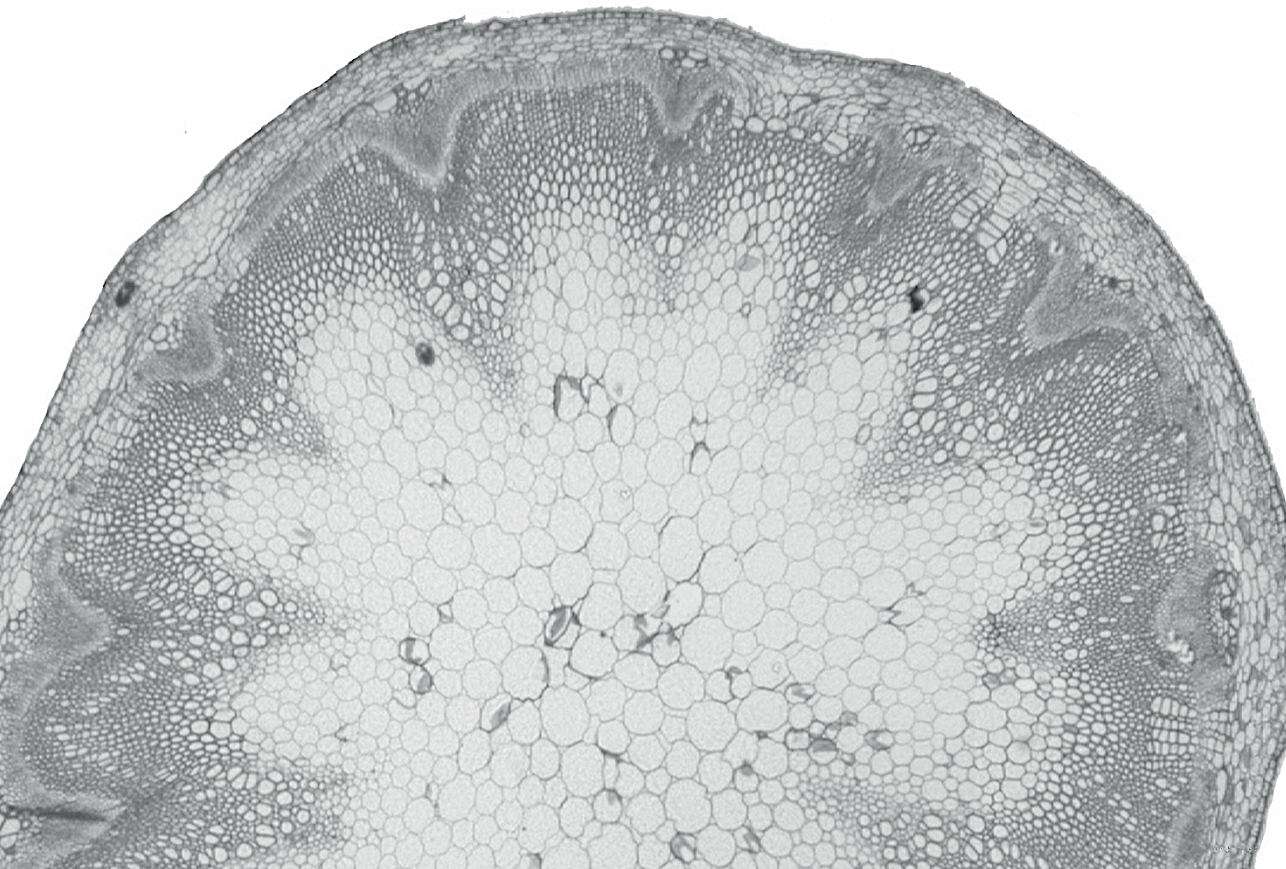


**Supplementary Figure S5** The relative importance of  $P_{50}$ ,  $P_{12}$  and  $P_{88}$  evaluated based on  $R^2$  contribution averaged over orderings among regressors (Lindemann, Merenda, and Gold (LMG) method). (A) The relative importance of  $P_{50}$  variation is mainly explained by intervessel pit membrane thickness ( $T_{PM}$ ) and proportion of fibre wall area per fibre cell area ( $PF_{wFA}$ ). (B)  $T_{PM}$  is the most important parameter explaining the relative importance of  $P_{12}$  variation. (C) The relative importance of  $P_{88}$  variation is mainly explained by  $PF_{wFA}$



## Chapter 5

# **GENERAL DISCUSSION AND FUTURE PERSPECTIVES**





## General discussion

The increasing frequency and severity of drought events resulting from climate change already have significant implications on global forest mortality and agricultural productivity (Allen *et al.*, 2009, 2015; Brás *et al.*, 2021; Gleason *et al.*, 2022; Hammond *et al.*, 2022). As plants heavily rely on an adequate water supply in the soil, the limitations imposed by reduced water availability have far-reaching effects on their overall development and ability to thrive (Choat *et al.*, 2018; Martinez-Vilalta *et al.*, 2019; Sapes *et al.*, 2019; Brodribb *et al.*, 2020). Therefore, identifying the key traits that underlie drought response mechanisms and a comprehensive understanding of the diverse range of plant adaptive strategies to drought is essential for accurately estimating the risk of forest die-off and crop yield loss and improving plant resilience and productivity in water-limited environments.

### ***The role of ecophysiological traits on drought response***

Plant desiccation and mortality are tightly linked to the failure of the water transport system, primarily due to the accumulation of embolism caused by drought within xylem conduits that surpasses the threshold beyond where water transport becomes irrecoverable (Sperry and Tyree, 1988; Venturas *et al.*, 2017; McDowell *et al.*, 2022; Johnson *et al.*, 2022). Consequently, the ability to avoid and/or resist embolism formation under the highly negative pressure induced by soil water deficit holds great significance in plant survival. Two sets of key ecophysiological traits are thought to be associated with plant hydraulic failure: (1) stomatal regulation that maintains the water potential ( $\psi$ ) and optimizes water use efficiency at the leaf level (Klein, 2014; Buckley, 2019; Papastefanou *et al.*, 2020; Joshi *et al.*, 2022) (discussed in chapter 2 and 3), and (2) embolism resistance in the xylem conduits that ensures the integrity of the water transport system under water deficit conditions (Choat *et al.*, 2012; Tng *et al.*, 2018) (discussed in chapter 1 and 2). Consequently, attaining a harmonious synergy between these two types of traits is imperative for an effective response to drought, enabling optimal plant growth without encountering hydraulic failure.

Stomatal regulation plays a crucial role in enabling plants to effectively balance water conservation and photosynthetic activity when faced with limited water availability (Assmann and Wang, 2001; Buckley, 2005; Messinger *et al.*, 2006; Ainsworth and Rogers, 2007). The closure of stomata is one of the earliest drought responses, considerably reduces water loss due to transpiration, and delays the decrease of leaf water potential ( $\Psi_l$ ) (Bartlett *et al.*, 2016; Choat *et al.*, 2018). Importantly, stomatal closure precedes substantial embolism formation, thereby effectively preventing/delaying detrimental levels of embolism that can result in hydraulic failure (Brodribb *et al.*, 2003; Mencuccini *et al.*, 2015; Martin-StPaul *et al.*, 2017; Scoffoni *et al.*, 2017; Choat *et al.*, 2018; Creek *et al.*, 2020). However, stomata closure also limits photosynthetic rates due to reduced gas exchange, potentially impairing carbon metabolic function, especially during long drought episodes (McDowell *et al.*, 2008; Brodribb *et al.*, 2017b; Martin-StPaul *et al.*, 2017; Martínez-Vilalta and Garcia-Forner, 2017; Knipfer *et al.*, 2020). The findings presented in chapters 2 and 3 highlight the distinct stomatal regulation behaviors in response to drought observed among the Arabidopsis and tomato genotypes studied. However, regardless of the specific regulatory mechanisms, the results underscore the importance of maintaining a high and stable leaf water potential ( $\Psi_l$ ) during drought stress. This can be achieved through strict stomatal regulation, as observed in Arabidopsis genotypes, or through alternative mechanisms, as seen in the case of tomato and Arabidopsis *JUB1OX* (discussed further in the last paragraph). In Arabidopsis, most genotypes exhibiting higher drought resistance have low stomatal conductance under well-watered conditions ( $g_s$ ; chapter 2). This stomatal regulation limits excessive decreases in  $\Psi_l$ , ensuring that the water demand from the leaves remains within the capacity of the hydraulic system (Li *et al.*, 2017; Dayer *et al.*, 2020; Lemaire *et al.*, 2021a). Additionally, these genotypes can keep their stomata open for a longer duration during drought, maximizing carbon assimilation, meaning that their stomatal control is rather relaxed. Conversely, drought-sensitive genotypes exhibit a stricter stomatal control, characterized by higher initial  $g_s$  and more rapid complete closure of stomata at the onset of drought. Interestingly, our dataset reveals that the rate of  $g_s$  under well-watered conditions is more crucial in responding to drought than the speed of stomatal closure. This is evident in the sensitive genotypes (Cvi, Col-0, Kel-4, and *jub1kd*), which experience higher transpiration rates and hence lose more water, despite closing their stomata earlier than the more drought-



tolerant genotypes that have lower initial  $g_s$ . These findings suggest that genotypes with higher drought resilience allow for a more effective balance between water loss and gas exchange.

The maintenance of the root-to-shoot hydraulic system depends on a species' ability to withstand embolism formation under the negative pressure caused by soil water deficit. Embolism resistance is often quantified as the xylem water potential inducing a 50% loss of maximum conductivity ( $P_{50}$ ), which is often used as a proxy for drought resilience: species exhibiting more negative  $P_{50}$  are thought to be more drought tolerant, while those with less negative  $P_{50}$  values tend to be more sensitive to drought (Choat *et al.*, 2012; Anderegg *et al.*, 2016; Brodribb, 2017). Embolism resistance can vary considerably between and within species, with species inhabiting drier habitats generally displaying greater resistance to embolism compared to those from wetter areas (Larter *et al.*, 2015; Lens *et al.*, 2016; Trueba *et al.*, 2017; Dória *et al.*, 2019).  $P_{50}$  has recently been considered a mechanistic 'super-trait' due to its strong predictive power of plant performance and distribution across environmental gradients (Brodribb, 2017; Larter *et al.*, 2017). The results presented in this thesis also show a similar trend: more drought-tolerant *Arabidopsis* genotypes demonstrate more negative  $P_{50}$  values, while the most sensitive genotype, Cvi, exhibits the least negative  $P_{50}$  (chapter 1-2). This suggests that resistant genotypes likely enhanced their intrinsic embolism resistance, allowing them to close stomata later during drought, thereby maximizing plant productivity (Klein, 2014; Skelton *et al.*, 2015; Anderegg *et al.*, 2016). However, there is a concern that assessing embolism resistance solely based on  $P_{50}$  does not fully capture its physiological relevance, especially under non-extreme conditions where water status is primarily regulated by the stomatal control (Meinzer *et al.*, 2009). In this regard, the stomatal safety margin (SSM), defined as the difference between the water potential at stomatal closure ( $\Psi_{gs90}$ ) and  $P_{50}$ , carries more physiological significance and reflects the strength of the hydraulic system in estimating a plant's ability to tolerate drought (Sperry and Tyree, 1988; Meinzer *et al.*, 2009; Anderegg *et al.*, 2016; Martin-StPaul *et al.*, 2017; Creek *et al.*, 2020; Dayer *et al.*, 2020; Skelton *et al.*, 2021). Numerous studies have shown that across angiosperms (mainly woody), a large positive safety margin is generally associated with a lower risk of lethal levels of drought-induced embolism compared to species with narrower (or even negative) safety margins (Choat *et al.*, 2012;

Anderegg *et al.*, 2016; Martin-StPaul *et al.*, 2017; Eller *et al.*, 2018; Creek *et al.*, 2020; Skelton *et al.*, 2021; Nolan *et al.*, 2021; Oliveira *et al.*, 2021). The findings presented in chapters 2 support that the more resilient genotypes display wider SSMs, whereas the susceptible ones show narrower SSMs and even a negative SSM in the case of Cvi. However, the drought-resistant genotype *p35S:AHL15*, despite its resilience, surprisingly exhibits a relatively narrow SSM, suggesting that a narrow SSM can be compensated by other drought-responsive traits to improve the drought resilience of an individual. For instance, the width of the SSM does not account for all aspects of stomatal regulation (i.e., rate of  $g_s$ ) and the dynamics of leaf water potential during drought (Martínez-Vilalta and Garcia-Forner, 2017; Knipfer *et al.*, 2020). Interestingly, among Arabidopsis genotypes studied with comparable levels of drought tolerance, there are substantial variations in stomatal regulation, while  $P_{50}$  values consistently align with the whole plant's drought tolerance, except for *JUB1* overexpression line that employs a totally different drought response (Figure 1). This observation suggests that  $P_{50}$  outperforms SSM in explaining the responses to drought among the genotypes studied.

### ***The role of xylem anatomical traits on embolism resistance***

The resistance to embolism in plants could be determined by various xylem anatomical features such as wood density, fiber wall thickness, vessel wall thickness and conduit diameter, and intervessel pit membrane. These traits provide mechanical support to plants, which in turn might help mitigate the potential damage caused by high tensions and enable plants to maintain water transport during drought. In recent years, the significant role of intervessel pit membranes in embolism resistance has been increasingly put forward in structure-function studies (Meyra *et al.*, 2007; Choat *et al.*, 2008; Jansen *et al.*, 2009; Lens *et al.*, 2013; Li *et al.*, 2016; Dória *et al.*, 2018; Simioni *et al.*, 2023). In angiosperms, thicker membranes, characterized by longer multiconstriction paths, exhibit smaller pore constriction sizes that act as bottlenecks for fluid (and gas) transport. In addition, the increased thickness of pit membranes corresponds to a higher number of constrictions, which further promotes the occurrence of gas bubble snap-offs that are assumed to be coated with a stabilizing layer of surfactants (Berg *et al.*, 2013; Schenk *et al.*, 2015; Park *et al.*, 2019; Lens *et al.*, 2022). This functionally explains why species with thicker intervessel pit

membranes are more drought-tolerant compared to species with thinner pit membranes (Kaack *et al.*, 2019, 2021; Yang *et al.*, 2020; Zhang *et al.*, 2020). However, most of these observations have been made at the interspecific level (Jansen *et al.*, 2009; Lens *et al.*, 2011; Plavcová and Hacke, 2012; Plavcová *et al.*, 2013; Scholz *et al.*, 2013; Li *et al.*, 2016; Dória *et al.*, 2018; Trueba *et al.*, 2019; Guan *et al.*, 2022), with limited focus on intraspecific variation (Schuldt *et al.*, 2016). Therefore, in this thesis, I emphasized the correlation between  $T_{PM}$  and embolism resistance among different genotypes of *Arabidopsis*. The findings from chapters 1 and 2 consistently demonstrate that  $T_{PM}$  is the key trait that best explains the variation of embolism resistance, with the more drought-resilient genotypes (more negative  $P_{50}$ ) possessing thicker intervessel pit membranes, while the *JUB1* overexpression genotypes increasing drought tolerance using another set of traits (Figure 1).

In addition to the thickness of intervessel pit membranes, the degree of lignification or woodiness also plays a crucial role in determining the embolism resistance in both woody (Greenwood *et al.*, 2017; Liang *et al.*, 2021) and predominantly herbaceous angiosperm lineages (Tixier *et al.*, 2013; Lens *et al.*, 2016; Dória *et al.*, 2018). Species with woodier or more lignified stems generally exhibit better resistance to drought-induced embolism (Hacke *et al.*, 2001; Jacobsen *et al.*, 2007a; Willson *et al.*, 2008; Hoffmann *et al.*, 2011; Lens *et al.*, 2013, 2016; Dória *et al.*, 2018, 2019). Accordingly, our findings indicate a strong correlation between the proportion of lignified area per total stem area ( $P_{LIG}$ ) and embolism resistance. Although  $P_{LIG}$  is not considered a key functional trait contributing to vulnerability to embolism in stems of the *Arabidopsis* genotypes studied, as it is not included in the most parsimonious multiple regression  $P_{50}$  model (chapters 1, 2, and 3), it still possesses significant predictive value due to its association with other traits that are thought to be more relevant such as  $T_{PM}$ . Plants with higher levels of embolism resistance are also believed to develop thicker vessel walls (Jansen *et al.*, 2009; Bouche *et al.*, 2014; Li *et al.*, 2016) or an increased fiber matrix (more and thicker fiber wall) (Jacobsen *et al.*, 2005, 2007b; Pratt and Jacobsen, 2017; Dória *et al.*, 2018), as is supported by our *Arabidopsis* dataset (chapter 1-2): the more resistant genotypes exhibit thicker vessel walls and a higher proportion of fiber wall area per fiber cell area ( $PF_{WF_A}$ ), suggesting the functional roles of these traits in explaining the variation of embolism resistance. It is noteworthy that the

majority of studies investigating functional-structure traits have primarily focused on trees, with limited attention given to herbaceous plants. Nevertheless, our study reveals that the herbaceous *Arabidopsis* exhibits a similar pattern of functional traits as those observed in trees. This finding implies that irrespective of being trees or herbs, both types of plants show the need to regulate stomata to balance water conservation and photosynthetic efficiency, alongside the development of resistance against embolism to ensure survival during drought conditions.

### ***Unraveling the diversity of drought response strategies in Arabidopsis thaliana***

Drought resilience in plants requires a complex interaction of traits influenced by a range of functional attributes (Violle *et al.*, 2007). As a result, the effectiveness and degree of drought tolerance can vary across species, depending on the synergistic interactions among these traits. This thesis has revealed remarkable findings, demonstrating that even in species with a short life cycle, like *Arabidopsis*, multiple strategies can be employed to achieve their respective levels of drought tolerance (Figure 1). These strategies primarily involve two key approaches: the development of xylem resistance through specific anatomical traits (Levionnois *et al.*, 2021), and the maintenance of high and stable leaf water potential to prevent sap pressure from reaching critical thresholds through precise stomatal regulation (Martin-StPaul *et al.*, 2017). Among the *Arabidopsis* genotypes studied, the *soc1ful* knockout mutant demonstrates the greatest tolerance to drought. *Soc1ful* shows a unique combination of traits, including the most negative  $P_{50}$ , widest stomatal safety margin (SSM), thickest intervessel pit membranes, and highest stem lignification, along low initial stomatal conductance that gradually decreases during drought, ensuring a stable leaf water potential ( $\psi_l$ ) (Figure 1; chapter 2; Thonglim *et al.*, 2021, 2023). The other two genotypes, Sha and *p35S: AHL15*, demonstrate a comparably high level of drought tolerance (Figure 1) despite exhibiting some variation in the drought-responsive traits. For instance, Sha has a relatively high initial stomatal conductance, but its  $g_s$  decreases rapidly during drought. *p35S: AHL15* has considerably lower  $g_s$ , enabling it to sustain a relatively high and stable  $\psi_l$ , but its stem  $P_{50}$  value is less negative, resulting in a smaller SSM compared to Sha. The three most resilient *Arabidopsis* genotypes also showed a similar expression of four drought-responsive genes (*RD29A*,

*DREB2A*, *ABI2*, and *AREB1*) compared to the more sensitive genotypes during our drought experiment (chapter 2). This pattern was also supported by an analysis of the chlorophyll content in the leaves at the end of the drought experiment (chapter 2).

Unlike the other drought-resistant genotypes, the resilient *Arabidopsis JUB1OX* does not possess hydraulic and stem anatomical traits that have been associated with increased drought resilience (observed in chapter 3). Instead, *A-JUB1OX* plants have less negative  $P_{50}$ , thin intervessel pit membranes, and a less lignified stem (Figure 1). *A-JUB1OX* (but not tomato *JUB1OX*) compensates for these characteristics by displaying a lower initial stomatal conductance ( $g_s$ ) that gradually decreases during drought. Interestingly, *JUB1OX* in tomato exhibit similar  $g_s$  to the wild-type, indicating that overexpression of *JUB1* does not lead to lowered stomatal conductance. This implies that the high  $\Psi_l$  during drought stress is driven by another mechanism that has not been investigated in this PhD (see next section). With respect to the sensitive *Arabidopsis* genotypes, including Col-0, Cvi, Kel-4, and *jub1kd*, we have observed traits that are typically associated with low resilience to drought. These traits encompass a less negative  $P_{50}$ , thin intervessel pit membranes, narrow SSMs, low levels of stem lignification, high initial  $g_s$ , and stomatal closure occurring later during drought (Figure 1; chapters 1-2). Altogether, these traits contribute to increased water loss through transpiration, a rapid decline in  $\Psi_l$  during drought, resulting in immediate wilting, and a significant reduction in chlorophyll content.

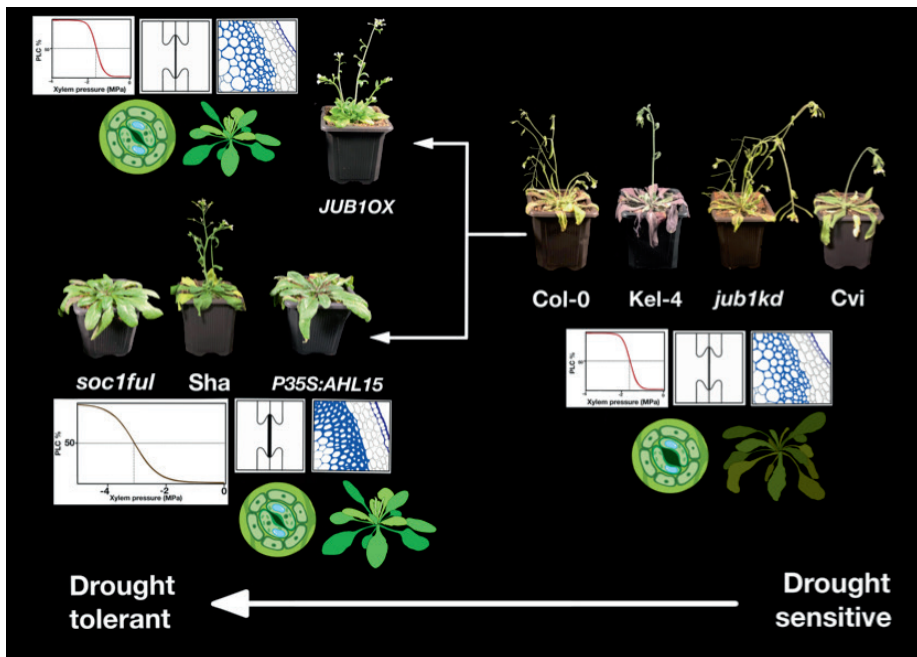


**Figure 1** Diverse drought response strategies observed in *Arabidopsis* genotypes studied. The figure illustrates the phenotype of each *Arabidopsis* genotype during the same drought period highlighting a set of key traits used by each genotype in response to drought, with two distinct drought strategies in *JUB1OX* compared to *soc1ful*, *Sha*, and *p35S:AHL15*. Genotypes that are highly susceptible to drought are depicted on the right side, while the more resistant genotypes are depicted on the left side.

***JUB1* mediates drought response in *Arabidopsis* slightly differs from that in tomato**

Although the drought response strategy of *JUB1OX* in *Arabidopsis* is clearly different from the other drought-resilient genotype (Figure 1), there are some differences when comparing *Arabidopsis* and tomato *JUB1OX* with their wild-types, highlighting the species-specific effects of these mechanisms. Unlike the *A-JUB1OX*, the tomato genotype displays a high initial stomatal conductance and keeps its stomata fully open for extended periods, resembling the drought-sensitive genotypes of *Arabidopsis*. However, despite these traits, tomato *JUB1OX* demonstrates a greater tolerance to drought by maintaining a high and stable  $\Psi_1$  compared to the Money Maker wild type. It is intriguing to observe that the increased

drought tolerance in tomato *JUB1OX* does not rely on either stomatal regulation or anatomical and hydraulic traits. According to literature, the observed elevation in  $\psi_l$  during drought periods in tomato *JUB1OX* can potentially be attributed to the accumulation of osmoprotectants, such as proline (Pro), in its leaves (Wu *et al.*, 2012; Shahnejat-Bushehri *et al.*, 2017; Tak *et al.*, 2017; Alshareef *et al.*, 2019; Welsch, 2022). Proline functions as an osmolyte, enabling the uptake of additional water and minimizing the negative impact of water deficit by adjusting cellular osmotic potential and stabilizing cellular structures (Heuer, 2010; Blum, 2017; Hasanuzzaman *et al.*, 2019; Ahmad *et al.*, 2020; Ozturk *et al.*, 2021). Additionally, the overexpression of *JUB1* may hamper the accumulation of reactive oxygen species (ROS) during drought stress (Shahnejat-Bushehri *et al.*, 2012, 2016; Wu *et al.*, 2012; Ebrahimian-Motlagh *et al.*, 2017; Thirumalaikumar *et al.*, 2018). This helps prevent oxidative damage in plant cells, thereby promoting drought tolerance in *JUB1OX* plants. Although the concentration of osmoprotectants and ROS was not analyzed in this thesis, the potential role of *JUB1* as discussed in the literature provides a promising starting point for a following up study to investigate the precise mechanisms by which *JUB1* influences osmoprotectants accumulation and ROS mitigation at the molecular level.

In conclusion, this study has shed light on the complex mechanisms of drought resilience in plants. Two different mechanisms have been identified in *Arabidopsis*: (1) a synergistic interplay among hydraulic ( $P_{50}$  and SSM) and anatomical traits ( $T_{PM}$  and stem lignification), along with low stomatal conductance and high leaf water potential  $\psi_l$ , and (2) high  $\psi_l$  likely driven by osmoprotectants accumulation in leaves. These two distinct drought response strategies within a single annual species highlight the remarkable adaptive capabilities of plants to respond to challenging environmental conditions. It is therefore crucial to do in-depth drought experiments based on multiple accessions within a single species to understand the full breadth of drought responses in for instance crops. This in-depth screening at the population-ecotype level will benefit the development of more resilient crops in an era characterized by global warming where the human population is still exponentially growing.

## Future perspectives

The presence of diverse drought strategies observed in this thesis showcases the remarkable adaptive capabilities of plants in coping with drought stress. However, it is important to acknowledge that the majority of research in the field of ecophysiology has predominantly focused on trees (Poorter *et al.*, 2010; Choat *et al.*, 2012; Mitchell *et al.*, 2013; Binks *et al.*, 2016*a, b*; Inoue *et al.*, 2017; Domingues *et al.*, 2018; Levionnois *et al.*, 2021; McDowell *et al.*, 2022; Johnson and Brodribb, 2023), while herbaceous plants have received far less attention (Lens *et al.*, 2016; Scoffoni *et al.*, 2018; Brodribb *et al.*, 2021; Fletcher *et al.*, 2022). Furthermore, the existing observations have primarily centered around individual species or generalized findings to the level of genera (Jansen *et al.*, 2009; Lens *et al.*, 2011; Plavcová and Hacke, 2012; Plavcová *et al.*, 2013; Scholz *et al.*, 2013*b*; Li *et al.*, 2016; Dória *et al.*, 2018; Trueba *et al.*, 2019; Guan *et al.*, 2022), disregarding the significance of intraspecific variation. This underestimation of intraspecific variability has hindered the comprehensive understanding of how plants respond to drought. To bridge this critical knowledge gap, it is crucial to prioritize and conduct more drought experiments that encompass a wide range of genotypes and species. By doing so, we can gain a broader perspective and develop a more comprehensive understanding of the diverse range of plant drought-responsive strategies. However, conducting drought experiments across numerous genotypes and species is a time-consuming task, particularly when precise measurements of key physiological traits are required. Advancements in technology have started to revolutionize this process, enabling efficient experimentation with hundreds of plants at once. One such innovative technology is PlantArray (Plant-Ditech, Rehobot, Israel) (Halperin *et al.*, 2017), a fully automated, multi-sensor gravimetric-based platform that streamlines the analysis of whole-plant performance. It facilitates the simultaneous measurements of various physiological traits, including plant transpiration, biomass accumulation, water, and nutrient use efficiency. This system provides accurate in-depth information on plant-environment interactions and the impact of environmental stresses on plant development and behavior under specific growth conditions, allowing for the efficient selection of optimal plant varieties and growing conditions that contribute to enhanced yields and stress response.



Given the significant findings regarding the integration of information from leaves and stems highlighted in chapter 2, it becomes evident that also the investigation of additional plant organs and associated traits would greatly contribute to our understanding of plant drought response. An often overlooked but fundamental aspect of the soil–plant–atmosphere continuum is the below-ground component. Roots play an important role in supplying water to compensate for transpiration losses during the process of gas exchange (Passioura, 1982; McCormack *et al.*, 2015; Cuneo *et al.*, 2021). Both woody and herbaceous species have been found to exhibit sensitivity to drought-induced declines in root hydraulic conductance ( $K_r$ ), as demonstrated by Bourbia *et al.* (2021). Additionally, studies have shown that  $K_r$  is a key factor in driving stomatal closure in olive plants (Rodriguez-Dominguez and Brodribb, 2020). Thus, investigating the below-ground dynamics and understanding the implications of root hydraulic conductance on plant responses to drought is crucial for a comprehensive assessment of drought tolerance and resistance at the whole-plant level. In addition, considering the crucial role of the intervessel pit membrane in enhancing embolism resistance, it becomes imperative to conduct detailed investigations of this structure across all organs and at a fine scale. While some studies have dived into the three-dimensional structures of pit membranes, our knowledge regarding their fine-scale structures and chemical composition remains limited (Schenk *et al.*, 2015, 2017, 2018, 2021; Kaack *et al.*, 2019, 2021; Zhang *et al.*, 2020). The same applies to the composition of the xylem sap, which is much more than only water (Lens *et al.*, 2022), but how changes in xylem sap composition in time and space affect embolism resistance is not known.

Another black hole in our knowledge of mechanisms leading to plants' drought responses is how they manage to coordinate gene regulation leading to key traits, and how different gene regulatory pathways in different organs are intertwined to obtain a certain level of drought resilience. A promising approach to identifying key drought genes is to investigate the causal relationship between gene regulation and physiological responses, such as stomatal closure and osmoregulation, drought-associated traits like  $P_{50}$ . To achieve this, ecophysiologicals and molecular biologists should team up and perform a high-resolution time-course gene expression analysis during drought and during the recovery

phase after rewatering across different organs and plant developmental stages.

In conclusion, our current understanding of plant responses to drought remains limited. By embracing the future perspectives mentioned above, we can propel our knowledge of plant drought tolerance forward. This progress will not only enable us to accurately predict plant mortality on both crop and large forest scales but also facilitate the development of more resilient crop varieties capable of withstanding water scarcity. Through continued research and implementation of effective strategies, we can ultimately ensure a sustainable and secure agricultural future, even in the face of climate change.

# SUMMARIES

## Summary

In recent decades, the frequency and severity of drought events have significantly increased due to climate change. This rise in drought occurrences has led to adverse consequences, including reduced global water availability which results in increased forest mortality or significant losses in crop yield. Consequently, there is an urgent need to gain a comprehensive understanding of the mechanisms underlying drought-induced plant mortality, particularly in herbaceous species that include numerous economically important crops. Acquiring this knowledge is crucial for the precise prediction of plant mortality and for the development of drought-resilient crop varieties. To deepen our comprehension of drought responses in herbaceous species and to gain insights into the diverse strategies employed by a single species to withstand drought stress, we analyzed a comprehensive dataset of anatomical and hydraulic traits of stems and leaves in eight different genotypes of *Arabidopsis thaliana*, including both wild-type and transgenic mutants. This dataset, discussed primarily in chapters 1 and 2 (and partly also in chapter 3), is used to showcase the strategies utilized by these genotypes during drought experiments (discussed in chapters 2 and 3). We also included a preliminary screen of the expression levels of four well-known drought marker genes associated with ABA-dependent and ABA-independent pathways (discussed in chapter 2). In chapter 3, we specifically focused on the impact of the overexpression of the *JUNGBRUNNEN1* (*JUB1*) gene on drought response in *Arabidopsis* and tomato.

The findings of our study highlight that each *Arabidopsis* genotype employed a unique combination of anatomical and hydraulic traits in stems and leaves to respond to water deficit conditions. This variation can be summarized into two distinct strategies: (1) one group of plants (*soc1ful* knockout, Sha ecotype, and *AHL15* overexpression) improved their drought response by developing a more negative stem  $P_{50}$ , thicker intervessel pit membranes, a more lignified inflorescence stem, and a gradual reduction of the low initial stomatal conductance ( $g_s$ ) during drought, allowing for a relatively high and stable leaf water potential ( $\Psi$ ) during onset of drought.

Additionally, these three genotypes showed reduced transcript levels of drought stress marker genes and minimized chlorophyll loss in leaves during drought. (2) Another group of plants (*JUB1* overexpression genotypes in *Arabidopsis* and tomato) relies solely on maintaining high  $\Psi_i$  for drought tolerance, possibly due to the accumulation of osmoprotectants in leaves, while the other drought-responsive traits have not been recorded (except for lower initial stomatal conductance in *Arabidopsis JUB1OX*). The ability to maintain high  $\Psi_i$  is particularly critical during the early stages of drought, prior to stomatal closure, as it prevents the water potential from reaching a critical threshold that could lead to cavitation and embolism formation. Once embolism occurs in the xylem, the synergistic effects with anatomical traits become significant, as these functional xylem traits (in)directly contribute to preventing the formation and spread of embolism. Overall, our results underscore the remarkable adaptive capabilities of herbaceous plants in responding to challenging drought conditions and highlight marked differences among genotypes within the same species. This intraspecific variation in drought responses shows that a more detailed assessment of drought-responsive traits is required to explore the full potential of increasing crop yield in a world facing global warming that needs to feed billions of people.

## Samenvatting

In de afgelopen decennia is de frequentie en intensiteit van droogteperiodes aanzienlijk toegenomen als gevolg van klimaatverandering. Deze toename van droogte heeft geleid tot nadelige gevolgen, waaronder verminderde wereldwijde waterbeschikbaarheid, wat resulteert in een verhoogde sterfte van bossen of aanzienlijke verliezen in gewasopbrengsten. Daarom is er een dringende behoefte aan een diepgaande opheldering van de mechanismen die ten grondslag liggen aan droogtegeïnduceerde plantensterfte, met name bij kruidachtige soorten, waartoe talrijke economisch belangrijke gewassen horen. Het verkrijgen van deze kennis is cruciaal voor de nauwkeurige voorspelling van plantensterfte en voor de ontwikkeling van droogtebestendige gewasvariëteiten. Om ons begrip van droogteresponsen bij kruidachtige soorten te verdiepen en inzicht te krijgen in de diverse strategieën die door een enkele soort worden gebruikt om droogtestress te weerstaan, hebben we een uitgebreide dataset geanalyseerd van anatomische en hydraulische eigenschappen van stengels en bladeren in acht verschillende genotypen van *Arabidopsis thaliana*, waaronder zowel wildtypes als transgene mutanten. Deze dataset, die voornamelijk wordt besproken in hoofdstukken 1 en 2 (en deels ook in hoofdstuk 3), wordt gebruikt om de strategieën te illustreren die deze genotypen hebben toegepast tijdens de droogte-experimenten (besproken in hoofdstukken 2 en 3). Ook hebben we een voorlopige screening uitgevoerd van de expressieniveaus van vier bekende marker-genen voor droogte die geassocieerd zijn met ABA-afhankelijke en ABA-onafhankelijke reactiepaden (besproken in hoofdstuk 2). In hoofdstuk 3 hebben we specifiek gekeken naar de impact van de overexpressie van het *JUNGBRUNNEN1* (*JUB1*) gen op de droogterespons bij *Arabidopsis* en de tomatenplant.

De bevindingen van ons onderzoek benadrukken dat elk *Arabidopsis* genotype een unieke combinatie van anatomische en hydraulische eigenschappen in stengels en bladeren gebruikt om te reageren op watertekort. Deze variatie kan worden samengevat in twee duidelijke strategieën: (1) één groep planten (*soc1ful* knockout, Sha ecotype en *AHL15* overexpressie) verbeterde hun droogterespons door een meer negatieve stengel  $P_{50}$  te ontwikkelen, dikkere stippelmembranen tussen xyleemvaten, een meer verhoutte bloeiwijzestengel en een geleidelijke vermindering van

het initiële gastransport door de huidmondjes in bladeren ( $g_s$ ) tijdens droogte, waardoor een relatief hoge en stabiele bladwaterpotentiaal ( $\psi_l$ ) bekomen werd tijdens de eerste fasen van het droogte-experiment. Bovendien vertoonden deze drie genotypen verminderde transcriptieniveaus van marker-genen voor droogtestress en minimaliseerden ze chlorofylverlies in bladeren tijdens droogte. (2) Een andere groep planten (*JUB1* overexpressie genotypen in *Arabidopsis* en tomaat) vertrouwdde uitsluitend op het handhaven van een hoge  $\psi_l$  voor droogtetolerantie, mogelijk door de ophoping van osmoprotectanten in bladeren, terwijl de andere droogteresponsieve eigenschappen niet werden waargenomen (behalve een lagere initiële gastransport door de huidmondjes in bladeren van *Arabidopsis JUB1OX*). Het vermogen om een hoge  $\psi_l$  te handhaven is met name cruciaal tijdens de vroege stadia van droogte, vóór de sluiting van de huidmondjes, omdat dit voorkomt dat de waterpotentiaal een kritische drempel bereikt die kan leiden tot cavitatie en embolievorming. Zodra gasembolie in het xyleem optreedt, worden de synergetische effecten met anatomische eigenschappen belangrijk, omdat deze functionele xyleemeigenschappen (in)direct bijdragen aan het voorkomen van de vorming en verspreiding van die gasembolieën. Over het algemeen benadrukken onze resultaten de opmerkelijke aanpassingsvermogens van kruidachtige planten in het reageren op uitdagende droogteomstandigheden, en vertonen ze opvallende verschillen tussen genotypen binnen dezelfde soort. Deze intraspecifieke variatie in droogteresponsen laat zien dat een gedetailleerdere beoordeling van droogteresponsieve eigenschappen nodig is om het volledige potentieel van het verbeteren van gewasopbrengsten te verkennen in een wereld die te maken heeft met wereldwijde opwarming en waarin miljarden mensen moeten worden gevoed.

# REFERENCES

**Adams HD, Luce CH, Breshears DD, Allen CD, Weiler M, Hale VC, Smith AMS, Huxman TE.** 2012. Ecohydrological consequences of drought- and infestation- triggered tree die-off: insights and hypotheses. *Ecohydrology* **5**, 145–159.

**Adams HD, Zeppel MJB, Anderegg WRL, et al.** 2017. A multi-species synthesis of physiological mechanisms in drought-induced tree mortality. *Nature Ecology & Evolution* **1**, 1285–1291.

**Agnolucci P, De Lipsis V.** 2020. Long-run trend in agricultural yield and climatic factors in Europe. *Climatic Change* **159**, 385–405.

**Agusti J, Herold S, Schwarz M, et al.** 2011. Strigolactone signaling is required for auxin-dependent stimulation of secondary growth in plants. *Proceedings of the National Academy of Sciences* **108**, 20242–20247.

**Ahmad HB, Lens F, Capdeville G, Burlett R, Lamarque LJ, Delzon S.** 2018. Intraspecific variation in embolism resistance and stem anatomy across four sunflower (*Helianthus annuus* L.) accessions. *Physiologia Plantarum* **163**, 59–72.

**Ahmad F, Singh A, Kamal A.** 2020. Osmoprotective role of sugar in mitigating abiotic stress in plants. In: Roychoudhury A, Tripathi DK, eds. *Protective Chemical Agents in the Amelioration of Plant Abiotic Stress*. Wiley, 53–70.

**Ainsworth EA, Rogers A.** 2007. The response of photosynthesis and stomatal conductance to rising [CO<sub>2</sub>]: mechanisms and environmental interactions: Photosynthesis and stomatal conductance responses to rising [CO<sub>2</sub>]. *Plant, Cell & Environment* **30**, 258–270.

**Al Abdallat AM, Ayad JY, Abu Elenein JM, Al Ajlouni Z, Harwood WA.** 2014. Overexpression of the transcription factor HvSNAC1 improves drought tolerance in barley (*Hordeum vulgare* L.). *Molecular Breeding* **33**, 401–414.

- Alder NN, Pockman WT, Sperry JS, Nuismer S.** 1997. Use of centrifugal force in the study of xylem cavitation. *Journal of Experimental Botany* **48**, 665–674.
- Allen CD, Breshears DD, McDowell NG.** 2015. On underestimation of global vulnerability to tree mortality and forest die-off from hotter drought in the Anthropocene. *Ecosphere* **6**, art129.
- Allen CD, Macalady AK, Chenchouni H, et al.** 2009. A global overview of drought and heat-induced tree mortality reveals emerging climate change risks for forests. *Forest Ecology and Management* **259**, 660–684.
- Alshareef NO, Wang JY, Ali S, Al-Babili S, Tester M, Schmöckel SM.** 2019. Overexpression of the NAC transcription factor JUNGBRUNNEN1 (JUB1) increases salinity tolerance in tomato. *Plant Physiology and Biochemistry* **140**, 113–121.
- Altamura MM, Possenti M, Matteucci A, Baima S, Ruberti I, Morelli G.** 2001. Development of the vascular system in the inflorescence stem of *Arabidopsis*. *New Phytologist* **151**, 381–389.
- Alves ES, Angyalossy-Alfonso V.** 2000. Ecological trend in wood anatomy of some Brazilian species. 1. growth rings and vessels. *IAWA Journal* **21**, 3–30.
- Anderegg WRL, Hicke JA, Fisher RA, et al.** 2015. Tree mortality from drought, insects, and their interactions in a changing climate. *New Phytologist* **208**, 674–683.
- Anderegg WRL, Kane JM, Anderegg LDL.** 2013. Consequences of widespread tree mortality triggered by drought and temperature stress. *Nature Climate Change* **3**, 30–36.
- Anderegg WRL, Klein T, Bartlett M, Sack L, Pellegrini AFA, Choat B, Jansen S.** 2016. Meta-analysis reveals that hydraulic traits explain cross-species patterns of drought-induced tree mortality across the globe. *Proceedings of the National Academy of Sciences* **113**, 5024–5029.
- Aoki S, Toh S, Nakamichi N, Hayashi Y, Wang Y, Suzuki T, Tsuji H, Kinoshita T.** 2019. Regulation of stomatal opening and histone



modification by photoperiod in *Arabidopsis thaliana*. *Scientific Reports* **9**, 10054.

**Asseng S, Ewert F, Martre P, et al.** 2015. Rising temperatures reduce global wheat production. *Nature Climate Change* **5**, 143–147.

**Assmann SM, Wang X-Q.** 2001. From milliseconds to millions of years: guard cells and environmental responses. *Current Opinion in Plant Biology* **4**, 421–428.

**Augspurger CK, Kelly CK.** 1984. Pathogen mortality of tropical tree seedlings: experimental studies of the effects of dispersal distance, seedling density, and light conditions. *Oecologia* **61**, 211–217.

**Awad H, Herbette S, Brunel N, Tixier A, Pilate G, Cochard H, Badel E.** 2012. No trade-off between hydraulic and mechanical properties in several transgenic poplars modified for lignins metabolism. *Environmental and Experimental Botany* **77**, 185–195.

**Baas P.** 1976. Some functional and adaptive aspects of vessel member morphology. *Leiden Botanical Series* **3**, 157–181.

**Baas P, Ewers FW, Davis SD, Wheeler EA.** 2004. Evolution of xylem physiology. *The Evolution of Plant Physiology*. Elsevier, 273–295.

**Baas P, Werker E, Fahn A.** 1983. Some ecological trends in vessel characters. *IAWA Journal* **4**, 141–159.

**Bac-Molenaar JA, Granier C, Keurentjes JJB, Vreugdenhil D.** 2016. Genome-wide association mapping of time-dependent growth responses to moderate drought stress in *Arabidopsis*. *Plant, Cell & Environment* **39**, 88–102.

**Bai H, Qian X, Fan J, Qian Y, Duo Y, Liu Y, Wang X.** 2020. Computing pore size distribution in non-woven fibrous filter media. *Fibers and Polymers* **21**, 196–203.

**Barbosa EGG, Leite JP, Marin SRR, et al.** 2013. Overexpression of the ABA-dependent AREB1 transcription factor from *Arabidopsis thaliana* improves

soybean tolerance to water deficit. *Plant Molecular Biology Reporter* **31**, 719–730.

**Barcelo AR.** 1997. Lignification in Plant Cell Walls. *International Review of Cytology*. Elsevier, 87–132.

**Barros J, Serk H, Granlund I, Pesquet E.** 2015. The cell biology of lignification in higher plants. *Annals of Botany* **115**, 1053–1074.

**Bartlett MK, Klein T, Jansen S, Choat B, Sack L.** 2016. The correlations and sequence of plant stomatal, hydraulic, and wilting responses to drought. *Proceedings of the National Academy of Sciences* **113**, 13098–13103.

**Basu S, Ramegowda V, Kumar A, Pereira A.** 2016. Plant adaptation to drought stress. *F1000Research* **5**, 1554.

**Bauerle WL, Whitlow TH, Setter TL, Vermeylen FM.** 2004. Abscisic acid synthesis in *Acer rubrum* L. leaves—a vapor pressure deficit mediated response. *Journal of the American Society for Horticultural Science* **129**, 182–187.

**Benjamin JG, Nielsen DC.** 2006. Water deficit effects on root distribution of soybean, field pea and chickpea. *Field Crops Research* **97**, 248–253.

**Berg S, Ott H, Klapp SA, et al.** 2013. Real-time 3D imaging of Haines jumps in porous media flow. *Proceedings of the National Academy of Sciences* **110**, 3755–3759.

**Billon LM, Blackman CJ, Cochard H, Badel E, Hitmi A, Cartailier J, Souchal R, Torres-Ruiz JM.** 2020. The droughtbox: a new tool for phenotyping residual branch conductance and its temperature dependence during drought. *Plant, Cell & Environment* **43**, 1–11.

**Binks O, Meir P, Rowland L, Costa ACL, Vasconcelos SS, Oliveira AAR, Ferreira L, Christoffersen B, Nardini A, Mencuccini M.** 2016a. Plasticity in leaf-level water relations of tropical rainforest trees in response to experimental drought. *New Phytologist* **211**, 477–488.

**Binks O, Meir P, Rowland L, Da Costa ACL, Vasconcelos SS, De Oliveira AAR, Ferreira L, Mencuccini M.** 2016b. Limited acclimation in leaf anatomy

to experimental drought in tropical rainforest trees. (G Goldstein, Ed.). *Tree Physiology* **36**, 1550–1561.

**Blackman CJ, Brodribb TJ, Jordan GJ.** 2012. Leaf hydraulic vulnerability influences species' bioclimatic limits in a diverse group of woody angiosperms. *Oecologia* **168**, 1–10.

**Blackman CJ, Creek D, Maier C, et al.** 2019. Drought response strategies and hydraulic traits contribute to mechanistic understanding of plant dry-down to hydraulic failure. (F Meinzer, Ed.). *Tree Physiology* **39**, 910–924.

**Blum A.** 2017. Osmotic adjustment is a prime drought stress adaptive engine in support of plant production: Osmotic adjustment and plant production. *Plant, Cell & Environment* **40**, 4–10.

**Bonal D, Guehl J-M.** 2001. Contrasting patterns of leaf water potential and gas exchange responses to drought in seedlings of tropical rainforest species. *Functional Ecology* **15**, 490–496.

**Bosio F, Soffiatti P, Boeger MRT.** 2010. Ecological wood anatomy of *Miconia Sellowiana* (Melastomataceae) in three vegetation types of paraná state, Brazil. *IAWA Journal* **31**, 179–190.

**Bouche PS, Larter M, Domec J-C, Burlett R, Gasson P, Jansen S, Delzon S.** 2014. A broad survey of hydraulic and mechanical safety in the xylem of conifers. *Journal of Experimental Botany* **65**, 4419–4431.

**Bouda M, Windt CW, McElrone AJ, Brodersen CR.** 2019. In vivo pressure gradient heterogeneity increases flow contribution of small diameter vessels in grapevine. *Nature Communications* **10**, 5645.

**Bourbia I, Carins-Murphy MR, Gracie A, Brodribb TJ.** 2020. Xylem cavitation isolates leaky flowers during water stress in pyrethrum. *New Phytologist*, [nph.16516](https://doi.org/10.1111/nph.16516).

**Bourbia I, Pritzkow C, Brodribb TJ.** 2021. Herb and conifer roots show similar high sensitivity to water deficit. *Plant Physiology* **186**, 1908–1918.

**Brackmann K, Qi J, Gebert M, et al.** 2018. Spatial specificity of auxin responses coordinates wood formation. *Nature Communications* **9**, 875.

- Brando PM, Balch JK, Nepstad DC, et al.** 2014. Abrupt increases in Amazonian tree mortality due to drought–fire interactions. *Proceedings of the National Academy of Sciences* **111**, 6347–6352.
- Brás TA, Seixas J, Carvalhais N, Jägermeyr J.** 2021. Severity of drought and heatwave crop losses tripled over the last five decades in Europe. *Environmental Research Letters* **16**, 065012.
- Bréda N, Cochard H, Dreyer E, Granier A.** 1993. Field comparison of transpiration, stomatal conductance and vulnerability to cavitation of *Quercus petraea* and *Quercus robur* under water stress. *Annales des Sciences Forestières* **50**, 571–582.
- Briggs LJ.** 1950. Limiting negative pressure of water. *Journal of Applied Physics* **21**, 721–722.
- Brodersen CR, Lee EF, Choat B, Jansen S, Phillips RJ, Shackel KA, McElrone AJ, Matthews MA.** 2011. Automated analysis of three-dimensional xylem networks using high-resolution computed tomography. *New Phytologist* **191**, 1168–1179.
- Brodersen CR, McElrone AJ, Choat B, Matthews MA, Shackel KA.** 2010. The dynamics of embolism repair in xylem: in vivo visualizations using high-resolution computed tomography. *Plant Physiology* **154**, 1088–1095.
- Brodribb TJ.** 2009. Xylem hydraulic physiology: the functional backbone of terrestrial plant productivity. *Plant Science* **177**, 245–251.
- Brodribb TJ.** 2017. Progressing from ‘functional’ to mechanistic traits. *New Phytologist* **215**, 9–11.
- Brodribb TJ, Bienaimé D, Marmottant P.** 2016a. Revealing catastrophic failure of leaf networks under stress. *Proceedings of the National Academy of Sciences* **113**, 4865–4869.
- Brodribb T, Brodersen CR, Carriqui M, Tonet V, Rodriguez Dominguez C, McAdam S.** 2021. Linking xylem network failure with leaf tissue death. *New Phytologist* **232**, 68–79.

**Brodribb TJ, Carriqui M, Delzon S, Lucani C.** 2017*a*. Optical measurement of stem xylem vulnerability. *Plant Physiology* **174**, 2054–2061.

**Brodribb TJ, Cochard H.** 2009. Hydraulic failure defines the recovery and point of death in water-stressed conifers. *Plant Physiology* **149**, 575–584.

**Brodribb T, Hill RS.** 1999. The importance of xylem constraints in the distribution of conifer species. *New Phytologist* **143**, 365–372.

**Brodribb TJ, Hill RS.** 2000. Increases in water potential gradient reduce xylem conductivity in whole plants. evidence from a low-pressure conductivity method. *Plant Physiology* **123**, 1021–1028.

**Brodribb TJ, Holbrook NM.** 2003. Stomatal closure during leaf dehydration, correlation with other leaf physiological traits. *Plant Physiology* **132**, 2166–2173.

**Brodribb TJ, Holbrook NM, Edwards EJ, Gutiérrez MV.** 2003. Relations between stomatal closure, leaf turgor and xylem vulnerability in eight tropical dry forest trees: Stomatal closure and xylem cavitation. *Plant, Cell & Environment* **26**, 443–450.

**Brodribb TJ, McAdam SA, Carins Murphy MR.** 2017*b*. Xylem and stomata, coordinated through time and space: functional linkages between xylem and stomata. *Plant, Cell & Environment* **40**, 872–880.

**Brodribb TJ, Powers J, Cochard H, Choat B.** 2020. Hanging by a thread? forests and drought. *Science* **368**, 261–266.

**Brodribb TJ, Skelton RP, McAdam S, Bienaimé D, Lucani C, Marmottant P.** 2016*b*. Visual quantification of embolism reveals leaf vulnerability to hydraulic failure. *New Phytologist* **209**, 1403–1409.

**Brown HR.** 2013*a*. The theory of the rise of sap in trees: some historical and conceptual remarks. *Physics in Perspective* **15**, 320–358.

**Brown HR.** 2013*b*. The Theory of the Rise of Sap in Trees: Some Historical and Conceptual Remarks. *Physics in Perspective* **15**, 320–358.

- Buckley TN.** 2005. The control of stomata by water balance. *New Phytologist* **168**, 275–292.
- Buckley TN.** 2019. How do stomata respond to water status? *New Phytologist* **224**, 21–36.
- Canelles Q, Aquilué N, James PMA, Lawler J, Brotons L.** 2021. Global review on interactions between insect pests and other forest disturbances. *Landscape Ecology* **36**, 945–972.
- Carlquist S.** 1966. Wood anatomy of Compositae: a summary, with comments on factors controlling wood evolution. *Aliso: A Journal of Systematic and Floristic Botany* **6**, 25–44.
- Carlquist S.** 1975. *Ecological strategies of xylem evolution*. Berkeley: University of California Press.
- Carlquist S.** 1977. Ecological factors in wood evolution: a floristic approach. *American Journal of Botany* **64**, 887–896.
- Carlquist S.** 1980. Further concepts in ecological wood anatomy, with comments on recent work in wood anatomy and evolution. *Aliso: A Journal of Systematic and Floristic Botany* **9**, 499–553.
- Carlquist S.** 1984. Vessel grouping in dicotyledon wood: significance and relationship to imperforate tracheary elements. *Aliso* **10**, 505–525.
- Carlquist S, Hoekman DA.** 1985. Ecological wood anatomy of the woody Southern Californian flora. *IAWA Journal* **6**, 319–347.
- Chaffey N, Cholewa E, Regan S, Sundberg B.** 2002. Secondary xylem development in *Arabidopsis*: a model for wood formation. *Physiologia Plantarum* **114**, 594–600.
- Chao K-J, Phillips OL, Gloor E, Monteagudo A, Torres-Lezama A, Martínez RV.** 2008. Growth and wood density predict tree mortality in Amazon forests. *Journal of Ecology* **96**, 281–292.

**Charrier G, Delzon S, Domec J-C, et al.** 2018. Drought will not leave your glass empty: Low risk of hydraulic failure revealed by long-term drought observations in world's top wine regions. *Science Advances* **4**, eaao6969.

**Charrier G, Torres-Ruiz JM, Badel E, et al.** 2016. Evidence for hydraulic vulnerability segmentation and lack of xylem refilling under tension. *Plant Physiology* **172**, 1657–1668.

**Chave J, Coomes D, Jansen S, Lewis SL, Swenson NG, Zanne AE.** 2009. Towards a worldwide wood economics spectrum. *Ecology Letters* **12**, 351–366.

**Chen K, Li G, Bressan RA, Song C, Zhu J, Zhao Y.** 2020. Abscisic acid dynamics, signaling, and functions in plants. *Journal of Integrative Plant Biology* **62**, 25–54.

**Chen I-T, Sessoms DA, Sherman Z, Choi E, Vincent O, Stroock AD.** 2016*a*. Stability limit of water by metastable vapor–liquid equilibrium with nanoporous silicon membranes. *The Journal of Physical Chemistry B* **120**, 5209–5222.

**Chen W, Yao Q, Patil GB, et al.** 2016*b*. Identification and comparative analysis of differential gene expression in soybean leaf tissue under drought and flooding stress revealed by RNA-Seq. *Frontiers in Plant Science* **7**, 1044.

**Choat B, Ball MC, Lully JG, Holtum JAM.** 2005. Hydraulic architecture of deciduous and evergreen dry rainforest tree species from north-eastern Australia. *Trees* **19**, 305–311.

**Choat B, Brodie TW, Cobb AR, Zwieniecki MA, Holbrook NM.** 2006. Direct measurements of intervessel pit membrane hydraulic resistance in two angiosperm tree species. *American Journal of Botany* **93**, 993–1000.

**Choat B, Brodribb TJ, Brodersen CR, Duursma RA, López R, Medlyn BE.** 2018. Triggers of tree mortality under drought. *Nature* **558**, 531–539.

**Choat B, Cobb AR, Jansen S.** 2008. Structure and function of bordered pits: new discoveries and impacts on whole-plant hydraulic function. *New Phytologist* **177**, 608–626.

- Choat B, Drayton WM, Brodersen C, Matthews MA, Shackel KA, Wada H, Mcelrone AJ.** 2010. Measurement of vulnerability to water stress-induced cavitation in grapevine: a comparison of four techniques applied to a long-veined species: comparison of vulnerability curve technique in grapevine. *Plant, Cell & Environment* **33**, 1502–1512.
- Choat B, Jansen S, Brodribb TJ, et al.** 2012a. Global convergence in the vulnerability of forests to drought. *Nature* **491**, 752–755.
- Choat B, Jansen S, Brodribb TJ, et al.** 2012b. Global convergence in the vulnerability of forests to drought. *Nature* **491**, 752–755.
- Choi H, Hong J, Ha J, Kang J, Kim SY.** 2000. ABFs, a family of ABA-responsive element binding factors. *Journal of Biological Chemistry* **275**, 1723–1730.
- Choudhury S, Panda P, Sahoo L, Panda SK.** 2013. Reactive oxygen species signaling in plants under abiotic stress. *Plant Signaling & Behavior* **8**, e23681.
- Choudhury FK, Rivero RM, Blumwald E, Mittler R.** 2017. Reactive oxygen species, abiotic stress and stress combination. *The Plant Journal* **90**, 856–867.
- Clark JS, Iverson L, Woodall CW, et al.** 2016. The impacts of increasing drought on forest dynamics, structure, and biodiversity in the United States. *Global Change Biology* **22**, 2329–2352.
- Cochard H.** 2002. A technique for measuring xylem hydraulic conductance under high negative pressures. *Plant, Cell and Environment* **25**, 815–819.
- Cochard H.** 2006. Cavitation in trees. *Comptes Rendus Physique* **7**, 1018–1026.
- Cochard H, Badel E, Herbette S, Delzon S, Choat B, Jansen S.** 2013. Methods for measuring plant vulnerability to cavitation: a critical review. *Journal of Experimental Botany* **64**, 4779–4791.
- Cochard H, Cruziat P, Tyree MT.** 1992. Use of positive pressures to establish vulnerability curves: further support for the air-seeding



hypothesis and implications for pressure-volume analysis. *Plant Physiology* **100**, 205–209.

**Cochard H, Damour G, Bodet C, Tharwat I, Poirier M, Améglio T.** 2005. Evaluation of a new centrifuge technique for rapid generation of xylem vulnerability curves. *Physiologia Plantarum* **124**, 410–418.

**Cochard H, Delzon S.** 2013. Hydraulic failure and repair are not routine in trees. *Annals of Forest Science* **70**, 659–661.

**Cochard H, Herbette S, Barigah T, Badel E, Ennajeh M, Vilagrosa A.** 2010. Does sample length influence the shape of xylem embolism vulnerability curves? a test with the cavitron spinning technique: shape of xylem embolism vulnerability curves. *Plant, Cell & Environment* **33**, 1543–1552.

**Corso D, Delzon S, Lamarque LJ, Cochard H, Torres-Ruiz JM, King A, Brodribb T.** 2020. Neither xylem collapse, cavitation, or changing leaf conductance drive stomatal closure in wheat. *Plant, Cell & Environment* **43**, 854–865.

**Creek D, Blackman CJ, Brodribb TJ, Choat B, Tissue DT.** 2018. Coordination between leaf, stem, and root hydraulics and gas exchange in three arid-zone angiosperms during severe drought and recovery: Coordination between hydraulics and gas exchange during drought and recovery. *Plant, Cell & Environment* **41**, 2869–2881.

**Creek D, Lamarque LJ, Torres-Ruiz JM, Parise C, Burlett R, Tissue DT, Delzon S.** 2020. Xylem embolism in leaves does not occur with open stomata: evidence from direct observations using the optical visualization technique. *Journal of Experimental Botany* **71**, 1151–1159.

**Crouchet SE, Jensen J, Schwartz BF, Schwinning S.** 2019. Tree mortality after a hot drought: distinguishing density-dependent and -independent drivers and why it matters. *Frontiers in Forests and Global Change* **2**, 21.

**Cruz De Carvalho MH.** 2008. Drought stress and reactive oxygen species: production, scavenging and signaling. *Plant Signaling & Behavior* **3**, 156–165.

- Cuneo IF, Barrios-Masias F, Knipfer T, Uretsky J, Reyes C, Lenain P, Brodersen CR, Walker MA, McElrone AJ.** 2021. Differences in grapevine rootstock sensitivity and recovery from drought are linked to fine root cortical lacunae and root tip function. *New Phytologist* **229**, 272–283.
- Cutler SR, Rodriguez PL, Finkelstein RR, Abrams SR.** 2010. Abscisic acid: emergence of a core signaling network. *Annual Review of Plant Biology* **61**, 651–679.
- Dayer S, Herrera JC, Dai Z, Burlett R, Lamarque LJ, Delzon S, Bortolami G, Cochard H, Gambetta GA.** 2020. The sequence and thresholds of leaf hydraulic traits underlying grapevine varietal differences in drought tolerance. *Journal of Experimental Botany* **71**, 4333–4344.
- De Guzman ME, Acosta-Rangel A, Winter K, Meinzer FC, Bonal D, Santiago LS.** 2021. Hydraulic traits of Neotropical canopy liana and tree species across a broad range of wood density: implications for predicting drought mortality with models. (M Ball, Ed.). *Tree Physiology* **41**, 24–34.
- De Roo L, Vergeynst L, De Baerdemaeker N, Steppe K.** 2016. Acoustic emissions to measure drought-induced cavitation in plants. *Applied Sciences* **6**, 71.
- Déjardin A, Laurans F, Arnaud D, Breton C, Pilate G, Leplé J-C.** 2010. Wood formation in Angiosperms. *Comptes Rendus Biologies* **333**, 325–334.
- Delzon S, Cochard H.** 2014. Recent advances in tree hydraulics highlight the ecological significance of the hydraulic safety margin. *New Phytologist* **203**, 355–358.
- Desikan R, Last K, Harrett-Williams R, Tagliavia C, Harter K, Hooley R, Hancock JT, Neill SJ.** 2006. Ethylene-induced stomatal closure in *Arabidopsis* occurs via AtrbohF-mediated hydrogen peroxide synthesis. *The Plant Journal* **47**, 907–916.
- Dixon HH, Joly J.** 1895. On the ascent of sap. *Philosophical Transactions of the Royal Society of London. B* **186**, 563–576.

**Domingues TF, Ometto JPHB, Nepstad DC, Brando PM, Martinelli LA, Ehleringer JR.** 2018. Ecophysiological plasticity of Amazonian trees to long-term drought. *Oecologia* **187**, 933–940.

**Dória LC, Meijs C, Podadera DS, Del Arco M, Smets E, Delzon S, Lens F.** 2019. Embolism resistance in stems of herbaceous Brassicaceae and Asteraceae is linked to differences in woodiness and precipitation. *Annals of Botany* **124**, 1–14.

**Dória LC, Podadera DS, Arco M, Chauvin T, Smets E, Delzon S, Lens F.** 2018. Insular woody daisies (*Argyranthemum*, Asteraceae) are more resistant to drought-induced hydraulic failure than their herbaceous relatives. *Functional Ecology* **32**, 1467–1478.

**Ebrahimian-Motlagh S, Ribone PA, Thirumalaikumar VP, Allu AD, Chan RL, Mueller-Roeber B, Balazadeh S.** 2017. JUNGBRUNNEN1 confers drought tolerance downstream of the HD-Zip I transcription factor AtHB13. *Frontiers in Plant Science* **8**, 2118.

**Eller C, de V. Barros F, R.L. Bittencourt P, Rowland L, Mencuccini M, S. Oliveira R.** 2018. Xylem hydraulic safety and construction costs determine tropical tree growth: Tree growth vs hydraulic safety trade-off. *Plant, Cell & Environment* **41**, 548–562.

**Emonet A, Hay A.** 2022. Development and diversity of lignin patterns. *Plant Physiology* **190**, 31–43.

**Ennajeh M, Nouriri M, Khemira H, Cochard H.** 2011. Improvement to the air-injection technique to estimate xylem vulnerability to cavitation. *Trees* **25**, 705–710.

**Esau K.** 1965. *Plant Anatomy*. New York: John Wiley.

**Esquivel-Muelbert A, Phillips OL, Brienen RJW, et al.** 2020. Tree mode of death and mortality risk factors across Amazon forests. *Nature Communications* **11**, 5515.

**Evert R.** 2006. *Esau's Plant Anatomy: Meristems, Cells, and Tissues of the Plant Body: Their Structure, Function, and Development*. John Wiley & Sons, Ltd.

- Ewers FW, Jacobsen AL, López-Portillo J.** 2023. Carlquist's indices for vulnerability and mesomorphy of wood: are they relevant today? *IAWA Journal*, 1–13.
- Fang Y, Liao K, Du H, Xu Y, Song H, Li X, Xiong L.** 2015. A stress-responsive NAC transcription factor SNAC3 confers heat and drought tolerance through modulation of reactive oxygen species in rice. *Journal of Experimental Botany* **66**, 6803–6817.
- Feldpausch TR, Phillips OL, Brienen RJW, et al.** 2016. Amazon forest response to repeated droughts: Amazon forest response to droughts. *Global Biogeochemical Cycles* **30**, 964–982.
- Fischer EM, Sippel S, Knutti R.** 2021. Increasing probability of record-shattering climate extremes. *Nature Climate Change* **11**, 689–695.
- Fletcher LR, Scoffoni C, Farrell C, Buckley TN, Pellegrini M, Sack L.** 2022. Testing the association of relative growth rate and adaptation to climate across natural ecotypes of *Arabidopsis*. *New Phytologist* **236**, 413–432.
- Förster S, Schmidt LK, Kopic E, et al.** 2019. Wounding-Induced Stomatal Closure Requires Jasmonate-Mediated Activation of GORK K<sup>+</sup> Channels by a Ca<sup>2+</sup> Sensor-Kinase CBL1-CIPK5 Complex. *Developmental Cell* **48**, 87–99.
- Fortunel C, Ruelle J, Beauchêne J, Fine PVA, Baraloto C.** 2014. Wood specific gravity and anatomy of branches and roots in 113 Amazonian rainforest tree species across environmental gradients. *New Phytologist* **202**, 79–94.
- Fu X, Meinzer FC.** 2019. Metrics and proxies for stringency of regulation of plant water status (iso/anisohydry): a global data set reveals coordination and trade-offs among water transport traits. (J Martinez-Vilalta, Ed.). *Tree Physiology* **39**, 122–134.
- Gao H, Chen Y-J, Zhang Y-J, Maenpuen P, Lv S, Zhang J-L.** 2019. Vessel-length determination using silicone and air injection: are there artifacts? (K Steppe, Ed.). *Tree Physiology* **39**, 1783–1791.
- Gauthey A, Peters JMR, López R, Carins-Murphy MR, Rodriguez-Dominguez CM, Tissue DT, Medlyn BE, Brodrick TJ, Choat B.** 2022.

Mechanisms of xylem hydraulic recovery after drought in *Eucalyptus saligna*. *Plant, Cell & Environment* **45**, 1216–1228.

**Gleason SM, Barnard DM, Green TR, et al.** 2022. Physiological trait networks enhance understanding of crop growth and water use in contrasting environments. *Plant, Cell & Environment*, pce.14382.

**Gleason SM, Blackman CJ, Cook AM, Laws CA, Westoby M.** 2014. Whole-plant capacitance, embolism resistance and slow transpiration rates all contribute to longer desiccation times in woody angiosperms from arid and wet habitats. *Tree Physiology* **34**, 275–284.

**Gleason SM, Butler DW, Ziemińska K, Waryszak P, Westoby M.** 2012. Stem xylem conductivity is key to plant water balance across Australian angiosperm species: Plant stem hydraulic traits. *Functional Ecology* **26**, 343–352.

**Gleason SM, Westoby M, Jansen S, et al.** 2016a. On research priorities to advance understanding of the safety–efficiency tradeoff in xylem: a response to Bittencourt et al.’s (2016) comment ‘On xylem hydraulic efficiencies, wood space-use and the safety–efficiency tradeoff’. *New Phytologist* **211**, 1156–1158.

**Gleason SM, Westoby M, Jansen S, et al.** 2016b. Weak tradeoff between xylem safety and xylem-specific hydraulic efficiency across the world’s woody plant species. *New Phytologist* **209**, 123–136.

**Goodsman DW, Lusebrink I, Landhäusser SM, Erbilgin N, Lieffers VJ.** 2013. Variation in carbon availability, defense chemistry and susceptibility to fungal invasion along the stems of mature trees. *New Phytologist* **197**, 586–594.

**Goulart HMD, van der Wiel K, Folberth C, Balkovic J, van den Hurk B.** 2021. Storylines of weather-induced crop failure events under climate change. *Earth System Dynamics* **12**, 1503–1527.

**Greenwood S, Ruiz-Benito P, Martínez-Vilalta J, et al.** 2017. Tree mortality across biomes is promoted by drought intensity, lower wood density and higher specific leaf area. (J Chave, Ed.). *Ecology Letters* **20**, 539–553.

- Guan X, Pereira L, McAdam SAM, Cao K, Jansen S.** 2021. No gas source, no problem: Proximity to pre-existing embolism and segmentation affect embolism spreading in angiosperm xylem by gas diffusion. *Plant, Cell & Environment* **44**, 1329–1345.
- Guan X, Werner J, Cao K -F., Pereira L, Kaack L, McAdam SAM, Jansen S.** 2022. Stem and leaf xylem of angiosperm trees experiences minimal embolism in temperate forests during two consecutive summers with moderate drought. *Plant Biology*, plb.13384.
- Hacke UG, Jansen S.** 2009. Embolism resistance of three boreal conifer species varies with pit structure. *New Phytologist* **182**, 675–686.
- Hacke UG, Sperry JS, Pockman WT, Davis SD, McCulloh KA.** 2001. Trends in wood density and structure are linked to prevention of xylem implosion by negative pressure. *Oecologia* **126**, 457–461.
- Hacke UG, Sperry JS, Wheeler JK, Castro L.** 2006. Scaling of angiosperm xylem structure with safety and efficiency. *Tree Physiology* **26**, 689–701.
- Hacke UG, Venturas MD, MacKinnon ED, Jacobsen AL, Sperry JS, Pratt RB.** 2014. The standard centrifuge method accurately measures vulnerability curves of long-vesselled olive stems. *New Phytologist* **205**, 116–127.
- Halperin O, Gebremedhin A, Wallach R, Moshelion M.** 2017. High-throughput physiological phenotyping and screening system for the characterization of plant-environment interactions. *The Plant Journal* **89**, 839–850.
- Hamann T, Smets E, Lens F.** 2011. A comparison of paraffin and resin-based techniques used in bark anatomy. *Taxon* **60**, 841–851.
- Hammond WM, Williams AP, Abatzoglou JT, Adams HD, Klein T, López R, Sáenz-Romero C, Hartmann H, Breshears DD, Allen CD.** 2022. Global field observations of tree die-off reveal hotter-drought fingerprint for Earth's forests. *Nature Communications* **13**, 1761.
- Hammond WM, Yu K, Wilson LA, Will RE, Anderegg WRL, Adams HD.** 2019. Dead or dying? Quantifying the point of no return from hydraulic failure in drought-induced tree mortality. *New Phytologist* **223**, 1834–1843.

**Hanin M, Brini F, Ebel C, Toda Y, Takeda S, Masmoudi K.** 2011. Plant dehydrins and stress tolerance: versatile proteins for complex mechanisms. *Plant Signaling & Behavior* **6**, 1503–1509.

**Hartmann H, Moura CF, Anderegg WRL, et al.** 2018. Research frontiers for improving our understanding of drought-induced tree and forest mortality. *New Phytologist* **218**, 15–28.

**Hasanuzzaman M, Hakeem KR, Nahar K, Alharby HF (Eds.).** 2019. *Plant abiotic stress tolerance: agronomic, molecular and biotechnological approaches*. Cham: Springer International Publishing.

**Heuer B.** 2010. Role of proline in plant response to drought and salinity. In: Pessarakli M, ed. *Books in Soils, Plants, and the Environment. Handbook of Plant and Crop Stress*, Third Edition. CRC Press, 213–238.

**Hoekstra FA, Golovina EA, Buitink J.** 2001. Mechanisms of plant desiccation tolerance. *Trends in Plant Science* **6**, 431–438.

**Hoffmann WA, Marchin RM, Abit P, Lau OL.** 2011. Hydraulic failure and tree dieback are associated with high wood density in a temperate forest under extreme drought: tree responses to severe drought. *Global Change Biology* **17**, 2731–2742.

**Holloway-Phillips M-M, Brodribb TJ.** 2011. Minimum hydraulic safety leads to maximum water-use efficiency in a forage grass. *Plant, Cell & Environment* **34**, 302–313.

**Hwang K, Susila H, Nasim Z, Jung J-Y, Ahn JH.** 2019. Arabidopsis ABF3 and ABF4 transcription factors act with the NF-YC complex to regulate SOC1 expression and mediate drought-accelerated flowering. *Molecular Plant* **12**, 489–505.

**Ingram S, Salmon Y, Lintunen A, Hölttä T, Vesala T, Vehkamäki H.** 2021. Dynamic surface tension enhances the stability of nanobubbles in xylem sap. *Frontiers in Plant Science* **12**, 732701.

**Inoue Y, Ichie T, Kenzo T, Yoneyama A, Kumagai T, Nakashizuka T.** 2017. Effects of rainfall exclusion on leaf gas exchange traits and osmotic adjustment in mature canopy trees of *Dryobalanops aromatica*

(Dipterocarpaceae) in a Malaysian tropical rain forest. *Tree Physiology* **37**, 1301–1311.

**IPCC.** 2022. *Climate Change 2022: Impacts, Adaptation, and Vulnerability. Contribution of Working Group II to the Sixth Assessment Report of the Intergovernmental Panel on Climate Change*. Cambridge, UK and New York, NY, USA: Cambridge University Press.

**Isasa E, Link RM, Jansen S, Tezeh FR, Kaack L, Sarmento Cabral J, Schuldt B.** 2023. Addressing controversies in the xylem embolism resistance–vessel diameter relationship. *New Phytologist*, nph.18731.

**Jacobsen AL, Agenbag L, Esler KJ, Pratt RB, Ewers FW, Davis SD.** 2007a. Xylem density, biomechanics and anatomical traits correlate with water stress in 17 evergreen shrub species of the Mediterranean-type climate region of South Africa. *Journal of Ecology* **95**, 171–183.

**Jacobsen AL, Ewers FW, Pratt RB, Paddock WA, Davis SD.** 2005. Do xylem fibers affect vessel cavitation resistance? *Plant Physiology* **139**, 546–556.

**Jacobsen AL, Pratt RB.** 2012. No evidence for an open vessel effect in centrifuge-based vulnerability curves of a long-vesselled liana (*Vitis vinifera*). *New Phytologist* **194**, 982–990.

**Jacobsen AL, Pratt RB, Davis SD, Ewers FW.** 2007b. Cavitation resistance and seasonal hydraulics differ among three arid Californian plant communities. *Plant, Cell & Environment* **30**, 1599–1609.

**Jacobsen AL, Pratt RB, Ewers FW, Davis SD.** 2007c. Cavitation resistance among 26 chaparral species of Southern California. *Ecological Monographs* **77**, 99–115.

**Jansen S, Choat B, Pletsers A.** 2009. Morphological variation of intervessel pit membranes and implications to xylem function in angiosperms. *American Journal of Botany* **96**, 409–419.

**Johnson KM, Brodersen C, Carins-Murphy MR, Choat B, Brodribb TJ.** 2020. Xylem embolism spreads by single-conduit events in three dry forest angiosperm stems. *Plant Physiology* **184**, 212–222.



**Johnson KM, Brodribb TJ.** 2023. Evidence for a trade-off between growth rate and xylem cavitation resistance in *Callitris rhomboidea*. (F Meinzer, Ed.). *Tree Physiology*, tpad037.

**Johnson DM, Katul G, Domec J.** 2022. Catastrophic hydraulic failure and tipping points in plants. *Plant, Cell & Environment* **45**, 2231–2266.

**Johnson KM, Lucani C, Brodribb TJ.** 2021. In vivo monitoring of drought-induced embolism in *Callitris rhomboidea* trees reveals wide variation in branchlet vulnerability and high resistance to tissue death. *New Phytologist* **233**, 207–218.

**Johnson DM, Wortemann R, McCulloh KA, Jordan-Meille L, Ward E, Warren JM, Palmroth S, Domec J-C.** 2016. A test of the hydraulic vulnerability segmentation hypothesis in angiosperm and conifer tree species. (N Phillips, Ed.). *Tree Physiology* **36**, 983–993.

**Joshi J, Stocker BD, Hofhansl F, Zhou S, Dieckmann U, Prentice IC.** 2022. Towards a unified theory of plant photosynthesis and hydraulics. *Nature Plants* **8**, 1304–1316.

**Joshi R, Wani SH, Singh B, Bohra A, Dar ZA, Lone AA, Pareek A, Singla-Pareek SL.** 2016. Transcription factors and plants response to drought stress: current understanding and future directions. *Frontiers in Plant Science* **7**, 1029.

**Kaack L, Altaner CM, Carmesin C, et al.** 2019. Function and three-dimensional structure of intervessel pit membranes in angiosperms: a review. *IAWA Journal* **40**, 673–702.

**Kaack L, Weber M, Isasa E, et al.** 2021. Pore constrictions in intervessel pit membranes provide a mechanistic explanation for xylem embolism resistance in angiosperms. *New Phytologist* **230**, 1829–1843.

**Kanduč M, Schneck E, Loche P, Jansen S, Schenk HJ, Netz RR.** 2020. Cavitation in lipid bilayers poses strict negative pressure stability limit in biological liquids. *Proceedings of the National Academy of Sciences* **117**, 10733–10739.

- Kannenberg SA, Driscoll AW, Malesky D, Anderegg WRL.** 2021. Rapid and surprising dieback of Utah juniper in the southwestern USA due to acute drought stress. *Forest Ecology and Management* **480**, 118639.
- Karami O, Rahimi A, Khan M, Bemmer M, Hazarika RR, Mak P, Compier M, van Noort V, Offringa R.** 2020. A suppressor of axillary meristem maturation promotes longevity in flowering plants. *Nature Plants* **6**, 368–376.
- Karnovsky MJ.** 1965. A formaldehyde-glutaraldehyde fixative of high osmolality for use in electron microscopy. **27**, 137-138A.
- Khurmatov KK.** 1982. Heterogeneity of natural populations of *Arabidopsis thaliana* (pamiro-alay) in the flowering time. *Arabidopsis Inf Serv.* **19**, 62–66.
- Kim T-W, Jehanzaib M.** 2020. Drought risk analysis, forecasting and assessment under climate change. *Water* **12**, 1862.
- Kim J-S, Mizoi J, Yoshida T, et al.** 2011. An ABRE promoter sequence is involved in osmotic stress-responsive expression of the DREB2A gene, which encodes a transcription factor regulating drought-inducible genes in *Arabidopsis*. *Plant and Cell Physiology* **52**, 2136–2146.
- Kimura Y, Aoki S, Ando E, et al.** 2015. A flowering integrator, SOC1, affects stomatal opening in *Arabidopsis thaliana*. *Plant and Cell Physiology* **56**, 640–649.
- Klein T.** 2014. The variability of stomatal sensitivity to leaf water potential across tree species indicates a continuum between isohydric and anisohydric behaviours. (S Niu, Ed.). *Functional Ecology* **28**, 1313–1320.
- Klein T, Hartmann H.** 2018. Climate change drives tree mortality. (J Sills, Ed.). *Science* **362**, 758–758.
- Knipfer T, Bambach N, Hernandez MI, Bartlett MK, Sinclair G, Duong F, Kluepfel DA, McElrone AJ.** 2020. Predicting stomatal closure and turgor loss in woody plants using predawn and midday water potential. *Plant Physiology* **184**, 881–894.

**Ko J-H, Han K-H, Park S, Yang J.** 2004. Plant body weight-induced secondary growth in *Arabidopsis* and its transcription phenotype revealed by whole-transcriptome profiling. *Plant Physiology* **135**, 1069–1083.

**Kolb TE, Fettig CJ, Ayres MP, Bentz BJ, Hicke JA, Mathiasen R, Stewart JE, Weed AS.** 2016. Observed and anticipated impacts of drought on forest insects and diseases in the United States. *Forest Ecology and Management* **380**, 321–334.

**Kolb KJ, Sperry JS.** 1999. Differences in drought adaptation between subspecies of sagebrush (*Artemisia tridentata*). *Ecology* **80**, 2373–2384.

**Konrad W, Katul G, Roth-Nebelsick A, Jensen KH.** 2019. Xylem functioning, dysfunction and repair: a physical perspective and implications for phloem transport. (T Holta, Ed.). *Tree Physiology* **39**, 243–261.

**Koornneef M, Meinke D.** 2010. The development of *Arabidopsis* as a model plant. *The Plant Journal* **61**, 909–921.

**Koster KL, Leopold AC.** 1988. Sugars and desiccation tolerance in seeds. *Plant Physiology* **88**, 829–832.

**Kuromori T, Seo M, Shinozaki K.** 2018. ABA transport and plant water stress responses. *Trends in Plant Science* **23**, 513–522.

**Lamarque LJ, Delzon S, Toups H, et al.** 2020. Over-accumulation of abscisic acid in transgenic tomato plants increases the risk of hydraulic failure. *Plant, Cell & Environment* **43**, 548–562.

**Larter M, Brodribb TJ, Pfautsch S, Burrett R, Cochard H, Delzon S.** 2015. Extreme aridity pushes trees to their physical limits. *Plant Physiology* **168**, 804–807.

**Larter M, Pfautsch S, Domec J, Trueba S, Nagalingum N, Delzon S.** 2017. Aridity drove the evolution of extreme embolism resistance and the radiation of conifer genus *Callitris*. *New Phytologist* **215**, 97–112.

**Lata C, Prasad M.** 2011. Role of DREBs in regulation of abiotic stress responses in plants. *Journal of Experimental Botany* **62**, 4731–4748.

- Lawson T, Vialet-Chabrand S.** 2019. Speedy stomata, photosynthesis and plant water use efficiency. *New Phytologist* **221**, 93–98.
- Le DT, Nishiyama R, Watanabe Y, Mochida K, Yamaguchi-Shinozaki K, Shinozaki K, Tran L-SP.** 2011. Genome-wide survey and expression analysis of the plant-specific NAC transcription factor family in soybean during development and dehydration stress. *DNA Research* **18**, 263–276.
- Lemaire C, Blackman CJ, Cochard H, Menezes-Silva PE, Torres-Ruiz JM, Herbette S.** 2021a. Acclimation of hydraulic and morphological traits to water deficit delays hydraulic failure during simulated drought in poplar. *Tree Physiology* **41**, 2008–2021.
- Lemaire C, Quilichini Y, Brunel-Michac N, Santini J, Berti L, Cartailier J, Conchon P, Badel É, Herbette S.** 2021b. Plasticity of the xylem vulnerability to embolism in *Populus tremula x alba* relies on pit quantity properties rather than on pit structure. (J Martinez-Vilalta, Ed.). *Tree Physiology* **41**, 1384–1399.
- Lens F, Eeckhout S, Zwartjes R, Smets E, Janssens SB.** 2012a. The multiple fuzzy origins of woodiness within Balsaminaceae using an integrated approach. where do we draw the line? *Annals of Botany* **109**, 783–799.
- Lens F, Gleason SM, Bortolami G, Brodersen C, Delzon S, Jansen S.** 2022a. Functional xylem characteristics associated with drought-induced embolism in angiosperms. *New Phytologist* doi: 10.1111/nph.18447.
- Lens F, Gleason SM, Bortolami G, Brodersen C, Delzon S, Jansen S.** 2022b. Functional xylem characteristics associated with drought-induced embolism in angiosperms. *New Phytologist* **236**, 2019–2036.
- Lens F, Luteyn JL, Smets E, Jansen S.** 2004. Ecological trends in the wood anatomy of Vaccinioideae (Ericaceae s.l.). *Flora - Morphology, Distribution, Functional Ecology of Plants* **199**, 309–319.
- Lens F, Picon-Cochard C, Delmas CE, et al.** 2016. Herbaceous angiosperms are not more vulnerable to drought-induced embolism than angiosperm trees. *Plant Physiology* **172**, 661–667.

**Lens F, Schönenberger J, Baas P, Jansen S, Smets E.** 2007. The role of wood anatomy in phylogeny reconstruction of Ericales. *Cladistics* **23**, 229–294.

**Lens F, Smets E, Melzer S.** 2012*b*. Stem anatomy supports *Arabidopsis thaliana* as a model for insular woodiness: Letter. *New Phytologist* **193**, 12–17.

**Lens F, Sperry JS, Christman MA, Choat B, Rabaey D, Jansen S.** 2011*a*. Testing hypotheses that link wood anatomy to cavitation resistance and hydraulic conductivity in the genus *Acer*. *New Phytologist* **190**, 709–723.

**Lens F, Sperry JS, Christman MA, Choat B, Rabaey D, Jansen S.** 2011*b*. Testing hypotheses that link wood anatomy to cavitation resistance and hydraulic conductivity in the genus *Acer*. *New Phytologist* **190**, 709–723.

**Lens F, Tixier A, Cochard H, Sperry JS, Jansen S, Herbette S.** 2013. Embolism resistance as a key mechanism to understand adaptive plant strategies. *Current Opinion in Plant Biology* **16**, 287–292.

**Lesk C, Rowhani P, Ramankutty N.** 2016. Influence of extreme weather disasters on global crop production. *Nature* **529**, 84–87.

**Levionnois S, Jansen S, Wandji RT, Beauchêne J, Ziegler C, Coste S, Stahl C, Delzon S, Authier L, Heuret P.** 2021. Linking drought-induced xylem embolism resistance to wood anatomical traits in Neotropical trees. *New Phytologist* **229**, 1453–1466.

**Levionnois S, Ziegler C, Jansen S, Calvet E, Coste S, Stahl C, Salmon C, Delzon S, Guichard C, Heuret P.** 2020. Vulnerability and hydraulic segmentations at the stem–leaf transition: coordination across Neotropical trees. *New Phytologist* **228**, 512–524.

**Li S, Feifel M, Karimi Z, Schuldt B, Choat B, Jansen S.** 2015. Leaf gas exchange performance and the lethal water potential of five European species during drought. *Tree Physiology* **36**, 179–192.

**Li S, Lens F, Espino S, Karimi Z, Klepsch M, Schenk HJ, Schmitt M, Schuldt B, Jansen S.** 2016. Intervessel pit membrane thickness as a key dominant of embolism resistance in angiosperm xylem. *IAWA Journal* **37**, 152–171.

- Li Y, Li H, Li Y, Zhang S.** 2017. Improving water-use efficiency by decreasing stomatal conductance and transpiration rate to maintain higher ear photosynthetic rate in drought-resistant wheat. *The Crop Journal* **5**, 231–239.
- Li Y, Sperry JS, Shao M.** 2009. Hydraulic conductance and vulnerability to cavitation in corn (*Zea mays* L.) hybrids of differing drought resistance. *Environmental and Experimental Botany* **66**, 341–346.
- Liang X, Ye Q, Liu H, Brodribb TJ.** 2021. Wood density predicts mortality threshold for diverse trees. *New Phytologist* **229**, 3053–3057.
- Lima TRA, Carvalho ECD, Martins FR, et al.** 2018. Lignin composition is related to xylem embolism resistance and leaf life span in trees in a tropical semiarid climate. *New Phytologist* **219**, 1252–1262.
- Limousin J, Roussel A, Rodríguez-Calcerrada J, Torres-Ruiz JM, Moreno M, Jalon LG de, Ourcival J, Simioni G, Cochard H, Martin-StPaul N.** 2022. Drought acclimation of *Quercus ilex* leaves improves tolerance to moderate drought but not resistance to severe water stress. *Plant, Cell & Environment* **45**, 1967–1984.
- Liu Q, Luo L, Zheng L.** 2018. Lignins: Biosynthesis and Biological Functions in Plants. *International Journal of Molecular Sciences* **19**, 335.
- Lobin W.** 1983. The occurrence of *Arabidopsis thaliana* in the Cape Verde Islands. *Arab Info Ser* **20**, 119–123.
- Lobo A, Torres-Ruiz JM, Burlett R, et al.** 2018. Assessing inter- and intraspecific variability of xylem vulnerability to embolism in oaks. *Forest Ecology and Management* **424**, 53–61.
- Loepfe L, Martinez-Vilalta J, Piñol J, Mencuccini M.** 2007. The relevance of xylem network structure for plant hydraulic efficiency and safety. *Journal of Theoretical Biology* **247**, 788–803.
- Lohse D, Zhang X.** 2015. Surface nanobubbles and nanodroplets. *Reviews of Modern Physics* **87**, 981–1035.

**Lopez FB, Barclay GF.** 2017. Plant Anatomy and Physiology. Pharmacognosy. Elsevier, 45–60.

**Losso A, Bär A, Dämon B, et al.** 2019. Insights from *in vivo* micro-CT analysis: testing the hydraulic vulnerability segmentation in *Acer pseudoplatanus* and *Fagus sylvatica* seedlings. *New Phytologist* **221**, 1831–1842.

**Lübbe T, Lamarque LJ, Delzon S, Torres Ruiz JM, Burlett R, Leuschner C, Schuldt B.** 2022. High variation in hydraulic efficiency but not xylem safety between roots and branches in four temperate broad-leaved tree species. *Functional Ecology* **36**, 699–712.

**Lucas WJ, Groover A, Lichtenberger R, et al.** 2013. The plant vascular system: evolution, development and functions <sup>F</sup>. *Journal of Integrative Plant Biology* **55**, 294–388.

**Maherali H, Pockman WT, Jackson RB.** 2004. Adaptive variation in the vulnerability of woody plants to xylem cavitation. *Ecology* **85**, 2184–2199.

**Mantova M, Cochard H, Burlett R, Delzon S, King A, Rodriguez-Dominguez CM, Ahmed MA, Trueba S, Torres-Ruiz JM.** 2022a. On the path from xylem hydraulic failure to downstream cell death. *New Phytologist* **237**, 793–806.

**Mantova M, Herbette S, Cochard H, Torres-Ruiz JM.** 2022b. Hydraulic failure and tree mortality: from correlation to causation. *Trends in Plant Science* **27**, 335–345.

**Mantova M, Menezes-Silva PE, Badel E, Cochard H, Torres-Ruiz JM.** 2021. The interplay of hydraulic failure and cell vitality explains tree capacity to recover from drought. *Physiologia Plantarum* **172**, 247–257.

**Maris H, Balibar S.** 2000. Negative pressures and cavitation in liquid helium. *Physics Today* **53**, 29–34.

**Martínez-Cabrera HI, Jones CS, Espino S, Schenk HJ.** 2009. Wood anatomy and wood density in shrubs: responses to varying aridity along transcontinental transects. *American Journal of Botany* **96**, 1388–1398.

- Martinez-Vilalta J, Anderegg WRL, Sapes G, Sala A.** 2019. Greater focus on water pools may improve our ability to understand and anticipate drought-induced mortality in plants. *New Phytologist* **223**, 22–32.
- Martínez-Vilalta J, Garcia-Forner N.** 2017. Water potential regulation, stomatal behaviour and hydraulic transport under drought: deconstructing the iso/anisohydric concept: Deconstructing the iso/anisohydric concept. *Plant, Cell & Environment* **40**, 962–976.
- Martinez-Vilalta J, Mencuccini M, Alvarez X, Camacho J, Loepfe L, Pinol J.** 2012. Spatial distribution and packing of xylem conduits. *American Journal of Botany* **99**, 1189–1196.
- Martínez-Vilalta J, Santiago LS, Poyatos R, Badiella L, Cáceres M, Aranda I, Delzon S, Vilagrosa A, Mencuccini M.** 2021. Towards a statistically robust determination of minimum water potential and hydraulic risk in plants. *New Phytologist* **232**, 404–417.
- Martin-StPaul N, Delzon S, Cochard H.** 2017. Plant resistance to drought depends on timely stomatal closure. *Ecology Letters* **20**, 1437–1447.
- Martin-StPaul NK, Longepierre D, Huc R, Delzon S, Burlett R, Joffre R, Rambal S, Cochard H.** 2014. How reliable are methods to assess xylem vulnerability to cavitation? The issue of ‘open vessel’ artifact in oaks. *Tree Physiology* **34**, 894–905.
- Maruyama K, Todaka D, Mizoi J, et al.** 2012. Identification of Cis-Acting Promoter Elements in Cold- and Dehydration-Induced Transcriptional Pathways in Arabidopsis, Rice, and Soybean. *DNA Research* **19**, 37–49.
- Matiu M, Ankerst DP, Menzel A.** 2017. Interactions between temperature and drought in global and regional crop yield variability during 1961–2014. (JL Gonzalez-Andujar, Ed.). *PLOS ONE* **12**, e0178339.
- Matros A, Peshev D, Peukert M, Mock H-P, Van den Ende W.** 2015. Sugars as hydroxyl radical scavengers: proof-of-concept by studying the fate of sucralose in Arabidopsis. *The Plant Journal* **82**, 822–839.



**Mauri R, Cardoso AA, da Silva MM, Oliveira LA, Avila RT, Martins SCV, DaMatta FM.** 2020. Leaf hydraulic properties are decoupled from leaf area across coffee species. *Trees* **34**, 1507–1514.

**McCormack ML, Dickie IA, Eissenstat DM, et al.** 2015. Redefining fine roots improves understanding of below-ground contributions to terrestrial biosphere processes. *New Phytologist* **207**, 505–518.

**McDowell NG, Beerling DJ, Breshears DD, Fisher RA, Raffa KF, Stitt M.** 2011. The interdependence of mechanisms underlying climate-driven vegetation mortality. *Trends in Ecology & Evolution* **26**, 523–532.

**McDowell N, Pockman WT, Allen CD, et al.** 2008. Mechanisms of plant survival and mortality during drought: why do some plants survive while others succumb to drought? *New Phytologist* **178**, 719–739.

**McDowell NG, Sapes G, Pivovarov A, et al.** 2022. Mechanisms of woody-plant mortality under rising drought, CO<sub>2</sub> and vapour pressure deficit. *Nature Reviews Earth & Environment* **3**, 294–308.

**Mehrotra R, Bhalothia P, Bansal P, Basantani MK, Bharti V, Mehrotra S.** 2014. Abscisic acid and abiotic stress tolerance – Different tiers of regulation. *Journal of Plant Physiology* **171**, 486–496.

**Meinzer FC, Campanello PI, Domec J-C, Gatti MG, Goldstein G, Villalobos-Vega R, Woodruff DR.** 2008a. Constraints on physiological function associated with branch architecture and wood density in tropical forest trees. *Tree Physiology* **28**, 1609–1617.

**Meinzer FC, Johnson DM, Lachenbruch B, McCulloh KA, Woodruff DR.** 2009. Xylem hydraulic safety margins in woody plants: coordination of stomatal control of xylem tension with hydraulic capacitance. *Functional Ecology* **23**, 922–930.

**Meinzer FC, McCulloh KA, Lachenbruch B, Woodruff DR, Johnson DM.** 2010. The blind men and the elephant: the impact of context and scale in evaluating conflicts between plant hydraulic safety and efficiency. *Oecologia* **164**, 287–296.

- Meinzer FC, Woodruff DR, Domec J-C, Goldstein G, Campanello PI, Gatti MG, Villalobos-Vega R.** 2008b. Coordination of leaf and stem water transport properties in tropical forest trees. *Oecologia* **156**, 31–41.
- Melzer S, Lens F, Gennen J, Vanneste S, Rohde A, Beeckman T.** 2008. Flowering-time genes modulate meristem determinacy and growth form in *Arabidopsis thaliana*. *Nature Genetics* **40**, 1489–1492.
- Ménard D, Blaschek L, Kriechbaum K, et al.** 2022. Plant biomechanics and resilience to environmental changes are controlled by specific lignin chemistries in each vascular cell type and morphotype. *The Plant Cell* **34**, 4877–4896.
- Mencuccini M, Minunno F, Salmon Y, Martínez-Vilalta J, Hölttä T.** 2015. Coordination of physiological traits involved in drought-induced mortality of woody plants. *New Phytologist* **208**, 396–409.
- Messinger SM, Buckley TN, Mott KA.** 2006. Evidence for involvement of photosynthetic processes in the stomatal response to CO<sub>2</sub>. *Plant Physiology* **140**, 771–778.
- Meyra AG, Kuz VA, Zarragoicoechea GJ.** 2007. Geometrical and physicochemical considerations of the pit membrane in relation to air seeding: the pit membrane as a capillary valve. *Tree Physiology* **27**, 1401–1405.
- Mitchell PJ, O’Grady AP, Tissue DT, White DA, Ottenschlaeger ML, Pinkard EA.** 2013. Drought response strategies define the relative contributions of hydraulic dysfunction and carbohydrate depletion during tree mortality. *New Phytologist* **197**, 862–872.
- Monda K, Negi J, Iio A, Kusumi K, Kojima M, Hashimoto M, Sakakibara H, Iba K.** 2011. Environmental regulation of stomatal response in the *Arabidopsis* Cvi-0 ecotype. *Planta* **234**, 555–563.
- Mrad A, Johnson DM, Love DM, Domec J.** 2021. The roles of conduit redundancy and connectivity in xylem hydraulic functions. *New Phytologist* **231**, 996–1007.

**Nakashima K, Yamaguchi-Shinozaki K, Shinozaki K.** 2014. The transcriptional regulatory network in the drought response and its crosstalk in abiotic stress responses including drought, cold, and heat. *Frontiers in Plant Science* **5**, 170.

**Nardini A, Battistuzzo M, Savi T.** 2013. Shoot desiccation and hydraulic failure in temperate woody angiosperms during an extreme summer drought. *New Phytologist* **200**, 322–329.

**Netherer S, Matthews B, Katzensteiner K, et al.** 2015. Do water-limiting conditions predispose Norway spruce to bark beetle attack? *New Phytologist* **205**, 1128–1141.

**Neufeld HS, Grantz DA, Meinzer FC, Goldstein G, Crisosto GM, Crisosto C.** 1992. Genotypic Variability in Vulnerability of Leaf Xylem to Cavitation in Water-Stressed and Well-Irrigated Sugarcane. *Plant Physiology* **100**, 1020–1028.

**Nieminen KM, Kauppinen L, Helariutta Y.** 2004. A weed for wood? *Arabidopsis* as a genetic model for xylem development. *Plant Physiology* **135**, 653–659.

**Niklas KJ.** 1997. Mechanical properties of black locust (*Robinia pseudoacacia*) wood: correlations among elastic and rupture moduli, proportional limit, and tissue density and specific gravity. *Annals of Botany* **79**, 479–485.

**Nolan RH, Gauthey A, Losso A, et al.** 2021. Hydraulic failure and tree size linked with canopy die-back in eucalypt forest during extreme drought. *New Phytologist* **230**, 1354–1365.

**Nolf M, Pagitz K, Mayr S.** 2014. Physiological acclimation to drought stress in *Solidago canadensis*. *Physiologia Plantarum* **150**, 529–539.

**Nolf M, Rosani A, Ganthaler A, Beikircher B, Mayr S.** 2016. Herb hydraulics: inter and intraspecific variation in three *Ranunculus* species. *Plant Physiology* **170**, 2085–2094.

- O'Brien MJ, Leuzinger S, Philipson CD, Tay J, Hector A.** 2014. Drought survival of tropical tree seedlings enhanced by non-structural carbohydrate levels. *Nature Climate Change* **4**, 710–714.
- Oletić D, Rosner S, Bilas V.** 2023. Field-experiences of tracking plant's xylem embolism formation with embedded acoustic emission sensors. *e-Journal of Nondestructive Testing* **28**.
- Oliveira RS, Eller CB, Barros F de V, Hirota M, Brum M, Bittencourt P.** 2021. Linking plant hydraulics and the fast–slow continuum to understand resilience to drought in tropical ecosystems. *New Phytologist* **230**, 904–923.
- Olson ME, Pace MR, Anfodillo T.** 2023. The vulnerability to drought-induced embolism-conduit diameter link: breaching the anatomy-physiology divide. *IAWA Journal*, 1–20.
- Ozturk M, Turkyilmaz Unal B, García-Caparrós P, Khursheed A, Gul A, Hasanuzzaman M.** 2021. Osmoregulation and its actions during the drought stress in plants. *Physiologia Plantarum* **172**, 1321–1335.
- Pammenter NW, Van der Willigen C.** 1998. A mathematical and statistical analysis of the curves illustrating vulnerability of xylem to cavitation. *Tree Physiology* **18**, 589–593.
- Papastefanou P, Zang CS, Pugh TAM, Liu D, Grams TEE, Hickler T, Rammig A.** 2020. A dynamic model for strategies and dynamics of plant water-potential regulation under drought conditions. *Frontiers in Plant Science* **11**, 373.
- Park J, Go T, Ryu J, Lee SJ.** 2019. Air spreading through wetted cellulose membranes: Implications for the safety function of hydraulic valves in plants. *Physical Review E* **100**, 032409.
- Passardi F, Dobias J, Valério L, Guimil S, Penel C, Dunand C.** 2007. Morphological and physiological traits of three major *Arabidopsis thaliana* accessions. *Journal of Plant Physiology* **164**, 980–992.

**Passioura JB.** 1982. Water in the soil-plant-atmosphere continuum. In: Lange OL, Nobel PS, Osmond CB, Ziegler H, eds. *Physiological Plant Ecology II*. Berlin, Heidelberg: Springer Berlin Heidelberg, 5–33.

**Pereira H.** 2007. *Cork: Biology, Production and Uses*. Amsterdam: Elsevier.

**Pereira L, Bittencourt PRL, Oliveira RS, Junior MBM, Barros FV, Ribeiro RV, Mazzafera P.** 2016. Plant pneumatics: stem air flow is related to embolism – new perspectives on methods in plant hydraulics. *New Phytologist* **211**, 357–370.

**Pereira L, Bittencourt PRL, Pacheco VS, et al.** 2020. The pneumatron: an automated pneumatic apparatus for estimating xylem vulnerability to embolism at high temporal resolution. *Plant, Cell & Environment* **43**, 131–142.

**Pereira L, Domingues-Junior AP, Jansen S, Choat B, Mazzafera P.** 2018. Is embolism resistance in plant xylem associated with quantity and characteristics of lignin? *Trees* **32**, 349–358.

**Pfautsch S, Renard J, Tjoelker MG, Salih A.** 2015. Phloem as Capacitor: Radial Transfer of Water into Xylem of Tree Stems Occurs via Symplastic Transport in Ray Parenchyma. *Plant Physiology* **167**, 963–971.

**Pickard WF.** 1981. The ascent of sap in plants. *Progress in Biophysics and Molecular Biology* **37**, 181–229.

**Pittermann J.** 2010. The evolution of water transport in plants: an integrated approach. *Geobiology* **8**, 112–139.

**Pittermann J, Sperry JS, Wheeler JK, Hacke UG, Sikkema EH.** 2006. Mechanical reinforcement of tracheids compromises the hydraulic efficiency of conifer xylem. *Plant, Cell and Environment* **29**, 1618–1628.

**Pivovarov AL, Sack L, Santiago LS.** 2014. Coordination of stem and leaf hydraulic conductance in southern California shrubs: a test of the hydraulic segmentation hypothesis. *New Phytologist* **203**, 842–850.

**Plavcová L, Hacke UG.** 2012. Phenotypic and developmental plasticity of xylem in hybrid poplar saplings subjected to experimental drought,

nitrogen fertilization, and shading. *Journal of Experimental Botany* **63**, 6481–6491.

**Plavcová L, Hacke UG, Sperry JS.** 2011. Linking irradiance-induced changes in pit membrane ultrastructure with xylem vulnerability to cavitation: Irradiance-induced changes in pit structure. *Plant, Cell & Environment* **34**, 501–513.

**Plavcová L, Jansen S.** 2015. The Role of Xylem Parenchyma in the Storage and Utilization of Nonstructural Carbohydrates. In: Hacke U, ed. *Functional and Ecological Xylem Anatomy*. Cham: Springer International Publishing, 209–234.

**Plavcová L, Jansen S, Klepsch M, Hacke UG.** 2013. Nobody's perfect: can irregularities in pit structure influence vulnerability to cavitation? *Frontiers in Plant Science* **4**, 453.

**Pockman WT, Sperry JS.** 2000. Vulnerability to xylem cavitation and the distribution of Sonoran Desert vegetation. *American Journal of Botany* **87**, 1287–1299.

**Pockman WT, Sperry JS, O'Leary JW.** 1995. Sustained and significant negative water pressure in xylem. *Nature* **378**, 715–716.

**Poorter L.** 2008. The Relationships of wood-, gas- and water fractions of tree stems to performance and life history variation in Tropical trees. *Annals of Botany* **102**, 367–375.

**Poorter L, McDonald I, Alarcón A, Fichtler E, Licona J, Peña-Claros M, Sterck F, Villegas Z, Sass-Klaassen U.** 2010. The importance of wood traits and hydraulic conductance for the performance and life history strategies of 42 rainforest tree species. *New Phytologist* **185**, 481–492.

**Powers JS, Vargas G. G, Brodribb TJ, et al.** 2020. A catastrophic tropical drought kills hydraulically vulnerable tree species. *Global Change Biology* **26**, 3122–3133.

**Pratt RB, Jacobsen AL.** 2017. Conflicting demands on angiosperm xylem: tradeoffs among storage, transport and biomechanics: Tradeoffs in xylem function. *Plant, Cell & Environment* **40**, 897–913.

**Pratt RB, Jacobsen AL, Ewers FW, Davis SD.** 2007*a*. Relationships among xylem transport, biomechanics and storage in stems and roots of nine Rhamnaceae species of the California chaparral. *New Phytologist* **174**, 787–798.

**Pratt RB, Jacobsen AL, Golgotiu KA, Sperry JS, Ewers FW, Davis SD.** 2007*b*. Life history type and water stress tolerance in nine California chaparral species (Rhamnaceae).pdf. *Ecological Monographs* **77**, 239–253.

**Puranik S, Sahu PP, Srivastava PS, Prasad M.** 2012. NAC proteins: regulation and role in stress tolerance. *Trends in Plant Science* **17**, 369–381.

**Rabara RC, Tripathi P, Rushton PJ.** 2014. The potential of transcription factor-based genetic engineering in improving crop tolerance to drought. *OMICS: A Journal of Integrative Biology* **18**, 601–614.

**Ragni L, Greb T.** 2018. Secondary growth as a determinant of plant shape and form. *Seminars in Cell & Developmental Biology* **79**, 58–67.

**Rahimi A, Karami O, Balazadeh S, Offringa R.** 2022. miR156-independent repression of the ageing pathway by longevity-promoting AHL proteins in Arabidopsis. *New Phytologist* **235**, 2424–2438.

**Ramel F, Sulmon C, Bogard M, Couée I, Gouesbet G.** 2009. Differential patterns of reactive oxygen species and antioxidative mechanisms during atrazine injury and sucrose-induced tolerance in Arabidopsis thaliana plantlets. *BMC Plant Biology* **9**, 28.

**Rawlings JO, Cure WW.** 1985. The Weibull Function as a Dose-Response Model to Describe Ozone Effects on Crop Yields <sup>1</sup>. *Crop Science* **25**, 807–814.

**Reiterer A, Burgert I, Sinn G, Tschegg S.** 2002. The radial reinforcement of the wood structure and its implication on mechanical and fracture mechanical properties—a comparison between two tree species. 935–940.

**Rissanen K, Hölttä T, Bäck J, Rigling A, Wermelinger B, Gessler A.** 2021. Drought effects on carbon allocation to resin defences and on resin

dynamics in old-grown Scots pine. *Environmental and Experimental Botany* **185**, 104410.

**Rockwell FE, Wheeler JK, Holbrook NM.** 2014. Cavitation and its discontents: opportunities for resolving current controversies. *Plant Physiology* **164**, 1649–1660.

**Rodriguez-Dominguez CM, Brodribb TJ.** 2020. Declining root water transport drives stomatal closure in olive under moderate water stress. *New Phytologist* **225**, 126–134.

**Rodriguez-Dominguez CM, Carins Murphy MR, Lucani C, Brodribb TJ.** 2018. Mapping xylem failure in disparate organs of whole plants reveals extreme resistance in olive roots. *New Phytologist* **218**, 1025–1035.

**Rodriguez-Dominguez CM, Forner A, Martorell S, et al.** 2022. Leaf water potential measurements using the pressure chamber: synthetic testing of assumptions towards best practices for precision and accuracy. *Plant, Cell & Environment* **45**, 2037–2061.

**Rosas T, Mencuccini M, Barba J, Cochard H, Saura-Mas S, Martínez-Vilalta J.** 2019. Adjustments and coordination of hydraulic, leaf and stem traits along a water availability gradient. *New Phytologist* **223**, 632–646.

**Rosenthal DM, Stiller V, Sperry JS, Donovan LA.** 2010. Contrasting drought tolerance strategies in two desert annuals of hybrid origin. *Journal of Experimental Botany* **61**, 2769–2778.

**Russo SE, Jenkins KL, Wiser SK, Uriarte M, Duncan RP, Coomes DA.** 2010. Interspecific relationships among growth, mortality and xylem traits of woody species from New Zealand: Tree growth, mortality and woody traits. *Functional Ecology* **24**, 253–262.

**Saha S, Holbrook NM, Montti L, Goldstein G, Cardinot GK.** 2009. Water relations of *Chusquea ramosissima* and *Merostachys clausenii* in Iguazu national park, Argentina. *Plant Physiology* **149**, 1992–1999.

**Sakuma Y, Maruyama K, Osakabe Y, Qin F, Seki M, Shinozaki K, Yamaguchi-Shinozaki K.** 2006a. Functional analysis of an *Arabidopsis*



transcription factor, DREB2A, involved in drought-responsive gene expression. *The Plant Cell* **18**, 1292–1309.

**Sakuma Y, Maruyama K, Qin F, Osakabe Y, Shinozaki K, Yamaguchi-Shinozaki K.** 2006*b*. Dual function of an *Arabidopsis* transcription factor DREB2A in water-stress-responsive and heat-stress-responsive gene expression. *Proceedings of the National Academy of Sciences* **103**, 18822–18827.

**Sakuraba Y, Kim Y-S, Han S-H, Lee B-D, Paek N-C.** 2015. The *Arabidopsis* transcription factor NAC016 promotes drought stress responses by repressing *AREB1* transcription through a trifurcate feed-forward regulatory loop involving NAP. *The Plant Cell* **27**, 1771–1787.

**Salleo S, Hinckley TM, Kikuta SB, Gullo MA, Weilgony P, Yoon T-M, Richter H.** 1992. A method for inducing xylem emboli in situ: experiments with a field-grown tree. *Plant, Cell and Environment* **15**, 491–497.

**Salmon Y, Torres-Ruiz JM, Poyatos R, Martinez-Vilalta J, Meir P, Cochard H, Mencuccini M.** 2015. Balancing the risks of hydraulic failure and carbon starvation: a twig scale analysis in declining Scots pine: Twig role in Scots pine drought-induced mortality. *Plant, Cell & Environment* **38**, 2575–2588.

**Sangüesa-Barreda G, Linares JC, Camarero JJ.** 2015. Reduced growth sensitivity to climate in bark-beetle infested Aleppo pines: Connecting climatic and biotic drivers of forest dieback. *Forest Ecology and Management* **357**, 126–137.

**Sapes G, Demaree P, Lekberg Y, Sala A.** 2021. Plant carbohydrate depletion impairs water relations and spreads via ectomycorrhizal networks. *New Phytologist* **229**, 3172–3183.

**Sapes G, Roskilly B, Dobrowski S, Maneta M, Anderegg WRL, Martinez-Vilalta J, Sala A.** 2019. Plant water content integrates hydraulics and carbon depletion to predict drought-induced seedling mortality. *Tree Physiology* **39**, 1300–1312.

**Schenk HJ, Espino S, Rich-Cavazos SM, Jansen S.** 2018. From the sap's perspective: the nature of vessel surfaces in angiosperm xylem. *American Journal of Botany* **105**, 172–185.

- Schenk HJ, Espino S, Romo DM, et al.** 2017. Xylem surfactants introduce a new element to the cohesion-tension theory. *Plant Physiology* **173**, 1177–1196.
- Schenk HJ, Michaud JM, Mocko K, Espino S, Melendres T, Roth MR, Welti R, Kaack L, Jansen S.** 2021. Lipids in xylem sap of woody plants across the angiosperm phylogeny. *The Plant Journal* **105**, 1477–1494.
- Schenk HJ, Steppe K, Jansen S.** 2015. Nanobubbles: a new paradigm for air-seeding in xylem. *Trends in Plant Science* **20**, 199–205.
- Schindelin J, Arganda-Carreras I, Frise E, et al.** 2012. Fiji: an open-source platform for biological-image analysis. *Nature Methods* **9**, 676–682.
- Scholz A, Klepsch M, Karimi Z, Jansen S.** 2013*a*. How to quantify conduits in wood? *Frontiers in Plant Science* **4**, 56.
- Scholz FG, Phillips NG, Bucci SJ, Meinzer FC, Goldstein G.** 2011. Hydraulic Capacitance: Biophysics and Functional Significance of Internal Water Sources in Relation to Tree Size. In: Meinzer FC, Lachenbruch B, Dawson TE, eds. *Tree Physiology. Size- and Age-Related Changes in Tree Structure and Function*. Dordrecht: Springer Netherlands, 341–361.
- Scholz A, Rabaey D, Stein A, Cochard H, Smets E, Jansen S.** 2013*b*. The evolution and function of vessel and pit characters with respect to cavitation resistance across 10 *Prunus* species. *Tree Physiology* **33**, 684–694.
- Schuldt B, Buras A, Arend M, et al.** 2020. A first assessment of the impact of the extreme 2018 summer drought on Central European forests. *Basic and Applied Ecology* **45**, 86–103.
- Schuldt B, Knutzen F, Delzon S, Jansen S, Müller-Haubold H, Burlett R, Clough Y, Leuschner C.** 2016. How adaptable is the hydraulic system of European beech in the face of climate change-related precipitation reduction? *New Phytologist* **210**, 443–458.
- Schweingruber FH.** 2006. Anatomical characteristics and ecological trends in the xylem and phloem of Brassicaceae and Resedaceae. *IAWA Journal* **27**, 419–442.

**Schweingruber FH.** 2007. *Wood structure and environment*. Berlin; New York: Springer.

**Schweingruber FH, Börner A, Schulze E-D.** 2011. *Atlas of Stem Anatomy in Herbs, Shrubs and Trees*. Berlin, Heidelberg: Springer Berlin Heidelberg.

**Scoffoni C, Albuquerque C, Brodersen CR, Townes SV, John GP, Bartlett MK, Buckley TN, McElrone AJ, Sack L.** 2017. Outside-xylem vulnerability, not xylem embolism, controls leaf hydraulic decline during dehydration. *Plant Physiology* **173**, 1197–1210.

**Scoffoni C, Albuquerque C, Cochard H, et al.** 2018. The causes of leaf hydraulic vulnerability and its influence on gas exchange in *Arabidopsis thaliana*. *Plant Physiology* **178**, 1584–1601.

**Segala Alves E, Angyalossy-Alfonso V.** 2002. Ecological trends in the wood anatomy of some Brazilian species. 2. axial parenchyma, ray and fibres. *IAWA Journal* **23**, 391–418.

**Shahnejat-Bushehri S, Allu AD, Mehterov N, Thirumalaikumar VP, Alseekh S, Fernie AR, Mueller-Roeber B, Balazadeh S.** 2017. Arabidopsis NAC transcription factor JUNGBRUNNEN1 exerts conserved control over gibberellin and brassinosteroid metabolism and signaling genes in tomato. *Frontiers in Plant Science* **8**, 214.

**Shahnejat-Bushehri S, Mueller-Roeber B, Balazadeh S.** 2012. Arabidopsis NAC transcription factor JUNGBRUNNEN1 affects thermomemory-associated genes and enhances heat stress tolerance in primed and unprimed conditions. *Plant Signaling & Behavior* **7**, 1518–1521.

**Shahnejat-Bushehri S, Tarkowska D, Sakuraba Y, Balazadeh S.** 2016. Arabidopsis NAC transcription factor JUB1 regulates GA/BR metabolism and signalling. *Nature Plants* **2**, 1–9.

**Shinozaki K, Yamaguchi-Shinozaki K.** 2006. Gene networks involved in drought stress response and tolerance. *Journal of Experimental Botany* **58**, 221–227.

**Shinozaki K, Yamaguchi-Shinozaki K, Seki M.** 2003. Regulatory network of gene expression in the drought and cold stress responses. *Current Opinion in Plant Biology* **6**, 410–417.

**Simioni PF, Emilio T, Giles AL, Viana De Freitas G, Silva Oliveira R, Setime L, Pierre Vitoria A, Pireda S, Vieira Da Silva I, Da Cunha M.** 2023. Anatomical traits related to leaf and branch hydraulic functioning on Amazonian savanna plants. (A Martin, Ed.). *AoB PLANTS* **15**, plad018.

**Singh PK, Indoliya Y, Agrawal L, et al.** 2022. Genomic and proteomic responses to drought stress and biotechnological interventions for enhanced drought tolerance in plants. *Current Plant Biology* **29**, 100239.

**Skelton RP, Anderegg LDL, Diaz J, Kling MM, Papper P, Lamarque LJ, Delzon S, Dawson TE, Ackerly DD.** 2021. Evolutionary relationships between drought-related traits and climate shape large hydraulic safety margins in western North American oaks. *Proceedings of the National Academy of Sciences* **118**, e2008987118.

**Skelton RP, Anderegg LDL, Papper P, Reich E, Dawson TE, Kling M, Thompson SE, Diaz J, Ackerly DD.** 2019. No local adaptation in leaf or stem xylem vulnerability to embolism, but consistent vulnerability segmentation in a North American oak. *New Phytologist* **223**, 1296–1306.

**Skelton RP, Brodribb TJ, Choat B.** 2017. Casting light on xylem vulnerability in an herbaceous species reveals a lack of segmentation. *New Phytologist* **214**, 561–569.

**Skelton RP, West AG, Dawson TE.** 2015. Predicting plant vulnerability to drought in biodiverse regions using functional traits. *Proceedings of the National Academy of Sciences* **112**, 5744–5749.

**Słupianek A, Dolzblasz A, Sokołowska K.** 2021. Xylem Parenchyma—Role and Relevance in Wood Functioning in Trees. *Plants* **10**, 1247.

**Smith-Martin CM, Skelton RP, Johnson KM, Lucani C, Brodribb TJ.** 2020. Lack of vulnerability segmentation among woody species in a diverse dry sclerophyll woodland community. (A Sala, Ed.). *Functional Ecology* **34**, 777–787.

**Soma F, Takahashi F, Yamaguchi-Shinozaki K, Shinozaki K.** 2021. Cellular phosphorylation signaling and gene expression in drought stress responses: ABA-dependent and ABA-independent regulatory systems. *Plants* **10**, 756.

**Somssich M.** 2019. *A short history of Arabidopsis thaliana (L.) Heynh. Columbia-0.* PeerJ Preprints.

**Song J, Trueba S, Yin X-H, Cao K-F, Brodribb TJ, Hao G-Y.** 2022. Hydraulic vulnerability segmentation in compound-leaved trees: evidence from an embolism visualization technique. *Plant Physiology* **189**, 204–214.

**Sorek Y, Greenstein S, Hochberg U.** 2022. Seasonal adjustment of leaf embolism resistance and its importance for hydraulic safety in deciduous trees. *Physiologia Plantarum* **174**, e13785.

**Sperry JS.** 1995. Limitations on Stem Water Transport and Their Consequences. *Plant Stems*. Elsevier, 105–124.

**Sperry JS.** 2003. Evolution of water transport and xylem structure. *International Journal of Plant Sciences* **164**, S115–S127.

**Sperry JS, Christman MA, Torres-Ruiz JM, Taneda H, Smith DD.** 2012. Vulnerability curves by centrifugation: is there an open vessel artefact, and are ‘r’ shaped curves necessarily invalid?: Vulnerability curves by centrifugation. *Plant, Cell & Environment* **35**, 601–610.

**Sperry JS, Hacke UG.** 2004. Analysis of circular bordered pit function I. Angiosperm vessels with homogenous pit membranes. *American Journal of Botany* **91**, 369–385.

**Sperry JS, Hacke UG, Pittermann J.** 2006. Size and function in conifer tracheids and angiosperm vessels. *American Journal of Botany* **93**, 1490–1500.

**Sperry JS, Hacke UG, Wheeler JK.** 2005. Comparative analysis of end wall resistivity in xylem conduits. *Plant, Cell and Environment* **28**, 456–465.

**Sperry JS, Meinzer FC, McCULLOH KA.** 2008. Safety and efficiency conflicts in hydraulic architecture: scaling from tissues to trees. *Plant, Cell & Environment* **31**, 632–645.

**Sperry JS, Saliendra NZ.** 1994. Intra- and inter-plant variation in xylem cavitation in *Betula occidentalis*. *Plant, Cell and Environment* **17**, 1233–1241.

**Sperry JS, Tyree MT.** 1988. Mechanism of water stress-induced xylem embolism. *Plant Physiology* **88**, 581–587.

**Steudle E.** 2001*a*. The cohesion-tension mechanism and the acquisition of water by plant roots. *Annual Review of Plant Physiology and Plant Molecular Biology* **52**, 847–875.

**Steudle E.** 2001*b*. The cohesion-tension mechanism and the acquisition of water by plant roots. *Annual review of plant physiology and plant molecular biology* **52**, 847–875.

**Stiller V.** 2002. Cavitation fatigue and its reversal in sunflower (*Helianthus annuus* L.). *Journal of Experimental Botany* **53**, 1155–1161.

**Stiller V.** 2009. Soil salinity and drought alter wood density and vulnerability to xylem cavitation of baldcypress (*Taxodium distichum* (L.) Rich.) seedlings. *Environmental and Experimental Botany* **67**, 164–171.

**Sultan B, Defrance D, Iizumi T.** 2019. Evidence of crop production losses in West Africa due to historical global warming in two crop models. *Scientific Reports* **9**, 12834.

**Swemmer A.** 2020. Locally high, but regionally low: the impact of the 2014–2016 drought on the trees of semi-arid savannas, South Africa. *African Journal of Range & Forage Science* **37**, 31–42.

**Tak H, Negi S, Ganapathi TR.** 2017. Banana NAC transcription factor MusaNAC042 is positively associated with drought and salinity tolerance. *Protoplasma* **254**, 803–816.

**Takasaki H, Maruyama K, Kidokoro S, Ito Y, Fujita Y, Shinozaki K, Yamaguchi-Shinozaki K, Nakashima K.** 2010. The abiotic stress-responsive

NAC-type transcription factor OsNAC5 regulates stress-inducible genes and stress tolerance in rice. *Molecular Genetics and Genomics* **284**, 173–183.

**Temperli C, Bugmann H, Elkin C.** 2013. Cross-scale interactions among bark beetles, climate change, and wind disturbances: a landscape modeling approach. *Ecological Monographs* **83**, 383–402.

**Thirumalaikumar VP, Devkar V, Mehterov N, Ali S, Ozgur R, Turkan I, Mueller-Roeber B, Balazadeh S.** 2018. NAC transcription factor JUNGBRUNNEN1 enhances drought tolerance in tomato. *Plant Biotechnology Journal* **16**, 354–366.

**Thoen MPM, Davila Olivas NH, Kloth KJ, et al.** 2017. Genetic architecture of plant stress resistance: multi-trait genome-wide association mapping. *New Phytologist* **213**, 1346–1362.

**Thonglim A, Bortolami G, Delzon S, Larter M, Offringa R, Keurentjes JJB, Smets E, Balazadeh S, Lens F.** 2022. Drought response in *Arabidopsis* displays synergistic coordination between stems and leaves. (J Zhang, Ed.). *Journal of Experimental Botany* **74**, 1004–1021.

**Thonglim A, Delzon S, Larter M, Karami O, Rahimi A, Offringa R, Keurentjes JJB, Balazadeh S, Smets E, Lens F.** 2020. Intervessel pit membrane thickness best explains variation in embolism resistance amongst stems of *Arabidopsis thaliana* accessions. *Annals of Botany* **128**, 171–182.

**Tixier A, Cochard H, Badel E, Dusotoit-Coucaud A, Jansen S, Herbette S.** 2013. *Arabidopsis thaliana* as a model species for xylem hydraulics: does size matter? *Journal of Experimental Botany* **64**, 2295–2305.

**Tng DYP, Apgaua DMG, Ishida YF, Mencuccini M, Lloyd J, Laurance WF, Laurance SGW.** 2018. Rainforest trees respond to drought by modifying their hydraulic architecture. *Ecology and Evolution* **8**, 12479–12491.

**Tobin MF, Pratt RB, Jacobsen AL, Guzman MED.** 2012. Xylem vulnerability to cavitation can be accurately characterised in species with long vessels using a centrifuge method. *Plant Biology* **15**, 496–504.

- Todaka D, Shinozaki K, Yamaguchi-Shinozaki K.** 2015. Recent advances in the dissection of drought-stress regulatory networks and strategies for development of drought-tolerant transgenic rice plants. *Frontiers in Plant Science* **6**, 84.
- Tomasella M, Petrusa E, Petruzzellis F, Nardini A, Casolo V.** 2019. The possible role of non-structural carbohydrates in the regulation of tree hydraulics. *International Journal of Molecular Sciences* **21**, 144.
- Tombesi S, Nardini A, Frioni T, Soccolini M, Zadra C, Farinelli D, Poni S, Palliotti A.** 2015. Stomatal closure is induced by hydraulic signals and maintained by ABA in drought-stressed grapevine. *Scientific Reports* **5**, 12449.
- Torres-Ruiz JM, Cochard H, Choat B, et al.** 2017. Xylem resistance to embolism: presenting a simple diagnostic test for the open vessel artefact. *New Phytologist* **215**, 489–499.
- Torres-Ruiz JM, Cochard H, Mayr S, Beikircher B, Diaz-Espejo A, Rodriguez-Dominguez CM, Badel E, Fernández JE.** 2014. Vulnerability to cavitation in *Olea europaea* current-year shoots: further evidence of an open-vessel artifact associated with centrifuge and air-injection techniques. *Physiologia Plantarum* **152**, 465–474.
- Tran L-SP, Nakashima K, Sakuma Y, Simpson SD, Fujita Y, Maruyama K, Fujita M, Seki M, Shinozaki K, Yamaguchi-Shinozaki K.** 2004. Isolation and functional analysis of *Arabidopsis* stress-inducible NAC transcription factors that bind to a drought-responsive cis-element in the early responsive to dehydration stress 1 Promoter. *The Plant Cell* **16**, 2481–2498.
- Trontin C, Tisné S, Bach L, Loudet O.** 2011. What does *Arabidopsis* natural variation teach us (and does not teach us) about adaptation in plants? *Current Opinion in Plant Biology* **14**, 225–231.
- Trueba S, Delzon S, Isnard S, Lens F.** 2019. Similar hydraulic efficiency and safety across vesselless angiosperms and vessel-bearing species with scalariform perforation plates. *Journal of Experimental Botany* **70**, 3227–3240.



**Trueba S, Pouteau R, Lens F, Feild TS, Isnard S, Olson ME, Delzon S.** 2017. Vulnerability to xylem embolism as a major correlate of the environmental distribution of rain forest species on a tropical island. *Plant, Cell & Environment* **40**, 277–289.

**Tyree MT, Alexander J, Machado J-L.** 1992. Loss of hydraulic conductivity due to water stress in intact juveniles of *Quercus rubra* and *Populus deltoides*. *Tree Physiology* **10**, 411–415.

**Tyree MT, Ewers FW.** 1991. The hydraulic architecture of trees and other woody plants. *New Phytologist* **119**, 345–360.

**Tyree MT, Fiscus EL, Wullschlegel SD, Dixon MA.** 1986. Detection of xylem cavitation in corn under field conditions. *Plant Physiology* **82**, 597–599.

**Tyree MT, Sperry JS.** 1989. Vulnerability of xylem to cavitation and embolism. *Annual Review of Plant Physiology and Plant Molecular Biology* **40**, 19–36.

**Tyree MT, Stephen D. D, Herve C.** 1994. Biophysical perspectives of xylem evolution: is there a tradeoff of hydraulic efficiency for vulnerability to dysfunction? *IAWA Journal* **15**, 335–360.

**Tyree MT, Zimmermann MH.** 2002. *Xylem structure and the ascent of sap*. Berlin, Heidelberg: Springer Berlin Heidelberg.

**Uno Y, Furihata T, Abe H, Yoshida R, Shinozaki K, Yamaguchi-Shinozaki K.** 2000. *Arabidopsis* basic leucine zipper transcription factors involved in an abscisic acid-dependent signal transduction pathway under drought and high-salinity conditions. *Proceedings of the National Academy of Sciences* **97**, 11632–11637.

**Urli M, Porte AJ, Cochard H, Guengant Y, Burlett R, Delzon S.** 2013. Xylem embolism threshold for catastrophic hydraulic failure in angiosperm trees. *Tree Physiology* **33**, 672–683.

**Venturas MD, Sperry JS, Hacke UG.** 2017a. Plant xylem hydraulics: what we understand, current research, and future challenges. *Journal of Integrative Plant Biology* **59**, 356–389.

- Venturas MD, Sperry JS, Hacke UG.** 2017*b*. Plant xylem hydraulics: What we understand, current research, and future challenges: Plant xylem hydraulics. *Journal of Integrative Plant Biology* **59**, 356–389.
- Venturas MD, Todd HN, Trugman AT, Anderegg WRL.** 2021. Understanding and predicting forest mortality in the western United States using long-term forest inventory data and modeled hydraulic damage. *New Phytologist* **230**, 1896–1910.
- Vergeynst LL, Dierick M, Bogaerts JAN, Cnudde V, Steppe K.** 2015*a*. Cavitation: a blessing in disguise? New method to establish vulnerability curves and assess hydraulic capacitance of woody tissues. *Tree Physiology* **35**, 400–409.
- Vergeynst LL, Sause MGR, De Baerdemaeker NJF, De Roo L, Steppe K.** 2016. Clustering reveals cavitation-related acoustic emission signals from dehydrating branches. (N Phillips, Ed.). *Tree Physiology* **36**, 786–796.
- Vergeynst LL, Sause MGR, Hamstad MA, Steppe K.** 2015*b*. Deciphering acoustic emission signals in drought stressed branches: the missing link between source and sensor. *Frontiers in Plant Science* **6**.
- Vermeirssen V, De Clercq I, Van Parys T, Van Breusegem F, Van De Peer Y.** 2015. *Arabidopsis* ensemble reverse-engineered gene regulatory network discloses interconnected transcription factors in oxidative stress. *The Plant Cell* **26**, 4656–4679.
- Violle C, Navas M-L, Vile D, Kazakou E, Fortunel C, Hummel I, Garnier E.** 2007. Let the concept of trait be functional! *Oikos* **116**, 882–892.
- Volaire F, Lens F, Cochard H, Xu H, Chacon-Doria L, Bristiel P, Balachowski J, Rowe N, Violle C, Picon-Cochard C.** 2018. Embolism and mechanical resistances play a key role in dehydration tolerance of a perennial grass *Dactylis glomerata* L. *Annals of Botany* **122**, 325–336.
- Wall S, Violet-Chabrand S, Davey P, Van Rie J, Galle A, Cockram J, Lawson T.** 2022. Stomata on the abaxial and adaxial leaf surfaces contribute differently to leaf gas exchange and photosynthesis in wheat. *New Phytologist* **235**, 1743–1756.

- Wang J, Li Q, Mao X, Li A, Jing R.** 2016a. Wheat transcription factor TaAREB3 participates in drought and freezing tolerances in *Arabidopsis*. *International Journal of Biological Sciences* **12**, 257–269.
- Wang G, Zhang S, Ma X, Wang Y, Kong F, Meng Q.** 2016b. A stress-associated NAC transcription factor (SINAC35) from tomato plays a positive role in biotic and abiotic stresses. *Physiologia Plantarum* **158**, 45–64.
- Wang R, Zhang L, Zhang S, Cai J, Tyree MT.** 2014. Water relations of *Robinia pseudoacacia* L.: do vessels cavitate and refill diurnally or are r-shaped curves invalid in *Robinia*? *Plant, Cell & Environment* **37**, 2667–2678.
- Waring KM, Reboletti DM, Mork LA, Huang C-H, Hofstetter RW, Garcia AM, Fulé PZ, Davis TS.** 2009. Modeling the Impacts of Two Bark Beetle Species Under a Warming Climate in the Southwestern USA: Ecological and Economic Consequences. *Environmental Management* **44**, 824–835.
- Wason JW, Anstreicher KS, Stephansky N, Huggett BA, Brodersen CR.** 2018. Hydraulic safety margins and air-seeding thresholds in roots, trunks, branches and petioles of four northern hardwood trees. *New Phytologist* **219**, 77–88.
- Welsch M.** 2022. Untersuchung des Stresstoleranz-Regulationsnetzwerks des NAC-Transkriptionsfaktors JUNGBRUNNEN1 (JUB1) Investigation of the stress tolerance regulatory network integration of the NAC transcription factor JUNGBRUNNEN1 (JUB1). Universität Potsdam.
- West AG, Hultine KR, Jackson TL, Ehleringer JR.** 2007. Differential summer water use by *Pinus edulis* and *Juniperus osteosperma* reflects contrasting hydraulic characteristics. *Tree Physiology* **27**, 1711–1720.
- Wheeler JK, Huggett BA, Tofte AN, Rockwell FE, Holbrook NM.** 2013. Cutting xylem under tension or supersaturated with gas can generate PLC and the appearance of rapid recovery from embolism: Sampling induced embolism. *Plant, Cell & Environment* **36**, 1938–1949.
- Wheeler JK, Sperry JS, Hacke UG, Hoang N.** 2005. Inter-vessel pitting and cavitation in woody Rosaceae and other vesselled plants: a basis for a

safety versus efficiency trade-off in xylem transport. *Plant, Cell and Environment* **28**, 800–812.

**Wheeler TD, Stroock AD.** 2008. The transpiration of water at negative pressures in a synthetic tree. *Nature* **455**, 208–212.

**Wiley E, Rogers BJ, Hodgkinson R, Landhäuser SM.** 2016. Nonstructural carbohydrate dynamics of lodgepole pine dying from mountain pine beetle attack. *New Phytologist* **209**, 550–562.

**Willson CJ, Manos PS, Jackson RB.** 2008. Hydraulic traits are influenced by phylogenetic history in the drought-resistant, invasive genus *Juniperus* (Cupressaceae). *American Journal of Botany* **95**, 299–314.

**Wu A, Allu AD, Garapati P, et al.** 2012. *JUNGBRUNNEN1*, a Reactive Oxygen Species-Responsive NAC Transcription Factor, Regulates Longevity in *Arabidopsis*. *The Plant Cell* **24**, 482–506.

**Xu Z-Y, Kim SY, Hyeon DY, et al.** 2013. The *Arabidopsis* NAC transcription factor ANAC096 cooperates with bZIP-type transcription factors in dehydration and osmotic stress responses. *The Plant Cell* **25**, 4708–4724.

**Yamaguchi-Shinozaki K, Shinozaki K.** 2005. Organization of cis-acting regulatory elements in osmotic- and cold-stress-responsive promoters. *Trends in Plant Science* **10**, 88–94.

**Yang J, M Michaud J, Jansen S, Schenk HJ, Zuo YY.** 2020. Dynamic surface tension of xylem sap lipids. *Tree Physiology* **40**, 433–444.

**Yoshida T, Fujita Y, Maruyama K, Mogami J, Todaka D, Shinozaki K, Yamaguchi-Shinozaki K.** 2015. Four *Arabidopsis* AREB ABF transcription factors function predominantly in gene. *Plant, Cell & Environment* **38**, 35–49.

**Yoshida T, Fujita Y, Sayama H, Kidokoro S, Maruyama K, Mizoi J, Shinozaki K, Yamaguchi-Shinozaki K.** 2010. AREB1, AREB2, and ABF3 are master transcription factors that cooperatively regulate ABRE-dependent ABA signaling involved in drought stress tolerance and require ABA for full activation. *The Plant Journal* **61**, 672–685.

**Yu S-M.** 1999. Cellular and Genetic Responses of Plants to Sugar Starvation. *Plant Physiology* **121**, 687–693.

**Zhang F-P, Brodribb TJ.** 2017. Are flowers vulnerable to xylem cavitation during drought? *Proceedings of the Royal Society B: Biological Sciences* **284**, 20162642.

**Zhang Y, Carmesin C, Kaack L, et al.** 2020. High porosity with tiny pore constrictions and unbending pathways characterize the 3D structure of intervessel pit membranes in angiosperm xylem. *Plant, Cell & Environment* **43**, 116–130.

**Zhang Y-J, Rockwell FE, Graham AC, Alexander T, Holbrook NM.** 2016. Reversible leaf xylem collapse: a potential “circuit breaker” against cavitation. *Plant Physiology* **172**, 2261–2274.

**Zheng J, Martínez-Cabrera HI.** 2013. Wood anatomical correlates with theoretical conductivity and wood density across China: evolutionary evidence of the functional differentiation of axial and radial parenchyma. *Annals of Botany* **112**, 927–935.

**Zimmerman MH, Brown CL.** 1971. *Trees: structure and function*. New York, USA: Springer-Verlag.

**Zimmermann MH.** 1983. *Xylem Structure and the Ascent of Sap*. Berlin-Heidelberg, Germany: Springer-Verlag.



# ACKNOWLEDGEMENTS

*In December 2018, my Ph.D. journey began as I left the bright hot days of Thailand for the chilly winters in the Netherlands. This transition was both challenging and eye-opening, as it introduced me to a whole new world. I can honestly say that it was tough, but it turned out to be an amazing experience. I am grateful for all the obstacles that came my way because, with each difficulty, I discovered wonderful people and learned valuable lessons. Every hurdle shaped me into the person I am today. Therefore, I want to express my heartfelt gratitude to the amazing people and institutions who have been a constant source of support and guidance throughout my incredible PhD journey, especially during the difficult times brought on by the COVID-19 pandemic. Their presence and contributions have deeply touched my heart.*

*First and foremost, I am forever thankful to my daily supervisor, Dr. Frederic Lens. Your guidance, knowledge, and patience have been priceless to me. Despite the personal challenges we faced, you always encouraged me, shared your insights, and stood by my side throughout every step of this journey. I am also grateful to my fellow researchers and colleagues who directly collaborated on this PhD project. Your time and valuable contributions were not only helpful but also your positive and uplifting vibes cheered me up during the hard times. Special thanks also go to the technicians from Naturalis Biodiversity Center, Leiden University, and the University of Bordeaux for their mentorship and assistance in processing numerous samples with perfect results.*

*To the incredible Functional Traits group, thank you for your support and empathy, both academically and emotionally. Despite the physical distance imposed by the pandemic, our intellectual connections remained strong. Engaging in meaningful discussions, sharing constructive feedback, and creating a supportive environment enriched my understanding and shaped my research in incredible ways. Together, we have proven that even in the darkest times, collaboration and friendship can bring light. A big thanks to all the fellow PhDs at Naturalis –without citing names (to not forget anyone).*

*You were always kind and cheerful, even though I could not attend all the activities. You all made my journey full of joy turning this cold part of the world warmer ☺. Special thanks also go to the 'spicy girls' - Dewi, Deyi, Eka, Le Qin, and Richa - for making me feel at home. Our time was amazing, and you filled the Netherlands with smiles and laughter. It was truly priceless.*

*To my cherished family, your unconditional love and unwavering support have been my pillar of strength and my driving force throughout this journey. A very special thanks to Pablo for always being there for me. Your love, belief in me, and patience during tough moments have carried me through the most challenging times. And to Pablo's family, thank you for being a second home that I can always come to. I deeply appreciate it. Muchas Gracias!*



# CURRICULUM VITAE

**Ajaree Thonglim** was born on January 14<sup>th</sup>, 1993, in Nakhon Pathom, Thailand. She completed her four - year bachelor's degree in biology with First-class honors in 2015 at Kasetsart University, Thailand. During her undergraduate course,



she studied the morphological and anatomical features of the leaves of various species of the genus *Cycas* L. and used these traits to build a species identification key. Driven by her fascination with plant anatomy and functional traits, she pursued a master's degree in Botany at Kasetsart University, investigating the anatomical adaptation of mangrove species in the genus *Rhizophora* (Rhizophoraceae), and she successfully completed her MSc degree in 2018. Throughout her bachelor's and master's studies, she actively shared her research findings at scientific meetings, particularly those organized by the Botanical Society of Thailand. During her university education, a scholarship from the Development and Promotion of Science and Technology Talents Project (DPST) was awarded to her, jointly administered by the Ministry of Science and Technology, the Ministry of Education, and The Institute for the Promotion of Teaching Science and Technology (IPST). Later in 2018, she received another scholarship from the same funding agency. This scholarship granted her the opportunity to pursue her PhD at Leiden University and Naturalis Biodiversity Center in the Netherlands under the supervision of Dr. Frederic Lens and Prof. Dr. Erik Smets. Her PhD project was focused on drought-responsive strategies in different genotypes of *Arabidopsis thaliana*, with a small focus on *Solanum lycopersicum*.

During her PhD, she had the opportunity to regularly visit the laboratory of Dr. Sylvain Delzon at the University of Bordeaux, France, where she conducted water transport measurements on stems under special laboratory conditions that simulate drought stress. She also collaborated

with Dr. Giovanni Bortolami at Naturalis Biodiversity Center on a project involving root pressure and used advanced X-ray scanning technology at the University of Ghent, Belgium, to examine the impact of root pressure on drought recovery in tomato plants. She actively participated in international scientific meetings and adapted to the challenges posed by the COVID-19 pandemic by presenting her research online. Her PhD research resulted in two peer-reviewed SCI papers published as first author, with another manuscript in preparation for publication. The findings of her research are compiled in this thesis, showcasing her dedication and contributions to the scientific community.

## List of publications

### Articles in peer-reviewed proceedings and journals

**Thonglim A.**, Jintana V., Kermanee P. 2017. Root anatomy of *Rhizophora apiculata* Blume. Proceedings of 55th Kasetsart University Annual Conference: Plants, Animals, Veterinary Medicine, Fisheries, Agricultural Extension and Home Economics. Bangkok (Thailand). 296-303.

**Thonglim A.**, Delzon S., Larter M., Karami O., Rahimi A., Offringa R., Keurentjes J. J., Balazadeh S., Smets E., Lens F. 2021. Intervessel pit membrane thickness best explains variation in embolism resistance amongst stems of *Arabidopsis thaliana* accessions. *Annals of Botany*, 128(2): 171-182.

**Thonglim A.**, Bortolami G., Delzon S., Larter M., Offringa R., Keurentjes, J. J., Smets E., Balazadeh S., Lens F. 2023. Drought response in *Arabidopsis* displays synergistic coordination between stems and leaves. *Journal of Experimental Botany*, 74(3): 1004-1021.

## Abstracts

**Thonglim A.**, Kermanee P. 2015. Morphology and anatomy of leaves in the genus *Cycas* L. The 7th International Kasetsart University Science and Technology Annual Research Symposiums, Bangkok, Thailand, 28-29 May 2015. (Poster presentation)

**Thonglim A.**, Kermanee P. 2015. Morphology and anatomy of leaves in some species of the genus *Cycas* L. The 9th Botanical Conference of Thailand, Bangkok, Thailand. 3-5 June 2015. (Poster presentation)

**Thonglim A.**, Jintana V., Kermanee P. 2015. Root anatomy of primary and prop roots of *Rhizophora apiculata*. The 10th Science and Technology Conference for Youth 2015, Pathum Thani, Thailand, 4-6 November 2015. (Oral and Poster presentations)

**Thonglim A.**, Delzon S., Lens F. 2019. Embolism resistance in herbaceous and woody accessions of *Arabidopsis thaliana*. Fourth Xylem International Meeting, Padua, Italy, 25-27 September 2019. (Poster presentation)

**Thonglim A.**, Delzon S., Larter M., Karami O., Rahimi A., Offringa R., Keurentjes J. J., Balazadeh S., Smets E., Lens F. 2020. Intervessel pit membrane thickness functionally explains best the differences in embolism formation in stems amongst *Arabidopsis thaliana* accessions. Botanical Society of America Conference (virtual), 27-31 July 2020. (Oral presentation)

**Thonglim A.**, Bortolami G., Delzon S., Larter M., Offringa R., Keurentjes, J. J., Smets E., Balazadeh S., Lens F. 2022. Different drought response strategies in six *Arabidopsis* genotypes with contrasting stem lignification. Fifth Xylem International Meeting, Würzburg, Germany, 19-21 September 2022. (Poster presentation)

**Thonglim A.**, Bortolami G., Delzon S., Larter M., Offringa R., Karami O., Rahimi A., Keurentjes J. J., Smets E., Balazadeh S., Lens F. 2022. Disentangling drought tolerance in six *Arabidopsis* genotypes with contrasting stem lignification. The 2022 International Youth Forum for Wood Anatomy and the 9th IAWA-China Group Annual Meeting, Guangzhou, China, 9-12 December 2022. (Oral presentation)



